Electrochemical study of the interaction between magnetic beads functionalized with nucleobase derivatives and selected heavy metals

Simona Sawan

N°d'ordre NNT : 2021LYSE1119

THESE de DOCTORAT DE L'UNIVERSITE DE LYON
opérée au sein de
l'Université Claude Bernard Lyon 1

Ecole Doctorale ED 206
Ecole Doctorale de Chimie

Spécialité de doctorat : Chimie
Discipline : Chimie Analytique

Soutenue publiquement le 01/07/2021, par :
Simona Sawan

Electrochemical study of the interaction between magnetic beads functionalized with nucleobase derivatives and selected heavy metals

Devant le jury composé de :

Nom, prénom	grade/qualité	établissement/entreprise	
Leonard, Didier	Professeur des universités	Université Lyon 1	Président
Hou-Broutin, Yanxia	Chargée de Recherche	CNRS Grenoble	Rapporteure
Korri-Youssoufi, Hafsa	Directrice de Recherche	CNRS Paris	Rapporteure
Chehimi, Mohamed	Directeur de Recherche	CNRS Paris	Examinateur
Errachid el-Salhi, Abdelhamid	Professeur des universités	Université Lyon 1	Directeur de thèse
Maalouf, Rita	Professeure Associée	Notre Dame University	Co-directrice de thèse
Jaffrezic-Renault, Nicole	Directrice de Recherche Emérite	CNRS Lyon	Invitée

Université Claude Bernard – LYON 1

Président de l'Université	M. Frédéric FLEURY
Président du Conseil Académique	M. Hamda BEN HADID
Vice-Président du Conseil d'Administration	M. Didier REVEL
Vice-Président du Conseil des Etudes et de la Vie Universitaire	M. Philippe CHEVALLIER
Vice-Président de la Commission de Recherche	M. Jean-François MORNEX
Directeur Général des Services	M. Pierre ROLLAND

COMPOSANTES SANTE

Département de Formation et Centre de Recherche en Biologie Humaine	Directrice : Mme Anne-Marie SCHOTT
Faculté d'Odontologie	Doyenne : Mme Dominique SEUX
Faculté de Médecine et Maïeutique Lyon Sud - Charles Mérieux	Doyenne : Mme Carole BURILLON
Faculté de Médecine Lyon-Est	Doyen : M. Gilles RODE
Institut des Sciences et Techniques de la Réadaptation (ISTR)	Directeur : M. Xavier PERROT
Institut des Sciences Pharmaceutiques et Biologiques (ISBP)	Directrice : Mme Christine VINCIGUERRA

COMPOSANTES & DEPARTEMENTS DE SCIENCES & TECHNOLOGIE

Département Génie Electrique et des Procédés (GEP)	Directrice : Mme Rosaria FERRIGNO
Département Informatique	Directeur : M. Behzad SHARIAT
Département Mécanique	Directeur M. Marc BUFFAT
Ecole Supérieure de Chimie, Physique, Electronique (CPE Lyon)	Directeur : Gérard PIGNAULT
Institut de Science Financière et d'Assurances (ISFA)	Directeur : M. Nicolas LEBOISNE
Institut National du Professorat et de l'Education	Administrateur Provisoire : M. Pierre CHAREYRON
Institut Universitaire de Technologie de Lyon 1	Directeur : M. Christophe VITON
Observatoire de Lyon	Directrice : Mme Isabelle DANIEL
Polytechnique Lyon	Directeur : Emmanuel PERRIN
UFR Biosciences	Administratrice provisoire : Mme Kathrin GIESELER
UFR des Sciences et Techniques des Activités Physiques et Sportives (STAPS)	Directeur : M. Yannick VANPOULLE
UFR Faculté des Sciences	Directeur : M. Bruno ANDRIOLETTI

Abstract

Even though some heavy metals are essential in small quantities for human life, exposure to increased levels of heavy metal ions is known to cause several disorders and diseases. Not only are they harmful to human beings, but also to the ecological system in general due to their non-biodegradability. Since they can reach the environment through natural and/or anthropogenic sources, their detection and removal from different environmental matrices are of great importance. The present work involves using magnetic nanoparticles (Fe_3O_4 NPs) coated with (3-aminopropyl)triethoxysilane (APTES) and functionalized with nucleobase derivatives for the adsorption studies of arsenic, cadmium, copper and lead ions. The physical and chemical characterization of the nanoparticles was done using Fourier transform infrared (FTIR) spectroscopy, energy-dispersive X-ray analysis, scanning electron microscopy and X-ray diffraction. The successful functionalization of the nanoparticles was confirmed using FTIR. The suitability of electrochemical methods, and specifically square wave voltammetry, for adsorption studies was investigated. The electrochemical signal was shown to decrease with increasing heavy metal concentrations. Kinetic studies showed the superiority of one nucleobase derivative, guanine hydrazide, compared to the other nucleobases. Both Langmuir and Freundlich isotherms were used to assess the adsorption behavior of the functionalized nanoparticles and the experimental data were better fitted with the Langmuir model. The highest adsorption capacity was observed for arsenic ions with Q_0 of 446.43 $\mu g.g^{-1}$, decreasing as the ionic radii increased. Moreover, the signals generated by square wave voltammetry were used to assess the analytical performances of the different functionalized nanoparticles. For all heavy metals, two distinct linear response ranges were detected. Using the nanoparticles functionalized with guanine hydrazide, the sensitivities and limits of detection of the heavy metals were as follows: 171.6 µA/µM and 0.069 µM for copper, 156 µA/µM and 0.011 µM for lead, 101.4 µA/µM and 0.077 µM for cadmium and 144 µA/µM and 0.021 µM for arsenic, respectively.

Key words: iron oxide nanoparticles, nucleobase derivatives, adsorption, arsenic, copper, cadmium, lead, analytical performance

Resumé

Certains métaux lourds sont essentiels en petites quantités à la vie humaine. Cependant, l'exposition à de fortes doses est impliquée dans de nombreuses pathologies sévères et des maladies neurodégénératives. Ils sont non seulement nocifs pour les êtres humains, mais aussi pour le système écologique dans la mesure où ils sont non biodégradables. La pollution environnementale par les métaux lourds provient de diverses sources, naturelles et/ou anthropiques, d'où la necessité de disposer des techniques de detection et de décontamination efficaces. Le présent travail consiste à utiliser des nanoparticules magnétiques (Fe_3O_4 NPs) enrobées de (3-aminopropyl) triéthoxysilane (APTES) et fonctionnalisées avec des dérivés de nucléobases pour l'étude d'adsorption des ions arsenic, cadmium, cuivre et plomb. La caractérisation physique et chimique des nanoparticules a été réalisée à l'aide de la spectroscopie infrarouge à transformée de Fourier (FTIR), de l'analyse par rayons X à dispersion d'énergie, de la microscopie électronique à balayage et de la diffraction de rayons X. La fonctionnalisation des nanoparticules a été confirmée par FTIR. La pertinence des méthodes électrochimiques, et en particulier de la voltampérométrie à onde carrée, pour les études d'adsorption a été étudiée. Il a été montré que le signal électrochimique des nucléobases diminuait avec l'augmentation des concentrations de métaux lourds. Les études cinétiques ont montré la supériorité d'un dérivé de nucléobase, la guanine hydrazide, par rapport aux autres nucléobases. Les isothermes de Langmuir et de Freundlich ont été utilisés pour évaluer le comportement d'adsorption des nanoparticules fonctionnalisées et les données expérimentales ont montré que le modèle Langmuir simulait mieux l'adsorption. La capacité d'adsorption la plus élevée a été observée pour l'arsenic avec un Q_0 de 446,43 $\mu g.g^{-1}$, diminuant à mesure que les rayons ioniques augmentaient. De plus, les signaux générés par voltampérométrie à onde carrée ont été utilisés pour évaluer les performances analytiques des différentes nanoparticules fonctionnalisées. Deux gammes de réponses linéaires distinctes ont été détectées pour tous les métaux lourds. La sensibilité et la limite de détection des différents métaux lourds mesurés via les nanoparticules fonctionnalisées avec de l'hydrazide de guanine correspondent respectivement à 171,6 µA / µM et 0,069 µM pour le cuivre, 156 µA / µM et 0,011 µM pour le plomb, 101,4 µA / µM et 0,077 µM pour le cadmium et 144 µA / µM et 0,021 µM pour l'arsenic.

Mot clés: nanoparticules d'oxyde de fer, dérivés de nucléobases, adsorption, arsenic, cuivre, cadmium, plomb, performances analytiques

Acknowledgements

A three-year journey with all its ups and downs could not have been done without the direct and indirect support of the people whom this section is devoted to. First and foremost, I would like to express my gratitude to Notre Dame University-Louaize (NDU) and University Claude Bernard-Lyon (UCBL) for giving me the opportunity to do this work.

I am extremely grateful for my committee members Pr. Yanxia Hou-Broutin, Pr. Hafsa Korri-Youssoufi, Pr. Mohamed Chehimi and Pr. Didier Leonard for their insightful comments and challenging questions.

I have been blessed and privileged to work under the supervision of three highly accomplished scientists and incredible human beings. Pr. Abdelhamid Errachid el Salhi, I was so lucky to have been part of the team of an expert and "one of the best in his field"! Your enthusiasm and energy are simply contagious. Pr. Nicole Jaffrezic-Renault, the thought of having you as a supervisor is both frightening and exciting. You made home seem not that far away during my stay in France. Dr. Rita Maalouf, your warm heart and beautiful intentions are the cherry on top of your scientific expertise. Never did I think when I first started at NDU that you will be a colleague-turned-friend and sister. Thank you all for believing in my abilities and entrusting me to work under your supervision. Thank you for the fruitful dialogs and countless weekends and holidays you had to work with me. I couldn't have imagined going through the past three years with better advisors and mentors. I would also like to thank our collaborators at the American University of Beirut for providing us with the needed chemicals and expertise.

My colleagues and friends, I wish I could write about each and every one of you, but that would make a whole new doctorate manuscript. I thank you all for the encouragement and motivation, and for your willingness to brighten the days and keep me going.

My housemate and sister, Ms. Lina Moussa, I'm sorry you had to put up with me in the last three years. Thank you for staying by my side through it all. Thank you for always trying to find a solution for any problem. The sarcasm, drinks and pomelo surely did magic! To my favorite roommate and sister Ms. Rania Kazan, thank you for proving to me that distance is just a number and for showing me what strong women in science really means. Even though in

different countries, I can always count on you to have my back. Ms. Sylvie Khattar, our bride-to-be, your never-ending prayers and beautiful heart are inspiring!

I am forever indebted to my parents and brothers for their unconditional love, prayers, care and continuous support that have gotten me thus far. To my bigger family; aunts, uncle and cousins, I say thank you for believing in me and always standing by my side both personally and professionally. You've been there since the beginning, and I have no doubt that wherever I end up, you'll always be there.

When I first started my PhD, I was fully aware that it wasn't going to be the easiest experience; conducting experiments while having a full-time job. Nonetheless, I knew it was something I wanted and I was prepared to fight for. Little did I know that I would have to do so while my beloved country was going through a revolution, an economic crisis, a pandemic and one of the most powerful non-nuclear explosions in history. The resultant levels of stress, frustration, depression and grief were too much to handle in a lifetime, let alone a year. For that, I thank God for all I have and for where I stand today. Thank you for granting me the strength, will and capabilities to fulfill my ambitions.

“We must have perseverance and above all confidence in ourselves. We must believe that we are gifted for something and that this thing must be attained.” — *Marie Curie*

Contents

List of Abbreviations and Symbols

A	Adenine
AAS	Atomic Absorption Spectroscopy
AdSV	Adsorptive Stripping Voltammetry
AES	Atomic Emission Spectroscopy
AFS	Atomic Fluorescence Spectroscopy
Ag	Silver
AgCl	Silver chloride
$AgNO_3$	Silver nitrate
AH	Adenine hydrazide
APTES	(3-aminopropyl)triethoxysilane
As	Arsenic
ASV	Anodic Stripping Voltammetry
Au	Gold
b	Langmuir constant related to energy of adsorption
BDD	Boron doped diamond
BSA	Bovine Serum Albumin
C	Cytosine
CB	Carbon Black
Cd	Cadmium
$CDCl_3$	Deuterated chloroform
CE	Capillary Electrophoresis
c_e	Concentration at equilibrium
CeO_2	Cerium oxide
CH_2Cl_2	Dichloromethane
CL	Chemiluminescence
CNNF	Carbon Nitride Nanofibers
Co_3O_4	Cobalt oxide
CPE	Carbon Paste Electrode
Cr	Chromium
CS	Chitosan
CTAB	Cethyltrimethylammonium Bromide
CV	Cyclic Voltammetry
CV-AFS	Cold vapor- Atomic Fluorescence Spectroscopy
Cu	Copper
CµF	Carbon ultra-microfiber
DMA	N,N-dimethylacetamide
DMSO	Dimethyl sulfoxide
DNA	Deoxyribonucleic acid
DPASV	Differential Pulse Anodic Stripping Voltammetry
DPV	Differential Pulse Voltammetry
DSS	Sodium trimethylsilylpropanesulfonate
ΔI	Variation in peak maximum
EC	European Commission
ECL	Electrochemiluminescence

EDTA	Ethylenediaminetetraacetic acid
EDX	Energy Dispersive X-ray
EIS	Electrochemical Impedance Spectroscopy
$EMIMBF_4$	1-ethyl-3-methylimidazolium tetrafluoroborate
EPA	Environmental Protection Agency
EU	European Union
FDA	Food and Drug Administration
Fe	Iron
Fe_3O_4	Iron oxide
$FeCl_2.4H_2O$	Ferrous chloride tetrahydrate
$FeCl_3.6H_2O$	Ferric chloride hexahydrate
FTIR	Fourier transform infrared
G	Guanine
GA	Glutaraldehyde
GCE	Glassy Carbon Electrode
GCME	Carbon nanotube flow-through membrane electrode
GH	Guanine hydrazide
GNEE	Gold nanoelectrode ensembles
GNP	Gold Nanoparticles
GO	Graphene Oxide
GSH	Glutathione
H	Hydrogen
h	Hour
H_2O	Water
HEPES	4-(2-hydroxyethyl)-1-piperazineethanesulfonic acid
Hg	Mercury
HI	Hydrogen iodide
HRMS	High-Resolution Mass Spectroscopy
HS	Thiol
Hz	Hertz
ICP-AES	Inductively Coupled Plasma- Atomic Emission Spectroscopy
ICP-MS	Inductively Coupled Plasma- Mass Spectrometry
ICP-OES	Inductively Coupled Plasma- Optical Emission Spectroscopy
k	Rate constant
KCl	Potassium chloride
keV	kiloelectronvolt
K_F	Freundlich constant
$KMnO_4$	Potassium permanganate
LC	Liquid Chromatography
LIBS	Laser-Induced Breakdown Spectroscopy
LOD	Limit of detection
LSASV	Linear Sweep Anodic Stripping Voltammetry
LSPR	Localized Surface Plasma Resonance
LSV	Linear Sweep Voltammetry
MB	Methylene Blue
MCH	6-mercapto-hexanol

MeOH	Methanol
min	Minute
MgO	Magnesium oxide
$MgSO_4$	Magnesium sulfate
MnO_2	Manganese oxide
MNP	Magnetic nanoparticles
$MnSO_4.H_2O$	Manganese sulfate monohydrate
MoS_2	Molybdenum Disulfide
MRS	Magnetic Relaxation Switching
MWCNT	Multiwalled Carbon Nanotubes
N	Nitrogen
n	Freundlich exponent
$N_2H_4.H_2O$	Hydrazine monohydrate
NaOEt	Sodium ethoxide
NaOH	Sodium hydroxide
$(NH_4)_2S_2O_8$	Ammonium persulfate
NH_4OH	Ammonium hydroxide
NMR	Nuclear Magnetic Resonance
NPs	Nanoparticles
O	Oxygen
ODR	Optical Darkness Ratio
PAC	Porous Activated Carbon
Pb	Lead
Pd	Palladium
PEC	Photoelectrochemistry
ppb	Parts per billion
ppm	Parts per million
Pt	Platinum
py	Polypyrrole
q_0	Adsorption capacity
QCM	Quartz Crystal Microbalance
QD	Quantum Dots
r^2	Correlation coefficient
rGO	Reduced graphene oxide
R_L	Separation factor
Sb	Antimony
Se	Selenium
SERS	Surface Enhanced Raman Spectroscopy
SELDI-MS	Surface Enhanced Laser Desorption – Ionization Mass Spectrometry
SELEX	Systematic Evolution of Ligands by Exponential Enrichment
SEM	Scanning Electron Microscopy
Si	Silicon
SiO_2	silica
Sn	Tin
$SnCl_4.5H_2O$	Tin chloride pentahydrate
SnO_2	Tin oxide

SPCE	Screen Printed Carbon Electrode
SPE	Screen Printed Electrode
SPR	Surface Plasma Resonance
SWASV	Square Wave Anodic Stripping Voltammetry
SWV	Square Wave Voltammetry
t	Time
T	Thymine
TB	Toluidine Blue
TiO_2	Titanium oxide
Tl	Thallium
TLC	Thin layer chromatography
TMS	Tetramethylsilane
U	Uracil
UCNP	Upconversion Nanoparticles
UH	Uracil hydrazide
UV-vis	Ultraviolet- visible spectroscopy
V	Volts
WHO	World Health Organization
XRD	X-ray diffraction
Zn	Zinc
ZnO	Zinc oxide

General Introduction and Aim

The accumulation of organic, inorganic and biological hazardous materials in various environmental matrices has become a global concern. With the industrial development, increasing quantities of run-offs containing chemical contaminants, and especially heavy metals, are being directly or indirectly discharged into the environment and specifically into water. Heavy metals are much harder to remove from environmental media compared to organic contaminants which are eventually degraded, producing carbon dioxide and water [1]. Even though some heavy metals are considered essential to human beings, and many are of natural sources, moderate and chronic effects have been reported in literature. Overexposure to heavy metals has led to several disorders and diseases including anemia, dyspnea, parakeratosis, eczema and several types of cancers, just to name a few [2]. The major natural and anthropogenic sources, and common effects of the exposure to some heavy metals [3, 4] are presented in figure 1.

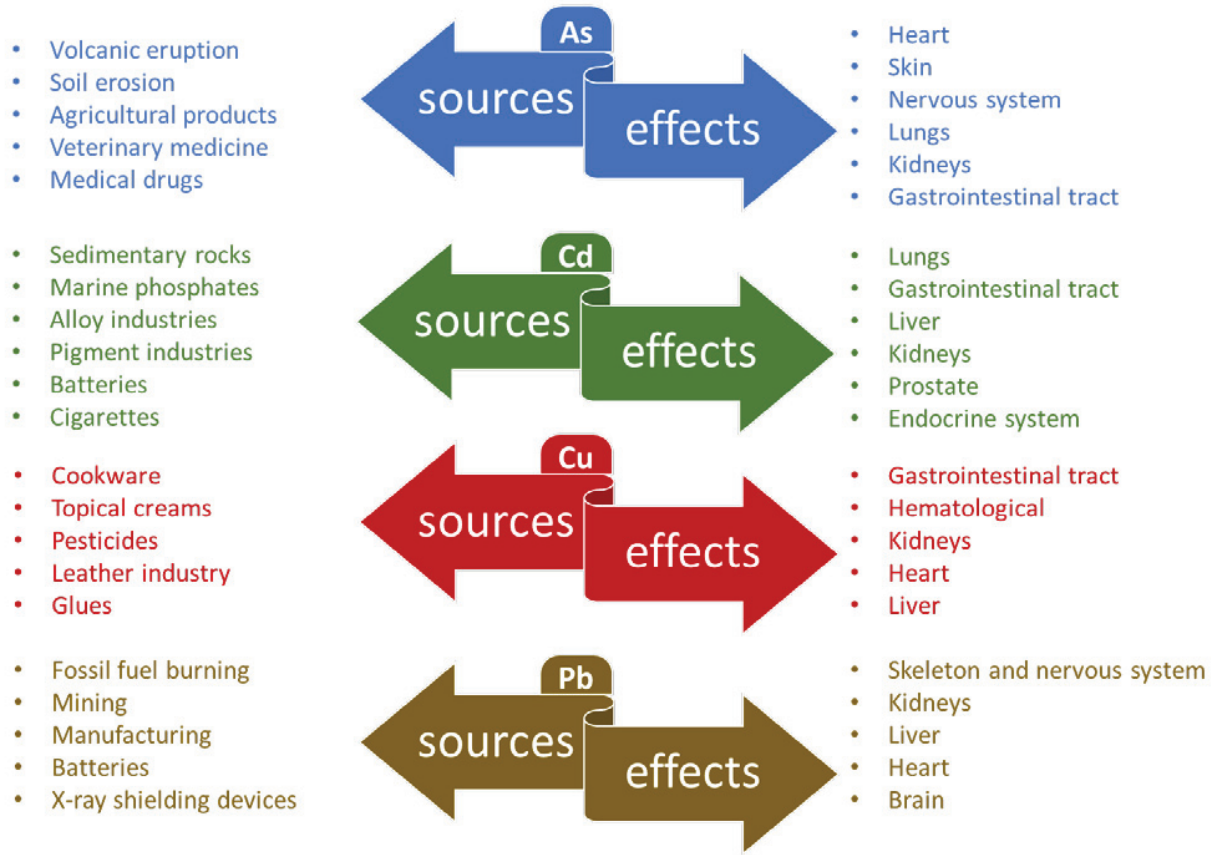

Figure 1: the major sources of arsenic, cadmium, copper and lead, and the most common human organs and systems affected by the exposure

Several studies have been conducted in areas with serious heavy metal pollution along with suggested treatment plans [5]. In France, and specifically in the Noyelles-Godaultand Auby, Douai area, which is a zinc-lead mine location, Sterckeman et al. found that the soil in that area is contaminated with zinc, lead and cadmium [6]. Audry et al. explored the Lot river basin where zinc ores are processed and not only did they find zinc, but also cadmium, copper and lead [7]. Cecchi et al. studied the surroundings of a lead recycling plant in Bazoches-les Gallérandes and were able to detect arsenic, chromium, copper, nickel, and zinc along with lead [8]. Most recently, Gardes et al. reconstructed the industrial trajectory of the Eure River confirming the high levels of zinc, copper and nickel reported back in the 1950s and 1960s and the high levels of lead in the 1990s and 2000s. As a result, a resilience period proves necessary for the system to recover [9].

In Lebanon, Houssainy et al. confirmed the significant contamination of the Saint Georges Bay in Beirut with mercury, copper, lead and silver [10]. Moustafa and Baroudi found that the groundwater in Akkar was contaminated with several heavy metals including lead and cadmium, rendering it undrinkable [11]. Halwani et al. also found lead and cadmium contamination, originating from dumps and industries, in Mount Lebanon reservoirs [12].

In efforts to minimize the harmful effects imposed by short-term and long-term exposure to heavy metals, several national and international agencies have set guideline values to be respected. The World Health Organization (WHO) [13], Environmental Protection Agency (EPA) [14] and European Commission (EC) [15] are among the international agencies that constantly update their permissible limits. Nevertheless, not all countries share the same levels of concern for heavy metal exposure, and consequently, reference values can differ between one governmental agency and the other [5]. France, as a member state of the European Union, implements regulations and policies set by the Union. On the other hand, in Lebanon, the Lebanese Ministry of Environment has set standards for the different types of water including sea and waste water [16], while still respecting the WHO guidelines.

Conventional technologies for the treatment of heavy metal ions include photocatalysis [17], reverse osmosis [18], flocculation [19] and coagulation [20]. Nevertheless, some drawbacks such as low efficiency, secondary pollution, high cost and restricted on-site application have limited the use of such techniques [21]. Benefiting from its low cost, feasibility and ease of operation, one of the methods used for heavy metal removal that has been largely exploited in the past few decades is adsorption [22]. Adsorption is the process by which a certain mass of a substrate or adsorbate is transferred to the surface of a solid or adsorbent resulting in physical and/or chemical interactions [23]. Depending on the strength of interaction between the two, several mechanisms have been used to explain the process [24]. Of the different adsorbents used, nanoparticles have emerged as alternatives for high-cost activated carbon while still demonstrating good adsorption efficiencies [25]. The role of surface modification was repeatedly highlighted to overcome a few setback characteristics of some nanoparticles such as the tendency of agglomeration of iron oxide nanoparticles and regeneration issues. Nucleobases and nucleotides are amongst those modifications used, specifically in heavy metal analysis. Not only

do they resolve the abovementioned drawbacks, but also contribute to increasing the sensitivity and selectivity of the nanoparticles [26].

The aim of this investigation is to develop low cost, effective and environmentally friendly adsorbents for the removal of heavy metal ions from water. The adsorbent will be based on iron oxide nanoparticles (Fe_3O_4 NPs) functionalized with nucleobase derivatives. The efficiency of the proposed biosorbents for the removal of four heavy metals will be assessed. The chosen heavy metals are arsenic (As^{3+}), cadmium (Cd^{2+}) and lead (Pb^{2+}) which are among the five most toxic heavy metals, in addition to copper (Cu^{2+}) which is among the most abundant in water. The technique chosen for the adsorption studies will be an electrochemical technique; square wave voltammetry. To the best of our knowledge, this technique is used for the first time in adsorption studies of heavy metal ions. Accordingly, this thesis is divided into the following chapters:

Chapter 1 briefly describes the voltametric studies, including square wave voltammetry, that have been reported lately to detect various heavy metal ions in several water samples. All the mentioned studies use either bare or functionalized metal and metal oxide nanoparticles. This chapter briefs the advantages of each type of nanoparticles used and presents the analytical performance of each. After comparing the different nanoparticles, it shows why iron oxide nanoparticles are perhaps the most advantageous in heavy metal detection.

Chapter 2 presents the studies combining nanotechnology with biotechnology for the detection and adsorption of heavy metal ions. In all the studies reported, nanoparticles were functionalized with aptamers or nucleobases and different sensing methods, from spectroscopic to electrochemical, were utilized. Compared to the numerous reports using aptamers, only a few have focused on using single nucloebases taking advantage of the simpler procedure and operation, while mainitaining the same selectivity and sensitivity obtained with aptamers. In this chapter, the different aspects of combining the two technologies together are highlighted, showing their advantages in heavy metal detection and removal.

Chapter 3 shows the experimental setup and procedure used in this work. It also introduces our synthesized magnetic nanoparticles and their functionalization with novel material, guanine hydrazide, for the electrochemical adsorption studies of the divalent heavy metals: cadmium, copper and lead. Following the synthesis, the different components were

characterized. Adsorption isotherms as well as the analytical performance of the functionalized nanoparticles were investigated.

Chapter 4 presents the square wave voltammetry adsorption studies of arsenic using several nucleobase hydrazides. It compares the performance of the different nucleobases and experimentally proves the preference of interaction. Adsorption isotherms, kinetics and analytical performances were also compared.

References

[1] J. Borjac, M. El Joumaa, L. Youssef, R. Kawach, D.A. Blake, Quantitative Analysis of Heavy Metals and Organic Compounds in Soil from Deir Kanoun Ras El Ain Dump, Lebanon, The Scientific World Journal, 2020 (2020) 8151676.

[2] J.G. Paithankar, S. Saini, S. Dwivedi, A. Sharma, D.K.J.C. Chowdhuri, Heavy metal associated health hazards: An interplay of oxidative stress and signal transduction, Chemosphere, 262 (2021) 128350.

[3] S.T. Royer A, Copper Toxicity, StatPearls {Internet}, Treasure Island (FL): StatPearls Publishing2020.

[4] P.B. Tchounwou, C.G. Yedjou, A.K. Patlolla, D.J. Sutton, Heavy metal toxicity and the environment, Exp Suppl, 101 (2012) 133-164.

[5] J.P. Vareda, A.J.M. Valente, L. Duraes, Assessment of heavy metal pollution from anthropogenic activities and remediation strategies: A review, J Environ Manage, 246 (2019) 101-118.

[6] T. Sterckeman, F. Douay, N. Proix, H. Fourrier, Vertical distribution of Cd, Pb and Zn in soils near smelters in the North of France, Environmental Pollution, 107 (2000) 377-389.

[7] S. Audry, J. Schäfer, G. Blanc, J.-M. Jouanneau, Fifty-year sedimentary record of heavy metal pollution (Cd, Zn, Cu, Pb) in the Lot River reservoirs (France), Environmental Pollution, 132 (2004) 413-426.

[8] M. Cecchi, C. Dumat, A. Alric, B. Felix-Faure, P. Pradere, M. Guiresse, Multi-metal contamination of a calcic cambisol by fallout from a lead-recycling plant, Geoderma, 144 (2008) 287-298.

[9] T. Gardes, M. Debret, Y. Copard, E. Patault, T. Winiarski, A.-L. Develle, P. Sabatier, A.-M. Dendievel, B. Mourier, S. Marcotte, B. Leroy, F. Portet-Koltalo, Reconstruction of anthropogenic activities in legacy sediments from the Eure River, a major tributary of the Seine Estuary (France), CATENA, 190 (2020) 104513.
[10] C.A.-G. Amonda El Houssainy, Duc Huy Dang, Céline Mahfouz,Dario Omanović, Gaby Khalaf, Stéphane Mounier, Cédric Garnier, Distribution and diagenesis of trace metals in marine sediments of a coastal Mediterranean area: St-Georges Bay (Lebanon), Marine Pollution Bulliten, 155 (2020) 11066.
[11] M.H. Ahmad Moustafa, Moomen Baroudi, Assessment of heavy metal and metalloids pollution in soils and groundwater in Akkar Northen Lebanon, Journal of Applied Sciences Research, 15 (2019) 28 - 38.
[12] D.A. Halwani, M. Jurdi, F.K. Abu Salem, M.A. Jaffa, N. Amacha, R.R. Habib, H.R. Dhaini, Cadmium Health Risk Assessment and Anthropogenic Sources of Pollution in Mount-Lebanon Springs, Exposure and Health, 12 (2020) 163-178.
[13] W.H.O. (WHO), Guidelines for Drinking-water Quality, 2006.
[14] U.S.E.P.A. (EPA), Drinking Water Requirements for States and Public Water Systems, https://www.epa.gov/dwreginfo/drinking-water-regulations, 2017.
[15] European Commision, Legislation, https://ec.europa.eu/environment/water/water-drink/legislation_en.html, 2020.
[16] MOE, State of the environment report, in: UNDP (Ed.) ECODITwww.undp.org, 2011.
[17] A. Ortega, I. Oliva, K.E. Contreras, I. González, M.R. Cruz-Díaz, E.P. Rivero, Arsenic removal from water by hybrid electro-regenerated anion exchange resin/electrodialysis process, Separation and Purification Technology, 184 (2017) 319-326.
[18] P. Benjwal, M. Kumar, P. Chamoli, K.K. Kar, Enhanced photocatalytic degradation of methylene blue and adsorption of arsenic(iii) by reduced graphene oxide (rGO)–metal oxide (TiO2/Fe3O4) based nanocomposites, RSC Advances, 5 (2015) 73249-73260.
[19] Y. Sun, S. Zhou, S.-Y. Pan, S. Zhu, Y. Yu, H. Zheng, Performance evaluation and optimization of flocculation process for removing heavy metal, Chem Eng J, 385 (2020) 123911.
[20] R.Y. Ning, Arsenic removal by reverse osmosis, Desalination, 143 (2002) 237-241.

[21] M. Usman, A. Ahmed, B. Yu, S. Wang, Y. Shen, H. Cong, Simultaneous adsorption of heavy metals and organic dyes by β-Cyclodextrin-Chitosan based cross-linked adsorbent, Carbohydr Polym, 255 (2021) 117486.
[22] R. Chakraborty, A. Asthana, A.K. Singh, B. Jain, A.B.H. Susan, Adsorption of heavy metal ions by various low-cost adsorbents: a review, Intern J Environ Anal Chem (2020) 1-38. https://doi.org/10.1080/03067319.2020.1722811
[23] C. Liu, Metal ions removal from polluted waters by sorption onto exhausted coffee waste. Application to metal finishing industries wastewater treatment, (2014) Doctoral dissertation, Universitat de Girona.
[24] B. Volesky, Equilibrium biosorption performance, Sorption and Biosorption, (2004) 103-116.
[25] M. Manyangadze, N.H.M. Chikuruwo, T.B. Narsaiah, C.S. Chakra, M. Radhakumari, G. Danha, Enhancing adsorption capacity of nano-adsorbents via surface modification: A review, South African Journal of Chemical Engineering, 31 (2020) 25-32.
[26] Q. Ren, L. Ga, Z. Lu, J. Ai, T. Wang, Aptamer-functionalized nanomaterials for biological applications, Materials Chemistry Frontiers, 4 (2020) 1569-1585.

Chapter I: Metal and Metal Oxide Nanoparticles in the Voltammetric Detection of Heavy Metals: A Review

Introduction

Heavy metals are a class of toxic and hazardous substances that can have a severe impact on the environment as well as human beings. They include, among others, mercury, lead, arsenic, cadmium, chromium, silver and antimony. Several techniques have been employed for the detection of heavy metal ions, of which electrochemical techniques proved to be the most advantageous. Highest sensitivities and lowest limits of detection are obtained with various voltammetry-based techniques. In addition to the fact that such techniques are simple and inexpensive, they allow on-site detection in several cases. A diversity of voltametric techniques is employed for heavy metal detection. The most common technique is square wave anodic stripping voltammetry. When using electrochemical sensors in real samples such as water, the complexity of such matrices due to the presence of competing ions and impurities should be taken into consideration, and consequently, a high sensitivity is required.

Nanoparticles are among the materials that have been used as modifiers in electrochemical sensors to enhance their sensitivity and selectivity. Due to their small sizes, they offer the advantages of larger surface areas and increased mass-transfer rate. Among the different nanoparticles used, metal and metal oxide nanoparticles are the most common. Gold nanoparticles are perhaps the most utilized metal nanoparticles for modifying electrochemical sensors. Various shapes and sizes of gold nanoparticles present different properties contributing to enhanced analytical performance. Not only is the use of gold nanoparticles investigated alone, but also with several modifiers. In fact, gold nanoparticles are rarely used alone and are usually associated with materials including carbon nanotubes, reduced graphene oxide and DNA. Similarly, silver, bismuth, platinum, palladium, tin and antimony nanoparticles are also used for heavy metal detection. Even though not as popular as gold nanoparticles, their catalytical, optical, chemical and mechanical properties have permitted them to be used as metal nanoparticles electrode modifiers.

On the other hand, the main disadvantage of using gold and some metal nanoparticles is their costly prices. Although some sensors using gold nanoparticles have shown excellent analytical performance, there remains a need to look for cheaper alternatives that can offer comparable sensitivities and limits of detection. Thus, metal oxide nanoparticles have been extensively studied in electrochemical detection of heavy metal ions in the past few years. The

different metal oxide nanoparticles recently used are titania, magnesium oxide, manganese oxide, cerium oxide, cobalt oxide, tin oxide, zinc oxide and magnetic nanoparticles. The latter nanoparticles, including iron oxide, are the most common. They offer great advantages, most notably, increased electrical conductivity as well as ease of separation from the matrix through an external magnet. Just like metallic nanoparticles, the use of these nanoparticles is also investigated with several modifiers including DNA, reduced graphene oxide and other nanoparticles such as gold nanoparticles.

Metal and Metal Oxide Nanoparticles in the Voltammetric Detection of Heavy Metals: A Review

This chapter is a slightly modified version of S. Sawan, R. Maalouf, A. Errachid, N. Jaffrezic-Renault, Metal and metal oxide nanoparticles in the voltammetric detection of heavy metals: A review, TrAC Trends in Analytical Chemistry, published 2020, Elsevier.

ABSTRACT

Most heavy metal ions are known to be toxic and carcinogenic when present in high amounts. Thus, rapid and reliable on-site detection of these ions is crucial. Voltammetry is a highly sensitive electrochemical method that has been widely used for heavy metal detection offering the advantages of sensitivity and rapidity. On the other hand, nanoparticles offer the advantages of high surface area and high selectivity. Thus, this review aims to highlight the application of metallic and metallic oxide nanoparticles for the voltammetric detection of heavy metals. The nanoparticles used were either applied solely on the electrode or as modifiers with various materials. In all cases, the synthesized devices showed an enhanced analytical performance, such that the limits of detection were lowered and the sensitivities were increased as compared to voltammetric systems not using nanoparticles. Moreover, the applicability of some of these systems was investigated in real samples.

1.1 Introduction

Heavy metals are defined as naturally occurring elements having a density or specific gravity greater than 5 $g.cm^{-3}$ and atomic weights between 63.5 and 200.6 $g.mol^{-1}$ [1]. Ions of heavy metals, even at trace levels, have been detected in different sources including food, beverages, soil, plants, natural waters, etc. The use of pesticides and fertilizers, burning of fossil fuels, mining, smelting and leaching from eating utensils and cookware are all sources of heavy

metal contamination [2, 3]. In addition to human activities, natural sources of heavy metals include: weathering of metal-bearing rocks, volcanic eruptions and forest fires.

Upon their release into the environment, whether through natural and anthropogenic sources, and since they are non-biodegradable, heavy metals accumulate and become toxic when present at high concentrations [4]. They are also known to hinder the developmental activity, yielding capacity and growth of plants. Moreover, heavy metals cause soil pollution and continuous exposure is very harmful to aquatic and terrestrial plants and animals [5]. In addition to their adverse impact on the environment, heavy metals are dangerous to the human health. They enter natural waters and start accumulating in sediments and living organisms, until they reach the final consumers in the food chain, which are human beings [6]. Continued exposure to heavy metals over a prolonged period of time can cause chronic poisoning, growth and developmental abnormalities, nephrotoxicity, encephalopathy, cardiovascular diseases and cancer [5].

For this reason, for each heavy metal, especially those considered as toxic, several agencies including the World Health Organization (WHO), Environmental Protection Agency (EPA) and Food and Drug Administration (FDA) [7, 8] have set guideline values for the allowable intake and exposure of humans to these heavy metals. Some of these limits are summarized in Table 1.

Table 1: Comparison between the allowable levels of some heavy metals in drinking water following the EPA, WHO and EU guidelines.

Heavy metal	EPA Guideline value in drinkable water (µg/L)	WHO Guideline value in drinkable water (µg/L)	EU Guideline value in foodstuff (µg/Kg)
Antimony	20	5	40
Arsenic	10	10	2
Cadmium	3	3	50
Chromium	50	50	250
Copper	2000	2000	3600
Lead	10	10	20
Mercury	6	1	1.6

Nickel	20	70	140

Conventional methods that have been used so far for the detection of heavy metals include Inductively Coupled Plasma- Mass Spectrometry (ICP-MS), Liquid Chromatography (LC) [9], UV-vis Spectrometry [10], Atomic Absorption Spectroscopy (AAS), Atomic Emission Spectrometry (AES) [11], Atomic Fluorescence Spectrometry (AFS) [12], Cold Vapor Atomic Fluorescence Spectrometry (CV-AFS) [13], Capillary Electrophoresis (CE) and Laser-Induced Breakdown Spectroscopy (LIBS) [14]. Even though these techniques are highly sensitive and selective, there still exists several challenges for their use in heavy metal detection [15]. These include high cost, complex operational procedures, long detection time and difficulty in achieving the detection in real environments [14].

On the other hand, electrochemical methods are gaining wide recognition in heavy metal detection. These methods offer the same sensitivity with a lower cost, less complex operational procedures and fast on-site detection. Different electrochemical platforms have been developed for heavy metal detection. Specifically, nanomaterials have brought several advantages in this area due to their unique electronic, chemical and mechanical properties. Accordingly, different electrochemical sensors using nanoparticles have been constructed for the detection of heavy metals [16, 17].

To the best of our knowledge, recent reviews focus on the detection of heavy metals using either a specific technique, or a specific type of nanoparticles [15, 17]. This review mainly discusses the use of voltammetry in the past fifteen years for heavy metal detection that can be applied to water samples using metal or metal oxide nanoparticles.

1.2. Voltammetric Techniques

Among the different known electrochemical methods, voltammetry is the most used in the detection of heavy metal ions. Voltammetry in general describes all electrochemical systems which are based on potential-dependent current measurements. A three-electrode electrochemical set-up typically consists of a working electrode, a counter electrode and a reference electrode. The potential is applied between the working and the reference electrodes, while the current is measured between the working and the counter electrodes. Upon varying the method of potential

change, one ends up with different techniques. Linear sweep voltammetry (LSV) is the simplest technique in which the potential is swept linearly with time [18]. Cyclic voltammetry (CV) consists of linearly scanning the potential in one direction followed by reversing the potential of a working electrode [17]. In other words, a single or multiple triangular potential waveforms [19] are involved.

The use of a pulse of voltage signal is the main concept behind pulsed voltammetry. By varying the shape and amplitude of the pulses, different types of pulsed voltammetry exist [17]. Differential pulse voltammetry (DPV) uses fixed magnitude pulses superimposed on a linear potential ramp [19]. Square wave voltammetry (SWV) is when a waveform of a symmetrical square wave is superimposed on a base staircase potential and applied to the working electrode [19].

Stripping voltammetry, and more specifically, anodic stripping voltammetry (ASV) is based on a two-step process. The first step is a pre-concentration or electrodeposition of the heavy metal at the electrode surface through the reduction of the metal ions. The second step is the stripping step, where the metal is oxidized back to give the ion. Having taken the 2 steps into consideration, several factors are known to influence the analysis, such as electrode material, deposition potential, deposition time [20] … When the preconcentration step is non-electrolytic, the analyte accumulates at the surface of the electrode by physical adsorption and a different method is obtained: Adsorptive Stripping Voltammetry (AdSV) [21]. Figure 1 summarizes how the potential is varied with time for CV, LSV, DPV, SWV and ASV to produce a signal.

A combination of some of these techniques results in increased sensitivities and limits of detection. The combinations include differential pulse anodic stripping voltammetry (DPASV), square wave anodic stripping voltammetry (SWASV) and linear sweep anodic stripping voltammetry (LSASV).

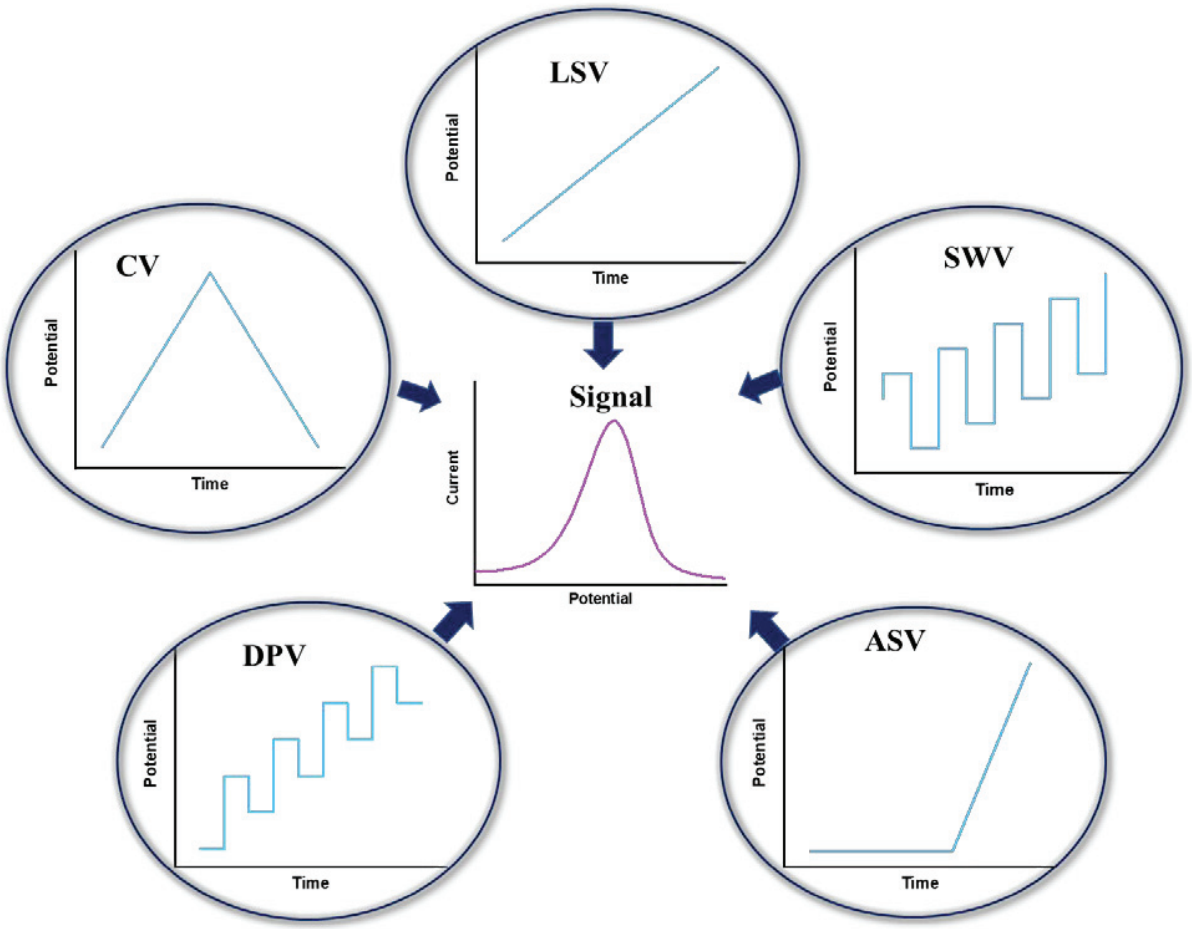

Figure 1: The graphs of potential vs time for some voltammetry techniques to produce a signal.

1.3. Metal Nanoparticles

Nanoparticles, specifically metal nanoparticles, present several advantages in the electrochemical sensing field. Due to their small sizes, nanoparticles can increase the surface area of the electrode being used. Moreover, metallic nanoparticles can increase the mass-transport rate and offer a fast electron transfer, both increasing the sensitivity of the used electrodes [16]. In this section, we will present the use of different types of metallic nanoparticles for the detection of the majority of heavy metals.

1.3.1. Silver Nanoparticles

Silver nanoparticles (Ag NPs) are one of the most well-developed nanoparticles because they are relatively inexpensive compared to noble metals and they have unique chemical and physical properties that make them useful in different catalytic, optical and chemical applications. Additionally, Ag NPs are stable with excellent catalytic activity and high conductivity. Silver nanoparticles have been combined with different materials for the detection of Cd^{2+}, Cr^{6+}, Cu^{2+}, Hg^{2+} and Sb^{3+}. Two different ways have been employed for the synthesis of spherical Ag NPs: reduction and electrodeposition. When the NPs were used along with graphene oxide, reduction of silver nitrate ($AgNO_3$) was employed, either hydrothermally to produce Ag NPs with an average size of 10 – 20 nm [22] or using hydrogen iodide HI as a reducing agent to yield Ag NPs with an average particle size of 9.7 nm [23]. The resultant nanoparticles in both reports were homogenously distributed on the reduced graphene oxide network. On the other hand, the electrodeposition of silver nanoparticles [24, 25] produced larger particles with sizes ranging between 30 and 50 nm.

Most recently, Cheng et al. synthesized reduced graphene oxide/silver nanoparticles composites for the simultaneous detection of several ions. Trace levels of Cu^{2+}, Cd^{2+} and Hg^{2+}, using cyclic voltammetry were detected with detection limits of 10^{-15} M, 10^{-21} M and 10^{-29} M respectively [22]. Although reporting exceptionally low LODs not reported elsewhere, specifically for mercury, the detection mechanism is different in all other papers such that it relies on the area of the entirety of the CV curve instead of using that of a peak. Moreover, the paper lacks important data on the analytical performance such as the linear range, sensitivity and reproducibility. Han et al. also used silver nanoparticles with reduced graphene oxide to detect Hg^{2+} ions by differential square wave anodic stripping voltammetry. The synthesized nanoparticles were spherical and uniformly distributed on the graphene sheet. The signal and analytical performance were compared with and without the nanoparticles, and it was shown that the presence of nanoparticles enhanced the signal significantly (figure 2). A linear concentration range was obtained between 0.1 and 1.8 μM, the limit of detection was calculated to be 0.11 μM and the sensitivity was 8 μA/μM. Moreover, no interferences were detected from Cd (II) and Cu (II) [23].

Xing et al. modified a glassy carbon electrode with Nafion and electrodeposited silver nanoparticles on its surface for the direct detection of Cr (VI) using linear sweep voltammetry. A

linear range was obtained between 2 and 230 ppb and the limit of detection was 0.67 ppb with no interference from different ions. The applicability of this sensor was studied using wastewater from a textile factory and the concentration of Cr (VI) was found to be 6.58 ± 0.04 µg/L with a recovery of 99 ± 5% for spiked samples [24]. Renedo and Arcos Martinez also conducted a study using silver nanoparticles modified screen printed electrodes for the detection of Sb by anodic stripping voltammetry. Differential pulse anodic stripping voltammetry was used and the linear concentration range was between 9.9×10^{-8} M and 9.09×10^{-7} M, whereas the LOD in case of silver nanoparticles was 6.79×10^{-10} M. Three different seawater samples were analyzed, and the amount of Sb (III) in all cases was below the detection limit and hence was not detected [25].

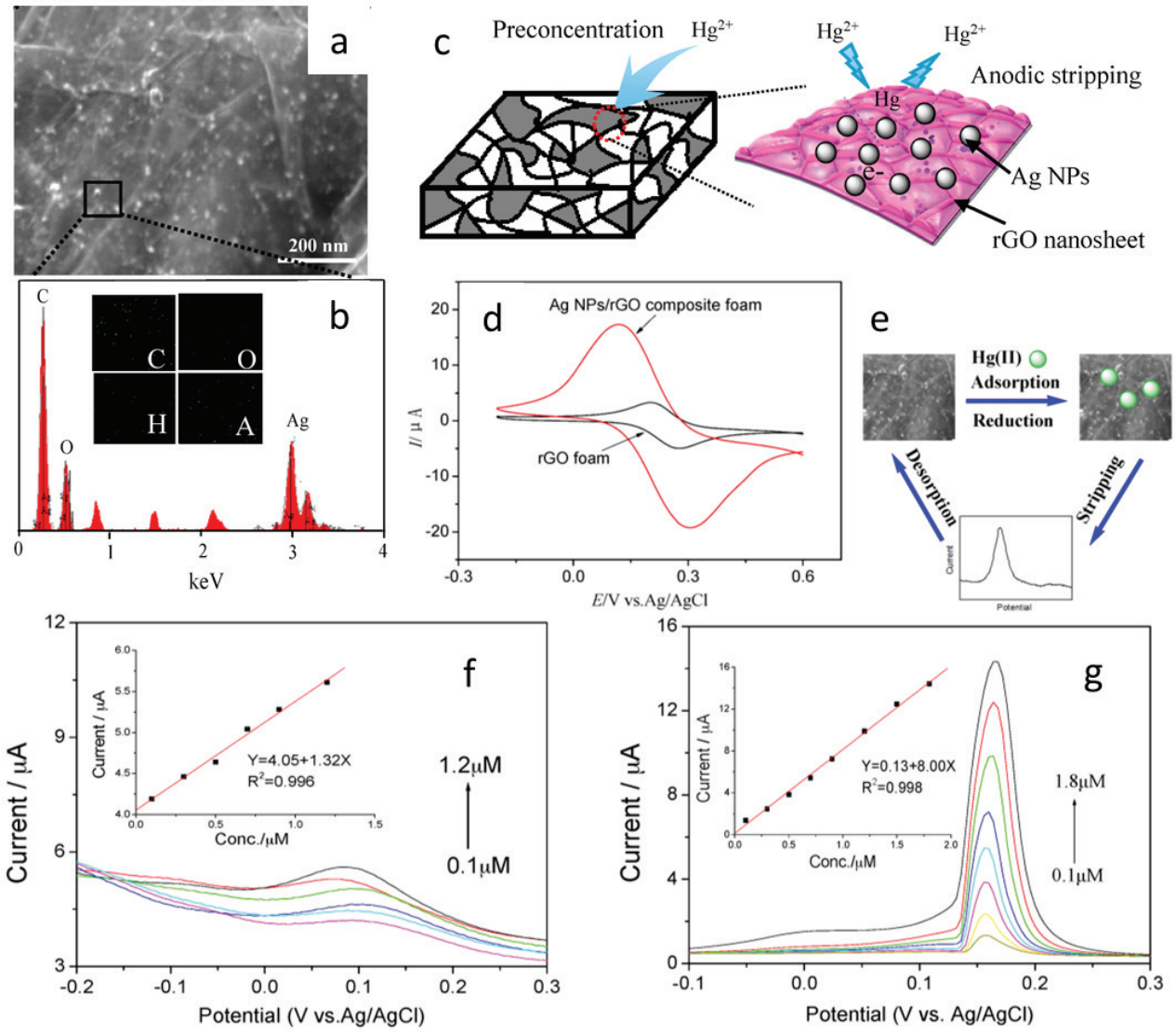

Figure 2: (a) Scanning electron microscopy (SEM) image and (b) energy dispersive spectroscopy (EDS) spectrum with elemental mapping of Ag NPs/reduced graphene oxide. (c) Schematic diagram of the Ag NPs/reduced graphene oxide structure. (d) Cyclic voltammetry of pure reduced graphene oxide and Ag NPs/reduced graphene oxide. (e) Schematic representation of the electrochemical detection towards Hg (II) ions. (f) and (g) SWASV response of pure reduced graphene oxide and Ag NPs/reduced graphene oxide towards Hg (II) at different concentrations in a 0.1 M NH_3 solution; the insets correspond to the calibration plots, respectively [23].

1.3.2. Gold Nanoparticles

The most used nanoparticles for the electrochemical detection of heavy metals are gold nanoparticles (Au NPs). Their properties vary depending on their size, but whatever the size, gold nanoparticles are known to be biocompatible and of low toxicity [26]. In addition to their high conductivity, Au NPs have a narrow size distribution that makes them good electrode modifiers. Table 2 summarizes the different voltammetric studies done to detect heavy metals using gold nanoparticles. Although Au NPs have enhanced the analytical performance of several sensors, only a few reports focus on the use of gold nanoparticles alone; nonetheless, different materials have been associated with gold nanoparticles for the detection of heavy metals, and especially mercury and lead.

Similar to Ag NPs, the most common methods utilized for the synthesis of Au NPs are either electrodeposition or reduction. However, different synthesis conditions lead to different shapes and sizes of the gold nanoparticles. The most common shape used in the electrochemical detection of heavy metals is spherical. Most groups have successfully synthesized spherical Au NPs of sizes ranging between 4 and 298 nm. Hassan et al. reported the synthesis and use of different gold nanostructures for the detection of As (III). The synthesis involved the reduction of chloroauric acid using ibuprofen in a basic medium. They investigated the effect of different heating times on the shape of the produced nanoparticles, and the results indicated that with increased heating time, nanoflowers formed along with other structures [27]. Ouyang et al. used a more complex method for the synthesis of nanoflowers. In brief, they modified a glassy carbon electrode with a layer of gold nanoparticles, followed by a layer of 3-mercaptopropyl-trimethoxysilane. Then, the electrode was immersed in a solution containing Au NPs to form a

second layer of nanoparticles and pyridinium was attached to the NPs after dipping in 4-pyridineethanethiol hydrochloride solution [28]. Dutta et al. synthesized gold nanostars and spherical gold nanoparticles and compared their performances in the detection of As (III), Hg (II) and Pb (II). The nanostars were prepared by mixing an auric chloride solution with 4-(2-hydroxyethyl)-l-piperazineethanesulfonic acid (HEPES) without stirring or shaking. Boiling the resultant nanostars for 5 minutes yielded spherical nanoparticles. Using these 2 structures, they modified a screen-printed electrode and optimized some conditions to conclude that the gold nanostar shape improved the detection of arsenic compared to the spherical shape (figure 3) [29]. Later on, different studies used the same procedure for the gold nanostars synthesis to detect Cr (II), Cd (II), As (III) and Se (IV) [30, 31].

It is worthy to note that the use of gold nanoparticles associated with different modifiers is gaining wide recognition. Even though the inhibition of enzymatic activity by heavy metals has been extensively studied, only one study uses enzyme-based biosensors with gold nanoparticles to detect mercury ions. The presence of gold nanoparticles considerably increased the analytical response [32]. Some researchers focus on the use of gold nanoparticles with amino acid-based biosensors. Amino acids and peptides (amino acid chains) have a high affinity towards some heavy metals which can be tuned by altering the peptide sequence [33]. Amino acids are known to bind heavy metal ions through cooperative metal-ligand interactions [34]. The use of gold nanoparticles with these biosensors amplifies the signal, improving the analytical performance [35]. The majority of authors focus on DNA-based biosensors with an emphasis on certain interactions between the DNA bases and certain heavy metal ions. Specifically, silver ion and mercury ion are well known to interact with cytosine-cytosine mismatch and thymine-thymine mismatch, respectively, to form stable base pairs [36 – 40].

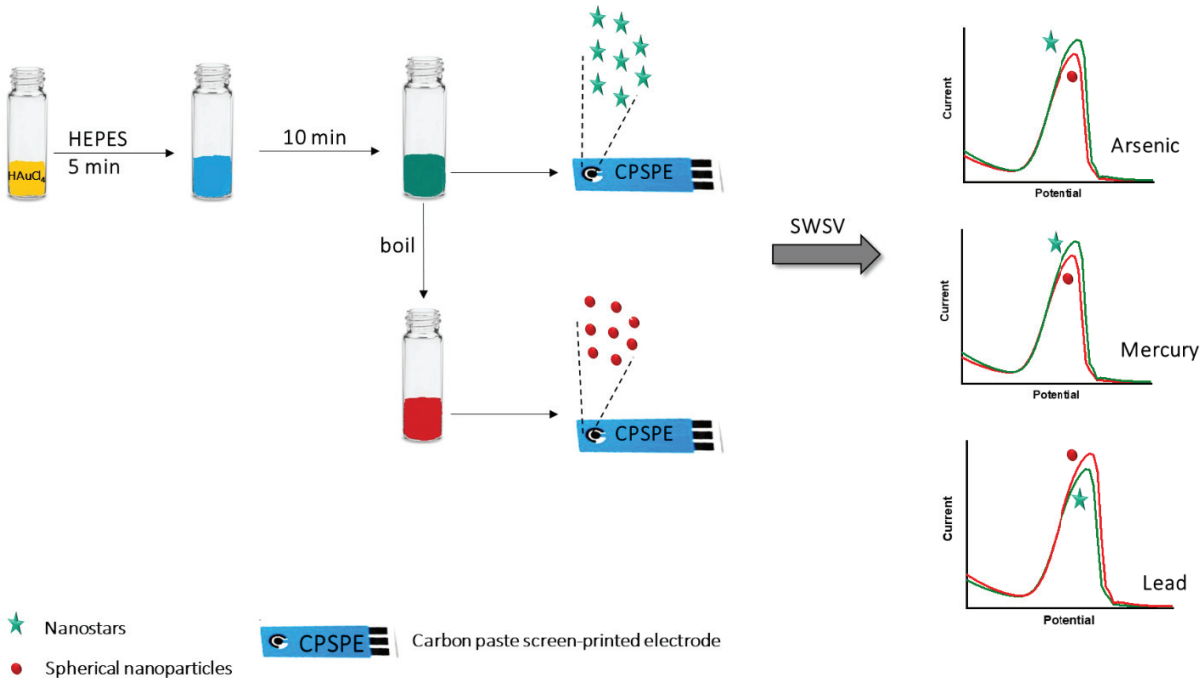

Figure 3: Modification of carbon paste screen-printed electrodes by Au NPs for the detection of As^{3+}, Hg^{2+} and Pb^{2+} [29].

Table 2: Comparison between the different studies using gold nanoparticles for heavy metal detection.

HM	Technique	Electrode	LOD (µM)	Sensitivity (µA/µM)	Linear range (µM)	Addition to Au NPs	Real sample	Ref
Ag^{+}	DPV	Au	3×10^{-5}	124.6	10^{-4} – 0.12	Oligonucleotide sequences		36
As^{3+}	SWV	GCE	10^{-3}	71.7			River water	41
	SWV	GCE	8.89×10^{-4}	1985		Multiwalled Carbon nanotubes		42
	ASV	CµF	67.43	1318	0.067 – 0.8		Tap, well water	43
	SWASV	GNEE	1.78×10^{-4}	0.7492	0 – 0.2	3-(mercaptopropyl)trimethoxy silane		44
	SWASV	SPE	6.53×10^{-3}				River water	31
	SWASV	GCE	1.06×10^{-3}	113.9	0.01 – 0.67			45
	SWASV	SPE	0.01		0.03 – 10.2		Ground water	29

	LSV	GCE	0.024		0 – 1.2			47
	LSV	GCE	5.34×10^{-3}	32.8		Multiwalled Carbon nanotubes		42
	LSV	GCE	2×10^{-3}	14.2			River water	41
	LSASV	GCME	0.01		0.01 – 10.01	Carbon nanotube		48
	LSASV	GCE	3.7×10^{-3}	940	0.005 – 3	Pt NPs	Tap, spring, river water	49
	LSASV	GCE	2.9×10^{-3}	230	0.005 – 1	Porous graphitic carbon nitride	Tap, spring, river water	50
	DPV	GCE	0.2	0.8075	4 – 40	Crystal violet	Drinking water	51
	DPSV	SPCE	8.01×10^{-4}		Up to 53.4	Poly(L-lactide)	Ground, surface water	52
	CV	Basal-plane pyrolytic praphite	0.8			Glassy carbon microsphere		53
	CV	SPCE	2.4×10^{-4}		1.3×10^{-3} – 24	Ibuprofen	Drinking, tap, river, ground water	27
Cd^{2+}	DPV	SPCE	0.023	26.19	0.07 – 4448		River, tap water	54
	DPV	GCE	0.022		0.05 – 300	Reduced graphene oxide, Tetraphenylporphyrin	Lake water	55
	DPASV	GCE	0.3	3.24	0 – 1.4			56
	SWV	GCE	8.89×10^{-4}		4.4×10^{-3} – 0.35	Graphene, cysteine	Spring water	35
	SWASV	GCE	0.1	1.88	0.1 – 1	Carbon nanofibers		57
	SWASV	SPE	0.015				River water	31
	SWASV	GCE	6×10^{-5}	2.2×10^{3}	10^{-3} – 0.01	L-cysteine, reduced graphene oxide	Lake, tap, sewage, ground water	58
Cr^{3+}	SWV	GCE			100 – 400			59
Cr^{6+}	SWV	SPE	0.096		0.19 – 96		River water	60
	SWV	GCE	1.92×10^{-4}	5.98	2.5×10^{-3} – 0.86		Sewage, tap water	61
	SWCSV	GCE	5.58×10^{-5}		1.9×10^{-4} – 23	3-mercaptopropyl-		28

						trimethoxysilane		
	AdSV	Graphene	0.02	1.94×10^{-4}	0.48 – 5.77	Reduced graphene oxide, 4-pyridylethylmercaptan hydrochloride	Waste water	73
	DPV	SPCE	0.4	2.01×10^{-8}	0.4 – 30		Tap, sea water	74
	CV	Indium tin oxide	2	0.3025	5 – 100		Tap, sea, stream water	75
	LSV	SPE	0.067		0.19 - 1442		Ground water	30
	LSV	SPCE	0.1	0.0572	0.38 – 3.8		River water	76
Cu^{2+}	DPV	SPCE	0.126		0.79 – 157	L-cysteine		33
	DPASV	GCE	0.3	4.18	0 – 1.4			56
	ASV	GCE	5×10^{-5}	3690	Logarithmic	Graphene quantum dots, cysteamine		68
	SWV	Au	10^{-7}	0.29435×10^{-6}	10^{-4} – 10	4-aminothiophenol, DNAzymes	Lake, tap water	37
	SWASV	SPE	0.025	4.368	0.31 – 4.72			70
	SWASV	GNEE	2.22×10^{-3}		6.67×10^{-3}– 0.2	3-(mercaptopropyl)trimethoxy silane		44
	SWASV	GCE	0.1	4.41	0.1 – 1	Carbon nanofibers		57
Hg^{2+}	SWASV	GNEE	9.97×10^{-5}	2.006	0 – 0.07	3-(mercaptopropyl)trimethoxy silane		44
	SWASV	SPE	2.49×10^{-3}		7.5×10^{-3} – 2.69		Ground water	29
	SWASV	GCE	2.99×10^{-5}	708.3 7.37	3.99×10^{-5} – 2.49×10^{-4} 4.98×10^{-4} – 0.3	Chitosan graphene	River water	77
	SWASV	SPCE	3.99×10^{-3}		2.49×10^{-5}– 10^{-4}		Rain, river water	78
	SWASV	GCE	4.2×10^{-4}	1370	0.64×10^{-3}– 4×10^{-3}			79
	SWASV	Pencil graphite	4×10^{-15}		10^{-13} –10^{-4}	DNA, L-methionine	Sea water, fish	80
	SWV	Au	5×10^{-4}		0.09-1.99	MSO, linker probes		81
	SWV	Carbon ionic liquid	2.3×10^{-3}		0.01 – 20	Thiolated amino acids	Waste, tap water	34
	SWV	SPE	9.97×10^{-4}	47.54	2.5×10^{-3} – 0.25	Carbon nanotubes	Tap, river water	71

	DPV	GCE	3×10^{-5}	35.88	10^{-4} – 0.02	Multi-walled C nanotubes, DNA	Tap, lake water	39
	DPV	GCE	7.48×10^{-6}	1603.6	4.98×10^{-5} – 4.98×10^{-3}	Reduced graphene oxide, thymine-1-acetic acid, cysteamine	Tap water	62
	DPV	Au	5×10^{-4}		10^{-3} – 0.1	DNA, methylene blue	Tap, river water	38
	DPV	Indium tin oxide	7.8×10^{-4}		5×10^{-3} – 0.11	Graphene oxide, 5-methyl-2-thiouracil	Tap, lake, bottled water	63
	DPV	Au	7.38×10^{-6}	333	5×10^{-5} – 2.5×10^{-3}	Thiolated probe DNA	Tap water	40
	DPASV	GCE	8×10^{-5}	749	4×10^{-4} – 0.096	Single walled C nanotubes, poly(2-mercaptobenzothiazole)	River, tap water	65
	DPASV	GCE	0.3	3.39	0 – 1.4			56
	DPASV	GCE	10^{-4}	0.09	5×10^{-4} – 1.25	Carbon nanotubes		82
	DPASV	Indium tin oxide	1.49×10^{-4}		4.98×10^{-4} – 0.05		Tap, lake water, milk, soil	66
	ASV	GCE	0.16		0.79 – 3.15		River water	77
	ASV	GCE	7.48×10^{-7}		Up to 0.25		Drinking water	67
	ASV	GCE	2×10^{-5}	2470	2×10^{-5} – 0.1	Graphene quantum dots, cysteamine		68
	CV	Au	0.01			MSO, ss-DNA		69
Pb^{2+}	SWASV	GCE	4×10^{-5}	3.2×10^{3}	10^{-3} – 0.01	L-cysteine, reduced graphene oxide	Lake, tap, sewage, ground water	58
	SWASV	SPE	0.02		0.06 – 1.56		Ground water	29
	SWASV	SPE	0.0106	31.91	0.096 – 0.96			70
	SWASV	GCE	0.1	19.08	0.1 – 1	Carbon nanofibers		57
	SWV	SPE	4.34×10^{-4}	17.612	0.01 – 1.2		Tap, river water	71
	SWV	GCE	2.4×10^{-4}		2.41×10^{-3} – 0.19	Graphene, cysteine	Spring water	72
	SWV	GCE	800	455.83	0.01 – 0.15	Graphene oxide	Tap water	83
	CV	Au	2.8×10^{-5}			DNA		32
	DPASV	GCE	0.3	17.63	0 – 1.4			56

	DPASV	CGE	4.83×10^{-5}	24.86	2.41×10^{-3} – 0.48	Graphene oxide, chitosan	River water	84
	DPV	Au	10^{-3}		5×10^{-3} – 0.1	DNAzymes		64
	DPV	GCE	4.3×10^{-9}		10^{-8} – 5×10^{-5}	Multi-walled carbon nanotubes, DNA	Tap, river, spring water	85
Sb^{3+}	DPASV	SPE	9.44×10^{-4}		9.9×10^{-2} – 0.909		Sea water, drugs	86
Se^{4+}	SWASV	SPE	0.01				River water	31

Abbreviations: Au gold, GCE glassy carbon electrode, CμF carbon ultra-microfiber, GNEE gold nanoelectrode ensembles, SPE screen printed electrode, GCME carbon nanotube flow-through membrane electrode, SPCE screen printed carbon electrode.

From the above table, it can be concluded that the best analytical performance for the detection of As (III) is obtained using gold nanoparticles modified carbon nanotubes [42]. The process of electrode modification and arsenic detection using square wave voltammetry can be achieved within minutes producing a very high sensitivity and low LOD compared to similar studies presented in the table. Although the authors claim that this sensor can be used for the detection of arsenic in natural waters, to the best of our knowledge, this study has not been conducted. The modification of a glassy carbon electrode with gold nanoparticles, L-cysteine and reduced graphene oxide showed a superior performance in the detection of Cd (II) by square wave voltammetry (figure 4). The modified electrode was used to assess the concentrations of cadmium in different water sources (lake, sewage, tap and ground water) and the obtained results were comparable with those of AAS [58]. The same electrode exhibited the highest reported sensitivity for the detection of Pb (II) as well; however, a better LOD was obtained by Zhu et al. [85] using differential pulse voltammetry. The latter team modified a glassy carbon electrode with gold nanoparticles, cysteine, graphene and bismuth film which exhibited a low LOD and good repeatability and reproducibility along with its possible usage in real water samples such as spring water. However, the preparation procedure was too complex compared with other studies. The modification of a GCE with graphene quantum dots and Au NPs is the method of choice for the detection of Cu (II) using anodic stripping voltammetry. Both the LOD and sensitivity are better than those obtained with different modifications, unfortunately the electrode was not tested with real samples [68]. This same electrode showed the highest sensitivity for the detection of Hg (II), while an outstanding LOD was obtained by Hasanjani and Zarei [80] who used DNA and L-methionine along with Au NPs for the modification of a pencil graphite electrode.

Interestingly, for the detection of Cr (VI), the sensitivities are either not reported, or are very small, with the best limit of detection obtained by Ouyang et al. [28] who modified a glassy carbon electrode with Au NPs and 3-mercaptopropyltrimethoxysilane.

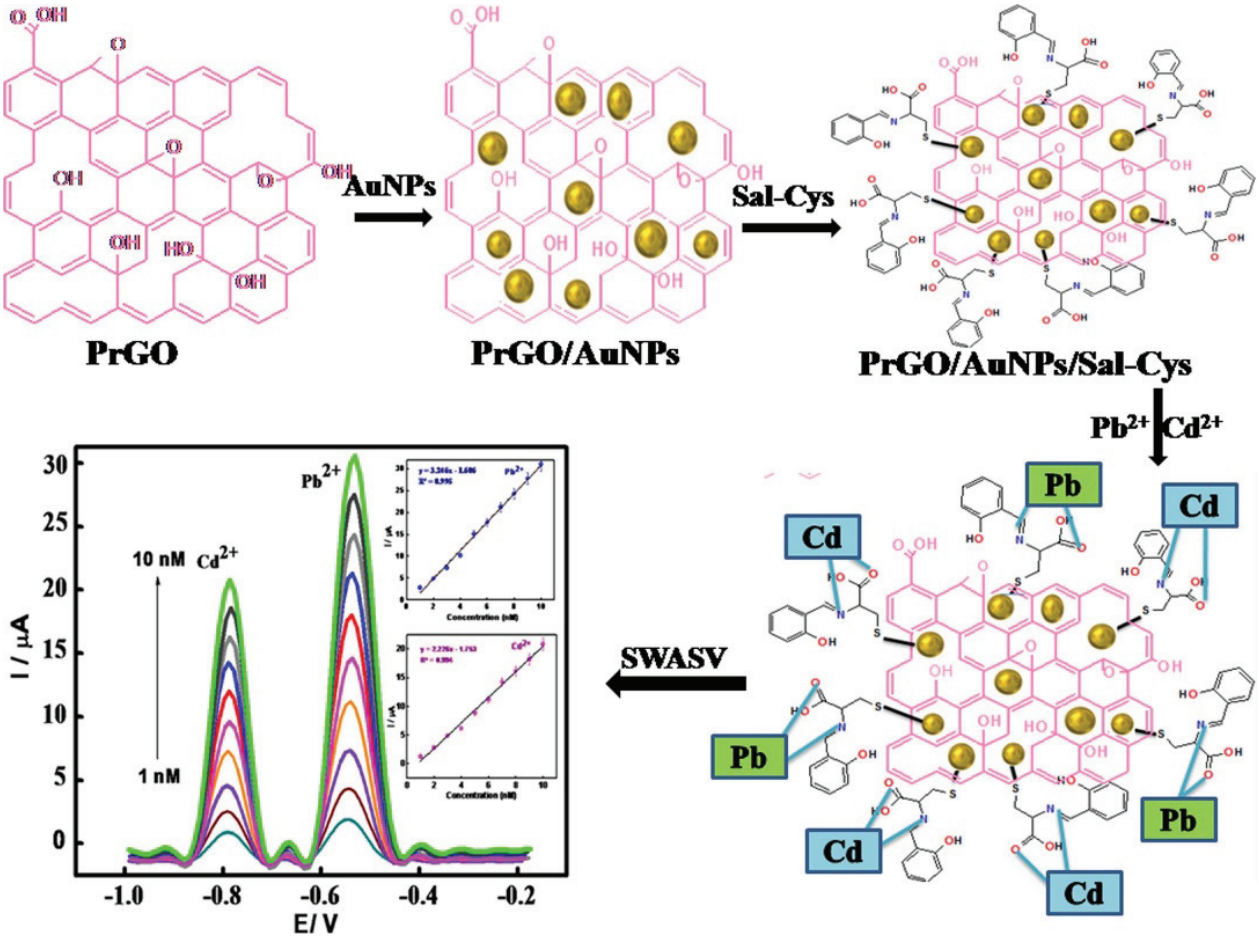

Figure 4: Schematic diagram of the possible interactions of Cd (II) and Pb (II) with gold nanoparticles, L-cysteine and reduced graphene oxide modified GCE electrode leading to the simultaneous analysis of the heavy metals [58]. Reproduced with permission from Elsevier

1.3.3. Bismuth Nanoparticles

The use of bismuth in different areas of chemistry (catalysis, organic synthesis, clusters…) has grown in the past decade. In electroanalytical chemistry, bismuth is used as an electrode coating, replacing the mercury electrode, because of its low toxicity and excellent peak resolution. Bismuth nanoparticles have a high electrocatalytic activity, high surface free energy and good conductivity suitable for heavy metal sensing.

Lee et al. used bismuth nanopowder modified electrode to detect Zn, Cd and Pb ions using square wave anodic stripping voltammetry. Spherical bismuth was prepared with different particle size distribution in order to investigate its effect on the sensitivity and limit of detection of the studied metals. It was concluded that as the particle size decreases from 406 to 166 nm, both the sensitivity and the limit of detection are improved [87]. In another work, the same group modified a thick-film graphite electrode with bismuth nanopowder for the detection of thallium (Tl). Applying the same procedure, a limit of detection of 0.03 μg/L was obtained with the possibility to overcome any interference from divalent ions through the addition of EDTA [88]. Rico et al. [89] adopted the method of Lee et al. [87], to modify a screen-printed carbon electrode and detect the heavy metals. Optimization of the method included the accumulation configuration; both convective and flow configurations were tested. The limits of detection that were obtained at the flow cell for Zn (II), Cd (II) and Pb (II) were better than those at the convective cell. Those limits were 2.6, 1.3 and 0.9 ng/mL, respectively. Moreover, the reproducibility and sensitivity of the method were good after analyzing a certified reference sample and tap water, but further tests showed that high concentrations of Cu (II) interfered with the results. Saturno et al. modified a glassy carbon electrode with micro-nanoparticles/bismuth film for the determination of cadmium and lead by differential pulse voltammetry. The shape and size of the nanoparticles were irregular, but they still obtained LODs of 11 μg/L for Cd (II) and 18 μg/L for Pb (II) with the response being highly reproducible [90]. Sahoo et al. modified a carbon paste electrode with graphene oxide and bismuth nanoparticles of diameter between 40 and 100 nm for the determination of zinc, cadmium, lead and copper ions using differential pulse anodic stripping voltammetry. A linear concentration range was obtained from 20 to 120 μg/L with limits of detection of 2.8, 0.55, 17 and 26 μg/L for Cd^{2+}, Pb^{2+}, Zn^{2+} and Cu^{2+}, respectively. The performance of the electrode was tested in two different water samples, ground and lake water, and the concentrations of the divalent metals were determined [91]. The obtained LODs were comparable in the different studies for lead and cadmium ions. However, the problem of Cu (II) interference was faced in more than one study.

1.3.4. Platinum Nanoparticles

Platinum metal has received a lot of attention in the catalysis industry. Platinum nanoparticles (Pt NPs) have also found a lot of applications in electrochemical analyses due to

their stability and conductivity [92]. Hrapovic and Luong electrodeposited spherical platinum nanoparticles on a glassy carbon electrode and on a boron doped diamond electrode for the detection of Arsenite (As (III)). The electrodeposition resulted in a non-homogenous and non-uniform distribution of the Pt NPs. Using linear sweep voltammetry, the boron-doped electrode was proven to have a superior performance with a limit of detection of 0.5 ppb without interference from copper (II) ions. Moreover, the analysis of drinking water and river water from Montreal confirmed that As (III) concentrations can be determined without any interference [93]. Spherical platinum nanoparticles of diameters between 105 and 180 nm were also electrodeposited on a glassy carbon electrode by Dai and Compton for the detection of Arsenic (III) ions. Cyclic voltammetry was applied and the measured limit of detection was 35 ppb. The performance of this electrode was compared using different techniques (square wave voltammetry and differential pulse voltammetry) all giving the same results. Moreover, possible interfering ions were investigated and the results still showed a clear peak for arsenic [94]. Both studies rely on the oxidation of As (III) to As (V) electrocatalyzed by Pt on a BDD electrode. Dai and Compton obtained a LOD that is higher than recommended guidelines for water. Moreover, even though Hrapovic and Luong obtained a lower LOD, the electrodeposited Pt NPs were not uniform in size.

1.3.5. Other metal nanoparticles

Owing to the advantages of nanoparticles in the modification of electrodes in electrochemical analysis, different metal nanoparticles have been used for the electrochemical detection of cadmium, copper, mercury and lead.

Palladium nanoparticles (Pd NPs) have unique mechanical properties along with excellent electrocatalytic activity important for electrochemical sensing. Two groups have reported the use of Pd NPs for the detection of heavy metals. Both groups synthesized porous activated carbon (PAC), followed by the decoration of PAC with palladium nanoparticles via a one-step thermal reduction method (with slightly different conditions). Spherical 20 – 30 nm Pd NPs were used by Zhang et al. for the simultaneous and individual determination of Cd^{2+}, Pb^{2+} and Cu^{2+} by applying square wave anodic stripping voltammetry (figure 5). The obtained limits of detection for individual determinations were 13.33, 6.6 and 11.92 nM for Cd^{2+}, Pb^{2+} and Cu^{2+}, while for simultaneous determinations the values were 20.9, 9.19 and 14.78 nM, respectively.

The applicability of the sensor was successfully tested in practical water, without specifying what this water is. [95]. Veerakumar et al. were able to obtain smaller crystals with an average size of 4 – 5 nm. They used differential pulse voltammetry for the detection of Cd^{2+}, Pb^{2+}, Cu^{2+} and Hg^{2+}. Results showed superior performance for both individual and simultaneous detections. For simultaneous detection of Cd^{2+}, Pb^{2+}, Cu^{2+} and Hg^{2+}, a linear response in the ion concentration ranges of 0.5 − 5.5, 0.5 − 8.9, 0.5 − 5.0 and 0.24 − 7.5 μM, with sensitivities of 66.7, 53.8, 41.1 and 50.3 μA $\mu M^{-1}.cm^{-2}$, and detection limits of 41, 50, 66 and 54 nM, respectively, were observed [96].

Lee et al. have used tin nanoparticles (Sn NPs) with reduced graphene oxide on glassy carbon electrode for the determination of Cd^{2+}, Pb^{2+} and Cu^{2+}. The Sn NPs of 50 nm diameter were synthesized using the electrochemical reduction of Sn^{2+} with graphene oxide solution. Individual analysis of metal ions using square wave anodic stripping voltammetry showed a high stability and detection limits of 0.63 nM, 0.60 nM and 0.52 nM, respectively. A high sensitivity for all metals was reported and was explained by the high absorptive ability of the nanoparticles. However, simultaneous analysis of the heavy metals increased the detection limits to 7.56 nM, 6.77 nM and 5.62 nM, respectively due to the possible formation of intermetallic compounds. The feasibility of the sensor was tested in tap water samples with and without spiking. No peaks were observed before spiking, while recoveries ranged between 97 and 102% after spiking [97].

Toghill et al. used an interesting and unsafe approach for the detection of cadmium and lead. They modified a BDD electrode with Sb nanoparticles for the detection of Cd^{2+} and Pb^{2+} using linear sweep anodic stripping voltammetry. The nanoparticles were electrochemically deposited on the electrode, with an average size of 108 ± 70 nm, but due to the toxicity of Sb, the team tried to use the smallest possible concentration of antimony. Based on this study, the addition of Sb nanoparticles did not improve the individual detection of each analyte as compared to the bare BDD. On the other hand, simultaneous detection of cadmium and lead was improved and Pb did not inhibit Cd from nucleating on the electrode surface like previous works [98].

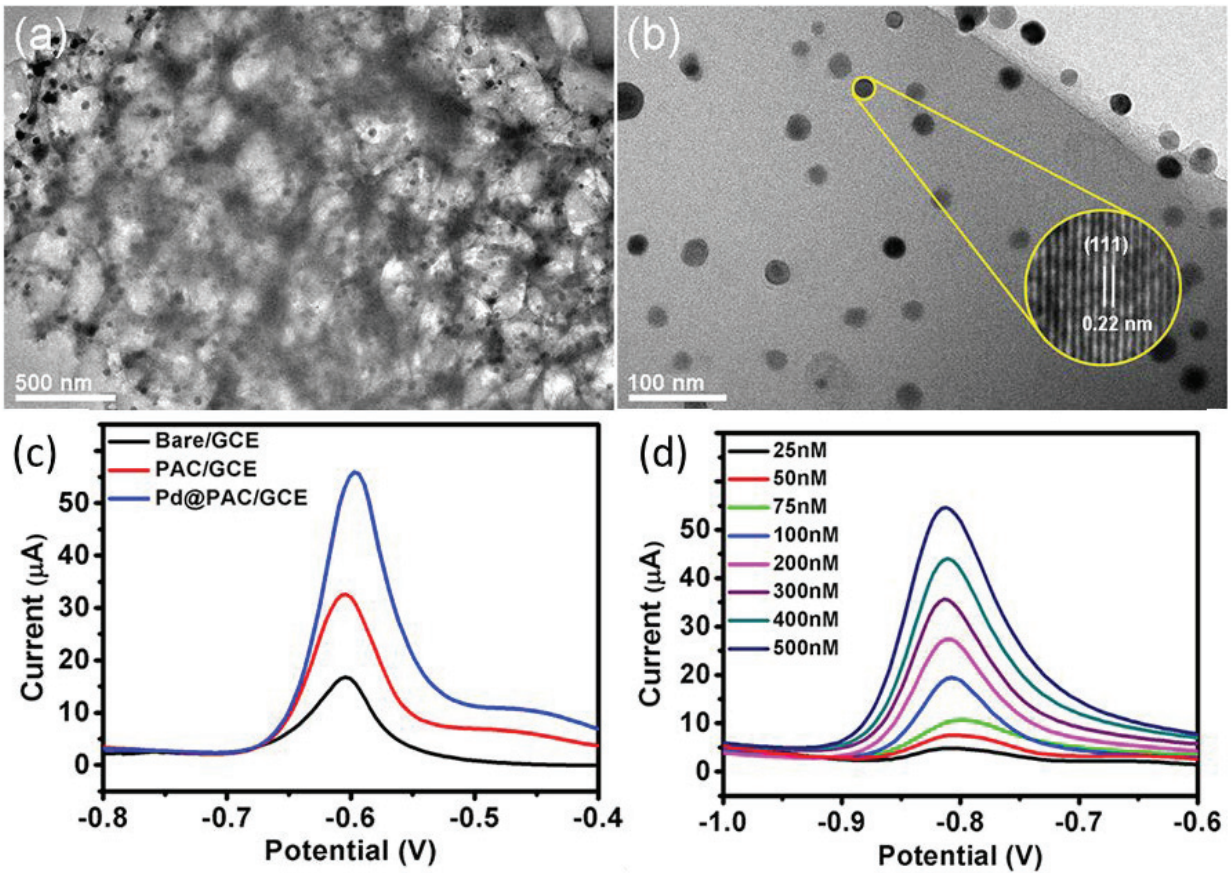

Figure 5: (a) and (b) TEM and HR-TEM images of Pd@Pac. (c) SWASV curves for 500 nM each of Cd^{2+}, Pb^{2+} and Cu^{2+} on the bare, PAC-modified and Pd@PAC-modified GCEs in 0.1 M acetate buffer solution (pH 4.8). Conditions: deposition potential: 2.1 V; deposition time: 210 s; room temperature; amplitude: 50 mV; increment potential: 4 mV; and frequency: 15 Hz. (d) SWASV curves of the Pd@PAC/GCE for the individual analysis of Cd^{2+} [95]. Reproduced with permission from Elsevier

1.4. Metal oxide nanoparticles

Metal oxide nanoparticles are being extensively studied in electrochemical detection these past few years. They have been synthesized using different methods to obtain different sizes, stability, and morphology. These differences allow them to exhibit various electrical and photochemical properties resulting in different applications [99]. Various oxides of metals, mainly transition metals, have been used in the modification of electrodes for the detection of

different analytes including heavy metals. Even though these oxides have been synthesized using almost all transition metals, only a few were used for the detection of heavy metals.

1.4.1. Iron oxide Nanoparticles

The most common metal oxide used for the detection of heavy metals is iron oxide in different forms ($MnFe_2O_4$, Fe_2O_3 and Fe_3O_4). While iron in the first 2 species is found as Fe^{3+}, both Fe^{2+} and Fe^{3+} are present in Fe_3O_4, which permits an electron hopping process between the 2 ions, and thus increasing the electrical conductivity compared to $MnFe_2O_4$ and Fe_2O_3.

Lee et al. were the first group to report the use of iron oxide in the form of Fe_2O_3. Briefly, graphene oxide was prepared and reduced, after which Fe_2O_3/graphene composites were prepared using a solvent-less method by mixing iron (III) acetylacetonate and oleic acid with the prepared graphene. The synthesized spherical maghemite nanoparticles had an average size of 30 nm and uniformly decorated the graphene sheets. Prior to be used in the detection of Pb^{2+}, Zn^{2+} and Cd^{2+} in tap water, the nanoparticles with graphene oxide were deposited on a cleaned glassy carbon electrode and dried under infrared heat lamp, and the electrode was modified with bismuth. Differential pulse anodic stripping voltammetry was applied and the analysis showed a linear range of detection between 1 and 100 $\mu g.L^{-1}$ for all the ions, and limits of detection of 0.11 $\mu g.L^{-1}$ for Zn (II), 0.08 $\mu g.L^{-1}$ for Cd (II) and 0.07 $\mu g.L^{-1}$ for Pb (II) [100]. Li et al. later reported the synthesis of 2 different morphologies (nanorods and nanocubes) of Fe_2O_3 for the electroanalysis of Pb (II) by anodic stripping voltammetry. The limit of detection of Pb (II) by nanorods was much smaller (0.0034 µM) than that with nanocubes (0.083 µM). Moreover, Fe_2O_3 nanorods proved to be much more sensitive (109.67 $\mu A.\mu M^{-1}$) compared to nanocubes (17.68 $\mu A.\mu M^{-1}$). The practicability of the proposed sensor was evaluated in drinking water, and good recoveries were observed with a slightly decreased sensitivity for lead that could be the result of interfering ions [101].

On the other hand, Fe_3O_4 is the most common form of iron oxide used to detect heavy metals. Most recently, Fe_3O_4 nanoparticles have been investigated for heavy metal detection. Fe_3O_4 is known for having a high affinity for heavy metal ions, but only a few reports that use iron oxide alone are available. This is due to the fact that iron oxide nanoparticles have the tendency to aggregate and become non-conductive units [102]. Most studies use either functionalized Fe_3O_4 or Fe_3O_4 combined with other materials. Table 3 summarizes the different studies done using Fe_3O_4 to detect heavy metals. Most of the magnetic nanoparticles used in

heavy metal detection were spherical or quasi-spherical with sizes ranging between 5.8 nm and 200 nm. Sun el al. synthesized different Fe_3O_4 shapes by varying the ratio of Fe^{2+} to Fe^{3+} ions. They used a one-step coprecipitation method with the following molar ratios of Fe^{2+}/Fe^{3+}: 2/5 to obtain spherical nanoparticles, 4/0 to get rod Fe_3O_4 (20 – 50 nm in width and 200 – 300 nm in length) and 5/4 to obtain band Fe_3O_4 (80 – 120 nm in width and 300 – 400 nm in length) (Figure 6). Along with reduced graphene oxide, the iron oxide nanoparticles were used for the detection of Pb (II) and it was shown that the sensitivity is best with the band nanoparticles followed by spherical nanoparticles and then rod nanoparticles (the results are shown in decreasing order in Table 3). On the other hand, the limit of detection did not differ much between the three structures. Band NPs were also used for the detection of Cu (II) and Cd (II) [103].

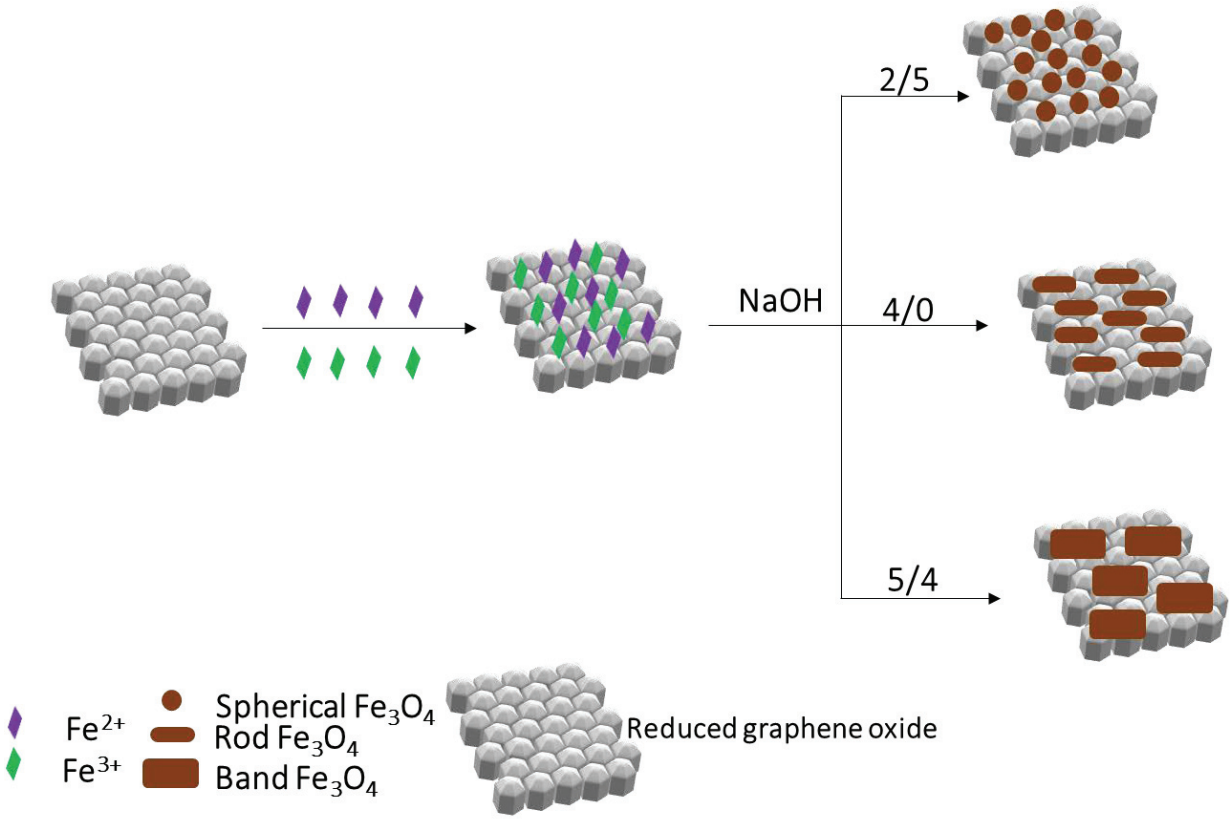

Figure 6: Synthesis of Fe_3O_4 nanoparticles, nanorods and nanobands done by Sun et al. [103]

Table 3: Comparison between the different studies using Fe_3O_4 to detect heavy metals.

HM	Technique	Electrode	LOD (µM)	Sensitivity (µA/µM)	Linear range (µM)	Addition to iron oxide NPs	Real sample	Ref

Pb^{2+}	SWV	GCE	2.41×10^{-4}		0 – 0.24	DMSA	Urine	104
Ag^{+}	SWV	GCE	3.4×10^{-3}		0.01 – 0.15	Au NPs, DNA	Natural water, orange juice, wine	105
Hg^{2+}			1.7×10^{-3}		0.01 – 0.1			
As^{3+}	SWASV	GCE	1.29×10^{-4}	1015	1.33×10^{-3} – 0.27	Au NPs	Natural water	106
Pb^{2+}	SWASV	GCE	0.15	10.07	0.5 – 8	Amine	Waste water	107
Pb^{2+}	SWASV	GCE	1.4×10^{-5}	235	5×10^{-3} – 0.6	polydopamine	Aqueous effluent	108
Cd^{2+}			9.2×10^{-5}	196	0.02 – 0.59			
Cd^{2+}	SWASV	GCE	0.056	14.82	0 – 0.8	Reduced graphene oxide		109
Pb^{2+}	SWASV	GCE	0.17	13.6	0.4 – 1.5	Reduced graphene oxide		103
			0.073	7.4	0.7 – 1.2			
			0.033	2.4	0.8 – 1.2			
Cu^{2+}			0.05	10.1	0.5 – 1.5			
Cd^{2+}			0.04	4.35	0.4 – 1.1			
Cd^{2+}	SWASV	CPE	1.78×10^{-3}			Macrocyclic Schiff-base ligand	Carrot, fish, rice, different waters	117
Cu^{2+}			0.014					
Hg^{2+}			4.98×10^{-3}					
Pb^{2+}	SWASV	GCE	0.119	14.9	0.3 – 1.3		River water	110
Cd^{2+}			0.154	3.18	0.3 – 1.3			
Hg^{2+}			0.0839	7.67	1.3 – 1.8			
Cu^{2+}			0.0765	4.73	0.3 – 1.7			
Pb^{2+}	SWASV	GCE	0.0422	50.6	0.1 – 1.3	Chitosan	River water	111
Hg^{2+}			0.0957	9.65	0.4 – 1.1			
Cu^{2+}			0.0967	4.24	0.3 – 1.2			
Cd^{2+}			0.0392	8.11	1.2 – 1.7			
Cd^{2+}	SWASV	GCE	0.2	12.15	0.4 – 1.1	Terephthalic acid	River water	102
Pb^{2+}			0.04	8.56	0.4 – 1.1			
Hg^{2+}			0.3	13.81	0.4 – 1.1			
Cd^{2+}	SWASV	GCE	1.52×10^{-3}	8.4	4.4×10^{-3} – 0.89	Glutathione	Natural water	112
Pb^{2+}			8.78×10^{-4}	27.37	2.41×10^{-3} – 0.48			
Ni^{2+}	LSV	Pt	3.5×10^{-3}		5×10^{-2} – 1	Chitosan	Sewage water, urine	113
					3 – 100			
Cr^{6+}	LSV	SPCE	0.01		0.5 – 10	Au NPs, Sephadex G-150	Lake water	114
Ag^{+}	DPV	GCE	0.059		0.117 – 17.7	Au NPs	Lake, tap, synthesized water	115

Cu^{2+}	DPV	GCE	0.5×10^{-3}	Multi-walled carbon nanotubes, poly-3-nitroaniline	116

Abbreviations: CPE carbon paste electrode

Lead and cadmium are the most studied heavy metal ions with Fe_3O_4 NPs. The lowest LODs and highest sensitivities for both ions were detected by Song et al. who coated the magnetic nanoparticles with polydopamine and reported that the high sensitivity is due to the interaction between the magnetic nanoparticles and the electrode allowing the electrodeposition of heavy metals. Additionally, the proposed method that uses SWASV was applied for the determination of lead in aqueous effluents of a factory. The method proved to be successful and comparable with ICP-AES [108]. Moreover, it is worthy to note that square wave voltammetry and glassy carbon electrodes are most commonly used when working with Fe_3O_4 NPs.

Recent studies have reported that the addition of another metal to iron oxide to produce spinel ferrites can enhance its electrochemical behavior towards some heavy metals. All the groups relied on a solvothermal method for the synthesis of $MnFe_2O_4$ along with surface modifications when applicable. The ferrite nanoparticles prepared had a spherical morphology with sizes ranging between 200 and 400 nm.

In this regard, one group has done different studies on $MnFe_2O_4$ to detect different heavy metals. Zhou et al. successfully synthesized $MnFe_2O_4$ nanocrystals and used them to modify a gold electrode and detect As (III) using SWASV. A linear response was obtained at As concentrations between 10 and 100 ppb with a limit of detection of 1.95 ppb and a sensitivity of 0.295 μA/ppb. The sensor was successfully applied for the detection of arsenic in tap water with a recovery of 95.6% [118]. In another attempt to detect As (III), they modified a glassy carbon electrode with $MnFe_2O_4$ and gold nanoparticles. Using SWASV, the electrode showed a sensitivity of 0.315 μA/ppb and a LOD of 3.37 ppb with the sensor also being used to test tap water [119]. Then, the same group modified a glassy carbon electrode with these nanoparticles for the selective determination of Pb^{2+}. Using SWASV, a sensitivity of 19.9 $\mu A.\mu M^{-1}$ and LOD of 0.054 μM were obtained under optimized conditions, while the response to Cd^{2+}, Hg^{2+}, $Cu^{2+}$and Zn^{2+} was poor. The modified electrode was successfully used to detect a spiked lead concentration in river water [120].

In a later study, and in attempt to obtain a better analytical performance, Zhou et al. also used $MnFe_2O_4$ and graphene oxide to modify a glassy carbon electrode for the detection of Pb (II), Cd (II), Cu (II) and Hg (II). Using square wave anodic stripping voltammetry, the best electrochemical response was obtained for Pb (II) with a sensitivity of 33.9 mA/mM and a LOD of 0.0883 mM. The sensitivities for Cd (II), Cu (II) and Hg (II) were 13.5 mA/mM, 13 mA/mM and 5.79 mA/mM, respectively. Moreover, the limits of detection were calculated to be 0.778 mM, 0.0997 mM and 1.16 mM, respectively, with a successful application in the analysis of river water [121]. They also tried modifying a glassy carbon electrode with L-cysteine functionalized $MnFe_2O_4$ to detect Pb (II), Hg (II), Cu (II) and Cd (II) by SWASV. The developed sensor was particularly selective towards lead, with sensitivities of 57 μA/μM and 35.3 μA/μM and LODs of 0.0843 μM and 0.0607 μM under individual and simultaneous conditions of detection. The sensor was also successfully used to monitor the concentration of lead in river water [122]. Thus, all attempts to modify $MnFe_2O_4$ nanoparticles to detect different heavy metal ions have showed a higher selectivity and preference for Pb (II). Moreover, although all studies have checked the practicability of the different modified sensors in real water samples, more experimentation should be done in this regard by monitoring the ions in water samples other than tap and river water.

1.4.2. Other metal oxide nanoparticles

Co_3O_4 nanoparticles are one of the most versatile transition metal oxides mainly because of their high reactivity, superior stability and excellent electrocatalytic activity. Salimi et al. electrodeposited cobalt oxide nanoparticles on a glassy carbon electrode in order to detect Arsenic (III) using cyclic voltammetry. The nanoparticles were small in size (100 nm) and uniformly distributed on the surface of the electrode. The results exhibited a detection limit of 0.6 μM and no interferences in presence of other heavy metal ions with a linear range of 10 – 50 μM. The possibility to use this sensor for the analysis of water samples was tested on drinking water from a village in Kurdistan and a concentration of 2.1 μM of As was found in water and confirmed by atomic absorption spectrometry [123].

On the other hand, titanium oxide nanoparticles have attracted attention due to their biocompatibility, high conductivity, stability and low cost. TiO_2 nanoparticles were used to detect Hg (II) by Zhou et al. Titanium oxide nanoparticles were prepared using sol-gel process.

Briefly, tetrabutyl titanate was dissolved in ethanol and acetic acid, after which water was added dropwise with vigorous stirring until a white transparent sol was formed. The sol was transformed into a gel, dried and calcinated to obtain TiO_2 powder. The nanoparticles, along with gold nanoparticles, were used to modify a gold electrode with the help of chitosan as a binder. Characterization showed that TiO_2 nanoparticles had a size range between 5 and 15 nm, with gold nanoparticles on their surface. In a medium buffered at a pH of 5 and using differential pulse anodic stripping voltammetry, the sensor showed a wide linear concentration range of Hg (II) from 5 to 400 nM and a low detection limit of 1 nM with a sensitivity of 3.133 $\mu A.\mu M^{-1}$ and no interference from different ions. Moreover, the sensor was tested for Hg (II) in some water samples, and the recoveries were between 98 and 106% for all samples [124]. Zhang et al. used purchased titanium oxide nanoparticles to modify a gold strip electrode to detect As (III) by linear sweep voltammetry. The linear range of analysis was obtained between 10 µg/L and 80 µg/L with a limit of detection of 10 µg/L and the possibility to use it for arsenic determination in real samples. Moreover, the stability of the electrodes was investigated and 96% of the initial response current was retained after 15 days [125]. Mao et al. incorporated TiO_2 nanoparticles into multiwalled carbon nanotubes and a cationic surfactant to modify a glassy carbon electrode. LSASV was used for the determination of mercury (II) and a linear range of 0.1 – 100 µM with a limit of detection of 0.025 µM were obtained. The potential applicability of the sensor was evaluated in spiked and non-spiked samples of river and industrial wastewater, and the sensor was able to successfully detect mercury in the wastewater even before spiking [126]. Ramezani et al. constructed an electrochemical sensor using spherical TiO_2 nanoparticles intermixed with graphite powder and 1,2-bis-[o-aminophenyl thio] ethane. Using DPASV, and under optimum conditions, Cd (II) was detected in a linear concentration range of 2.9 nM – 4.6 µM with a limit of detection of 2 nM. A spiked concentration of Cd (II) ions in tap water was successfully detected without requiring any treatment of the water [127]. Liu et al used an Fe_3O_4-TiO_2 core-shell nanoparticles on a glassy carbon electrode for the detection of Pb (II). Using square wave voltammetry (SWV), the limit of detection of the proposed sensor was calculated to be 7.5×10^{-13} M with a linear range of 4×10^{-13} M – 2.5×10^{-8} M. Different concentrations of Pb (II) were evaluated in river and rain water samples with recoveries ranging between 99 and 110% [128]. Each one of these modifications with TiO_2 NPs presents its advantages, from outstanding limit of detection of 7.5×10^{-13} M for Pb (II) [128] to the wide linear range of detection of 2.9 nM – 4.6

μM for Cd (II) [127]; nevertheless, more experimentation is required in order to be able to compare between the different methods.

Different forms of manganese oxide nanoparticles have been explored due to properties like low cost, non-toxicity and high activity (mainly in alkali media). Zhang et al. focused on investigating the difference between various MnO_2 structures, including nanoparticles, nanotubes and nanobowls on the mutual interference of Cd^{2+}, Pb^{2+} and Zn^{2+} (figure 7). The nanoparticles were prepared by dissolving potassium permanganate in ethanol, washing the product with water and drying it. The nanotubes were prepared by dissolving $MnSO_4.H_2O$ and $KMnO_4$ in water, heating the mixture for 12 hours, washing the product with water and drying it. The nanobowls were hydrothermally prepared by dissolving $MnSO_4.H_2O$ and $(NH_4)_2S_2O_8$ in water, heating the mixture for 24 h, washing the product with water and drying it. The group modified a glassy carbon electrode with MnO_2 and square wave anodic stripping voltammetry was applied. The individual response was studied for Cd (II) and Zn (II) and the higher sensitivities were observed with Cd (II) (18.05 μA/μM for the nanoparticles, 12.36 μA/μM for the nanotubes and 18.69 μA/μM for the nanobowls). However, the interference mechanism was not clearly understood and demonstrated. Upon fixing the concentration of Zn (II), the trend in the mutual interference between Cd (II) and Zn (II) was similar on the three morphologies of MnO_2. On the other hand, when fixing the Cd (II) concentration, the interference between Cd (II) and Zn (II) on MnO_2 nanoparticles was different from that on the other structures. Similarly, the interference between Cd (II) and Pb (II) on MnO_2 nanotubes was different from the other morphologies [129]. Fayazi et al. used MnO_2 nanotubes for the detection of Hg (II) using differential pulse voltammetry. A simple chemical precipitation followed by a hydrothermal method were used for the fabrication of halloysite nanotubes – iron oxide – manganese oxide nanocomposite. The electrode displayed a limit of detection of 0.2 $\mu g.L^{-1}$ in a linear range of 0.5 – 150 $\mu g.L^{-1}$. The proposed sensor was validated for mercury determination in well and aqueduct water where the concentration of Hg (II) before spiking was below the detection limit and the recoveries after spiking were close to 100%. [130]. Salimi et al. investigated the use of yet another form of manganese oxide nanoparticles: nanoflakes. A glassy carbon electrode was first modified with chitosan and multiwalled carbon nanotubes followed by the electrodeposition of manganese oxide. Using cyclic voltammetry, Cr (III) was detected in a linear range of 40 – 360 μM, and the electrode was used for the detection of chromium ions in drinking water samples such that the calculated Cr

(III) concentration agreed with that measured by AAS [131]. All these studies were nicely elaborated, but at the same time each one of them still misses some important data on the analytical performance of each electrode.

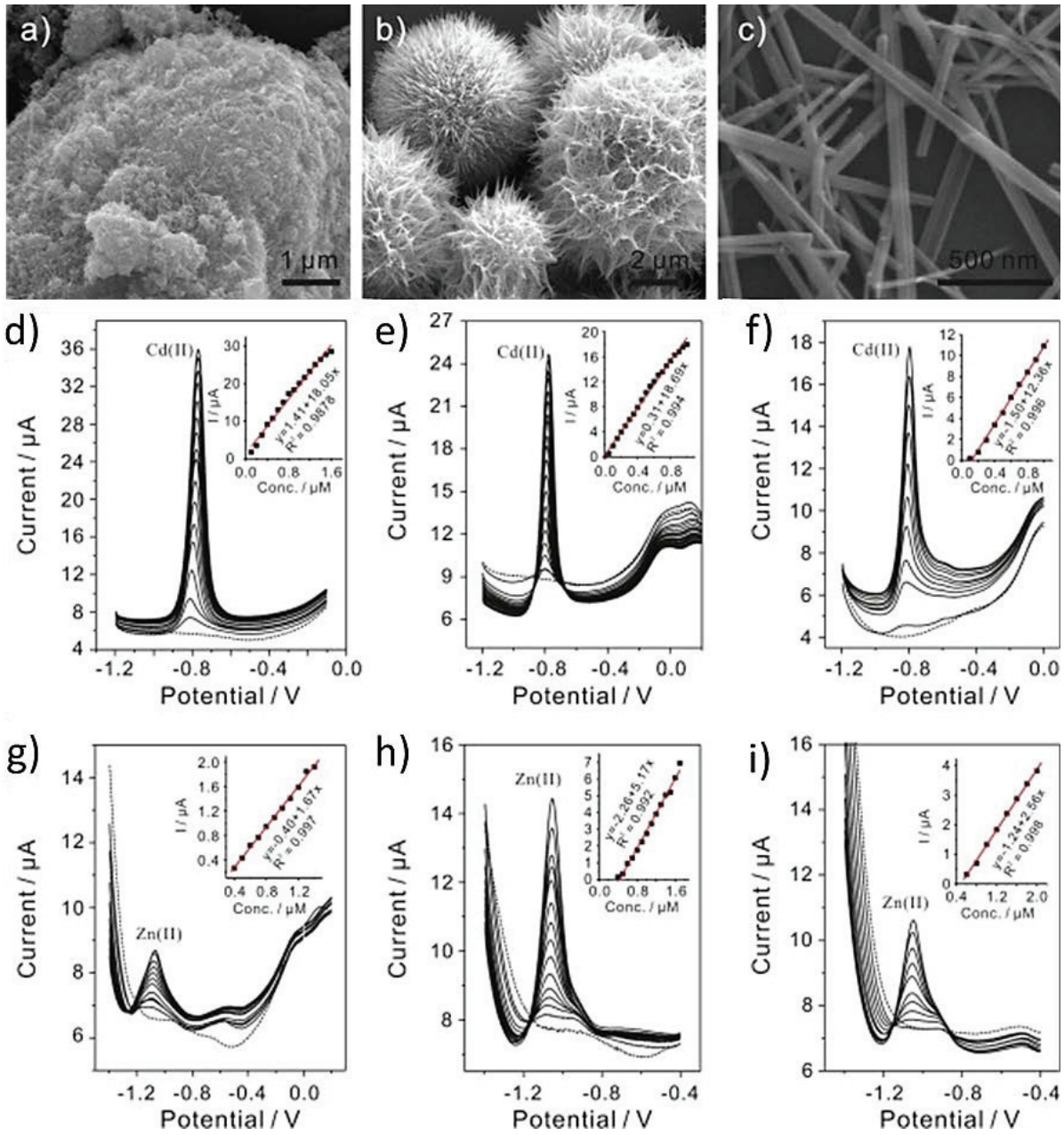

Figure 7: SEM images of (a) MnO_2 nanoparticles, (b) MnO_2 nanobowls and (c) MnO_2 nanotubes. SWASV responses of MnO_2 (d and g) nanoparticles, (e and h) nanobowls and (f and i) nanotubes modified electrode towards Cd (II) and Zn (II) at different concentrations in 0.1 M

NaAc–HAc (pH 5.0), respectively. The insets are plots of current vs concentration of Cd (II) and Zn (II), respectively [129]. Reproduced with permission from Elsevier

Wei et. al used tin oxide nanoparticles with reduced graphene oxide for the determination of Cd^{2+}, Pb^{2+}, Cu^{2+} and Hg^{2+} by square wave anodic stripping voltammetry. SnO_2 nanoparticles are known to have a high electric conductivity and chemical sensitivity, along with the ability to adsorb heavy metal ions. The nanoparticles were prepared by a one-step wet chemical method after the preparation of reduced graphene oxide. This step involved mixing graphene oxide with $SnCl_4.5H_2O$ in water. After stirring and centrifuging, the product was heated to improve its crystallinity. The obtained nanoparticles were uniformly distributed on the graphene network, with an average diameter of 4 – 5 nm. Individual and simultaneous determination of these ions were done, and the limits of detection of the ions were 1.015×10^{-10} M, 1.839×10^{-10} M, 2.269×10^{-10} M and 2.789×10^{-10} M, respectively, with an enhanced sensitivity for Cu (II) and Hg (II) when analyzed simultaneously. The authors reported that even though the sensitivities and LODs are not the best, but the electrode can be used without needing any regeneration [132]. Yang et al. synthesized an amino-based porous SnO_2 nanowires and modified a glassy carbon electrode for the detection of Cd (II) by means of SWASV. The sensor displayed a sensitivity of 124.03 $\mu A.\mu M^{-1}$ and a limit of detection of 0.0054 μM, with an effective determination of cadmium ions in water samples [133]. Cui and coworkers synthesized a 2-amino benzothiazole and 2-amino-4-thiazoleacetic acid derivative graphene enhanced with fluorine, chlorine and iodine on SnO_2 nanoparticles for the detection of Cu (II), Cd (II) and Hg (II). The nanoparticles were nearly spherical and well distributed on the graphene sheet. Using cyclic voltammetry, it was shown that the fluorine-SnO_2 sensor is the best suited for the detection of Cu (II), and thus differential pulse voltammetry was used. A linear range from 2 to 1000 nM and a LOD of 0.3 nM were obtained. The electrode was later used for the simultaneous detection of Cd (II), Cu (II) and Hg (II) such that all the linear ranges were between 20 and 2000 nM and the LODs were 5 nM, 3 nM and 5 nM, respectively, and hence the electrode was successfully evaluated for these ions in lake water, with results in agreement with those of AAS [134].

In addition to the general properties of nanoparticles, CeO_2 has a strong adsorption ability. Li et al. used a glassy carbon electrode modified with cerium oxide (CeO_2) nanoparticles, multi-wall carbon nanotubes, 1-ethyl-3-methylimidazolium tetrafluoroborate ($EMIMBF_4$) and DNA to detect Pb (II). Differential pulse voltammetry was applied and the linear range for Pb

(II) was between 10^{-8} and 10^{-5} M with the detection limit being 5×10^{-9} M hardly exhibiting any interference from five different metal ions with a practical application for the detection of lead in tap water [135].

Yukird et al. used thermal pyrolysis for the synthesis of ZnO nanorods mixed with graphene solution through colloidal coagulation for the modification of a screen-printed carbon electrode. Anodic stripping voltammetry was used for the concurrent determination of Cd^{2+} and Pb^{2+}. The limits of detection obtained were 0.6 $\mu g.L^{-1}$ for Cd (II) and 0.8 $\mu g.L^{-1}$ for Pb (II) in a linear range of 10 – 200 $\mu g.L^{-1}$, respectively. These heavy metal ions were simultaneously determined in wastewater samples, with measurements in accordance with those obtained by ICP-OES [136]. Yuan-Yuan et al. prepared a ZnO nanotubes/reduced graphene modified glassy carbon electrode via electrospinning and thermal decomposition of zinc acetate-polyacrylonitrile-polyvinyl pyrrolidone. SWASV was used for the analysis of Pb (II). A linear concentration range of 2.4×10^{-9}– 4.8×10^{-7} M and the limit of detection was 4.8×10^{-10} M [137].

MgO nanoflowers were also used for the detection of Pb (II) and Cd (II). Their synthesis involved mixing a magnesium precursor with potassium carbonate and heating the mixture to obtain a white precipitate that was later collected and calcinated. These nanoflowers along with Nafion® were used to modify a glassy carbon macroelectrode and SWASV was used under optimized conditions. The results for Pb (II) and Cd (II) detection showed linear ranges between 1 and 30 nM for lead and between 20 and 140 nM for cadmium, sensitivities of 0.706 and 0.077 $\mu A.nM^{-1}$ and limits of detection of 2.1×10^{-12} M and 8.1×10^{-11} M, respectively. The sensor was successfully tested for Pb (II) in Reservoir water samples from China [138].

1.5. Conclusion and Outlook

Electrochemical methods have been extensively used for the detection of heavy metals. However, the use of metal and metal oxide nanoparticles for modifying electrochemical sensors, for the voltammetric detection of heavy metals, proves to be more promising. Taking advantage of the unique properties of nanoparticles along with the advantages of electrochemical detection over conventional detection techniques, the analytical performance of all the reported electrodes was enhanced. The result was a rapid response time, increased sensitivity, very low limits of detection, simplified operational procedures and enhanced reproducibility.

In this review, the emphasis was on electrochemical sensors that could be applied for water samples. However, different water systems exist, from sea water, river water, tap water, drinking water to wastewater. Thus, these matrices are considered complex, some more than others, with the presence of different heavy metals either free or complexed, cations and anions, organic and inorganic materials… Despite the claims that some of the fabricated sensors were tested in these complex matrices, transition to commercialization remains shy. Moreover, most of these sensors require significant improvements, especially in the selectivity and capability of simultaneous analysis, before they can be applied for commercial use. Besides, commercialization also presents the challenges of reusability and mass production, which question the simplicity and cost-effectiveness of some of the sensors. For example, great focus has been given to gold nanoparticles and some excellent electrochemical sensors have been developed for the detection of heavy metals with LODs much lower than Fe_3O_4 NPs for instance. Nonetheless, noble metals such as gold and silver are known to be costly, and hence an alternative that presents high selectivity and can detect limits lower than the guidelines such as Fe_3O_4 NPs would be convenient. On the other hand, several materials were used along with the nanoparticles for the modification of the electrodes. However, with the use of certain materials, a few inconveniences, including toxicity and non-biocompatibility of the synthesized electrodes, still exist.

***References:**

[1] P. B. Tchounwou, C. G. Yedjou, A. K. Patlolla, D. J. Sutton, Heavy metal toxicity and the environment, Exp Suppl, 101 (2012) 133-164.

[2] J. Barton, M. B. G. García, D. H. Santos, P. Fanjul-Bolado, A. Ribotti, M. McCaul, D. Diamond, P. Magni, Screen-printed electrodes for environmental monitoring of heavy metal ions: a review, Microchimica Acta, 183(2) (2016) 503-517.

[3] C. Ariño, N. Serrano, J. M. Díaz-Cruz, M. Esteban, Voltammetric determination of metal ions beyond mercury electrodes. A review, Analytica chimica acta, 990 (2017) 11-53.

[4] P. Kumar, K. H. Kim, V. Bansal, T. Lazarides, N. Kumar, Progress in the sensing techniques for heavy metal ions using nanomaterials, Journal of industrial and engineering chemistry, 54 (2017) 30-43.

[5] S. Martin, W. Griswold, Human Health Effects of Heavy Metals, *Environmental Science and Technology Briefs for Citizens*, 15 (2009) 1–6 .

[6] G. L. Turdean, Design and Development of Biosensors for the Detection of Heavy Metal Toxicity, *Int. J. Electrochem.,* 2011, (2011) 1-15.

[7] N. Verma, M. Singh, Biosensors for heavy metals, *BioMetals, 18*(2) (2005) 121-129.

[8] WHO. *Guidelines for Drinking-water Quality* (4th ed.). 2011

[9] J. J. Corr, E. H. Larsen, Arsenic speciation by liquid chromatography coupled with ionspray tandem mass spectrometry, *J. Anal. At. Spectrom.*, 11(12), (1996) 1215.

[10] C. Yin, J. Iqbal, H. Hu, B. Liu, L. Zhang, B. Zhu, Y. Du, Sensitive determination of trace mercury by UV-visible diffuse reflectance spectroscopy after complexation and membrane filtration-enrichment, *J. Hazard. Mater., 233-234* (2012) 207-212.

[11] P. Pohl, Determination of metal content in honey by atomic absorption and emission spectrometries, *TrAC Trends Anal. Chem., 28*(1) (2009) 117-128.

[12] J. L. Gomez-Ariza, F. Lorenzo, T. Garcia-Barrera, Comparative study of atomic fluorescence spectroscopy and inductively coupled plasma mass spectrometry for mercury and arsenic multispeciation, *Anal. Bioanal. Chem., 382*(2) (2005) 485-492.

[13] P. R. Aranda, P. H. Pacheco, R. A. Olsina, L. D. Martinez, R. A. Gil, Total and inorganic mercury determination in biodiesel by emulsion sample introduction and FI-CV-AFS after multivariate optimization, *J. Anal. At. Spectrom.*, *24*(10) (2009) 1441-1445.

[14] S.-H. Chen, Y.-X. Li, P.-H. Li, X.-Y. Xiao, M. Jiang, S.-S. Li, W.-Q. Liu, Electrochemical spectral methods for trace detection of heavy metals: A review, *TrAC Trends Anal. Chem, 106* (2018) 139-150.

[15] Y. Lu, X. Liang, C. Niyungeko, J. Zhou, J. Xu, G. Tian, A review of the identification and detection of heavy metal ions in the environment by voltammetry, *Talanta, 178* (2018) 324-338.

[16] G. Aragay, A. Merkoçi, Nanomaterials application in electrochemical detection of heavy metals. *Electrochim. Acta, 84* (2012) 49-61.

[17] B. Bansod, T. Kumar, R. Thakur, S. Rana, I. Singh, A review on various electrochemical techniques for heavy metal ions detection with different sensing platforms, *Biosens. Bioelectron., 94* (2017) 443-455.

[18] Y. Lu, X. Liang, C. Niyungeko, J. Zhou, J. Xu, G. Tian, A review of the identification and detection of heavy metal ions in the environment by voltammetry, *Talanta*, 178 (2018) 324–338.

[19] J. Hoyos-Arbeláez, M. Vázquez, J. Contreras-Calderón, Electrochemical methods as a tool for determining the antioxidant capacity of food and beverages: A review, Food Chemistry, 221 (2017) 1371–1381.

[20] A. Borrill, N. E. Reily, J. V. Macpherson, Addressing the Practicalities of Anodic Stripping Voltammetry for Heavy Metal Detection: A Tutorial Review, The Analyst, 144(23) (2019) 6834-6849.

[21] J. Barek, A. G. Fogg, A. Muck, J. Zima, Polarography and Voltammetry at Mercury Electrodes, Critical Reviews in Analytical Chemistry, 31(4) (2001) 291–309.

[22] Y. Cheng, H. Li, C. Fang, L. Ai, J. Chen, J. Su, Q. Fu, Facile synthesis of reduced graphene oxide/silver nanoparticles composites and their application for detecting heavy metal ions, *J. Alloys Compd., 787* (2019) 683-693.

[23] T. Han, J. Jin, C. Wang, Y. Sun, Y. Zhang, Y. Liu, Ag Nanoparticles-Modified 3D Graphene Foam for Binder-Free Electrodes of Electrochemical Sensors, *Nanomaterials (Basel), 7*(2) (2017) 40.

[24] S. Xing, H. Xu, J. Chen, G. Shi, L. Jin, Nafion stabilized silver nanoparticles modified electrode and its application to Cr(VI) detection, *J. Electroanal. Chem., 652*(1-2) (2011) 60-65.

[25] O.D. Renedo, M. Julia Arcos Martínez, A novel method for the anodic stripping voltammetry determination of Sb(III) using silver nanoparticle-modified screen-printed electrodes, *Electrochem. Commun., 9*(4) (2007) 820-826.

[26] S. Zeng, K.-T. Yong, I. Roy, X.-Q. Dinh, X. Yu, F. Luan, A Review on Functionalized Gold Nanoparticles for Biosensing Applications, *Plasmonics, 6*(3) (2011) 491-506.

[27] S. S. Hassan, A. R. Solangi, T. G. Kazi, M. S. Kalhoro, Y. Junejo, N. H. Kalwar, Nafion stabilized ibuprofen–gold nanostructures modified screen printed electrode as arsenic(III) sensor, *J. Electroanal. Chem., 682* (2012) 77-82.

[28] R. Ouyang, S. A. Bragg, J. Q. Chambers, Z. L. Xue, Flower-like self-assembly of gold nanoparticles for highly sensitive electrochemical detection of chromium(VI), *Anal. Chim. Acta, 722* (2012) 1-7.

[29] S. Dutta, G. Strack, P. Kurup, Gold Nanostar Electrodes for Heavy Metal Detection, *Sensors and Actuators B: Chemical*, 281 (2019) 383-391.

[30] S. Dutta, G. Strack, P. Kurup, Gold nanostar-based voltammetric sensor for chromium(VI), *Microchim. Acta*, 186(11) (2019) 1-7.

[31] D. Lu, C. Sullivan, E. M. Brack, C. P. Drew, P. Kurup, Simultaneous voltammetric detection of cadmium(II), arsenic(III), and selenium(IV) using gold nanostar–modified screen-printed carbon electrodes and modified Britton-Robinson buffer, Analytical and Bioanalytical Chemistry, 412(17) (2020) 4113-4125.

[32] X. Yang, J. Xu, X. Tang, H. Liu, D. Tian, A novel electrochemical DNAzyme sensor for the amplified detection of Pb2+ ions, *Chem. Commun. (Camb), 46*(18) (2010) 3107-3109.

[33] W. Pooi See, S. Nathan, L. Yook Heng, A Disposable Copper (II) Ion Biosensor Based on Self-Assembly of L-Cysteine on Gold Nanoparticle-Modified Screen-Printed Carbon Electrode, *Journal of Sensors, 2011* (2011) 1-5.

[34] A. Safavi, E.Farjami, Construction of a carbon nanocomposite electrode based on amino acids functionalized gold nanoparticles for trace electrochemical detection of mercury, *Anal. Chim. Acta, 688*(1) (2011) 43-48.

[35] L. Zhu, L. Xu, B. Huang, N. Jia, L. Tan, S. Yao, Simultaneous determination of Cd(II) and Pb(II) using square wave anodic stripping voltammetry at a gold nanoparticle-graphene-cysteine composite modified bismuth film electrode, *Electrochim. Acta, 115* (2014) 471-477.

[36] G. Xu, G. Wang, X He, Y. Zhu, L. Chen, X. Zhang, An ultrasensitive electrochemical method for detection of Ag(+) based on cyclic amplification of exonuclease III activity on cytosine-Ag(+)-cytosine, *Analyst, 138*(22) (2013) 6900-6906.

[37] Z. Chen, L. Li, X. Mu, H. Zhao, L. Guo, Electrochemical aptasensor for detection of copper based on a reagentless signal-on architecture and amplification by gold nanoparticles, *Talanta, 85*(1) (2011) 730-735.

[38]R. M. Kong, X.B. Zhang, L. L.Zhang, X. Y. Jin, S. Y. Huan, G. L. Shen, R. Q. Yu, An ultrasensitive electrochemical "turn-on" label-free biosensor for Hg2+with AuNP-functionalized reporter DNA as a signal amplifier, *Chem. Commun. (Camb)*(37) (2009) 5633-5635.

[39] X. Lu, X. Dong, K. Zhang, Y. Zhang, An ultrasensitive electrochemical mercury(ii) ion biosensor based on a glassy carbon electrode modified with multi-walled carbon nanotubes and gold nanoparticles, *Analytical Methods, 4*(10) (2012) 3326-3331.

[40] X. Tang, H. Liu, B. Zou, D. Tian, H. Huang, A fishnet electrochemical Hg2+ sensing strategy based on gold nanoparticle-bioconjugate and thymine-Hg(2+)-thymine coordination chemistry, *Analyst, 137*(2) (2012) 309-311.

[41] X. Dai, O. Nekrassova, M. E. Hyde, R. G. Compton, Anodic Stripping Voltammetry of Arsenic(III) Using Gold Nanoparticle-Modified Electrodes, *Anal. Chem., 76*, (2004) 5924-5929.

[42] L. Xiao, G.G. Wildgoose, R. G. Compton, Sensitive electrochemical detection of arsenic (III) using gold nanoparticle modified carbon nanotubes via anodic stripping voltammetry, *Anal. Chim. Acta, 620*(1-2) (2008) 44-49.

[43] P. Carrera, P. J. Espinoza-Montero, L Fernández, H. Romero, J. Alvarado Electrochemical determination of arsenic in natural waters using carbon fiber ultra-microelectrodes modified with gold nanoparticles, Talanta, 166 (2017) 198–206.

[44] B. Kumar Jena, C. Retna Raj, Gold Nanoelectrode Ensembles for the Simultaneous Electrochemical Detection of Ultratrace Arsenic, Mercury, and Copper, *Anal. Chem., 80* (2008) 4836–4844.

[45] G. Zhao, G. Liu, Electrochemical Deposition of Gold Nanoparticles on Reduced Graphene Oxide by Fast Scan Cyclic Voltammetry for the Sensitive Determination of As(III), Nanomaterials, 9(1) (2018) 41.

[46] E. Majid, S. Hrapovic, Y. Liu, K. B. Male, J. H. Luong, J.H., Electrochemical Determination of Arsenite Using a Gold Nanoparticle Modified Glassy Carbon Electrode and Flow Analysis, *Anal. Chem, 78* (2006) 762-769.

[47] M. M. Hossain, M. M. Islam, M. M., S. Ferdousi, T. Okajima, T. Ohsaka, Anodic Stripping Voltammetric Detection of Arsenic(III) at Gold Nanoparticle-Modified Glassy Carbon Electrodes Prepared by Electrodeposition in the Presence of Various Additives, *Electroanalysis, 20*(22), (2008) 2435-2441.

[48] A. Buffa, D. Mandler, Arsenic(III) detection in water by flow-through carbon nanotube membrane decorated by gold nanoparticles, Electrochimica Acta, 318 (2019) 496-503.

[49] L. Bu, J. Liu, Q. Xie, S. Yao, Anodic stripping voltammetric analysis of trace arsenic(III) enhanced by mild hydrogen-evolution at a bimetallic Au–Pt nanoparticle modified glassy carbon electrode. Electrochemistry Communications, 59 (2015) 28–31.

[50] L. Bu, Q. Xie, H. Ming, Gold nanoparticles decorated three-dimensional porous graphitic carbon nitrides for sensitive anodic stripping voltammetric analysis of trace arsenic(III), Journal of Alloys and Compounds, (2020) 153723.

[51] M. Rajkumar, S. Thiagarajan, S. M. Chen, Electrochemical Detection of Arsenic in Various Water Samples, *Int. J. Electrochem. Sci., 6*, (2011) 3164 - 3177.

[52] Y. S. Song, G. Muthuraman, Y. Z. Chen, C. C. Lin, J. M. Zen, Screen Printed Carbon Electrode Modified with Poly(L-Lactide) Stabilized Gold Nanoparticles for Sensitive As(III) Detection, *Electroanalysis, 18*(18) (2006) 1763-1770.

[53] R. Baron, B. Šljukić, C. Salter, A. Crossley, R. G. Compton, Electrochemical detection of arsenic on a gold nanoparticle array, *Russ. J. Phys. Chem. A, 81*(9)(2007) 1443-1447.

[54] L. Zhang, D. W. Li, W. Song, L. Shi, Y. Li, Y. T. Long, High Sensitive On-Site Cadmium Sensor Based on AuNPs Amalgam Modified Screen-Printed Carbon Electrode, *IEEE Sensors Journal, 10(10)* (2010) *1583–1588.*

[55] Y. Si, J. Liu, Y. Chen, X. Miao, F. Ye, Z. Liu, J. Li, rGO/AuNPs/tetraphenylporphyrin nanoconjugate-based electrochemical sensor for highly sensitive detection of cadmium ions, *Analytical Methods, 10*(29) (2018) 3631-3636.

[56] X. Xu, G. Duan, Y. Li, G. Liu, J. Wang, H. Zhang, W. Cai, Fabrication of gold nanoparticles by laser ablation in liquid and their application for simultaneous electrochemical detection of Cd2+, Pb2+, Cu2+, Hg2+, *ACS Appl. Mater. Interfaces, 6*(1) (2014) 65-71.

[57] B. Zhang, J. Chen, H. Zhu, T. Yang, M. Zou, M. Zhang, M. Du, Facile and green fabrication of size-controlled AuNPs/CNFs hybrids for the highly sensitive simultaneous detection of heavy metal ions, *Electrochim. Acta, 196* (2016) 422-430.

[58] T. Priya, N. Dhanalakshmi, S. Thennarasu, V. Karthikeyan, N. Thinakaran, Ultra sensitive electrochemical detection of Cd2+ and Pb2+ using penetrable nature of graphene/gold nanoparticles/modified L-cysteine nanocomposite, Chemical Physics Letters, 731 (2019) 136621.

[59] C. M. Welch, O. Nekrassova, X. Dai, M. E. Hyde, R. G. Compton, Fabrication, characterisation and voltammetric studies of gold amalgam nanoparticle modified electrodes, *ChemPhysChem, 5*(9) (2004) 1405-1410.

[60] G. Liu, Y. Y. Lin, H. Wu, Y. Lin, Voltammetric Detection of Cr(VI) with Disposable Screen-Printed Electrode Modified with Gold Nanoparticles, *Environ. Sci. Technol., 41* (2007) 8129–8134.

[61] B. Liu, L. Lu, M. Wang Y. Zi, A study of nanostructured gold modified glassy carbon electrode for the determination of trace Cr(VI), *J. Chem. Sci., 120*(5) (2008) 493–498.

[62] N. Wang, M. Lin, H. Dai, H. Ma, Functionalized gold nanoparticles/reduced graphene oxide nanocomposites for ultrasensitive electrochemical sensing of mercury ions based on thymine-mercury-thymine structure, *Biosens. Bioelectron., 79* (2016) 320-326.

[63] N. Zhou, H. Chen, J. Li, L. Chen, Highly sensitive and selective voltammetric detection of mercury(II) using an ITO electrode modified with 5-methyl-2-thiouracil, graphene oxide and gold nanoparticles, *Microchim. Acta, 180*(5-6) (2013) 493-499.

[64] L. Shen, Z. C., Y. Li, S. He, S. Xie, X. Xu, Z. Liang, X. Meng, Q. Li, Z. Zhu, M. Li, X. Chris Le, Y. Shao, Electrochemical DNAzyme Sensor for Lead Based on Amplification of DNA-Au Bio-Bar Codes. *Anal. Chem., 80* (2008) 6323–6328.

[65] X. C. Fu, J. Wu, L. Nie, C. G. Xie, J. H. Liu, X. J. Huang, Electropolymerized surface ion imprinting films on a gold nanoparticles/single-wall carbon nanotube nanohybrids modified glassy carbon electrode for electrochemical detection of trace mercury(II) in water, *Anal. Chim. Acta, 720* (2012) 29-37.

[66] Y. Lin, Y. Peng, J. Di, Electrochemical detection of Hg(II) ions based on nanoporous gold nanoparticles modified indium tin oxide electrode, *Sens. Actuators, B 220* (2015) 1086-1090.

[67] O. Abollino, A. Giacomino, M. Malandrino, G. Piscionieri, E. Mentasti, Determination of mercury by anodic stripping voltammetry at a gold nanoparticle-modified glassy carbon electrode, Electroanalysis: An International Journal Devoted to Fundamental and Practical Aspects of Electroanalysis, 20(1) (2008) 75-83.

[68] S. L. Ting, S. J. Ee, A. Ananthanarayanan, K. C. Leong, P. Chen, Graphene quantum dots functionalized gold nanoparticles for sensitive electrochemical detection of heavy metal ions, *Electrochim. Acta, 172* (2015) 7-11.

[69] P. Miao, L. Liu, Y. Li, G. Li, A novel electrochemical method to detect mercury (II) ions, *Electrochem. Commun., 11*(10) (2009) 1904-1907.

[70] H. Wan, Q. Sun, H. Li, F. Sun, N. Hu, P. Wang, Screen-printed gold electrode with gold nanoparticles modification for simultaneous electrochemical determination of lead and copper, *Sens. Actuators, B, 209* (2015) 336-342.

[71] D. Martín-Yerga, M. B. González-García, A. Costa-García, Use of nanohybrid materials as electrochemical transducers for mercury sensors, *Sens. Actuators, B 165*(1) (2012) 143-150.

[72] L. Zhu, L. Xu, B. Huang, N. Jia, L. Tan, S. Yao, Simultaneous determination of Cd(II) and Pb(II) using square wave anodic stripping voltammetry at a gold nanoparticle-graphene-cysteine composite modified bismuth film electrode, *Electrochim. Acta, 115* (2014) 471-477.

[73] X. Yiwei, Z. Wen, H. Xiaowei, S. Jiyong, Z. Xiaobo, L. Zhihua, C. Xueping, Adsorptive stripping voltammetry determination of hexavalent chromium by a pyridine functionalized gold nanoparticles/three-dimensional graphene electrode. Microchemical Journal, (2019) 104022.

[74] O. Dominguez-Renedo, L. Ruiz-Espelt, N. Garcia-Astorgano, M. J. Arcos-Martinez, Electrochemical determination of chromium(VI) using metallic nanoparticle-modified carbon screen-printed electrodes, *Talanta, 76*(4) (2008) 854-858.

[75] M. C. Tsai, P. Y. Chen, Voltammetric study and electrochemical detection of hexavalent chromium at gold nanoparticle-electrodeposited indium tinoxide (ITO) electrodes in acidic media, *Talanta, 76*(3) (2008) 533-539.

[76] J. Tu, Y. Gan, T. Liang, H. Wan, P. Wang, A miniaturized electrochemical system for high sensitive determination of chromium(VI) by screen-printed carbon electrode with gold nanoparticles modification. *Sens. Actuators, B, 272* (2018) 582-588.

[77] J. Gong, T. Zhou, D. Song, L. Zhang, Monodispersed Au nanoparticles decorated graphene as an enhanced sensing platform for ultrasensitive stripping voltammetric detection of mercury(II), *Sensors and Actuators B: Chemical, 150*(2) (2010) 491-497.

[78] E. Bernalte, C. Marín Sánchez, E. Pinilla Gil, Gold nanoparticles-modified screen-printed carbon electrodes for anodic stripping voltammetric determination of mercury in ambient water samples, *Sens. Actuators, B, 161*(1) (2012) 669-674.

[79] T. Hezard, K. Fajerwerg, D. Evrard, V. Collière, P. Behra, P. Gros, Gold nanoparticles electrodeposited on glassy carbon using cyclic voltammetry: Application to Hg(II) trace analysis, *J. Electroanal. Chem., 664* (2012) 46-52.

[80] H. R. A. Hasanjani, K. Zarei, An electrochemical sensor for attomolar determination of mercury(II) using DNA/poly-L-methionine-gold nanoparticles/pencil graphite electrode, *Biosens. Bioelectron., 128* (2019) 1-8.

[81] Z. Zhu, Y. Su, J. Li, D. Li, J. Zhang, S. Song, C. Fan, Highly sensitive electrochemical sensor for mercury(II) ions by using a mercury-specific oligonucleotide probe and gold nanoparticle-based amplification, *Anal. Chem., 81*(18) (2009) 7660-7666.

[82] H. Xu, L. Zeng, S. Xing, G. Shi, Y. Xian, L. Jin, Microwave-radiated synthesis of gold nanoparticles/carbon nanotubes composites and its application to voltammetric detection of trace mercury(II), *Electrochem. Commun., 10*(12) (2008) 1839-1843.

[83] P. M. Lee, Z. Wang, X. Liu, Z. Chen, E. Liu, Glassy carbon electrode modified by graphene–gold nanocomposite coating for detection of trace lead ions in acetate buffer solution, *Thin Solid Films, 584* (2015) 85-89.

[84] Z. Lu, S. Yang, Q. Yang, S. Luo, C. Liu, Y. Tang, A glassy carbon electrode modified with graphene, gold nanoparticles and chitosan for ultrasensitive determination of lead(II), *Microchim. Acta, 180*(7-8) (2013) 555-562.

[85] Y. Zhu, G. M. Zeng, Y. Zhang, L. Tang, J. Chen, M. Cheng, L. H. Zhang, L. He, Y. Guo, X. X. He, M. Y. Lai, Y. B. He, Highly sensitive electrochemical sensor using a MWCNTs/GNPs-modified electrode for lead (II) detection based on Pb(2+)-induced G-rich DNA conformation, *Analyst, 139*(19) (2014) 5014-5020.

[86] O. Dominguez Renedo, M. J. Arcos Martinez, Anodic stripping voltammetry of antimony using gold nanoparticle-modified carbon screen-printed electrodes, *Anal. Chim. Acta, 589*(2) (2007) 255-260.

[87] G. J. Lee, C. K. Kim, M. K. Lee, C. K. Rhee, Simultaneous Voltammetric Determination of Zn, Cd and Pb at Bismuth Nanopowder Electrodes with Various Particle Size Distributions. *Electroanalysis, 22*(5) (2010) 530-535.

[88] G. J. Lee, H. M. Lee, Y. R. Uhm, M. K. Lee, C. K. Rhee, Square-wave voltammetric determination of thallium using surface modified thick-film graphite electrode with Bi nanopowder, *Electrochem. Commun., 10*(12) (2008) 1920-1923.

[89] M. A.Rico, M. Olivares-Marin, E. P. Gil, Modification of carbon screen-printed electrodes by adsorption of chemically synthesized Bi nanoparticles for the voltammetric stripping detection of Zn(II), Cd(II) and Pb(II), *Talanta, 80*(2) (2009) 631-635.

[90] J. Saturno, D. Valera, H. Carrero, L. Fernández, Electroanalytical detection of Pb, Cd and traces of Cr at micro/nano-structured bismuth film electrodes, *Sens. Actuators, B, 159*(1) (2011) 92-96.

[91] P. K. Sahoo, B. Panigrahy, S. Sahoo, A. K. Satpati, D. Li, D. Bahadur, In situ synthesis and properties of reduced graphene oxide/Bi nanocomposites: as an electroactive material for analysis of heavy metals, *Biosens. Bioelectron., 43* (2013) 293-296.

[92] F. W. Campbell, R. G. Compton, The use of nanoparticles in electroanalysis: an updated review, Analytical and Bioanalytical Chemistry, 396(1) (2009) 241–259.

[93] Y. L. Sabahudin Hrapovic, J. H. T. Luong, Reusable Platinum Nanoparticle Modified Boron Doped Diamond Microelectrodes for Oxidative Determination of Arsenite, *Anal. Chem., 79* (2007) 500-507.

[94] X. Dai, R. G. Compton, Detection of As(III) via oxidation to As(V) using platinum nanoparticle modified glassy carbon electrodes: arsenic detection without interference from copper, *Analyst, 131*(4) (2006) 516-521.

[95] T. Zhang, H. Jin, Y. Fang, J. Guan, S. Ma, Y. Pan, M. Zhang, H. Zhu, X. Liu, M. Du, Detection of trace Cd2+, Pb2+ and Cu2+ ions via porous activated carbon supported palladium nanoparticles modified electrodes using SWASV, *Mater. Chem. Phys., 225* (2019) 433-442.

[96] P. Veerakumar, V. Veeramani, S. M. Chen, R. Madhu, S. B. Liu, Palladium Nanoparticle Incorporated Porous Activated Carbon: Electrochemical Detection of Toxic Metal Ions, ACS Applied Materials & Interfaces, 8(2) (2016) 1319–1326.

[97] P. M. Lee, Z. Chen, L. Li, E. Liu, Reduced graphene oxide decorated with tin nanoparticles through electrodeposition for simultaneous determination of trace heavy metals, *Electrochim. Acta, 174* (2015) 207-214.

[98] K. E. Toghill, L. Xiao, G. G. Wildgoose, R. G. Compton, Electroanalytical Determination of Cadmium(II) and Lead(II) Using an Antimony Nanoparticle Modified Boron-Doped Diamond Electrode, *Electroanalysis, 21*(10) (2009) 1113-1118.

[99] J. M. George, A. Antony, B. Mathew, Metal oxide nanoparticles in electrochemical sensing and biosensing: a review, *Mikrochim Acta, 185*(7) (2018) 358.

[100] S. Lee, J. Oh, D. Kim, Y. Piao, A sensitive electrochemical sensor using an iron oxide/graphene composite for the simultaneous detection of heavy metal ions, *Talanta, 160* (2016) 528-536.

[101] S. S. Li, W. Y. Zhou, M. Jiang, L. N. Li, Y. F. Sun, Z. Guo, J. H. Liu, X. J. Huang, Insights into diverse performance for the electroanalysis of Pb(II) on Fe2O3 nanorods and hollow nanocubes: Toward analysis of adsorption sites, *Electrochimica Acta* 288 (2018) 42-51.

[102] S. Deshmukh, G. Kandasamy, R. K. Upadhyay, G. Bhattacharya, D. Banerjee, D. Maity, S. S. Roy, Terephthalic acid capped iron oxide nanoparticles for sensitive electrochemical detection of heavy metal ions in water, *J. Electroanal. Chem., 788*, (2017) 91-98.

[103] Y. Sun, W. Zhang, H. Yu, C. Hou, D. Li, Y. Zhang, Y. Liu, Controlled synthesis various shapes Fe3O4 decorated reduced graphene oxide applied in the electrochemical detection, *Journal of Alloys and Compounds,* 638, (2015) 182–187.

[104] W. Yantasee, K. Hongsirikarn, C. L. Warner, D. Choi, T. Sangvanich, M. B. Toloczko, C. Timchalk, Direct detection of Pb in urine and Cd, Pb, Cu, and Ag in natural waters using electrochemical sensors immobilized with DMSA functionalized magnetic nanoparticles, *Analyst, 133*(3), (2008) 348-355.

[105] P. Miao, Y. Tang, L. Wang, DNA Modified Fe3O4@Au Magnetic Nanoparticles as Selective Probes for Simultaneous Detection of Heavy Metal Ions, *ACS Appl. Mater. Interfaces, 9*(4), (2017) 3940-3947.

[106] H. Cui, W. Yang, X. Li, H. Zhao, Z. Yuan An electrochemical sensor based on a magnetic Fe3O4 nanoparticles and gold nanoparticles modified electrode for sensitive determination of trace amounts of arsenic(iii), *Analytical Methods, 4*(12), (2012) 4176-4181.

[107] S. Xiong, M. Wang, D. Cai, Y. Li, N. Gu, Z. Wu, Electrochemical Detection of Pb(II) by Glassy Carbon Electrode Modified with Amine-Functionalized Magnetite Nanoparticles, *Anal. Lett., 46*(6), (2013) 912-922.

[108] Q. Song, M. Li, L. Huang, Q. Wu, Y. Zhou, Y. Wang, Bifunctional polydopamine@Fe3O4 core-shell nanoparticles for electrochemical determination of lead(II) and cadmium(II), *Anal. Chim. Acta, 787*, (2013) 64-70.

[109] Y. F. Sun, W. K. Chen, W. J. Li, T. J. Jiang, J. H. Liu, Z. G. Liu, Selective detection toward Cd2+ using Fe3O4/RGO nanoparticle modified glassy carbon electrode, *J. Electroanal. Chem., 714-715*, (2014) 97-102.

[110] H. L. Fan, S. F. Zhou, J. Gao, Y. Z. Liu, Continuous preparation of Fe3O4 nanoparticles through Impinging Stream-Rotating Packed Bed reactor and their electrochemistry detection toward heavy metal ions, *J. Alloys Compd., 671*, (2016) 354-359.

[111] S. F. Zhou, X. J. Han, Y. Q. Liu, SWASV performance toward heavy metal ions based on a high-activity and simple magnetic chitosan sensing nanomaterials, *J. Alloys Compd., 684*, (2016) 1-7.

[112] M. Baghayeri, A. Amiri, B. Maleki, Z. Alizadeh, O. Reiser, A simple approach for simultaneous detection of cadmium(II) and lead(II) based on glutathione coated magnetic nanoparticles as a highly selective electrochemical probe. *Sens. Actuators, B 273*, (2018) 1442-1450.

[113] R. A. Ahmed, A. M. Fekry, Preparation and Characterization of a Nanoparticles Modified Chitosan Sensor and Its Application for the Determination of Heavy Metals from Different Aqueous Media. *Int. J. Electrochem. Sci., 8*, (2013) 6692 - 6708.

[114] H. Filik, A. A. Avan, Dextran modified magnetic nanoparticles based solid phase extraction coupled with linear sweep voltammetry for the speciation of Cr(VI) and Cr(III) in tea, coffee, and mineral water samples. Food Chemistry, 292, (2019) 151–159.

[115] H. Yang, X. Liu, R. Fei, Y. Hu, Sensitive and selective detection of Ag+ in aqueous solutions using Fe3O4@Au nanoparticles as smart electrochemical nanosensors. *Talanta, 116*, (2013) 548-553.

[116] L. Dedelaite, S. Kizilkaya, H. Incebay, H. Ciftci, M. Ersoz, Z. Yazicigil, A. Ramanavicius, Electrochemical determination of Cu(II) ions using glassy carbon electrode modified by some nanomaterials and 3-nitroaniline. *Colloids Surf., A, 483*, (2015) 279-284.

[117] A. Afkhami, R. Moosavi, T. Madrakian, H. Keypour, A. Ramezani-Aktij, M. Mirzaei-Monsef, Construction and Application of an Electrochemical Sensor for Simultaneous Determination of Cd(II), Cu(II) and Hg(II) in Water and Foodstuff Samples. *Electroanalysis, 26*(4), (2014) 786-795.

[118] S. F. Zhou, X. J. Han, H. L. Fan, Q. X. Zhang, Y. Q. Liu, Electrochemical detection of As(III) through mesoporous MnFe2O4 nanocrystal clusters by square wave stripping voltammetry, *Electrochim. Acta, 174*, (2015) 1160-1166.

[119] S. Zhou, X. Han, H. Fan, Y. Liu, Electrochemical Sensing toward Trace As(III) Based on Mesoporous MnFe(2)O(4)/Au Hybrid Nanospheres Modified Glass Carbon Electrode, *Sensors (Basel),* (2016) *16*(6).

[120] X. J. Han, S. F. Zhou, H. L. Fan, Q. X. Zhang, Y. Q. Liu, Mesoporous MnFe2O4 nanocrystal clusters for electrochemistry detection of lead by stripping voltammetry, Journal of Electroanalytical Chemistry, 755, (2015) 203–209.

[121] S. F. Zhou, X. J. Han, H. L. Fan, J. Huang, Y. Q. Liu, Enhanced electrochemical performance for sensing Pb(II) based on graphene oxide incorporated mesoporous MnFe2O4 nanocomposites, *J. Alloys Compd., 747*, (2018) 447-454.

[122] S. F. Zhou, J.J. Wang, L. Gan, X. J. Han, H. L. Fan, L. Y. Mei, Y. Q. Liu, Individual and simultaneous electrochemical detection toward heavy metal ions based on L-cysteine modified mesoporous MnFe2O4 nanocrystal clusters, *J. Alloys Compd., 721*, (2017) 492-500.

[123] A. Salimi, H. Mamkhezri, R. Hallaj, S. Soltanian, Electrochemical detection of trace amount of arsenic(III) at glassy carbon electrode modified with cobalt oxide nanoparticles, *Sens. Actuators, B, 129*(1), (2008) 246-254.

[124] L. Zhou, W. Xiong, S. Liu, Preparation of a gold electrode modified with Au–TiO2 nanoparticles as an electrochemical sensor for the detection of mercury(II) ions, *J. Mater. Sci.50*(2), (2014) 769-776.

[125] X. Zhang, T. Zeng, C. Hu, S. Hu, Q. QiulinTianStudies on fabrication and application of arsenic electrochemical sensors based on titanium dioxide nanoparticle modified gold strip electrodes. *Analytical Methods, 8*(5), , (2016) 1162-1169.

[126] A. Mao, H. Li, Z. Cai, X. Hu, Determination of mercury using a glassy carbon electrode modified with nano TiO2 and multi-walled carbon nanotubes composites dispersed in a novel cationic surfactant, Journal of Electroanalytical Chemistry, 751, (2015) 23–29.

[127] S. Ramezani, M. Ghobadi, B. N. Bideh, Voltammetric monitoring of Cd (II) by nano-TiO2 modified carbon paste electrode sensitized using 1,2-bis-[o-aminophenyl thio] ethane as a new ion receptor, Sensors and Actuators B: Chemical, 192, (2014) 648–657.

[128] F. Liu, Y. Zhang, W. Yin, C. Hou, D. Huo, B. He, L. Qian, H. Fa, A high–selectivity electrochemical sensor for ultra-trace lead (II) detection based on a nanocomposite consisting of nitrogen-doped graphene/gold nanoparticles functionalized with ETBD and Fe3O4 @TiO2 core–shell nanoparticles. Sensors and Actuators B: Chemical, 242, (2017) 889–896.

[129] Q. X. Zhang, H. Wen, D. Peng, Q. Fu, X. J. Huang, Interesting interference evidences of electrochemical detection of Zn(II), Cd(II) and Pb(II) on three different morphologies of MnO2 nanocrystals. *J. Electroanal. Chem., 739*, (2015) 89-96.

[130] M. Fayazi, M. A. Taher, D. Afzali, A. Mostafavi, (2016) Fe3O4 and MnO2 assembled on haloysite nanotubes: A highly efficient solid-phase extractant for electrochemical detection of mercury(II) ions. Sensors and Actuators B: Chemical, 228, (2016) 1–9.

[131] A. Salimi, B. Pourbahram, S. Mansouri-Majd, R. Hallaj, Manganese oxide nanoflakes/multi-walled carbon nanotubes/chitosan nanocomposite modified glassy carbon electrode as a novel electrochemical sensor for chromium (III) detection. Electrochimica Acta, 156, (2015) 207–215.

[132] Y. Wei, C. Gao, F. L. Meng, H. H. Li, L. Wang, J. H. Liu, X. J. Huang, SnO2/Reduced Graphene Oxide Nanocomposite for the Simultaneous Electrochemical Detection of Cadmium(II), Lead(II), Copper(II), and Mercury(II): An Interesting Favorable Mutual Interference, The Journal of Physical Chemistry C, 116(1), (2011) 1034–1041.

[133] M. Yang, T. J. Jiang, Z. Guo, J. H. Liu, Y. F. Sun, X. Chen, X. J. Huang, Sensitivity and selectivity sensing cadmium(II) using amination functionalized porous SnO2 nanowire bundles-room temperature ionic liquid nanocomposite: Combined efficient cation capture with control experimental conditions. Sensors and Actuators B: Chemical, 240, (2017) 887–894.

[134] X. Cui, X. Fang, H. Zhao, Z. Li, H. Ren, Fabrication of thiazole derivatives functionalized graphene decorated with fluorine, chlorine and iodine@SnO2 nanoparticles for highly sensitive detection of heavy metal ions. Colloids and Surfaces A: Physicochemical and Engineering Aspects, 546, (2018) 153–162.

[135] Y. Li, X. R. Liu, X. H. Ning, C. C. Huang, J. B. Zheng, J. C. Zhang, An ionic liquid supported CeO2 nanoparticles-carbon nanotubes composite-enhanced electrochemical DNA-based sensor for the detection of Pb(2). *J. Pharm. Anal., 1*(4), (2011) 258-263.

[136] J. Yukird, P. Kongsittikul, J. Qin, O. Chailapakul, N. Rodthongkum, ZnO@graphene nanocomposite modified electrode for sensitive and simultaneous detection of Cd (II) and Pb (II), Synth. Met. 245, (2018) 251–259.

[137] L. Yuan-Yuan, C. Meng-Ni, G. Yi-Li, Y. Jian-Mao, M. A. Xiao-Yu, L. Jian-Yun, Preparation of zinc oxide-graphene composite modified electrodes for detection of trace Pb(II), Chinese J. Anal. Chem. 43, (2015) 1395–1401.

[138] Y. Wei, R. Yang, X. Y. Yu, L. Wang, J. H. Liu, X. J. Huang, Stripping voltammetry study of ultra-trace toxic metal ions on highly selectively adsorptive porous magnesium oxide nanoflowers, The Analyst, 137(9), (2012) 2183.

Chapter II: Aptamers and nucleobases functionalized metal and metal oxide nanoparticles: Recent advances in heavy metal contamination

Introduction

The accumulation of heavy metal ions in living beings and the environment has led to serious disorders as well as disruption in the entire ecological system. The way of exposure, concentration of the heavy metal and the heavy metal itself are amongst the factors affecting the severity of the adverse consequences. Accordingly, agencies such as the World Health Organization have set safety limits, and numerous techniques have been established for the detection, quantitation and removal of heavy metals from different matrices.

One class of functional nucleic acids that has been successfully used in the recognition of various target molecules such as peptides, proteins and heavy metals is aptamers. They are artificial oligonucleotide sequences produced by systematic evolution of ligands by exponential enrichment (SELEX) method in vitro. Their most notable advantages are their high specificity and selectivity towards the analyte. On the other hand, nanoparticles (NPs) have also been investigated in the sensing and removal of heavy metal ions, among other analytes. The main advantage of using nanoparticles is the large surface area created by the small particle size, thus opening space for increased area for interaction with the analyte. In fact, the combination of aptamers and nanotechnology has created new properties different than the individual properties of each element alone. These new properties have led to the development of various sensing and removal platforms, especially in the past few years.

The interaction between heavy metal ions and aptamer-based approaches using nanoparticles happens through the aptamers themselves. Coordination studies have been carried out to identify the specific sites and preferences of interaction, as well as the factors influencing these interactions. In the past five years, six studies have reported the use of specific nucleobases along with gold and magnetic nanoparticles for the analysis of heavy metals, mainly mercury, along with arsenic, cadmium, copper and lead.

Different electrochemical, spectroscopic and optical methods have been investigated for aptamer-based nanoparticle approaches. Aptamers of different lengths and sequences were examined. The most common are electrochemical methods using gold nanoparticles for the detection of mercury, benefiting from the selective interaction between thymine nucleobases and mercury. Other approaches include colorimetry, fluorometry, surface enhanced Raman spectroscopy, quartz crystal microbalance, magnetic relaxation switching, chemiluminescence

and visual detection. Less commonly, other metallic and bimetallic nanoparticles such as silver and platinum were also studied, with electrochemical techniques being the most frequently used.

On the other hand, metal oxide nanoparticles have also been combined with aptamers for the analysis of heavy metals. Nanoparticles such as zinc oxide, copper(II) oxide, tin oxide, titanium oxide and manganese oxide are among those used for aptamer-based heavy metal detection. However, magnetic nanoparticles and specifically iron oxide Fe_3O_4 nanoparticles were the most utilized taking advantage of the fact that these nanoparticles can be easily separated from any solution using an external magnet. In the past five years, not only were they used as biosensors for the detection of heavy metals, but also as biosorbents for the adsorption and removal of heavy metal ions. Mercury was again the most commonly detected heavy metal followed by mercury and silver; whereas adsorption studies were performed with lead ions only.

Aptamers and nucleobases functionalized metal and metal oxide nanoparticles: Recent advances in heavy metal monitoring

ABSTRACT

Heavy metal contamination has long been a serious threat to the entire ecological system and human beings. Consequently, sensitive and reliable methods have been developed for the detection of heavy metal ions from different systems. Advancements in biotechnology, and in functional nucleic acids specifically, have offered new methods for heavy metal monitoring based on the specific interactions of aptamers with heavy metal ions. The introduction of nanoparticles to aptamer-based technologies has also presented its advantages of increased immobilization efficiency, sensitivity and selectivity. Thus, this review provides an update on the progress of using nanotechnology combined with biotechnology for the monitoring of heavy metal ions. The aptamer-based detection of heavy metal ions using metallic and metallic oxide nanoparticles, as well as the few studies on the adsorption of heavy metals are emphasized. Electrochemistry, colorimetry, fluorescence, surface plasmon resonance and surface-enhanced Raman scattering are among the detection modes of heavy metal ions. In all cases, the analytical performances of the studied systems were significantly improved.

Keywords

Heavy metals, metal nanoparticles, metal oxide nanoparticles, aptamers, oligonucleotides, detection, adsorption

2.1. Introduction

The upsurge in waste materials whether agricultural, industrial or medical has resulted in an increased risk of the population's exposure to pollutants [1]. These include dyes, pesticides,

pharmaceuticals, oils, organic molecules and heavy metals [2]. Heavy metals are neither biodegradable nor environmentally degradable, tending to accumulate in all living beings through the food chain [3]. Consequences of heavy metal exposure include diseases and disorders in several systems [4], and their severity depends on the heavy metal, way of exposure and concentration. The side effects of heavy metals on human beings and the environment have led several organizations including the World Health Organization (WHO) to set safety limits. However, adhering to these limits in some parts of the world can be somehow challenging due to rapid urbanization and industrialization [5]. Thus, speciation analysis and quantitative determination of toxic metals are of great importance.

Several methods have been employed for the detection of toxic heavy metals from different matrices. These include inductively coupled plasma mass spectrometry ICP-MS [6], inductively coupled plasma optical emission spectroscopy ICP-OES [7], inductively coupled plasma atomic emission spectroscopy ICP-AES [8], atomic absorption spectroscopy AAS [9] and cold vapor atomic fluorescence spectroscopy CV-AFS [10]. Despite all the advantages offered by these techniques, some challenges still exit. These techniques are expensive, with a complex operational procedure, long detection time and difficulty of on-site monitoring [11].

Aptamers are typically artificial oligonucleotides (mainly single-stranded DNA or RNA) or peptides produced by systematic evolution of ligands by exponential enrichment (SELEX) method in vitro. They present one type of functional nucleic acids that can form binding pockets and clefts within a well-defined three dimensional structure for the specific recognition of target molecules [12]. Aptamers have been successfully used for an extensive variety of target molecules including metal ions, peptides and proteins, cells [13], and most recently Covid-19 [14]. They offer the advantages of specificity, easy and cost-effective preparation and

modification and high binding affinity compared to small-molecule ligands [15]. They are known for their high temperature and chemical stability, as well as their target versatility. Accordingly, several bio-sorbents and biosensors have been designed based on these specific interactions. Additionally, aptamers designed for heavy metal sensors can be easily regenerated, and the sensors can be reused [13].

In recent years, nanotechnology has emerged as an interdisciplinary technology with numerous fields including physics, biology, chemistry, medicine and material science due to the predefined superstructure of nanoparticles [16]. Nanoparticles are the solid particles engineered at atomic or molecular scale with at least one dimension less than 100 nm [16]. Nanomaterials can be easily functionalized with different substrates through covalent bonding or non-covalent actions. Combining aptamers and nanoparticles not only exhibits dual properties pertaining to each element alone, but also demonstrates new properties that can be useful in many applications [17]. Utilizing nanomaterials with aptamers can convert the interaction between aptamers and their substrates into electrical, optical and other signals [18]. On the one hand, the intrinsic properties of nanoparticles along with the binding properties of aptamers lead to various possibilities in different applications. On the other hand, the use of nanoparticles increases the surface area of the used material thus increasing the density of the immobilized aptamers and the area of interaction between these aptamers and analyte molecules [17].

Several reviews have been published recently focusing on biosensors for specific heavy metals such as mercury [3, 19], lead [20] and arsenic [21]. In this review, an updated overview of the aptamer-based approaches developed in the past five years for the analysis of heavy metals by using metal and metal oxide nanoparticles is presented.

2.2. Interaction between heavy metals and nucleic acids

Metal ion coordination to single stranded nucleic acids has been reviewed, taking into consideration the phosphate diester backbone [22]. It was reported that metal ions can bind to the phosphate backbone stabilizing the DNA duplex. Nevertheless, such interaction disregards the chemical nature of the metal ions and DNA. The ability of cations to bind nucleobases can be ascribed to the cation's ionic radius, coordination behavior and hydration effects [23]. Sigel and Sigel summarized the nucleotide coordination affinity to various divalent ions [24]. It was shown that each nucleobase has a preferred binding site for the different metals. Cationic divalent metals bind preferentially to the N7 of guanine followed by N3 of cytosine, N7 of adenine, N1 of adenine and finally the N3 of adenine and guanine [22]. The affinity of arsenic, which is a trivalent heavy metal ion, towards nucleobases was investigated by Yu et al. [25]. Just like divalent heavy metals, it was proven that As^{3+} has preferred binding sites for nucleobases decreasing in the following order: guanine, adenine, uracil, cytosine and thymine. The high stability of the arsenic-guanine complex was also confirmed by our group [26]. According to the latest reports, the use of nanoparticle-modified electrodes is set to meet the commercial challenges in developing cost effective, field portable, and highly selective sensors and test kits to monitor arsenic in drinking water and other environmental samples [27].

The different and specific interactions between the nucleobases of aptamers and single-stranded DNA from one side, and heavy metal ions from the other side, have been the basis of heavy metal detection by DNA. Most commonly, mercury Hg^{2+} and silver Ag^{+} ions recognition has been based on thymine (T)-thymine and cytosine (C)-cytosine mismatches to form the more stable T-Hg^{2+}-T and C-Ag^{+}-C complexes [28, 29]. Lead Pb^{2+} ions have been detected using the conformational switch of a guanine (G)-rich aptamer from random coil to G-quadruplex structure

[30], whereas cadmium Cd^{2+} ions were captured using thymine and guanine-rich aptamers [31]. The detection mechanism differs depending on how the nucleobases make up the aptamer. The two most common structures are the G-quadruplex for the detection of lead using guanine-rich oligonucleotides, and hairpin structure that makes use of the guanine-lead and thymine-mercury interactions. These structures are represented in figure 1. The aptamer functionalization of nanoparticles can be either through adsorption or chemical bonding also leading to different sensing mechanisms.

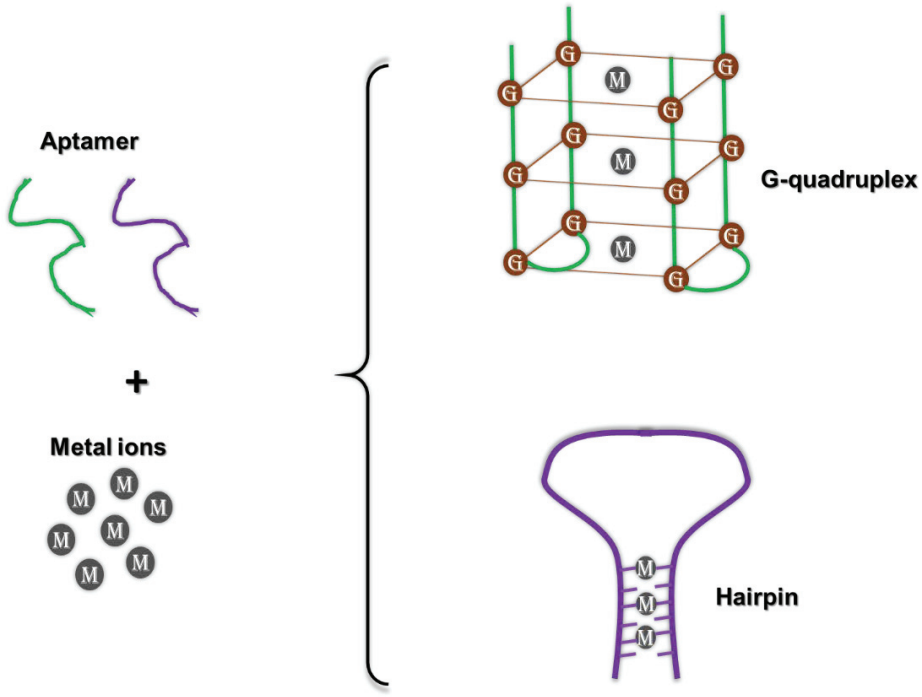

Figure 1: The most commonly formed structures after the interaction of aptamers with metal ions.

2.3. Metal nanoparticles

In addition to the increased surface area due to their small sizes, metallic nanoparticles present several advantages. They can increase the sensitivity of the used techniques by increasing the mass-transport rate and offering a fast electron transfer [32]. The various metallic nanoparticles that have been combined with aptamers for the detection of heavy metals are detailed in this section.

2.3.1. Gold nanoparticles

Aptamer-based strategies using gold nanoparticles (Au NPs) are the most common for the study of heavy metals. Au NPs are known for their easy and controllable synthesis and the stability in the synthesis process and application [33]. For the detection of heavy metals, gold nanoparticles have been integrated with aptamers either as a deposited layer on the surface of the signal transducer, or as a conjugated form with the aptamer to enhance the sensitivity and increase the surface area [34].

Electrochemical approaches are the most common aptamer-based strategies using gold nanoparticles, among which, differential pulse voltammetry (DPV) is the most used. Other electrochemical techniques include square wave voltammetry (SWV), electrochemical impedance spectroscopy (EIS), differential pulse stripping voltammetry (DPSV), differential pulse anodic stripping voltammetry (DPASV), electrochemiluminescence (ECL), photoelectrochemistry (PEC) chronocoulometry, and amperometry. The most recent applications are summarized in Table 1. Using electrochemistry, mercury is the most frequently detected heavy metal, making use of the thymine – mercury – thymine interaction. Other heavy metal ions detected include lead, cadmium, arsenic and silver. It is worth noting that several authors have used gold nanoparticles in combination with other metal and metal oxide nanoparticles such as silver nanoparticles Ag NPs [35, 36] and iron oxide nanoparticles Fe_3O_4 NPs [37-39].

Table 1: Electrochemical aptasensors using gold nanoparticles for the detection of heavy metals.

From Table 1, it can be noticed that almost all aptamers utilized for mercury detection are thymine-rich, and electrochemiluminescence along with differential pulse voltammetry are the two most used techniques. The lowest limit of detection (2 aM) was reported using electrochemiluminescence with two DNA strands; one immobilized on Fe_3O_4@SiO_2/dendrimers/QD and the other with gold nanoparticles [39]. Interestingly, most of the lowest LODs for Hg^{2+} detection were reported using electrochemiluminescence [39-43], whether the thymine-rich aptamers and gold nanoparticles were associated with other modifiers or not. In the case of the detection of lead, all the aptamers used were guanine-rich aptamers, with differential pulse voltammetry as the most used electrochemical technique. However, except for one study, the lowest LODs (as low as 4×10^{-5} nM) were obtained when no modifiers were added to the gold nanoparticles and aptamers [44-48]. The sensing mechanisms differed between the reported studies.

Most mechanisms relied on using gold nanoparticles as an immobilization layer for the aptamers. When one aptamer was immobilized on the nanoparticles, the detected signals were mainly the result of the formation or disassembly of stable structures such as G-quadruplex and hairpin. In other cases, when two aptamers were used, the signal was due to the formation of a double helix, or its disassembly to form a more stable structure. One study only relied on the disassembly of a triple helix [49]. A few studies have utilized gold nanoparticles as signal amplifiers and not for aptamer immobilization. A representation of some of the different sensing mechanisms is shown in figure 2.

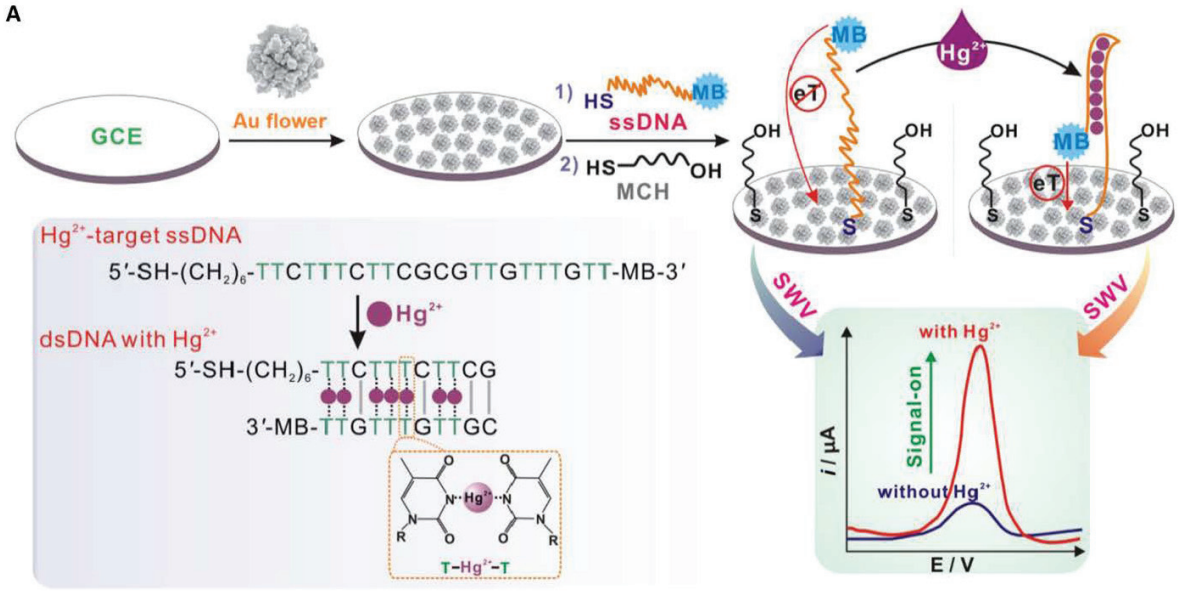
A
GCE
Au flower
1) HS
MB
ssDNA
2) HS
OH
MCH
Hg2+-target ssDNA
5′-SH-(CH2)6-TTCTTTCTTCGCGTTGTTTGTT-MB-3′
Hg2+
dsDNA with Hg2+
5′-SH-(CH2)6-TTCTTTCTTCG
3′-MB-TTGTTTGTTGC
T–Hg2+–T
eT
Hg2+
SWV
with Hg2+
Signal-on
without Hg2+
i / μA
E / V

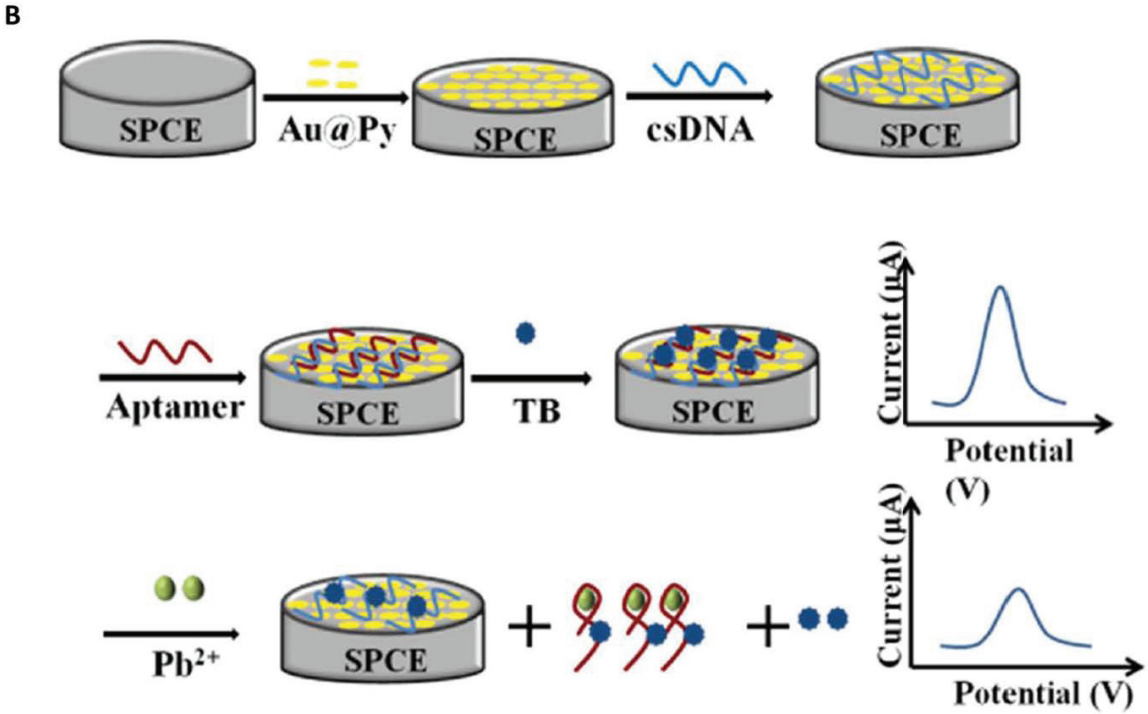
B
SPCE
Au@Py
csDNA
Aptamer
TB
Current (μA)
Potential (V)
Pb2+

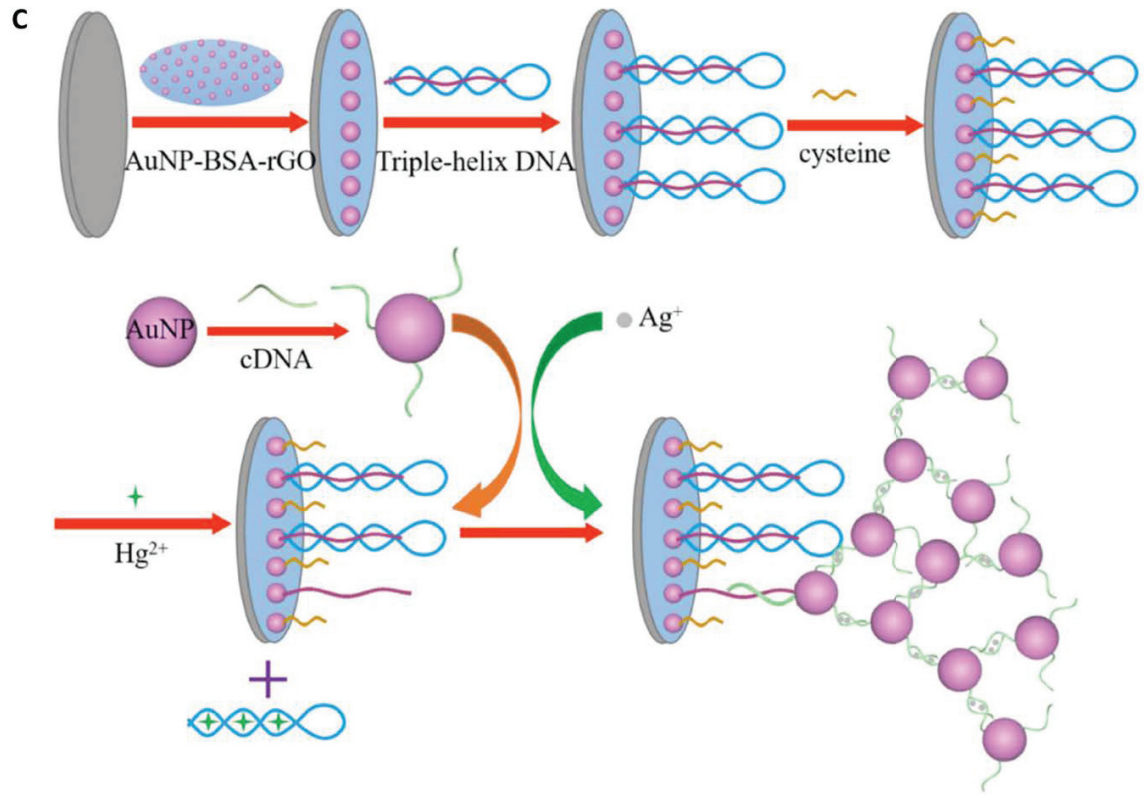

Figure 2: (A) Illustration of the single-step and specific detection of Hg^{2+} by using Au flowers-based electrochemical aptasensor. Lower left: conformational change of single-stranded DNA (ssDNA) upon binding to Hg^{2+}. Reprinted (adapted) with permission from [50]. Copyright 2018 American Chemical Society, (B) Presentation of the Pb^{2+} biosensor and detection principle. Reproduced from Ref. [51] with permission from the Royal Society of Chemistry, and (C) Fabrication of the electrochemical probe for Hg^{2+} detection based on triple helix disassembly [49]. Reproduced with permission from Elsevier

Abbreviations: GCE: glassy carbon electrode, MCH: 6-mercapto-hexanol, MB: methylene blue, SPCE: screen-printed carbon electrode, py: polypyrrole, TB: toluidine blue

Several other approaches have combined gold nanoparticles with aptamers for the detection of heavy metal ions (Table 2). Colorimetry has been extensively utilized for the detection of lead, mercury, arsenic, cadmium and platinum. In most cases, Au NPs were used alone; however, a few studies have reported the use of magnetic nanoparticles [52-54] among other modifications. Several detection strategies were employed. Unlike with electrochemical techniques, gold nanoparticles were mainly utilized as signal amplifiers making use of their catalytic and electrical properties. A lot of studies also relied on the change in color between colloidal gold nanoparticles (red) and aggregated nanoparticles (blue). Despite the expansive development of the detection mechanisms, the lowest limit of detection reported was 1.4 pM for the detection of mercury [55].

A number of studies have used fluorometry for the detection of lead [56-58] and mercury [59-61]. Interestingly, the LODs were in the nanomolar range except for one study where quantum dots were used along with gold nanoparticles to obtain an LOD of 2.5 pM [60]. Surface enhanced Raman spectroscopy (SERS) was also used for the detection of lead, mercury and arsenic [62-65]. The lowest limit of detection (0.4 pM) using a non-electrochemical technique was obtained using this method [65]. Less commonly, a few studies have attempted the detection of lead and mercury using quartz crystal microbalance (QCM), magnetic relaxation switching (MRS) and chemiluminescence (CL). Generally, it can be noticed that the limits of detection obtained using non-electrochemical methods were mostly higher than those obtained with electrochemical techniques.

Table 2: Non-electrochemical aptasensors using gold nanoparticles for the detection of heavy metals.

2.3.2. Other Metallic Nanoparticles

Silver Ag and platinum Pt are among the metal nanoparticles that have been combined with aptamers for the detection of heavy metal ions. In addition to the advantages of good electrical conductivity and larger surface area, these nanoparticles also have a favorable catalytic activity with a wide range of pH and temperature conditions.

Jin et al. developed a lead electrochemical aptasensor based on biomass porous carbon derived from soybean straws, platinum nanoparticles and several DNA strands: 5'-GGG TGG GTG GGT GGG TAT-3', complementary DNA: 5'-TCA TAC CCA CCC ACC-3', hairpin DNA 1: 5'-TTT TGG GTG GGT ATG ACC ACC GCC CAC CCA-3' and Bio-Hairpin DNA 2: 5'-bio-TAT GAC CAC CTG GGT GGG CGG TGG TCA TAC CCA C-3'. The biosensor exhibited a linear range of 50 pM – 1000 nM with a detection limit of 18 pM. The proposed sensor was also successfully tested in tap water and lake water [66].

Ma et al. were able to visually detect lead using the aptamer 5'-NH_2-C_6-GTGGGTAGGGCGGGTTGG-3' and silver nanoparticles based on the formation of G-quadruplex structure. The results showed that optical darkness ratio (ODR) and logarithmic value of Pb^{2+} concentration had a good linear relationship over a concentration range of 0.5–10 μM. In addition, there was no obvious interference of other common metal ions for the detection, proving the selectivity of the method. The method was also successfully applied for the qualitative and semi-quantitative analysis of lead in soil samples [67].

Song et al. proposed a portable ultrasensitive SERS sensor based on T-rich oligonucleotides 5′-thiol-TTTTTTTTTTTTTTT-Cy5-3′ immobilized on silver nanorods for the detection of mercury (II) ions. The mercury – thymine interaction led to a change in structure of the DNA and hence in the SERS signal. A linear range was obtained between 1 pM and 1 μM

with a detection limit of 0.16 pM. Good recovery rates were also obtained upon testing the sensor in tap and lake water [68].

Bimetallic AgPt nanoparticles can significantly increase the surface area and have good electrical conductivity and electrocatalytic activity. Xu et al. designed an electrochemical aptasensor for the detection of lead ions. The biosensor was made using metal-organic frameworks decorated with AgPt nanoparticles conjugated with single stranded DNA 3'-NH_2-$(CH_2)_6$-CCCACCCACC-5' complementary to a guanine-rich lead specific aptamer 5'-GGGTGGGTGGGTGGGT-$(CH_2)_6$-NH_2-3'. The developed sensor showed a linear response in the concentration range of 0.1 pM and 100 nM as well as a detection limit of 0.032 pM with potential application in tap and lake water [69].

2.4. Metal oxide nanoparticles

Some metal oxide nanoparticles such as ZnO, CuO, Fe_3O_4, SnO_2, TiO_2 and MnO_2 have been widely explored for the identification and detection of heavy metal ions because of their non-toxic and catalytic properties [70]. Magnetic nanoparticles, and specifically magnetite Fe_3O_4 and maghemite γ Fe_2O_3 have received considerable attention due to their low toxicity, ease of preparation and biocompatibility [71]. Metal oxide nanoparticles offer the advantages of significant electron transfer kinetics and larger specific area thus possessing a larger number of adsorption sites on the surface of the working electrode to accumulate more detected ions [70]. The different studies on the conjugation of metallic oxide nanoparticles with aptamers for the detection of heavy metals are thoroughly discussed in this section.

Even though Fe_3O_4 nanoparticles are the most common form of metal oxide nanoparticles used for the detection of heavy metal ions, some studies have used Co_3O_4, TiO_2 and CeO_2

nanoparticles. Liu and coworkers designed an electrochemical aptasensor based on Ti-modified Co_3O_4 nanoparticles and the aptamer 5'-GGA CTG TTG TGG TAT TAT TTT TGG TTG TGC AGT CC-3', for the detection of cadmium ions. Under optimal conditions, a linear range of 1.8 pM – 0.13 nM and a limit of detection of 4.36 pM were obtained in addition to the possibility of using it to test tap water and river water [72].

Song et al. developed an electrochemical biosensor using a one-step synthetic method for the detection of Pb(II). The method consisted on reducing cupric sulfate by ascorbic acid in presence of G-rich DNA with the sequence 5′- CAACGGTGGGTGTGGTTGG - 3' to produce spherical Cu_xO@DNA. Electrochemical impedance spectroscopy data presented a linear range of 0.1 to 100 nM with a detection limit of 6.8 nM and a feasibility to apply in blood serum [73].

Niu et al. fabricated a photoelectrochemical aptasensor for the detection of Pb(II) ions. CdS-TiO_2 nanocomposite was used as photoactive material along with Pb(II)-binding aptamers 5'-SH-GGG TGG GTG GGT GGG T-3' and 5'-A CCC ACC CAC CCA CCC-3' immobilized on gold nanochains and a copper(II) complex as an intercalator. After optimization, a linear concentration range was obtained between 5 pM and 10 nM with a detection limit of 1.6 pM. The method was successfully used to detect lead in water and soil samples [74].

Yang et al. developed an electrochemical biosensor for the detection of arsenate using CeO_2-DNA nanoprobe based on the competitive coordination effect. As(V) was detected using the methylene blue labelled aptamer 5'-MB-AAAAA-3' in a linear range of 50 nM – 2 μM with a detection limit of 20.5 nM. The system was also successfully used in natural water samples [75].

Magnetic nanoparticles possess numerous magnetic and physical properties of high susceptibility, biocompatibility, stability and superparamagnetism [76]. The analytical applications of magnetic nanoparticles benefit from their specific properties such as homogeneous size distribution, colloidal stability, presence of surface functional groups and fast response to an applied magnetic field [13]. For the immobilization of aptamers on magnetic nanoparticles can be functionalized with numerous reactive functional groups such as carboxyls, amines, epoxyls and tosyls [13].

Liu et al. developed a magnetic relaxation switching sensor based on iron oxide nanoparticles, gold nanoparticles and aptamers 5'-SH C_6-CGGCTTTTGTTTT-3'. The presence of mercury ions caused the aggregation of aptamers due to the thymine–Hg^{2+}–thymine interaction allowing the detection of these ions in two distinct concentration ranges, 10 – 100 nM and 100 nM – 5 μM. The limit of detection using this method was 2.7 nM and the authors reported a visual detection for concentrations of Hg^{2+} beyond 5 μM [77].

Tao and coworkers designed a graphene/Fe_3O_4-AuNPs composite colorimetric aptasensor for the detection of lead ions. The aptamer specific for Pb^{2+} was decorated on the surface of the amine magnetic beads, with complementary strands of the aptamer 5'-biotin-GGGTGGGTGGGTGGGT-3' and 3'-CCACCCTCCCAC-5' and Pb^{2+} competing to bind to it. Detection of lead was done in a linear concentration range of 4.8 nM – 1.4 μM with a limit of detection of 0.24 nM. This assay was successfully applied to test tap water samples, exhibiting good selectivity [78]. Wang and coworkers described a colorimetric assay using 5'-SH-TTTCTTTCTTCCCCCCTTGTTTGTTT-3', 3'- AAA GAA AGA AGG GGG GAA CAA ACA AAC ATC GAT TGT GTC CCC CCT TC-5' and 5'-GTA GCT AAC ACA GGG GGG AAG TTT CTTTCTTCCCCCCTTGTTTGTTT-3' aptamers immobilized on Fe_3O_4@Au nanoparticles

for the detection of Hg^{2+} ions. A linear calibration plot was obtained between 1 and 300 nM with a detection limit of 0.7 nM and selectivity over other ions and a possibility to use in river water samples [53].

Shan et al. designed a fluorescence biosensor for Hg^{2+} onsite detection using magnetic beads and 5'-Biotin-AAAAAAAAAACATGTTAGTCGTTGCT-3', and 5'-NH_2-AGC TTC GTC TAT CTTG-3' aptamers. The sensor showed a high sensitivity for mercury with a linear concentration range of 1 nM – 1 μM and a detection limit of 1 nM. The sensor was also successfully used for Hg^{2+} detection in tap water [79]. Sun et al. designed a fluorescent sensor using aptamers immobilized on the surface of magnetic beads for the detection of Hg^{2+}. The presence of mercury ions induced the formation of thymine–Hg^{2+}–thymine structure influencing the fluorescence signal. The results obtained showed that mercury can be detected in a concentration range of 2 – 160 nM with a detection limit of 0.2 nM. The method was also used to quantify Hg^{2+} in river water and ribbon fish with acceptable recoveries, agreeing with the results obtained by atomic fluorescence spectroscopy [80].

Babamiri et al. designed an electrochemiluminescence aptasensor for the detection of Hg^{2+} based on an "on-off-on" switching strategy. The assay used thymine-rich 5'-TTC TTT GTT CCC CTT CTT TGTT-NH_2-3' single stranded DNA immobilized on Fe_3O_4@SiO_2/dendrimers/QD and gold nanoparticles modified with a complementary aptamer. Under optimized conditions, mercury was detected in a linear range of 20 aM – 2 μM with a detection limit of 2 aM. The aptasensor was used for the detection of Hg^{2+} ions in tap water, carp and other fishes with satisfactory results [39].

Wu el al. developed an electrochemical aptasensor for the detection of mercury ions through the T – Hg^{2+} – T structure. Single stranded DNA 5'-Bio- TCTTTCTTCCCTTGTTTGT-

3'. were immobilized on streptavidin modified magnetic beads and the detection was done using DPV. Under optimized conditions, the detection limit was 0.33 nM and the linear range was between 1 and 200 nM with a potential application in tap and river water [81]. Miao et al. designed an electrochemical biosensor based on DNA modified Fe_3O_4@Au nanoparticles for the simultaneous detection of Hg^{2+} and Ag^{+}. Detection was based on the formation of thymine–Hg^{2+}–thymine and cytosine–Ag^{+}–cytosine structures and square wave voltammetry was applied. The limits of detection were 1.7 nM and 3.4 nM with linear concentration ranges of 10 – 100 nM and 0 – 400 nM for Hg^{2+} and Ag^{+}, respectively [37]. Luo et al. designed a sandwich-type aptasensor based on platinum nanotubes array and thionine labelled Fe_3O_4/reduced graphene oxide nanocomposite for the detection of mercury ions through thymine-Hg^{2+}-thymine pairing. Under optimized conditions, the aptasensor showed a low limit of detection of 30 pM, a linear range between 0.1 and 100 nM and an applicability for Hg^{2+} detection in tap and lake water [82].

Since most studies aim at analyzing mercury ions, the different reports using Fe_3O_4 nanoparticles for the detection of mercury can be compared in figure 3. The number of studies relying on iron oxide nanoparticles is insignificant compared to those using gold nanoparticles. Thus, we can say that the numerous possibilities of detection have not yet been explored. Nevertheless, an exceptionally low limit of detection of 2 aM was obtained electrochemically, proving that iron oxide nanoparticles can be considered as competitors for gold nanoparticles.

It is worth noting that there are two recent studies that used the combination of Fe_3O_4 nanoparticles and aptamers as biosorbents for lead ions for preconcentration before detection. On the one hand, aptamers specifically make use of the metal-oligonucleotide interaction that results in complexes. On the other hand, the use of magnetic nanoparticles allows these complexes to be easily separated from the supernatant.

Shamsipur et al. were able to determine Pb^{2+} by covalently binding a lead specific aptamer 5′-H_2N-$(CH_2)_6$-TTTTT ACCCA GGGTGGGTGGG TGGGT-3′) to a Fe_3O_4/graphene surface. In presence of Pb^{2+}, G-quadruplex was formed by the aptamer with hairpin structure. EDTA was used to elute the bound analyte from the biosorbents. Inductively coupled plasma mass spectrometry was used for the determination of the heavy metal ions and a detection limit of 0.24 nM with a linear range of 1.45 nM – 4.1 μM and an enrichment factor of 50 were obtained. The method was applied for the separation and preconcentration of lead from biological samples with good reproducibility [83].

Rahnama and coworkers also used aptamer-functionalized magnetic adsorbents for the enrichment of lead ions prior to flame atomic absorption spectrometric detection. Two steps were involved in the synthesis of the adsorbents: synthesis of silver-coated magnetite core-shell nanoparticles followed by the conjugation of a selective Pb^{2+} aptamer 5'-GGT TGG TGT GGT TGG-3' on the surface of the nanoparticles. After optimization, a calibration curve was obtained in the range of 33 – 1000 mg/L with a limit of detection of 10 mg/L. The method was successfully applied in the preconcentration and determination of lead ions in tap and seawater samples [84].

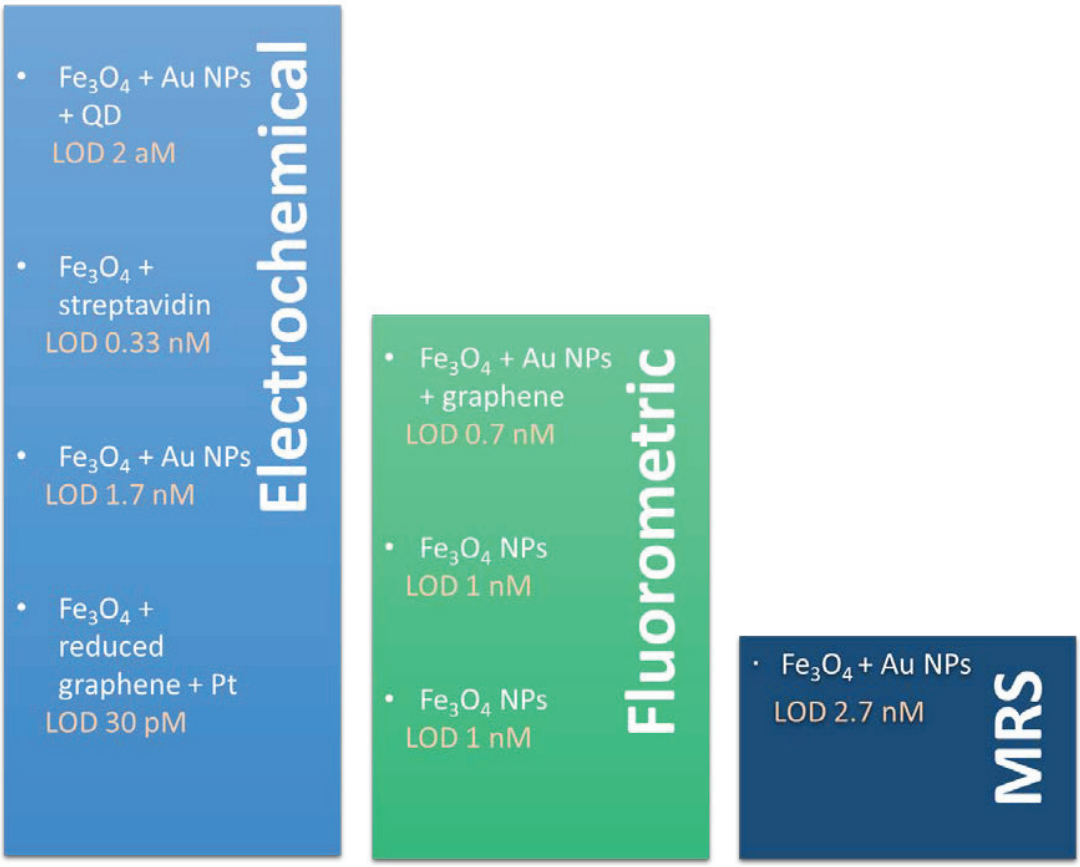

Figure 3: Comparison of the thymine aptamer-based techniques for the detection of mercury ions.

2.5. Single nucleobases

Despite the obvious advantages of increased sensitivity and selectivity offered when using aptamers, a few studies have reported the use of single nucleobases benefiting from less complex preparation and operational procedures.

Most recently, Butmee et al. used thymine acetic acid anchored with cysteamine-conjugated core shell Fe_3O_4@Au nanoparticles for the electrochemical detection of mercury ions. Hg^{2+} ions interacted with the immobilized thymine forming thymine– Hg^{2+} –thymine

mismatch and generating a signal detectable using differential pulse anodic stripping voltammetry (DPASV). After optimization, the sensor exhibited two linear ranges from 1 to 200 µg/L and 200 to 2200 µg/L with a detection limit of 0.5 µg/L. The sensor was successfully used for the detection of mercury in water and fish samples, with results comparable to those of flow injection atomic spectroscopy–inductively coupled plasma–optical emission spectroscopy (FIAS–ICP–OES) [38]. Yuan et al. also used thymine acetic acid functionalized gold nanoparticles for the detection of mercury ions, benefiting from the T-Hg^{2+}-T mismatch. The detection was done using surface plasma resonance (SPR) and under optimal conditions, a linear range of 80 nM – 20 µM with a limit of detection of 9.98 nM were obtained [85]. Wang et al. incorporated thymine acetic acid with gold nanoparticles and reduced graphene oxide for the detection of mercury by differential pulse voltammetry. A limit of detection of 1.5 ng/L and a linear concentration range of 10 ng/L – 1 µg/L were obtained [86].

Abdelhamid et al. on the other hand used thymine chitosan modified magnetic nanoparticles for the preconcentration of mercury ions prior to surface enhanced laser desorption – ionization mass spectrometry (SELDI–MS). The authors reported a limit of detection of 1 nM with a high selectivity and sensitivity to mercury ions and a possibility of application in real water samples [87].

Our group used different nucleobase hydrazides for the adsorption and affinity studies of different heavy metals. Guanine hydrazide was used to functionalize magnetic nanoparticles and the affinity towards the divalent heavy metal ions copper, cadmium and lead was evaluated. By applying square wave voltammetry, adsorption capacities and analytical performances towards the different heavy metals were assessed, and a sensitivity of 171.6 µA/µM towards copper ions was obtained [88]. In another study, the affinity between several nucleobase hydrazides and

arsenic was tested. Adsorption capacities, kinetics and the analytical performance were compared using magnetic nanoparticles functionalized with guanine hydrazide, adenine hydrazide or uracil hydrazide. Under the same conditions as before, the best analytical data were obtained with guanine hydrazide with a sensitivity of 1.92 $\mu A.\mu g^{-1}.L$ and a limit of detection of 1.6 µg/L [26].

2.6. Summary and perspectives

Aptamer-based technologies have been developed as effective sensing tools for various analytes. To the best of our knowledge, there hasn't been an update on heavy metal monitoring based on aptamers using nanoparticles in the past few years. Hence, this review presents the most recent metallic and metallic oxide nanoparticles combined with aptamer-based approaches for the monitoring of arsenic, cadmium, copper, lead, mercury, silver and platinum in various samples. It has been known that the affinity and specificity of aptamers towards their analytes are the main advantages supporting their use. Nonetheless, the advantages of nanoparticles and aptamers, as well as the new properties that result from combining the two technologies all contributed to enhance analytical performances of the proposed methods.

Even though gold nanoparticles are the most commonly used with aptamers for the detection of heavy metal ions reporting extremely low detection limits, several other nanoparticles have emerged as promising modifications to aptamers in heavy metal monitoring as well. Comparing the different techniques used, electrochemical methods have presented the best performance while offering their advantages over optical and spectrometric techniques. Despite all that, each proposed system was at best applied to one or a few environmental or biological samples. Numerous and complex matrices would probably impose further modifications and improvements to the developed sensors. It is worth noting that the use of

different nanomaterials such as quantum dots along with the nanoparticles, or even the use of bimetallic nanoparticles are proving to be promising in this field. Thus, we anticipate significant progress in developing novel aptamer-based sensors using various nanomaterials in the future.

References

[1] S.M. Shaban, D.H. Kim, Recent Advances in Aptamer Sensors, Sensors (Basel), 21 (2021) 979.

[2] K.G. Akpomie, J. Conradie, Banana peel as a biosorbent for the decontamination of water pollutants. A review, J Environmental Chemistry Letters, 18 (2020) 1085-1112.

[3] S. Sahin, M.O. Caglayan, Z. Ustundag, A review on nanostructure-based mercury (II) detection and monitoring focusing on aptamer and oligonucleotide biosensors, Talanta, 220 (2020) 121437.

[4] B. Bansod, T. Kumar, R. Thakur, S. Rana, I. Singh, A review on various electrochemical techniques for heavy metal ions detection with different sensing platforms, Biosens Bioelectron, 94 (2017) 443-455.

[5] M.R. Saidur, A.R. Aziz, W.J. Basirun, Recent advances in DNA-based electrochemical biosensors for heavy metal ion detection: A review, Biosens Bioelectron, 90 (2017) 125-139.

[6] M. Mittal, K. Kumar, D. Anghore, R. K Rawal, ICP-MS: Analytical method for identification and detection of elemental impurities, Curr Drug Discov Technol, 14 (2017) 106-120.

[7] G. Heltai, Z. Győri, I. Fekete, G. Halász, K. Kovács, A. Takács, L. Khumalo, M. Horváth, Application of flexible multi-elemental ICP-OES detection in fractionation of potentially toxic element content of solid environmental samples by a sequential extraction procedure, Microchem J, 149 (2019) 104029.

[8] F. Pan, Y. Yu, L. Yu, H. Lin, Y. Wang, L. Zhang, D. Pan, R. Zhu, Quantitative assessment on soil concentration of heavy metal–contaminated soil with various sample pretreatment techniques and detection methods, Environ Monit Assess 192 (2020) 1-8.

[9] S. Akram, R. Najam, G.H. Rizwani, S.A. Abbas, Determination of heavy metal contents by atomic absorption spectroscopy (AAS) in some medicinal plants from Pakistani and Malaysian origin, Pak J Pharm Sci, 28 (2015).

[10] P.R. Aranda, P.H. Pacheco, R.A. Olsina, L.D. Martinez, R.A. Gil, Total and inorganic mercury determination in biodiesel by emulsion sample introduction and FI-CV-AFS after multivariate optimization, J Anal Atom Spectrom, 24 (2009) 1441-1445.

[11] S.-H. Chen, Y.-X. Li, P.-H. Li, X.-Y. Xiao, M. Jiang, S.-S. Li, W.-Y. Zhou, M. Yang, X.-J. Huang, W.-Q. Liu, Electrochemical spectral methods for trace detection of heavy metals: A review, TrAC Trend. Anal. Chem, 106 (2018) 139-150.

[12] T.C. Chiu, C.C. Huang, Aptamer-functionalized nano-biosensors, Sensors (Basel), 9 (2009) 10356-10388.

[13] H. Modh, T. Scheper, J.G. Walter, Aptamer-Modified Magnetic Beads in Biosensing, Sensors (Basel), 18 (2018).

[14] S. Jain, S.P. Singh, C. Mayya, S. Majumdar, D.J.C.S. Bhatia, DNA aptamers in COVID-19 research, Current Science, 119 (2020) 1489.

[15] L. Wang, X. Peng, H. Fu, C. Huang, Y. Li, Z. Liu, Recent advances in the development of electrochemical aptasensors for detection of heavy metals in food, Biosens Bioelectron, 147 (2020) 111777.

[16] G. Sharma, A. Kumar, S. Sharma, M. Naushad, R. Prakash Dwivedi, Z.A. Alothman, G.T. Mola, Novel development of nanoparticles to bimetallic nanoparticles and their composites: A review, Journal of King Saud University - Science, 31 (2019) 257-269.

[17] Q. Ren, L. Ga, Z. Lu, J. Ai, T. Wang, Aptamer-functionalized nanomaterials for biological applications, Materials Chemistry Frontiers, 4 (2020) 1569-1585.

[18] X. Xu, X. Niu, X. Li, Z. Li, D. Du, Y. Lin, Nanomaterial-based sensors and biosensors for enhanced inorganic arsenic detection: A functional perspective, Sensors and Actuators B: Chemical, 315 (2020).

[19] T. Liu, Z. Chu, W. Jin, Electrochemical mercury biosensors based on advanced nanomaterials, Journal of Materials Chemistry B, 7 (2019) 3620-3632.

[20] S. Dolati, M. Ramezani, K. Abnous, S.M. Taghdisi, Recent nucleic acid based biosensors for Pb2+ detection, Sensors and Actuators B: Chemical, 246 (2017) 864-878.

[21] K. Mao, H. Zhang, Z. Wang, H. Cao, K. Zhang, X. Li, Z. Yang, Nanomaterial-based aptamer sensors for arsenic detection, Biosens Bioelectron, 148 (2020) 111785.

[22] W. Zhou, R. Saran, J. Liu, Metal Sensing by DNA, Chem Rev, 117 (2017) 8272-8325.

[23] L. Farzin, M. Shamsipur, S. Sheibani, A review: Aptamer-based analytical strategies using the nanomaterials for environmental and human monitoring of toxic heavy metals, Talanta, 174 (2017) 619-627.

[24] R.K.O. Sigel, H. Sigel, A Stability Concept for Metal Ion Coordination to Single-Stranded Nucleic Acids and Affinities of Individual Sites, Accounts of Chemical Research, 43 (2010) 974-984.

[25] H. Yu, M. Yuan, H. Cao, T. Ye, J. Yu, F. Xu, A computational investigation of the interaction between As3+ and deoxynucleotides, Molecular Simulation, 45 (2019) 769-776.

[26] S. Sawan, K. Hamze, A. Youssef, K. Bouhadir, A. Errachid, R. Maalouf, N. Jaffrezic-Renault, The use of voltammetry for sorption studies of arsenic (III) ions by magnetic beads functionalized with nucleobase hydrazide derivatives, Electroanalysis, 2021

[27] S. Kempahanumakkagari, A. Deep, K.H. Kim, S. Kumar Kailasa, H.O. Yoon, Nanomaterial-based electrochemical sensors for arsenic - A review, Biosens Bioelectron, 95 (2017) 106-116.

[28] Y. Zheng, C. Yang, F. Yang, X. Yang, Real-time study of interactions between cytosine–cytosine pairs in DNA oligonucleotides and silver ions using dual polarization interferometry, Anal Chem, 86 (2014) 3849-3855.

[29] G. Liu, Z. Li, J. Zhu, Y. Liu, Y. Zhou, J. He, Studies on the thymine–mercury–thymine base pairing in parallel and anti-parallel DNA duplexes, New J Chem, 39 (2015) 8752-8762.

[30] S. DasGupta, S.A. Shelke, N.-s. Li, J.A. Piccirilli, Spinach RNA aptamer detects lead (II) with high selectivity, Chem Comm, 51 (2015) 9034-9037.

[31] Y. Wu, S. Zhan, L. Wang, P. Zhou, Selection of a DNA aptamer for cadmium detection based on cationic polymer mediated aggregation of gold nanoparticles, Analyst, 139 (2014) 1550-1561.

[32] G. Aragay, A. Merkoçi, Nanomaterials application in electrochemical detection of heavy metals, Electrochimica Acta, 84 (2012) 49-61.

[33] M. Negahdary, Electrochemical aptasensors based on the gold nanostructures, Talanta, 216 (2020) 120999.

[34] S. Ebrahimi, R.E. Nahli, Nano-biosensors and Nano-aptasensors for Stimulant Detection, in: N. Dasgupta, S. Ranjan, E. Lichtfouse (Eds.) Environmental Nanotechnology: Volume 2, Springer International Publishing, Cham (2019)169-193.

[35] A.T. Ezhil Vilian, A. Shahzad, J. Chung, S.R. Choe, W.-S. Kim, Y.S. Huh, T. Yu, Y.-K. Han, Square voltammetric sensing of mercury at very low working potential by using oligomer-functionalized Ag@Au core-shell nanoparticles, Microchimica Acta, 184 (2017) 3547-3556.

[36] Y. Zhao, X. Xie, A Novel Electrochemical Aptamer Biosensor Based on DNAzyme Decorated Au@Ag Core-Shell Nanoparticles for Hg2+ Determination, Journal of the Brazilian Chemical Society, 29 (2018) 232-239.

[37] P. Miao, Y. Tang, L. Wang, DNA Modified Fe3O4@Au Magnetic Nanoparticles as Selective Probes for Simultaneous Detection of Heavy Metal Ions, ACS Appl Mater Interfaces, 9 (2017) 3940-3947.

[38] P. Butmee, J. Mala, C. Damphathik, K. Kunpatee, G. Tumcharern, M. Kerr, E. Mehmeti, G. Raber, K. Kalcher, A. Samphao, A portable selective electrochemical sensor amplified with Fe3O4@Au-cysteamine-thymine acetic acid as conductive mediator for determination of mercuric ion, Talanta, 221 (2021) 121669.

[39] B. Babamiri, A. Salimi, R. Hallaj, Switchable electrochemiluminescence aptasensor coupled with resonance energy transfer for selective attomolar detection of Hg(2+) via CdTe@CdS/dendrimer probe and Au nanoparticle quencher, Biosens Bioelectron, 102 (2018) 328-335.

[40] X. Fan, S. Wang, Z. Li, Y. Wang, X. Fan, L. Yu, An Electrochemiluminescence Biosensor for the Determination of Mercury Ion via Dual-Amplification Strategy, Journal of the Brazilian Chemical Society, 31 (2020) 2620-2627.

[41] D. Feng, P. Li, X. Tan, Y. Wu, F. Wei, F. Du, C. Ai, Y. Luo, Q. Chen, H. Han, Electrochemiluminescence aptasensor for multiple determination of Hg(2+) and Pb(2+) ions by using the MIL-53(Al)@CdTe-PEI modified electrode, Anal Chim Acta, 1100 (2020) 232-239.

[42] C. Wang, M. Chen, J. Wu, F. Mo, Y. Fu, Multi-functional electrochemiluminescence aptasensor based on resonance energy transfer between Au nanoparticles and lanthanum ion-doped cadmium sulfide quantum dots, Anal Chim Acta, 1086 (2019) 66-74.

[43] D.M. Wang, Q.Q. Gai, R.F. Huang, X. Zheng, Label-free electrochemiluminescence assay for aqueous Hg(2+) through oligonucleotide mediated assembly of gold nanoparticles, Biosens Bioelectron, 98 (2017) 134-139.

[44] Y. Peng, Y. Li, L. Li, J.J. Zhu, A label-free aptasensor for ultrasensitive Pb(2+) detection based on electrochemiluminescence resonance energy transfer between carbon nitride nanofibers and Ru(phen)3(2), J Hazard Mater, 359 (2018) 121-128.

[45] W. Tang, J. Yu, Z. Wang, I. Jeerapan, L. Yin, F. Zhang, P. He, Label-free potentiometric aptasensing platform for the detection of Pb(2+) based on guanine quadruplex structure, Anal Chim Acta, 1078 (2019) 53-59.

[46] Y. Wang, G. Zhao, Q. Zhang, H. Wang, Y. Zhang, W. Cao, N. Zhang, B. Du, Q. Wei, Electrochemical aptasensor based on gold modified graphene nanocomposite with different morphologies for ultrasensitive detection of Pb2+, Sensors and Actuators B: Chemical, 288 (2019) 325-331.

[47] S. Xu, X. Chen, G. Peng, L. Jiang, H. Huang, An electrochemical biosensor for the detection of Pb(2+) based on G-quadruplex DNA and gold nanoparticles, Anal Bioanal Chem, 410 (2018) 5879-5887.

[48] G. Zhao, C. Li, X. Wang, G. Liu, N.T.D. Thuy, A Reusable Electrochemical Aptasensor for the Sensitive Detection of Pb(II) with an Electrodeposited AuNP-Modified Electrode based on the Formation of a Target-Induced G- Quadruplex, International Journal of Electrochemical Science, 16 (2021) 150956.

[49] H. Wang, Y. Zhang, H. Ma, X. Ren, Y. Wang, Y. Zhang, Q. Wei, Electrochemical DNA probe for Hg(2+) detection based on a triple-helix DNA and Multistage Signal Amplification Strategy, Biosens Bioelectron, 86 (2016) 907-912.

[50] X. Zhang, C. Huang, Y. Jiang, Y. Jiang, J. Shen, E. Han, Structure-Switching Electrochemical Aptasensor for Single-Step and Specific Detection of Trace Mercury in Dairy Products, J Agric Food Chem, 66 (2018) 10106-10112.

[51] J. Ding, D. Zhang, Y. Liu, M. Yu, X. Zhan, D. Zhang, P. Zhou, An electrochemical aptasensor for detection of lead ions using a screen-printed carbon electrode modified with Au/polypyrrole composites and toluidine blue, Analytical Methods, 11 (2019) 4274-4279.

[52] Z. Tao, L. Wei, S. Wu, N. Duan, X. Li, Z. Wang, A colorimetric aptamer-based method for detection of cadmium using the enhanced peroxidase-like activity of Au-MoS2 nanocomposites, Anal Biochem, 608 (2020) 113844.

[53] L. Wang, F. Liu, N. Sui, M. Liu, W.W. Yu, A colorimetric assay for Hg(II) based on the use of a magnetic aptamer and a hybridization chain reaction, Microchimica Acta, 183 (2016) 2855-2860.

[54] D. Fan, Q. Zhai, W. Zhou, X. Zhu, E. Wang, S. Dong, A label-free colorimetric aptasensor for simple, sensitive and selective detection of Pt (II) based on platinum (II)-oligonucleotide coordination induced gold nanoparticles aggregation, Biosens Bioelectron, 85 (2016) 771-776.

[55] X. Liu, Z. Wu, Q. Zhang, W. Zhao, C. Zong, H. Gai, Single Gold Nanoparticle-Based Colorimetric Detection of Picomolar Mercury Ion with Dark-Field Microscopy, Anal Chem, 88 (2016) 2119-2124.

[56] M. Chen, M. Hassan, H. Li, Q. Chen, Fluorometric determination of lead(II) by using aptamer-functionalized upconversion nanoparticles and magnetite-modified gold nanoparticles, Mikrochim Acta, 187 (2020) 85.

[57] X. Niu, Y. Zhong, R. Chen, F. Wang, Y. Liu, D. Luo, A “turn-on” fluorescence sensor for Pb2+ detection based on graphene quantum dots and gold nanoparticles, Sensors and Actuators B: Chemical, 255 (2018) 1577-1581.

[58] Y. Wang, M. Lv, Z. Chen, Z. Deng, N. Liu, J. Fan, W. Zhang, A Fluorescence Resonance Energy Transfer Probe Based on DNA-Modified Upconversion and Gold Nanoparticles for Detection of Lead Ions, Front Chem, 8 (2020) 238.

[59] Y. Liu, Q. Ouyang, H. Li, M. Chen, Z. Zhang, Q. Chen, Turn-On Fluoresence Sensor for Hg(2+) in Food Based on FRET between Aptamers-Functionalized Upconversion Nanoparticles and Gold Nanoparticles, J Agric Food Chem, 66 (2018) 6188-6195.

[60] H. Tianyu, Y. Xu, N. Weidan, S. Xingguang, Aptamer-based aggregation assay for mercury(II) using gold nanoparticles and fluorescent CdTe quantum dots, Microchimica Acta, 183 (2016) 2131-2137.

[61] Z. Wu, H. Shen, J. Hu, Q. Fu, C. Yao, S. Yu, W. Xiao, Y. Tang, Aptamer-based fluorescence-quenching lateral flow strip for rapid detection of mercury (II) ion in water samples, Anal Bioanal Chem, 409 (2017) 5209-5216.

[62] Y. Lu, J. Zhong, G. Yao, Q. Huang, A label-free SERS approach to quantitative and selective detection of mercury (II) based on DNA aptamer-modified SiO2@Au core/shell nanoparticles, Sensors and Actuators B: Chemical, 258 (2018) 365-372.

[63] H. Ouyang, S. Ling, A. Liang, Z. Jiang, A facile aptamer-regulating gold nanoplasmonic SERS detection strategy for trace lead ions, Sensors and Actuators B: Chemical, 258 (2018) 739-744.

[64] L. Song, K. Mao, X. Zhou, J. Hu, A novel biosensor based on Au@Ag core-shell nanoparticles for SERS detection of arsenic (III), Talanta, 146 (2016) 285-290.

[65] Y. Wu, T. Jiang, Z. Wu, R. Yu, Novel ratiometric surface-enhanced raman spectroscopy aptasensor for sensitive and reproducible sensing of Hg(2), Biosens Bioelectron, 99 (2018) 646-652.

[66] H. Jin, D. Zhang, Y. Liu, M. Wei, An electrochemical aptasensor for lead ion detection based on catalytic hairpin assembly and porous carbon supported platinum as signal amplification, RSC Advances, 10 (2020) 6647-6653.

[67] L.H. Ma, H.B. Wang, B.Y. Fang, F. Tan, Y.C. Cao, Y.D. Zhao, Visual detection of trace lead ion based on aptamer and silver staining nano-metal composite, Colloids Surf B Biointerfaces, 162 (2018) 415-419.

[68] C. Song, B. Yang, Y. Zhu, Y. Yang, L. Wang, Ultrasensitive sliver nanorods array SERS sensor for mercury ions, Biosens Bioelectron, 87 (2017) 59-65.

[69] W. Xu, X. Zhou, J. Gao, S. Xue, J. Zhao, Label-free and enzyme-free strategy for sensitive electrochemical lead aptasensor by using metal-organic frameworks loaded with AgPt nanoparticles as signal probes and electrocatalytic enhancers, Electrochimica Acta, 251 (2017) 25-31.

[70] Y. Lu, X. Liang, C. Niyungeko, J. Zhou, J. Xu, G. Tian, A review of the identification and detection of heavy metal ions in the environment by voltammetry, Talanta, 178 (2018) 324-338.

[71] T. Jamshaid, E.T.T. Neto, M.M. Eissa, N. Zine, M.H. Kunita, A.E. El-Salhi, A. Elaissari, Magnetic particles: From preparation to lab-on-a-chip, biosensors, microsystems and microfluidics applications, TrAC Trends in Analytical Chemistry, 79 (2016) 344-362.

[72] Y. Liu, D. Zhang, J. Ding, K. Hayat, X. Yang, X. Zhan, D. Zhang, Y. Lu, P. Zhou, Label-Free and Sensitive Determination of Cadmium Ions Using a Ti-Modified Co3O4-Based Electrochemical Aptasensor, Biosensors (Basel), 10 (2020) 195.

[73] Y. Song, C. Guo, H. Ji, S. Zhang, M. Wang, L. He, D. Peng, Z. Zhang, Cu x O@DNA sphere-based electrochemical bioassay for sensitive detection of Pb(2), Mikrochim Acta, 185 (2018) 186.

[74] Y. Niu, G. Luo, H. Xie, Y. Zhuang, X. Wu, G. Li, W. Sun, Photoelectrochemical aptasensor for lead(II) by exploiting the CdS nanoparticle-assisted photoactivity of TiO2 nanoparticles and by using the quercetin-copper(II) complex as the DNA intercalator, Mikrochim Acta, 186 (2019) 826.

[75] L. Yang, B. An, X. Yin, F. Li, A competitive coordination-based immobilization-free electrochemical biosensor for highly sensitive detection of arsenic(v) using a CeO2-DNA nanoprobe, Chem Commun (Camb), 56 (2020) 5311-5314.

[76] S. Liu, B. Yu, S. Wang, Y. Shen, H. Cong, Preparation, surface functionalization and application of Fe3O4 magnetic nanoparticles, Adv Colloid Interface Sci, 281 (2020) 102165.

[77] Y. Liu, Z. Cai, L. Sheng, M. Ma, X. Wang, A magnetic relaxation switching and visual dual-mode sensor for selective detection of Hg(2+) based on aptamers modified Au@Fe3O4 nanoparticles, J Hazard Mater, 388 (2020) 121728.

[78] Z. Tao, Y. Zhou, N. Duan, Z. Wang, A Colorimetric Aptamer Sensor Based onthe Enhanced Peroxidase Activity of FunctionalizedGrapheneFe3O4-AuNPs for Detection ofLead (II) Ions, Catalysts 10 (2020) 600.

[79] Y. Shan, B. Wang, H. Huang, D. Jian, X. Wu, L. Xue, S. Wang, F. Liu, On-site quantitative Hg(2+) measurements based on selective and sensitive fluorescence biosensor and miniaturized smartphone fluorescence microscope, Biosens Bioelectron, 132 (2019) 238-247.

[80] C. Sun, R. Sun, Y. Chen, Y. Tong, J. Zhu, H. Bai, S. Zhang, H. Zheng, H. Ye, Utilization of aptamer-functionalized magnetic beads for highly accurate fluorescent detection of mercury (II) in environment and food, Sensors and Actuators B: Chemical, 255 (2018) 775-780.

[81] D. Wu, Y. Wang, Y. Zhang, H. Ma, X. Pang, L. Hu, B. Du, Q. Wei, Facile fabrication of an electrochemical aptasensor based on magnetic electrode by using streptavidin modified magnetic beads for sensitive and specific detection of Hg(2.), Biosens Bioelectron, 82 (2016) 9-13.

[82] J. Luo, D. Jiang, T. Liu, J. Peng, Z. Chu, W. Jin, High-performance electrochemical mercury aptasensor based on synergistic amplification of Pt nanotube arrays and Fe3O4/rGO nanoprobes, Biosens Bioelectron, 104 (2018) 1-7.

[83] M. Shamsipur, L. Farzin, M.A. Tabrizi, S. Sheibani, Functionalized Fe3O4 graphene oxide nanocomposites with hairpinaptamers for the separation and preconcentration of trace Pb2+frombiological samples prior to determination by ICP MS, Materials Science and Engineering C 77 (2017) 459–469.

[84] S. Rahnama, S. Shariati, F. Divsar, Selective aptamer conjugation to silver-coated magnetite nanoparticles for magnetic solid-phase extraction of trace amounts of Pb2+ ions, RSC Advances, 11 (2021) 4971-4982.

[85] H. Yuan, G. Sun, W. Peng, W. Ji, S. Chu, Q. Liu, Y. Liang, Thymine-Functionalized Gold Nanoparticles (Au NPs) for a Highly Sensitive Fiber-Optic Surface Plasmon Resonance Mercury Ion Nanosensor, Nanomaterials (Basel), 11 (2021).

[86] N. Wang, M. Lin, H. Dai, H. Ma, Functionalized gold nanoparticles/reduced graphene oxide nanocomposites for ultrasensitive electrochemical sensing of mercury ions based on thymine-mercury-thymine structure, Biosens Bioelectron, 79 (2016) 320-326.

[87] H.N. Abdelhamid, Y.C. Lin, H.-F. Wu, Thymine chitosan nanomagnets for specific preconcentration of mercury(II) prior to analysis using SELDI-MS, Microchimica Acta, 184 (2017) 1517-1527.

[88] S. Sawan, K. Hamze, A. Youssef, R. Boukarroum, K. Bouhadir, A. Errachid, R. Maalouf, N. Jaffrezic-Renault, Voltammetric study of the affinity of divalent heavy metals for guanine functionalized iron oxide nanoparticles, Monatshefte für Chemie - Chemical Monthly, 152 (2021) 229-240.

[89] S.M. Taghdisi, N.M. Danesh, P. Lavaee, M. Ramezani, K. Abnous, An electrochemical aptasensor based on gold nanoparticles, thionine and hairpin structure of complementary strand of aptamer for ultrasensitive detection of lead, Sensors and Actuators B: Chemical, 234 (2016) 462-469.

[90] M. Adabi, Detection of lead ions using an electrochemical aptasensor, Nanomed Res J 4(2019) 247-252.

[91] J. Ding, Y. Liu, D. Zhang, M. Yu, X. Zhan, D. Zhang, P. Zhou, An electrochemical aptasensor based on gold@polypyrrole composites for detection of lead ions, Microchim Acta, 185 (2018) 545.

[92] Y. Zhang, C. Zhang, R. Ma, X. Du, W. Dong, Y. Chen, Q. Chen, An ultra-sensitive Au nanoparticles functionalized DNA biosensor for electrochemical sensing of mercury ions, Mater Sci Eng C Mater Biol Appl, 75 (2017) 175-181.

[93] L.-L. He, L. Cheng, Y. Lin, H.-F. Cui, N. Hong, H. Peng, D.-R. Kong, C.-D. Chen, J. Zhang, G.-B. Wei, H. Fan, A sensitive biosensor for mercury ions detection based on hairpin hindrance by thymine-Hg(II)-thymine structure, Journal of Electroanalytical Chemistry, 814 (2018) 161-167.

[94] H. Jin, M. Zhang, M. Wei, J.H. Cheng, A voltammetric biosensor for mercury(II) using reduced graphene oxide@gold nanorods and thymine-Hg(II)-thymine interaction, Microchim Acta, 186 (2019) 264.

[95] A. Mohammadi, E. Heydari-Bafrooei, M.M. Foroughi, M. Mohammadi, Heterostructured Au/MoS2-MWCNT nanoflowers: A highly efficient support for the electrochemical aptasensing of solvated mercuric ion, Microchemical Journal, 158 (2020).

[96] F. Maatouk, M. Maatouk, K. Bekir, H. Barhoumi, A. Maaref, H. Ben Mansour, An electrochemical DNA biosensor for trace amounts of mercury ion quantification, J Water Health, 14 (2016) 808-815.

[97] L. Zhao, Y. Wang, G. Zhao, N. Zhang, Y. Zhang, X. Luo, B. Du, Q. Wei, Electrochemical aptasensor based on Au@HS-rGO and thymine-Hg2+-thymine structure for sensitive detection of mercury ion, Journal of Electroanalytical Chemistry, 848 (2019) 113308.

[98] J. Wang, J. Guo, J. Zhang, W. Zhang, Y. Zhang, Signal-on electrochemical sensor for the detection of two analytes based on the conformational changes of DNA probes, Analytical Methods, 8 (2016) 8059-8064.

[99] Y. Shi, G. Zhang, J. Li, Y. Zhang, Y. Yu, Q. Wei, Photoelectrochemical determination of Hg(II) via dual signal amplification involving SPR enhancement and a folding-based DNA probe, Microchimica Acta, 184 (2017) 1379-1387.

[100] L. Cui, J. Wu, H. Ju, Label-free signal-on aptasensor for sensitive electrochemical detection of arsenite, Biosens Bioelectron, 79 (2016) 861-865.

[101] A.A. Ensafi, F. Akbarian, E. Heydari-Soureshjani, B. Rezaei, A novel aptasensor based on 3D-reduced graphene oxide modified gold nanoparticles for determination of arsenite, Biosens Bioelectron, 122 (2018) 25-31.

[102] T. Talifhani Mushiana, N. Mabuba, A.O. Idris, G.M. Peleyeju, B.O. Orimolade, D. Nkosi, R.F. Ajayi, O.A. Arotiba, An aptasensor for arsenic on a carbon-gold bi-nanoparticle platform, Sensing and Bio-Sensing Research, 24 (2019) 100280.

[103] C.T. Fakude, O.A. Arotiba, N. Mabuba, Electrochemical aptasensing of cadmium (II) on a carbon black-gold nano-platform, Journal of Electroanalytical Chemistry, 858 (2020) 113796.

[104] Y. Liu, Y. Lai, G. Yang, C. Tang, Y. Deng, S. Li, Z. Wang, Cd-Aptamer Electrochemical Biosensor Based on AuNPs/CS Modified Glass Carbon Electrode, Journal of Biomedical Nanotechnology, 13 (2017) 1253-1259.

[105] M. Yuan, Z. Song, J. Fei, X. Wang, F. Xu, H. Cao, J. Yu, Aptasensor for lead(II) based on the use of a quartz crystal microbalance modified with gold nanoparticles, Microchimica Acta, 184 (2017) 1397-1403.

[106] S. Jia, C. Bian, J. Sun, J. Tong, S. Xia, A wavelength-modulated localized surface plasmon resonance (LSPR) optical fiber sensor for sensitive detection of mercury(II) ion by gold nanoparticles-DNA conjugates, Biosens Bioelectron, 114 (2018) 15-21.

[107] Y. Qi, F.R. Xiu, G. Yu, L. Huang, B. Li, Simple and rapid chemiluminescence aptasensor for Hg(2+) in contaminated samples: A new signal amplification mechanism, Biosens Bioelectron, 87 (2017) 439-446.

[108] H.-B. Wang, L.-H. Ma, B.-Y. Fang, F. Tan, Y.-C. Cao, Y.-D. Zhao, X.-B. Hu, Visual detection of Pb2+ using strip biosensor based on PS2M aptamer and sensitivity enhancement probe, Sensors and Actuators B: Chemical, 261 (2018) 307-315.

[109] S. Sajed, M. Kolahdouz, M.A. Sadeghi, S.F. Razavi, High-Performance Estimation of Lead Ion Concentration Using Smartphone-Based Colorimetric Analysis and a Machine Learning Approach, ACS Omega, 5 (2020) 27675-27684.

[110] D. Wang, C. Ge, K. Lv, Q. Zou, Q. Liu, L. Liu, Q. Yang, S. Bao, A simple lateral flow biosensor for rapid detection of lead(ii) ions based on G-quadruplex structure-switching, Chem Commun (Camb), 54 (2018) 13718-13721.

[111] A.N. Berlina, A.V. Zherdev, S.M. Pridvorova, M.S. Gaur, B.B. Dzantiev, Rapid Visual Detection of Lead and Mercury via Enhanced Crosslinking Aggregation of Aptamer-Labeled Gold Nanoparticles, J Nanosci Nanotechnol, 19 (2019) 5489-5495.

[112] L. Tan, Z. Chen, C. Zhang, X. Wei, T. Lou, Y. Zhao, Colorimetric Detection of Hg(2+) Based on the Growth of Aptamer-Coated AuNPs: The Effect of Prolonging Aptamer Strands, Small, 13 (2017) 1603370.

[113] L. Yao, J. Teng, H. Qu, M. Zhu, L. Zheng, F. Xue, W. Chen, Paper matrix based array for rapid and sensitive optical detection of mercury ions using silver enhancement, Microchimica Acta, 184 (2016) 569-576.

[114] X. Song, Y. Wang, S. Liu, X. Zhang, H. Wang, J. Wang, J. Huang, Colorimetric and visual mercury(II) assay based on target-induced cyclic enzymatic amplification, thymine-Hg(II)-thymine interaction, and aggregation of gold nanoparticles, Microchim Acta, 186 (2019) 105.

[115] A.G. Memon, X. Zhou, J. Liu, R. Wang, L. Liu, B. Yu, M. He, H. Shi, Utilization of unmodified gold nanoparticles for label-free detection of mercury (II): Insight into rational design of mercury-specific oligonucleotides, J Hazard Mater, 321 (2017) 417-423.

[116] W. Xiao, M. Xiao, Q. Fu, S. Yu, H. Shen, H. Bian, Y. Tang, A Portable Smart-Phone Readout Device for the Detection of Mercury Contamination Based on an Aptamer-Assay Nanosensor, Sensors (Basel), 16 (2016) 1871.

[117] Y. Qi, J. Ma, X. Chen, F.R. Xiu, Y. Chen, Y. Lu, Practical aptamer-based assay of heavy metal mercury ion in contaminated environmental samples: convenience and sensitivity, Anal Bioanal Chem, 412 (2020) 439-448.

[118] D. Zhang, Y. Liu, J. Ding, K. Hayat, X. Zhan, P. Zhou, D. Zhang, Label-free colorimetric assay for arsenic(III) determination based on a truncated short ssDNA and gold nanoparticles, Mikrochim Acta, 188 (2021) 38.

[119] N.L. Thao Nguyen, C.Y. Park, J.P. Park, S.K. Kailasa, T.J. Park, Synergistic molecular assembly of an aptamer and surfactant on gold nanoparticles for the colorimetric detection of trace levels of As3+ ions in real samples, New Journal of Chemistry, 42 (2018) 11530-11538.

[120] K. Matsunaga, Y. Okuyama, R. Hirano, S. Okabe, M. Takahashi, H. Satoh, Development of a simple analytical method to determine arsenite using a DNA aptamer and gold nanoparticles, Chemosphere, 224 (2019) 538-543.

[121] L. Xu, J. Liang, Y. Wang, S. Ren, J. Wu, H. Zhou, Z. Gao, Highly Selective, Aptamer-Based, Ultrasensitive Nanogold Colorimetric Smartphone Readout for Detection of Cd(II), Molecules, 24 (2019) 2745.

[122] Y. Gan, T. Liang, Q. Hu, L. Zhong, X. Wang, H. Wan, P. Wang, In-situ detection of cadmium with aptamer functionalized gold nanoparticles based on smartphone-based colorimetric system, Talanta, 208 (2020) 120231.

[123] M. Zhou, T. Lin, X. Gan, Colorimetric aggregation assay for silver(I) based on the use of aptamer modified gold nanoparticles and C-Ag(I)-C interaction, Microchimica Acta, 184 (2017) 4671-4677.

Table 1 Electrochemical aptasensors using gold nanoparticles for the detection of heavy metals

Modification	Aptamer	Technique	Heavy metal	LOD (nM)	Linear range (nM)	Ref
Au NPs	5′-CACCCACCCAC-$(CH_2)_6$-SH-3 ′; 5′-GGGTGGGTGGGTGGGT-3	Chronocoulometry	Pb^{2+}	4.2 $\times 10^{-3}$	0.01 – 200	[47]
Au NPs	5’-TGGGTGGGTGGGTGGG-3’; 5’-NH_2-CCCACCCACCCTTTTT-3’; 5’-NH_2-CCCACCCACCCACCCA-3’; 5’-NH_2-CCCACCCACCCATTTT-3’; 5’-NH_2-CCCACCCACCCTTTTT-3’; 5’-NH_2-CCCACCCACCTTTTTT-3’; 5’-NH_2-CCCACCCACTTTTTTT-3’; 5’-NH_2-CCCACCCATTTTTTTT-3’;	EIS	Pb^{2+}	0.0046	4.83 – 480	[48]

	5’- AAAAATGGGTGTGA-3’					
Au NPs-thionine	5'-GGGTGGGTGGGTGGGT-3'; 5'-Thiol-GAGGACCCACCCACCCACCCTCCTCAA-Thiol-3'	DPV	Pb^{2+}	0.312	0.6 – 50	[89]
Au NPs-thionine	5’-GGGTGGGTGGGTGGGT-3’; 5’-Thiol-GAGGACCCACCCACCCACCCTCCTCAAThiol-3’	DPV	Pb^{2+}	0.374	1 – 40	[90]
Au NPs-polypyrrole	5’-GGGTGGGTGGGTGGGT-3’; 5’-CCACCCACCC–$(CH_2)_6$–SH-3’	DPV	Pb^{2+}	2.9	2.4 – 120	[51]
Au NPs-polypyrrole	5-GGGTGGGTGGGTGGGT-3	DPV	Pb^{2+}	0.36	0.5 – 10	[91]
Au NPs@GO	5’-HS-TTTTTT CGATAACTCACTATrAGGA AGAGATG-3’; 5’-HS-TTTTTTCATCTCTTCTCCGA GCCGGTCGAAATAGTGAGT -3’	Amperometry	Pb^{2+}	1.67×10^{-3}	5×10^{-3} – 1000	[46]
Au NPs	HS-CACCCTCCCAC- 3’;	Potentiometry	Pb^{2+}	8.5	0.01 –	[45]

	HS-GGGTGGGTGGGTGGGTGGGT- 5’			$\times 10^{-3}$	1000	
Au NPs and QD	5’-COOH-$(CH_2)_{10}$-AAA AAA AAA GGG G-SH-3’ 5’-CCC CAA AAA A-3’	ECL	Pb^{2+}	0.24	0.1 – 10000	[41]
Au NPs and CNNF	5′-SH-$(CH_2)_6$-TTTTTTGTATACCCACCCACCCACCCATGA-3′ 5′-TCATGGGTGGGTGGGTGGGTATAC-3′	ECL	Pb^{2+}	4×10^{-5}	1 – 1000	[44]
Au NPs	5′-SH-$(CH_2)_6$-TTCTTTCTTCGCGTTGTTTGTT-MB-3′	SWV	Hg^{2+}	0.62 $\times 10^{-6}$	1×10^{-6} – 1	[50]
Au NPs	5′-SH-AAAAAAAAAAAAAAACGCGCG-3′; 5′-TTTTTTTTTTTTTTT-3′; 5′-SH-CGCGCGCGCGCG-3′	EIS	Hg^{2+}	0.05	0 – 200	[92]
Au NPs	5'-HS-GCGCGCGCCCTTTTTCCCCCCCCCCGCGCGCGC biotin-3'; 5'-FAM-GCGCGCGCCCTTTTTCCCCCCCCCCGCGCGCGC-Dabcyl-3'; 5'-	DPV	Hg^{2+}	0.21 $\times 10^{-3}$	0.35 $\times 10^{-3}$– 3.5	[93]

	TTTTGGGCGAACACACAC-3'; 5'-SH-TTTTTTTTTGGATTTTTTTTGACGATTTTTTT-MB-3'					
rGO/ Au nanorods	5'-SHTTTTTT T-3'; 5'-biotin-TTT TTT T-3'	DPV	Hg^{2+}	0.24	1 – 200	[94]
Au-BSA-rGO	5'-CTTCTTCCCCCCCCTTCTTC-3'	DPSV	Hg^{2+}	0.03	0.1 – 130	[49]
Fe_3O_4@Au NPs	5'-SH-AAAATCACCCATGAGGCATCTTTAGCG-3'; 5'- Fc-TCATCCGTGAT-3'; 5'- MB-CGCTTTAGATG-3'	SWV	Hg^{2+}	1.7	10 – 100	[37]
Ag@Au core shell	5'-CCC CCC CCC CCC TTC TTT CTT CCC CTT GTT TGT T-3'	SWV	Hg^{2+}	6×10^{-3}	0.01 – 0.16	[35]
Au@Ag core shell	5'-SH-$(CH_2)_6$-AAA ATT TTG CTT TGG TTT-3'; 5'-SH-$(CH_2)_6$-AAA AAT TTC CTT TGC TTT-3'; 5'-SH-(CH2)6-GGG TAG GGC GGG TTG GGT-3'	SWV	Hg^{2+}	2.99×10^{-3}	9.97×10^{-3} – 99.7	[36]
Au/MoS_2-	5'-SH-C6-CGGCTTTTGTTTT-	DPV	Hg^{2+}	0.05	0.1 –	[95]

MWCNT	3’				1000	
Au-GSH-cysteine	5’-NH2-(CH2)6-ATTTGTTCATGCCT-3’	DPV	Hg^{2+}	0.05	0.05 – 100	[96]
Au@HS-rGO	5′-SH-(CH2)6-TTGCTCTCTCGTT	DPV	Hg^{2+}	0.38	1 – 200	[97]
Au/MB/ferrocene	5'-SH-(CH2)6-CGTGCTTTCTGTCCCCTCTGTT TGCTCG-Fc-3'	DPV	Hg^{2+}	0.05	0.1 – 30	[98]
Au NPs and QD	5’-CCC CAA AAA A-3’ 5’-TTT TTT AAA ATT TTT T-SH-3’	ECL	Hg^{2+}	4.1 $\times10^{-3}$	0.01 – 0.1 $\times10^{-3}$	[41]
Fe_3O_4@SiO_2/dendrimers/QD + Au	5’-TTCTTTGTTCCCCTTCTTTGTT-NH2-3’; 5’-AACAAAGAACCCCCCCCCC-(CH2)3-SH-3’	ECL	Hg^{2+}	2 $\times10^{-9}$	20 $\times10^{-9}$ – 2000	[39]
Au NPs and QD	5’-CCA ACC ACA CCA ACC(CH2)6-NH2-3’; 5’-GGT TGG TGT GGT TGG TTC TTT CTT CCC TTG TTTGTT(CH2)6-SH-3’; 5’-SH-(CH2)6CAT ATC C-3’	ECL	Hg^{2+}	0.3 $\times10^{-3}$	1 $\times10^{-3}$ –10000	[42]

Au NPs	5’-TTCG TGTT GTGT TTCC AAA GGAT TCTC TACT CGTA-3’	ECL	Hg^{2+}	2×10^{-3}	0 – 0.2	[43]
Au NPs	5’-SH-(-CH2)6-TTGCTCTCTCGTT-(-CH2)6-NH2-3’; 5’-TTCGTGTGTGCTT-3’	ECL	Hg^{2+}	0.2×10^{-4}	1×10^{-3} – 100	[40]
Au@Ag-MoS_2 nanohybrid and QD	Calf thymus DNA	PEC	Hg^{2+}	5×10^{-3}	0.01-100	[99]
Au NPs	5’-HS-GGTAATACGACTCACTATA GGGAGATACCAGCTTATTC AATTTTAC AGAACAACCAACGTCGCTC CGGGTACTTCTTCATCGAG A- TAGTAAGTGCAATCT-3′	DPV	As^{3+}	0.15	0.2 – 100	[100]
3D-rGO-Au	5’-GGTAATACGACTCACTATA GGGAGATACCAGCTTATTC AAT TTTACAGAACAACCAACGT CGCTCCGGGTACTTCTTCAT CGAGATAGT	EIS	As^{3+}	1.9×10^{-6}	5.07×10^{-6} – 4×10^{-4}	[101]

	AAGTGCAATCT-3’					
Carbon Au binanoparticles	5’-HS-GGTAATACGACTCACTATAGGG AGATACCAGCTTATTCAATTTTACAGAACAACCAACGTCGCTCCGGGT ACTTCTTCATCGAGATAGTAAGTGCAATCT-3’	SWV	As^{3+}	1.22	6.7 – 1334	[102]
Au NPs– CB	5’HS$(CH_2)_6$GGACTGTTGTGGTATTATTTTTGG TTGTGCAGTATG3’	SWV	Cd^{2+}	1.2	8.9 – 400	[103]
Au NPs/CS	5’-HS-$(CH_2)_6$-ACCGACCGTGCTGGACTCTGGACTGTTGTGGTATTATTTTTGGTTGTGCAGTATGAGCGAGCGTTGCG-3’	DPV	Cd^{2+}	0.0499 5×10^{-3}	0.001 – 100	[104]
Fe_3O_4@Au NPs	5’-SH-AAAATCACCCATGAGGCATCTTTAGCG-3’; 5’- Fc-TCATCCGTGAT-3’; 5’- MB-CGCTTTAGATG-3’	SWV	Ag^{+}	3.4	0 – 400	[37]
Au/MB/ferrocene	5'-SH-$(CH_2)_6$-CTCTCTTCTCTTCATTTTTCAACA	DPV	Ag^{+}	0.05	0.1 – 40	[98]

	CAACACAC-MB-3'					

CNNF: carbon nitride nanofibers, GO: graphene oxide, QD: quantum dots, rGO: reduced graphene oxide, BSA: bovine serum albumin, MoS_2: molybdenum disulfide, MWCNT: multiwalled carbon nanotubes, GSH: glutathione, HS: thiol, MB: methylene blue, CB: carbon black, CS: chitosan.

Table 2 Non-electrochemical aptasensors using gold nanoparticles for the detection of heavy metals

Modification	Aptamer	Technique	Heavy metal	LOD (nM)	Linear range (nM)	Ref
Au NPs	5'-SH-$(CH_2)_6$-TTTTTTACCCAGGGTGGGTGGGTGGGT-3'; 5'-SH-$(CH_2)_6$-TTTTTTACCCACCC-3'	QCM	Pb^{2+}	4	5 – 200	[105]
Au@Fe_3O_4 NPs	5'-SH C6-CGGCTTTTGTTTT-3'	MRS	Hg^{2+}	2.7	10 – 100 100 – 5000	[77]
Au NPs	5'-GGTTGGTGTGGTGGTTGGT-GTTGG-3'	SERS	Pb^{2+}	-	various	[63]
Au@Ag NPs	5′Cy3-TTC TTT GTT CCC CTT CTT TGT TCC CCC CCC CC-SH-3′; 5′Rox-AAC AAA GAA-3′	SERS	Hg^{2+}	0.4 $\times 10^{-3}$	0.001 – 1	[65]
SiO_2@Au core/shell	5'-HS-(CH2)6-TTTTTTTTTTGGGGGGGGAAAAAAAA-3'	SERS	Hg^{2+}	10	10 – 10^6	[62]
Au@Ag NPs	5'-GGTAATACGACTCACTATAGGGAGATACCAGCTTATTCAA	SERS	As^{3+}	1.33	6.7 – 133	[64]

	TTTT-ACAGAACAACCAACGTCGCTCCGGGTACTTCTTCATCGAGATAGTAAG- TGCAATCT-3’					
Au NPs	5’-SH-(CH2)6-GATTCCGTGCATGACTCAG-3’; 5’-SH-(CH2)6-CTGTGTCTTGCTCGGTATC-3’	LSPR	Hg^{2+}	0.7	1 – 50	[106]
(+)Au NPs	5′-TTT TTT TTT T-3′; 5′-GGT TGG TGT GGT TGG-3′; 5′-CTC ACG TAA ACT CAC GTA AA-3′	Chemiluminescence	Hg^{2+}	0.016	0.62 – 120 120 – 1200	[107]
Au NPs	13 different aptamers	Visual	Pb^{2+}	2.5	10 – 500 500 – 25000	[108]
Au NPs	5’-GGTTGGGCGGGATGGGTG-3’	Colorimetry	Pb^{2+}	2.4	24 – 9660	[109]
Au NPs	5’-TCGGGTGTGGGTG GGTGGTGGTGGTTGTGGTGG TGGTGG-3’; 5’-CACCC ACACC CGATT TTTTT TTTTT-SH-3’; 5’-CCACC ACCAC CACAA CCACC ACCAC CACA-3’; 5’-TCGGG TGTGG GTGTC	Colorimetry	Pb^{2+}	25	10 – 500	[110]

	GGGTG TGGGTG-3’					
Au NPs	HS-$(CH_2)_6$-GGGTGGGTGGGTGG	Colorimetry	Pb^{2+}	0.58 $\times 10^3$	-	[111]
Fe_3O_4-Au NPs-graphene	5’-biotin-GGGTGGGTGGGTGGGT-3’; 3’-CCACCCTCCCAC-5’	Colorimetry	Pb^{2+}	3	4.8 – 1400	[78]
Au NPs	5’-TTT TTT TT-3’; 5’-TTT TTT TTT TTT TTT-3’; 5’-AAA AAA AAA AAA AAA-3’; 5’-AAA AAA AAA ATT TTT TTT TTT TTT T-3’; 5’-AAA AAA AAA AAA AAA AAA AAA AAA A-3’; 5’-AAA AAA AAA AAA AAA AAA AA-3’; 5’-AAA AAA AAA AAA AAA AAA AAA AAA AAA A-3’; 5’-AAA AAA AAA AAA AAA AAA AAA ATT TTT TTT TTT TTT TAA AAA AAA AAA AAA AAA AAA AA-3’; 5’-AAA AAA AAA AAA AAA AAA AAA AAA AAA AAA	Colorimetry	Hg^{2+}		various	[112]

	AAA AAA AAA AAA AAA AAA AAA AAA AAA AA-3’					
Au NPs	5′SH$(CH_2)_6$TCAGTTTGGC3′; 5′SH$(CH_2)_6$GCCTTTCTGA3′	Colorimetry	Hg^{2+}	1.4 $\times10^{-3}$	0.005 – 25	[55]
Au NPs	HS-$(CH_2)_6$-GGGTGGGTGGGTGG	Colorimetry	Hg^{2+}	2.49 $\times10^{3}$	-	[111]
Au NPs	5’-Biotin-TTC GCT CTC TTT GTG TTT TTG CAT GT-3’; 5’-SH-ACA CGC CAT CAA GCT TTA ACT CAT AGT GGC GTG TCG CG-3’	Colorimetry	Hg^{2+}	2.49 $\times10^{-3}$	2.49 $\times10^{-2}$ – 2.49	[113]
Au NPs	5’-GGTCACGCTTTCTTCTTTCTTTC-3’ 5’- GAA AGC GTG ACA CAG-3’ 5’- GTT TGT TTG TTG TTA GCG TGA CGG TC-3’ 5’- SH-TTT CAC GCT TTC-3’	Colorimetry	Hg^{2+}	0.9	1 – 10000	[114]
Au NPs	5’-TCA TGT TTG TTT GTT GGC CCCCCT TCT TTC TTA-3’; 5’-TTT GTT TGT TGG CCC CCC TTC TTT CTT A-3’	Colorimetry	Hg^{2+}	15	50 – 300	[115]

Au NPs	5’-AAAAAAAAAATTCTTTCTTCCCCTTGTTTGTT-3’	Colorimetry	Hg^{2+}	1.39	5 – 159	[116]
cationic AuNPs	5’-TTT TTT TTT T-3’; 5’-CCT CCC TCC TTT TCCACCCACC-3’; 5’-CCA ACCACA C -3’	Colorimetry	Hg^{2+}	0.049	0.82 – 62	[117]
Au/Fe_3O_4	5’-SH-TTTCTTTCTTCCCCCCTTGTTTGTTT-3’; 3’-AAAGAAAGAAGGGGGGAACAAACAAACATCGATTGTGTCCCCCCTTC-5’; 5’-GTAGCTAACACAGGGGGGAAGTTTCTTTCTTCCCCCCTTGTTTGTTT-3’	Colorimetry	Hg^{2+}	0.7	1 – 300	[53]
Au NPs	5’-TCGAGATAGTAAGTGCAATCT-3’	Colorimetry	As^{3+}	2.4	13 – 400 400 – 1335	[118]
CTAB-AuNPs	5’-GGTAATACGCTCACTATAGGGAGATACCAGCTTATTCAATTTTACAGAACAAC	Colorimetry	As^{3+}	225	0 – 1335	[119]

	CAACGTCGCTCCGGGTACTT CTTCATCGAGATAGTAAGTG CAATCT-3’					
AuNPs	5’GGTAATACGACTCACTATA GGGAGATACCAGCTTATTCA ATTTTACAGAACAACCAACG TCGCTCCGGGTACTTCTTCAT CGAGATAGTAAGTGCAATCT-3’	Colorimetry	As^{3+}	2100	1000 – 10000	[120]
Au NPs	5’-TTTTTTTTTT-3’	Colorimetry	Cd^{2+}	8.9×10^{-3}	8.9×10^{-3} – 3.5	[121]
Au NPs	5’-ACCGACCGTGCTGGACTCTG GACTGTTGTGG. TATTATTTTTGGTTGTGCAGT ATGAGCGAGCGTTGCG-3’	Colorimetry	Cd^{2+}	9.9	17.8 – 178	[122]
Au-MoS_2	5′-biotin-ACC GAC CGT GCT GGA CTC TGG ACT GTT GTG GTA TTA TTT TTG GTT GTG CAG TAT GAG CGA GCG TTG CG-3’; 5′–SH– CGC AAC GCT CGC TCA TAC TGC ACA ACC AAA -3’	Colorimetry	Cd^{2+}	6.2	8.9 – 4448	[52]
Au NPs	5’-CCCC CCCCCCCCCCCCCCCCC	Colorimetry	Ag^{+}	0.77	1 – 500	[123]

	CCCCC-3’					
Au NPs and magnetic beads	5’-ATAGACCGCTGTGTGACGCAACACTCTAT-3’ 5’-ATAGACCGCTGTGTGACGCAAGACTGTAT-3’	Colorimetry	Pt^{2+}	150	600 – 12500	[54]
UCNPs-MNPs-GNPs	5’-Biotin-CGATCA CTA ACTATr AGG AAG AGATG-HS-3’; 5’-NH2-TGA GTG ATA AAG CTG GCC GAG CCT CTTCTC TAC-3’	Fluorometry	Pb^{2+}	5.7	25 – 1400	[56]
Au NPs and QD	5’-/3ThioMC3-D/CGATAACTCACTATrAGGAAGAGATG-3’; 5’-/5AmMC6/CATCTCTTCTCCGAGCCGGTCGA-AATAGTGAGT-3’	Fluorometry	Pb^{2+}	16.7	50 – 4000	[57]
AuNP and UCNP	5’>AAGGGT GGGT GGGT<3’; 5’>AAAAA AAAAA AAAAA AAAAA TTTTT CACCC TCCC AC <3’	Fluorometry	Pb^{2+}	4.1	0 – 50	[58]
Au NPs	5′ - b i o t i n -	Fluorometry	Hg^{2+}	0.65	0.65 –	[61]

	AAAAAAAAAATTCTTTCTTC CCCTTGTTTGTT-3′; 5′-biotin-AAAAAAAAAACACA AACAAGGCCAACA-3′	ry			214.4	
Au NPs	5'NH2C6-CTA CAG TTT CAC CTT TTC CCC CGT TTT GGT GTT T-3'; 5′ SH C6-GAA ACT GTA G-3'	Fluorometry	Hg^{2+}	60	200 – 20000	[59]
Au NPs and QD	5'-TTTTTTTTTT-3'	Fluorometry	Hg^{2+}	2.5 $\times 10^{-3}$	0.05 – 1	[60]

QCM: quartz crystal microbalance, MRS: magnetic relaxation switching, SERS: surface enhanced Raman spectroscopy, SiO_2: silica, CTAB: cethyltrimetylammonium bromide, LSPR: localized surface plasma resonance, UCNP: upconversion nanoparticles, MNP: magnetic nanoparticles, GNP: gold nanoparticles.

Chapter III: Voltammetric study of the affinity of divalent heavy metals for guanine functionalized iron oxide nanoparticles

Introduction

Guanine is one of the natural nucleobases that has been exploited extensively along with its derivatives. Binding of heavy metals to guanine is known to depend on the heavy metal itself, but it mainly involves the carbonyl oxygen O(6) and/or the imidazolyl nitrogen N(7) of guanine. Consequently, these nucleobases are gaining wide popularity in heavy metal sensing considering the advantages of biodegradability, selectivity and ease of synthesis.

Thus, iron oxide nanoparticles with a homogeneous size distribution of 45 nm and spherical shape were prepared following a modified Massart's method, after which they were coated with (3-aminopropyl)triethoxysilane and functionalized with the novel material, *3-(2-amino-6-oxo-1,6-digydro-9H-purin-9-yl)propane hydrazide* also known as guanine hydrazide (GH). The nanoparticles were characterized using X-ray Diffraction (XRD), Energy Dispersive X-ray Spectroscopy (EDX), Scanning Electron Microscopy (SEM) and Fourier Transform Infrared Spectroscopy (FTIR). Guanine hydrazide was characterized by FTIR, Hydrogen Nuclear Magnetic Resonance (^{1}H NMR), Carbon Nuclear Magnetic Resonance (^{13}C NMR) and High-Resolution Mass Spectroscopy (HRMS), and the successful functionalization of the nanoparticles was confirmed using FTIR.

The interaction of the divalent heavy metal ions cadmium, copper and lead with guanine hydrazide was evaluated electrochemically using square wave voltammetry. The functionalized nanoparticles were used to modify the surface of a Boron Doped Diamond electrode, and the signal decreased with increasing heavy metal concentration. Adsorption isotherms using the Langmuir and Freundlich models were examined, and it was shown that the Langmuir model is a better fit to describe the interaction between the different heavy metals studied and guanine. Adsorption capacities were the highest for copper followed by lead and cadmium.

Detection of the heavy metal ions was also evaluated electrochemically, and the highest sensitivity was recorded for copper ions with 171.6 μA/μM. This sensitivity was in fact the highest reported sensitivity compared to those using electrochemical detections with iron oxide nanoparticles. The sensitivities and limits of detection with lead and cadmium ions were also comparable to those reported in literature.

Voltammetric study of the affinity of divalent heavy metals for guanine functionalized iron oxide nanoparticles

Material from: "S. Sawan, K. Hamze, A. Youssef, R. Boukarroum, K. Bouhadir, A. Errachid, R. Maalouf, N. Jaffrezic-Renault, Voltammetric study of the affinity of divalent heavy metals for guanine-functionalized iron oxide nanoparticles, Monatshefte für Chemie-Chemical Monthly, published 2021, Springer Nature.

ABSTRACT

In this study, a novel nanobiomaterial based on (3-aminopropyl)triethoxysilane (APTES) coated iron oxide (Fe_3O_4) nanoparticles functionalized with newly synthesized guanine hydrazide (GH) was elaborated. A boron-doped diamond electrode coated with GH-APTES-Fe_3O_4 nanoparticles was used to assess the interaction of heavy metal ions with guanine hydrazide. The adsorption isotherms were electrochemically investigated and it was shown that the adsorption capacity of the nanoparticles towards heavy metals decreased in the following order: Cu^{2+}>Pb^{2+}>Cd^{2+}. From the calibration curves, the sensitivities of detection were as follows: 171.6 µA/µM (2.7 $\mu A.\mu g^{-1}.L$) for Cu (II), 156 µA/µM (0.75 $\mu A.\mu g^{-1}.L$) for Pb (II) and 101.4 µA/µM (0.9 $\mu A.\mu g^{-1}.L$) for Cd (II).

Keywords Nucleosides, Heavy Metals, Nanostructures, Electrochemistry, Metal complexes

Graphical Abstract

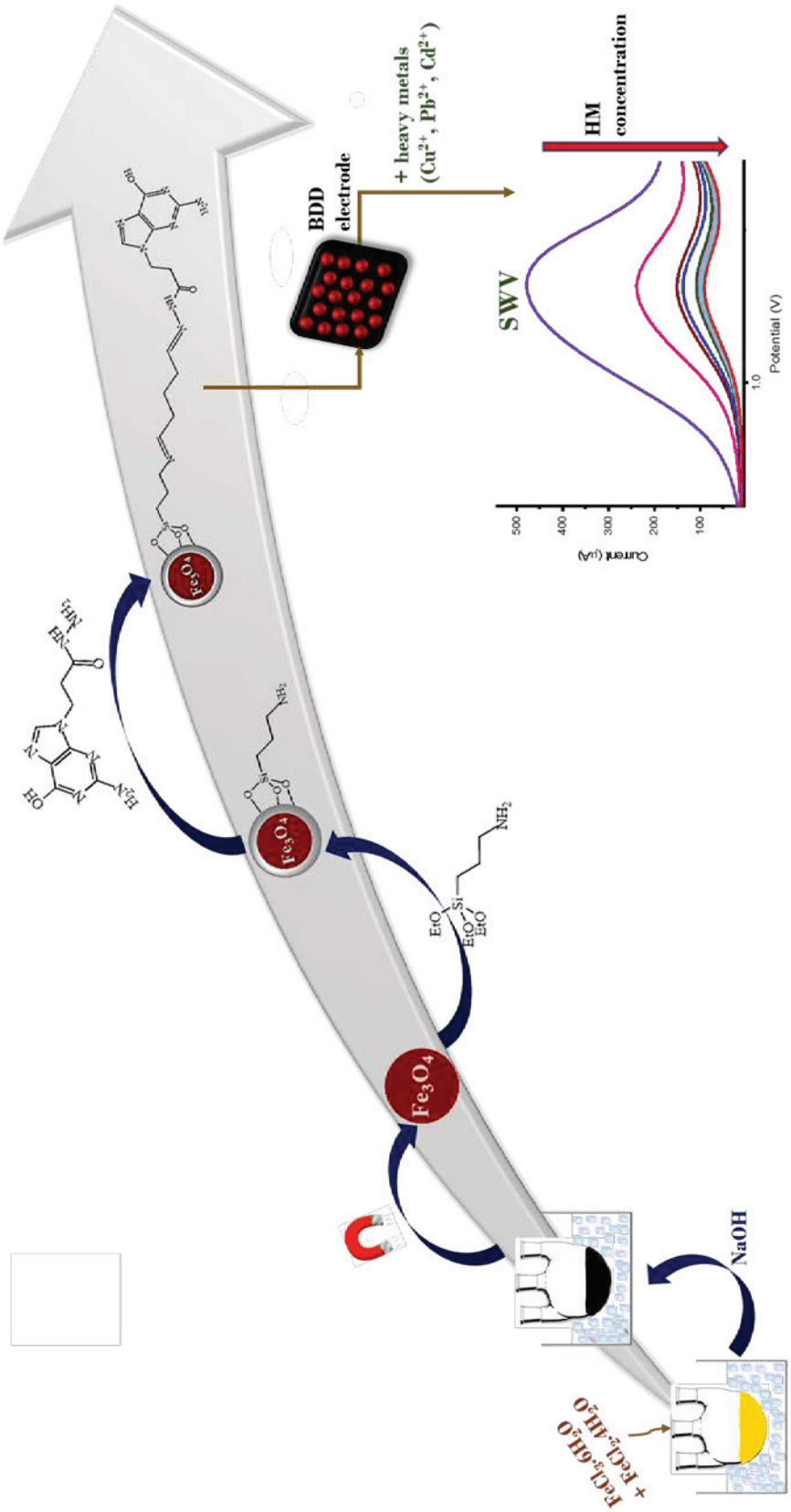

3.1. Introduction

Despite the many uses of heavy metals, excessive exposure, either externally or by ingestion, can be harmful to humans, animals and plants on several levels. They are nonbiodegradable and thus have the tendency to accumulate in living organisms. Besides being considered as environmental pollutants [1], some heavy metals can cause skin, liver, kidney, bone and neurological diseases [2]. Along with natural sources, heavy metals can be released from industrial sources such as fertilizers, household waste, cosmetics, paint, batteries and plastics [3]. The range of toxicity of heavy metals depends on several factors including their charges, concentrations, way of exposure…

Although the main function of nucleic acids is encoding genetic information in human beings, they have been widely explored in the fields of catalysis and ligand binding [4]. Nucleic acids are known to have different metal binding sites, binding capacity and affinity for heavy metals [5]. For years, the interaction of metal cations with nucleic acids has been investigated. It was noted that metal ions impact differently the stability and structure of nucleic acids depending on the type and concentration of metal ion and its relative affinity to the phosphate and nucleobases. It has been hypothesized that bioavailable metal ion-induced toxicity inactivates vital processes, inhibits metabolic pathways and directly or indirectly displaces essential metals from the active sites of macromolecules and/or disrupts depolymerization or repair of nucleotide bases with subsequent errors in protein synthesis [6]. The study of the interaction between nucleic acids and heavy metal ions can help to explain their biotoxicity mechanisms and these interactions can be used for the detection of toxic heavy metals in waters. Recently, nucleic acids, nucleotides, nucleosides, nucleobases and their derivatives have been gaining wide popularity in heavy metal sensing [7]. They are biodegradable, highly selective and can be produced by natural or synthetic methods. Many studies have relied on the stabilization or destabilization of G-quadruplex structure of guanine-rich DNA, formation of stable base pairs or catalytic cleavage of DNA substrates for the detection of heavy metals [8].

Among the five natural nucleobases, guanine and its derivatives have received considerable interest [9]. Guanine is a purine derivative that consists of a fused pyrimidine-imidazole ring system with conjugated double bonds. It has been well established that metal ions bind to the carbonyl oxygen O(6) and/or the imidazolyl nitrogen N(7) of guanine. Preference of the binding site depends on the metal ion itself [10]. In the present work, the voltametric behaviour of guanine in the presence of divalent heavy metal ions was studied. It is known that the redox moiety of guanine is the imidazolyl nitrogen N(7) [11]. The interaction of N(7) with heavy metal ions can then be monitored

through the change of the electron transfer rate. For the sensitive detection of the oxidation of guanine, synthesized guanine hydrazide (GH) was immobilized on iron oxide nanoparticles that present a large specific surface area and a high electrical conductivity. Recently, magnetic nanoparticles, particularly magnetite Fe_3O_4 nanoparticles, have attracted a lot of interest owing to their unique properties of superparamagnetism, low Curie temperature, high magnetic susceptibility, low toxicity and cost effectiveness [12,13]. The exclusive magnetic and electrical properties are the result of the transfer between Fe^{2+} and Fe^{3+} [14]. They have a wide variety of applications ranging from environmental to biological and medical. Synthesis conditions are crucial in determining their size and physicochemical properties, and thus several processes have been investigated for their production depending on the desired application. Moreover, Fe_3O_4 nanoparticles have the tendency to aggregate due to magnetic dipole-dipole interactions between particles [15], which is why in most electrochemical studies they are either coated or functionalized [16]; i.e. iron oxide core encapsulated in an organic or inorganic shell [17]. Owing to their versatile properties, Fe_3O_4 nanoparticles were extensively used in combination with biological recognition elements such as enzymes, antibodies and nucleic acids for various applications [18]. The guanine functionalized iron oxide nanoparticles were immobilized on the surface of a boron doped diamond (BDD) electrode. BDD electrodes are extensively investigated for electroanalytical applications, because of their electrochemical properties, as a low background current and a wide potential window in aqueous solutions (∼−1.35 to +2.3 V versus the normal hydrogen electrode), corrosion stability in aggressive media and resistance to biofouling [19]. The redox properties of guanine were detected in the presence of copper, lead and cadmium ions. From these results, adsorption of the three heavy metals on N(7) site of guanine was characterized and the sensitive electrochemical detection of these heavy metals could then be achieved.

3.2. Experimental

3.2.1. Chemical Reagents

All the reagents used in this study were of analytical grade and used as received without any further purification. Ammonium hydroxide (NH_4OH) (25% in H_2O), (3-aminopropyl)triethoxysilane (APTES) 99%, glutaraldehyde solution Grade II (25% in H_2O), potassium chloride (99 – 100.5%) and potassium citrate tribasic monohydrate (≥ 99%) were purchased from Sigma-Aldrich. Dimethyl sulfoxide (DMSO) (≥ 99.9%) was purchased from Riedel-de-Haën, sodium hydroxide (NaOH) (98.5 – 100%), cadmium, copper and lead standards from Fluka and ethanol (≥ 99.8%) from Honeywell. Ferric chloride hexahydrate $FeCl_3.6H_2O$ (98%) and ferrous chloride tetrahydrate $FeCl_2.4H_2O$ (99%) were purchased from Acros Organic. All the chemicals used in the synthesis and characterization of

guanine hydrazide were purchased from Sigma-Aldrich, Merck or Fluka Chemika. Deionized water (with a resistivity of 18.2 MΩ.cm) was used in the preparation of all solutions.

3.2.2. Synthesis and characterization of guanine hydrazide

A round bottom flask was charged with guanine (10 g, 66.22 mmol) *N*,*N*-dimethylacetamide (DMA, 30 mL) and acetic anhydride (16.5 mL, 168 mmol). The reaction mixture was stirring overnight at 165°C after which it was cooled to room temperature. The precipitate was collected and triturated with water/ethanol 1:1 (30 mL) at 80°C for 2-3 h. The precipitate was collected and dried under reduced pressure at 70°C to yield a white solid. The solid was transferred to a 500 mL round bottom flask with dimethylformamide (50 mL). An ethanolic solution of sodium ethoxide (NaOEt, 2 mL, 25.9 mmol) was added and the mixture was stirred for 15 min. Ethyl acrylate (3.8 mL, 34.96 mmol) was added and the mixture was refluxed at 165°C for 1h. The solvent was evaporated and the residue was dissolved in methylene chloride and washed with distilled water. The organic layer was separated, dried with anhydrous $MgSO_4$, filtered and the solvent evaporated under reduced pressure. The crude was then triturated with toluene (250 mL) with stirring overnight at room temperature. The precipitate was collected, dried under reduced pressure and purified by column chromatography on silica gel (CH_2Cl_2/MeOH 98:2) to yield a white solid (2.85 g). The white solid (7 g, 23.9 mmol) was mixed with ethanol (70 mL) and $N_2H_4.H_2O$ (4.1 mL, 83.6 mmol) and the mixture was stirred and heated at 80°C for 24 h. The precipitate was collected and dried at 70°C under reduced pressure to yield a white solid. ^{1}H and ^{13}C nuclear magnetic resonance (NMR) spectra were recorded on a Bruker 300 MHz NMR spectrometer in DMSO, $CDCl_3$ and D_2O or D_2O/D_2SO_4, using TMS and DSS as references; chemical shifts are reported in ppm. Fourier Transform Infrared (FTIR) spectra were collected using PerkinElmer Spectrum Two spectrometer.

3.2.3. Fabrication of APTES-coated iron oxide nanoparticles

Magnetic nanoparticles were synthesized according to a modified Massart's method [20] based on coprecipitation of an aqueous mixture of ferric and ferrous salt hydrates followed by the addition of a base. Briefly, 2.7 g of $FeCl_3.6H_2O$ and 1.2 g of $FeCl_2.4H_2O$ were mixed with a molar ratio of 2:1 and dissolved in 90 mL of deionized water. Afterwards, 100 mL of 1 mol/L NaOH solution was added dropwise under vigorous stirring and nitrogen gas at 0°C. A change in color indicated the formation of iron oxide nanoparticles. The solution was subjected to magnetic stirring for 4 hours to ensure nucleation and growth of magnetite nanoparticles. The latter were collected with an external magnet, washed several times with water followed by ethanol, and finally dried under vacuum. The solution was subjected to magnetic stirring for 60 minutes to ensure nucleation

and growth of magnetite particles. APTES coating was carried out afterwards. Iron oxide nanoparticles were sonicated for 25 minutes before the addition of NH_4OH and (3-aminopropyl)triethoxysilane under nitrogen atmosphere. The mixture was allowed to age for 24 hours, after which the nanoparticles were again washed with water followed by ethanol and dried for later use.

3.2.4. Characterization of iron oxide nanoparticles coated with APTES

FTIR spectra were collected at each step of the synthesis using PerkinElmer Spectrum Two spectrometer in order to verify the successful synthesis of the APTES coated magnetic nanoparticles. In order to identify the crystalline phase of the prepared nanoparticles, X-ray diffraction (XRD) was performed using a Bruker D4 ENDEAVOR with Cu/K-α radiation. The operating target voltage was 50 kV and the tube current was 50 mA. The morphology and size of the nanoparticles were investigated using Scanning Electron Microscopy (SEM) done using Tescan, Vega 3 LMU with Oxford EDX detector (Inca XmaW20).

3.2.5. Fabrication of the electrochemical sensor

Guanine hydrazide was immobilized on the APTES coated iron oxide nanoparticles using glutaraldehyde (GA) as a crosslinking agent. Briefly, a 1 mg/mL solution of GH dissolved in DMSO was mixed with 100 mg/L of the APTES coated nanoparticles. 20 µL of this mixture were dropped on a clean BDD electrode and left for 20 minutes in saturated glutaraldehyde vapor. The electrode was left to dry at room temperature. Afterwards, it was placed on the electrochemical cell where a 300 mT cylindrical magnet will permit the paramagnetic nanoparticles to remain attracted to the electrode surface.

3.2.6. Electrochemical measurements

All electrochemical measurements were performed using a PalmSens4. A conventional three-electrode system was employed: a bare or modified boron doped diamond electrode as the working electrode, Platinum plate as a counter electrode and Ag/AgCl as a reference electrode. The BDD electrodes were cleaned between the different measurements by sonicating in acetone for 5 minutes, followed by soaking in piranha solution for 3 min. The electrodes were then washed repeatedly with water and ethanol before being dried with nitrogen.

Citrate buffered solutions (0.1 mol/L, containing 0.5 mol/L KCl, pH 4) were used as electrolytes for all electrochemical measurements. The technique used in all the measurements was square wave voltammetry with the following optimized conditions: frequency 50 Hz; amplitude 50 mV; step potential 10 mV; time of equilibration 2 minutes.

3.3. Results and Discussion

3.3.1. Guanine hydrazide preparation and characterization

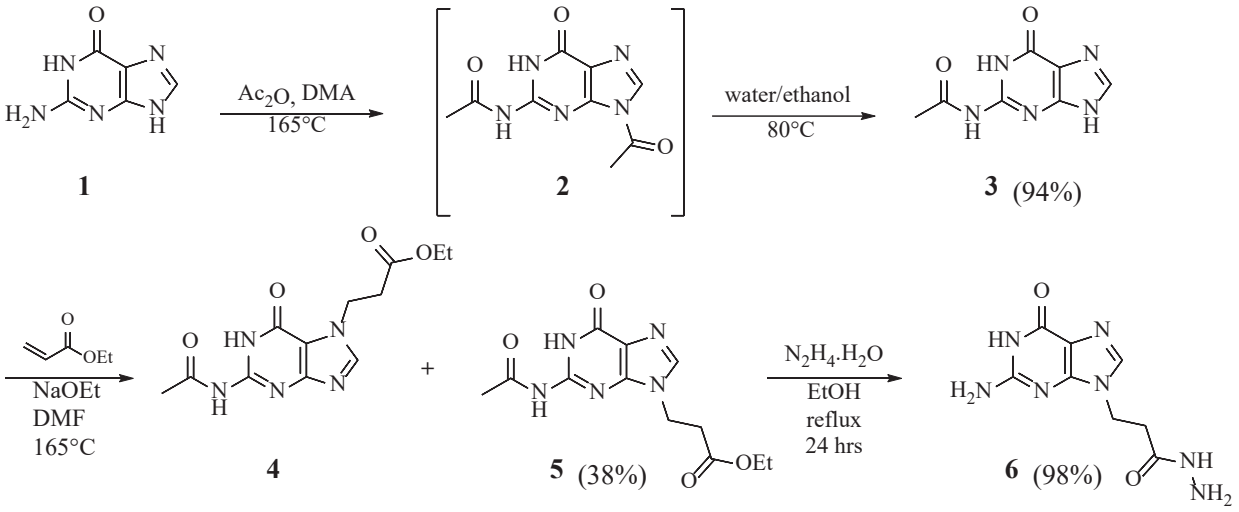

Figure 1: Schematic diagram showing the steps of guanine hydrazide synthesis.

Figure 1 summarizes the overall steps involved in the synthesis of *3-(2-amino-6-oxo-1,6-digydro-9H-purin-9-yl)propane hydrazide* (**6**, $C_8H_{10}N_7O_2$) or guanine hydrazide. The process of guanine hydrazide synthesis generated a white product with a yield of 98%. To prepare the guanine hydrazide **6** shown in figure 1, The exocyclic amine of guanine **1** was first protected by acetylation according to literature procedure [21]. Then reaction of N^2-acetylguanine **3** via a Michael addition with Ethyl acrylate and sodium ethoxide afforded, as expected, a mixture of two isomeric ethyl propionates resulting from guanine alkylation at either the N-9 (**5**) or N-7 (**4**) atom. These compounds were separated by Flash chromatography and, after their structural assignment, the reaction of the N-9 ester with hydrazine hydrate in ethanol led to the formation of the desired acyl hydrazide **6** according to an established literature procedure [22].

The synthesized guanine hydrazide was characterized using FTIR and ^1H and ^{13}C NMR. The infrared spectrum shown in figure 2a revealed peaks at 1695 cm^{-1} corresponding to C=O, 1657 and 3310 cm^{-1} corresponding to NH and 1440 cm^{-1} corresponding to C-N. Peaks at 2854 cm^{-1} correspond to C-H stretching of CH_2 in the hydrazide function, along with a weak peak at 1563 corresponding to

C=C stretching. ^{1}H NMR characterization (500 MHz, DMSO-d_6) showed that the two methylene group protons resonate at 3.36 (triplet, 2H) and 4.14 (triplet, 2H) while the proton from the methine group resonates at 7.54. Protons from the primary amine groups at 4.22 – 4.19 and 6.49 whereas those from secondary amines appear at 9.04 and 10.49 (figure 2b). ^{13}C NMR results in figure 2c are consistent with literature such that the signals corresponding to the guanine carbons appear at 156.8, 153.5, 151.0, 137.4 and 116.5 while those for the hydrazide function appear at 168.7, 39.5 and 33.5 [23].

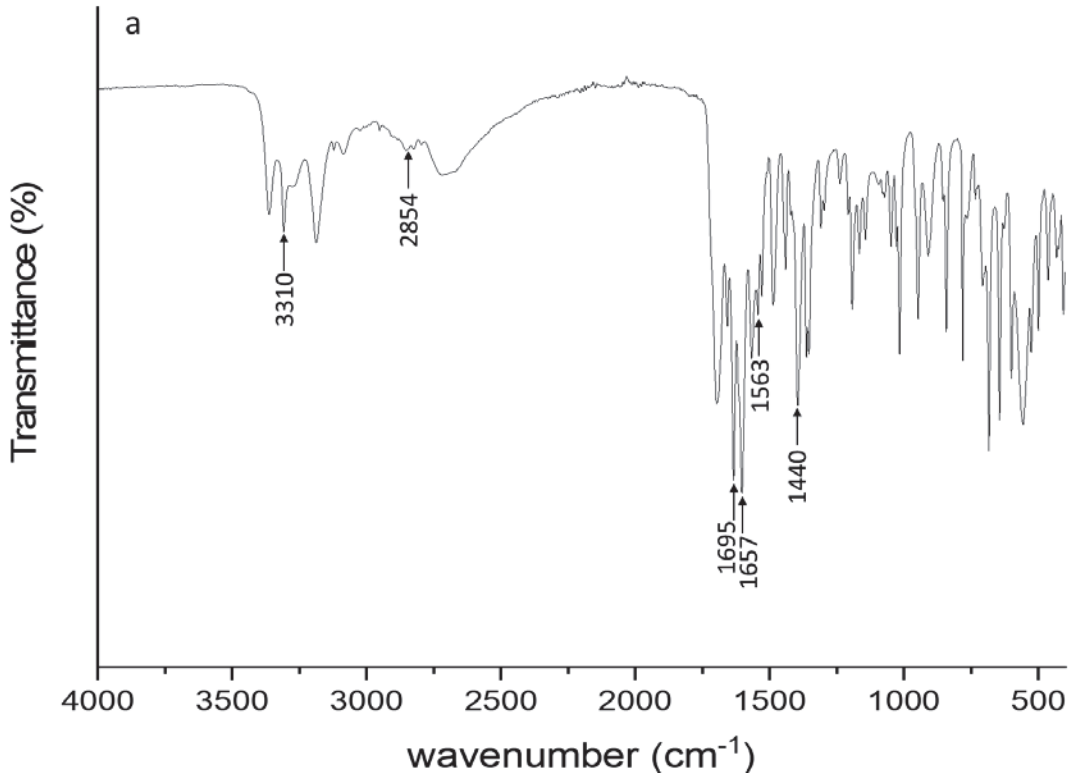

b

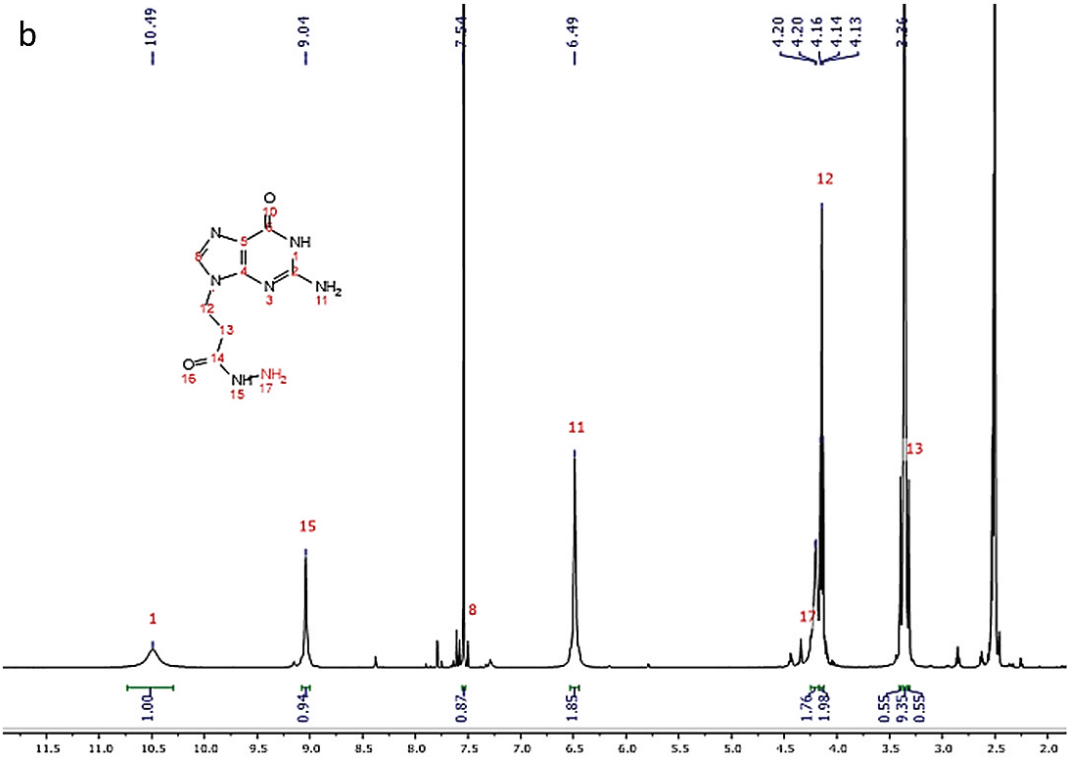
10.19
9.04
7.54
6.49
4.20
4.20
4.16
4.14
4.13
2.36
12
11
13
15
1
8
17
1.00
0.94
0.87
1.85
1.76
1.98
0.55
9.35
0.55

c

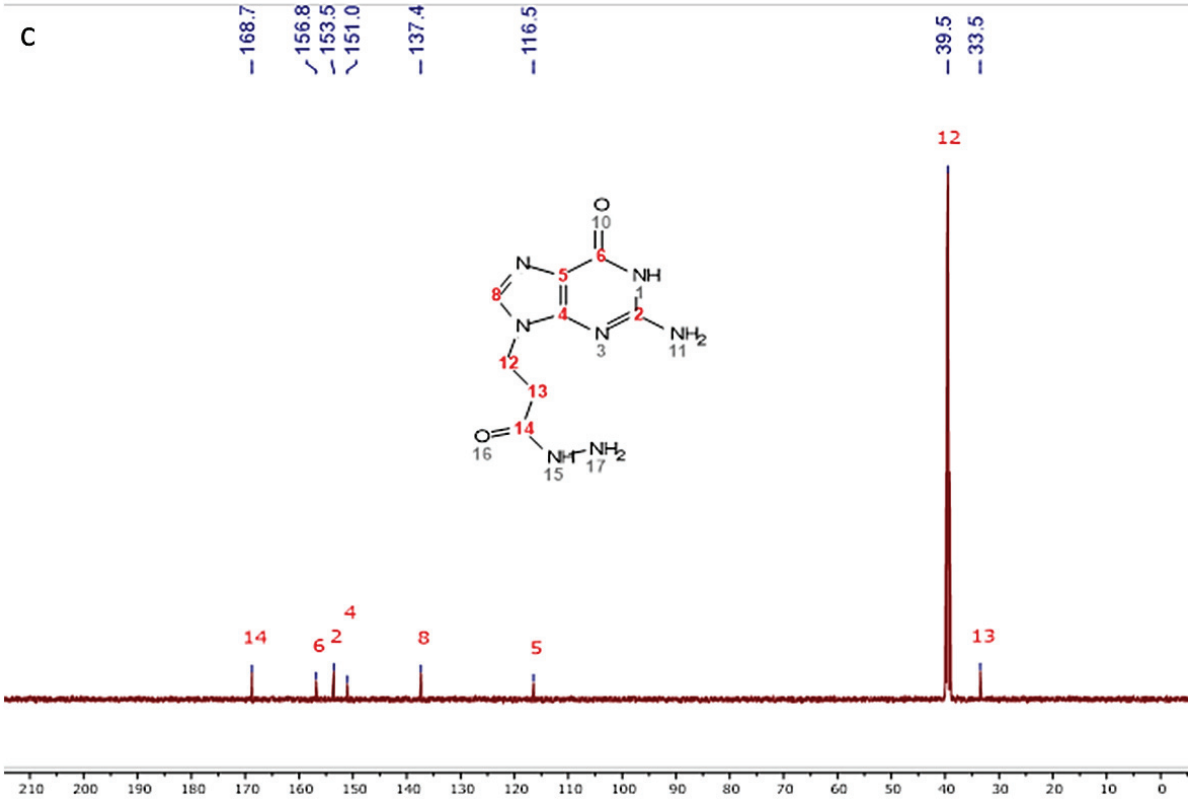
168.7
156.8
153.5
151.0
137.4
116.5
39.5
33.5
12
14
6
2
4
8
5
13

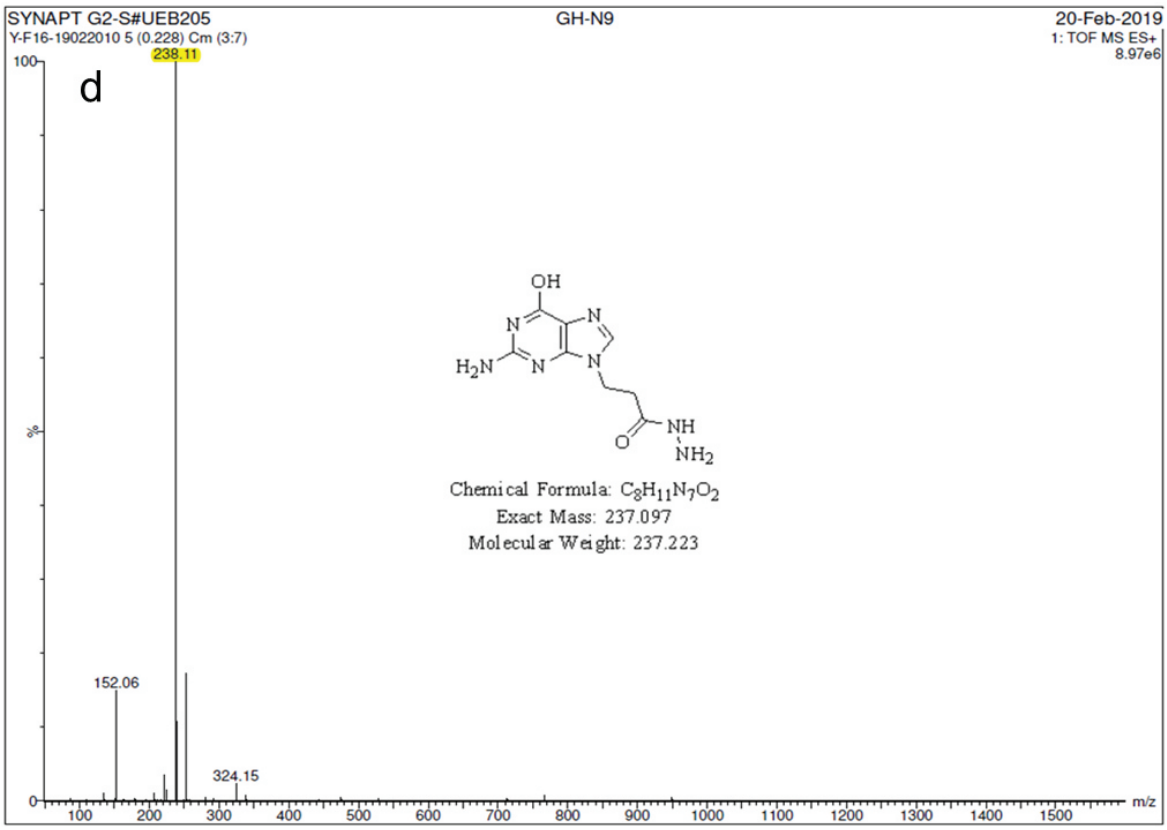

Figure 2: (a) FTIR spectrum, (b) ^{1}H NMR (c) ^{13}C NMR and (d) HRMS of guanine hydrazide.

3.3.2. Preparation of GH-APTES functionalized Fe_3O_4 nanoparticles

The co-precipitation of ferrous and ferric ions in a basic medium is a classical method for the preparation of Fe_3O_4. The size of the iron oxide nanoparticles directly affects their magnetic properties and should therefore be optimized based on the desired application [13]. Nanoparticles that are too small (less than 20 nm) cannot be manipulated by an external magnetic field. Hence, the coprecipitation procedure was carried out at 0 °C to ensure the synthesis of nanoparticles of adequate size. Upon the addition of NaOH, the color of the solution changed gradually from orange to brown to black. Precipitation of Fe_3O_4 is expected at pH > 7.5 [15]. The reactions involved in the production of Fe_3O_4 are:

$$Fe^{3+} + 3HO^{-} \rightleftharpoons Fe(OH)_3 \quad (1)$$

$$Fe(OH)_3 \rightleftharpoons FeO(OH) + H_2O \quad (2)$$

$$Fe^{2+} + 2HO^{-} \rightleftharpoons Fe(OH)_2 \quad (3)$$

$$Fe(OH)_2 + 2FeO(OH) \rightleftharpoons Fe_3O_4 + H_2O \quad (4)$$

The process of amino modification of Fe_3O_4 nanoparticles by direct immobilization of (3-aminopropyl)triethoxysilane on the surface of the nanoparticles can be expected to occur through a silanization reaction, leaving the NH_2 group of APTES exposed. This step is usually very complex and is influenced by several parameters including the reaction time, temperature and silane concentration.

Finally, the functionalization of the APTES-coated nanoparticles with guanine hydrazide was done using glutaraldehyde. The overall reaction for the synthesis of the functionalized electrode is shown in figure 3.

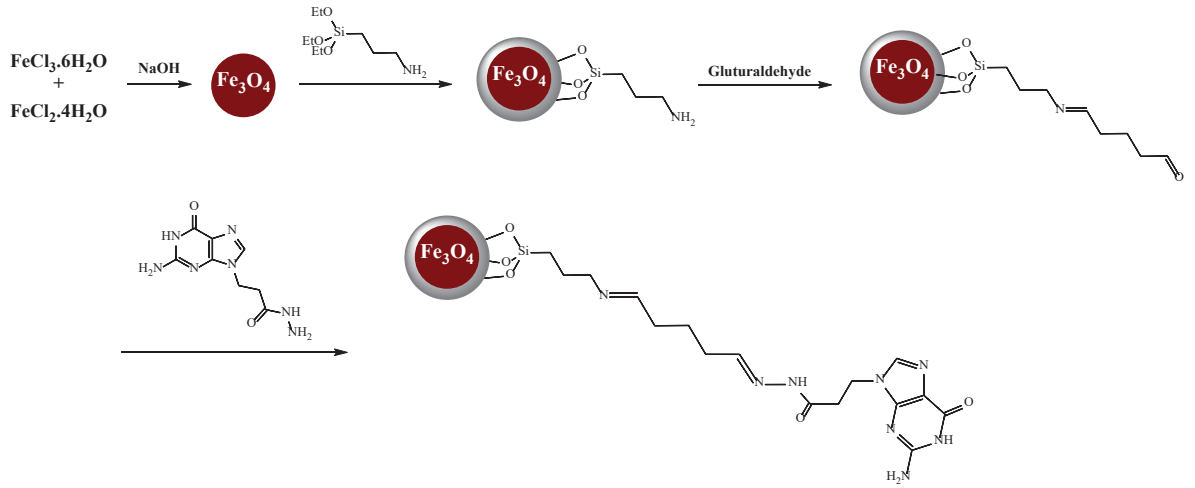

Figure 3: Schematic diagram showing the process of synthesizing the GH-APTES-Fe_3O_4 nanoparticles.

3.3.3. Characterization of the functionalized nanoparticles

FTIR spectroscopy was used to study the functionalization of the bare and coated nanoparticles, as shown in figure 4A. For the bare nanoparticles, one peak at 550 cm^{-1} is noticeable. This peak is the characteristic absorption peak of Fe-O. This band can also be observed with the coated nanoparticles, along with new bands confirming the adsorption of (3-aminopropyl)triethoxysilane on the surface of Fe_3O_4. Bands at 3672 cm^{-1} and 1624 cm^{-1} can be attributed to the N-H stretching and NH_2 bending modes, respectively, of a free NH_2 group. Bands at 1063 cm^{-1} and 1162 cm^{-1} can be attributed to Si-O-Si and SiO-H groups. The stretching of $-CH_2$ was confirmed with bands at 2902 cm^{-1} and 2973 cm^{-1} [13]. The absorption band corresponding to the Fe-O-Si bond cannot be seen since it overlaps with that of Fe-O vibration. However, the shift in the Fe-O band from 550 cm^{-1} to 562 cm^{-1} indicates that there is an Fe-O-Si bond [16]. FTIR measurement after the functionalization of APTES coated nanoparticles with GH confirmed the crosslinking of GH to the APTES by the appearance of new peaks not characteristic of APTES.

These include a peak at 1663 cm^{-1} corresponding at C=C. The shift in the peak corresponding to N-H stretching from 3672 cm^{-1} to 3440 cm^{-1} is consistent with N-H stretching of an amide group along with an increased peak intensity. The -CH_2 stretching peaks also increased in intensity due to the increased number of CH_2 groups from the hydrazide function.

Powder XRD patterns of the coated nanoparticles show diffraction peaks at 30.1°, 35.4°, 43.1°, 53.4°, 57.0°, and 62.6° corresponding to the characteristic pattern of pure magnetite Fe_3O_4 (figure 4B). The diffraction peaks can be assigned to the (220), (311) (400), (422), (511) and (440) diffraction planes, respectively [17]. This proves that the coating does not affect the core magnetite and doesn't lead to a phase change.

The morphology of the prepared nanoparticles capped with (3-aminopropyl)triethoxysilane was investigated using SEM as shown in figure 4C. The magnetic nanoparticles appear to be quasi-spherical, with uniform distribution and an average size of 45 nm. Energy-dispersive X-ray spectroscopy (EDX) was performed to study the elemental composition of the APTES coated Fe_3O_4 nanoparticles (figure 4D). Peaks corresponding to iron (Fe) at about 0.6, 6.3 and 7 keV and oxygen (O) confirm the formation of iron oxide nanoparticles [18]. The presence of peaks corresponding to Si and N confirm that the APTES coating was successful.

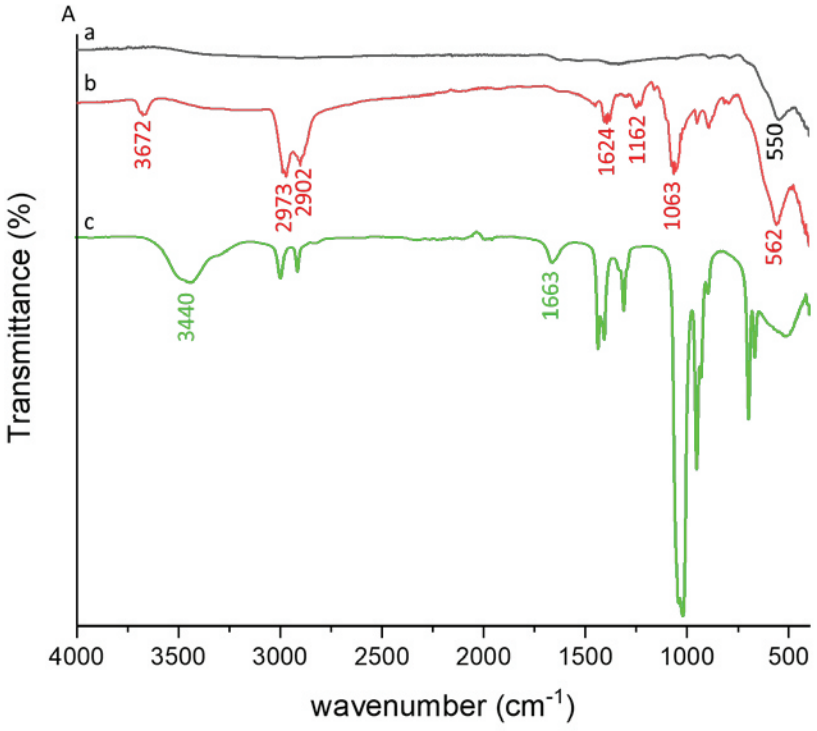

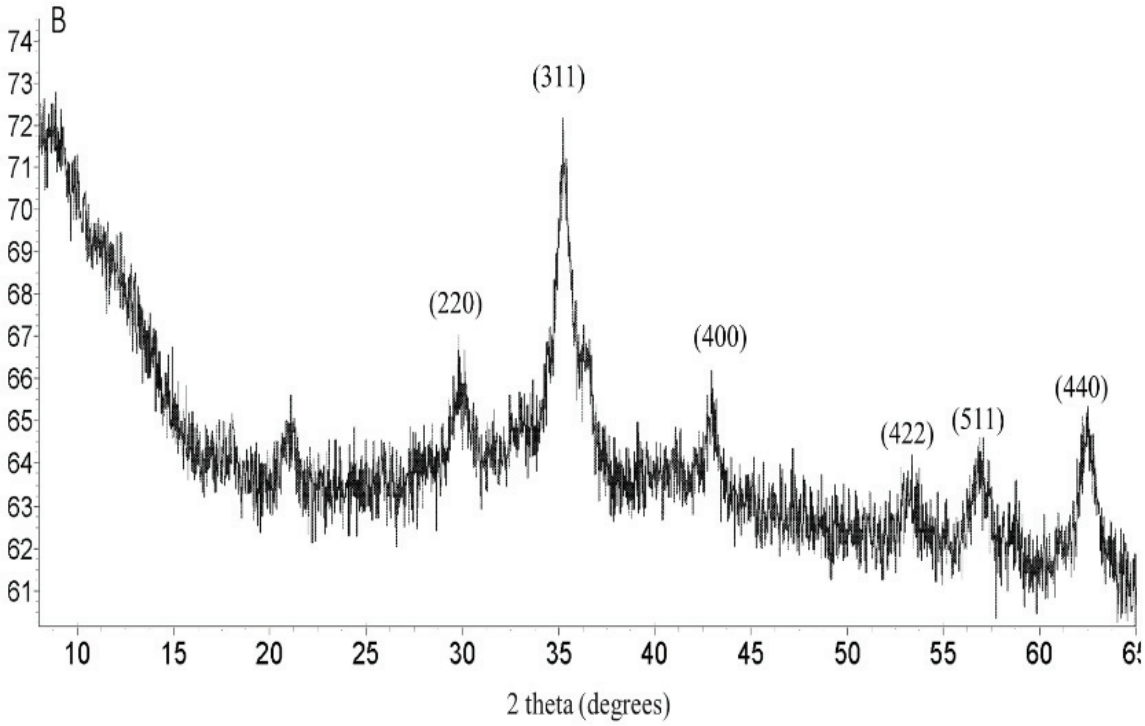
B
(311)
(220)
(400)
(422)
(511)
(440)
2 theta (degrees)

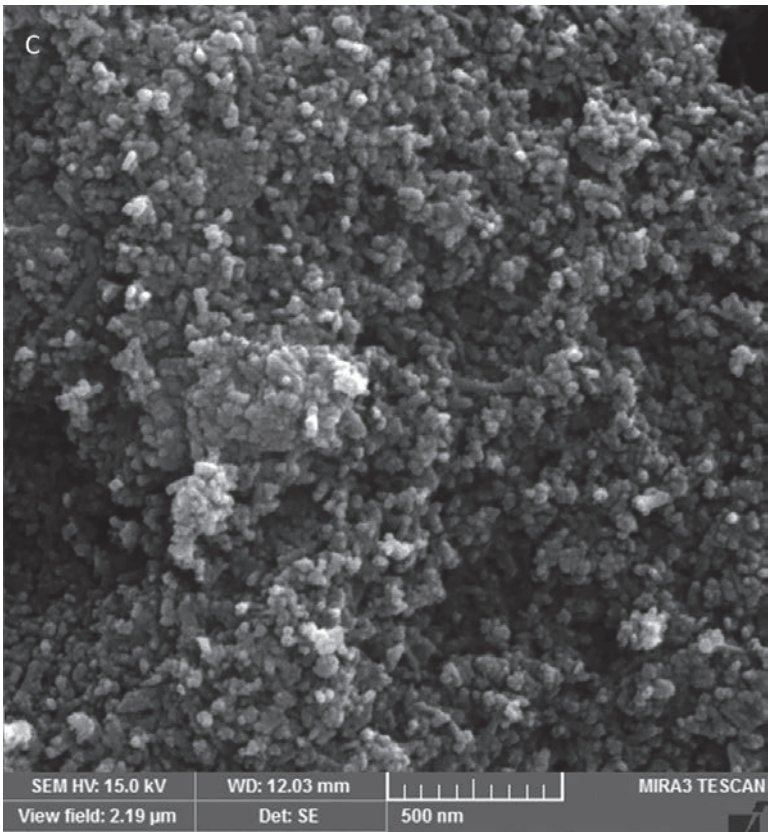
C
SEM HV: 15.0 kV
WD: 12.03 mm
MIRA3 TESCAN
View field: 2.19 µm
Det: SE
500 nm

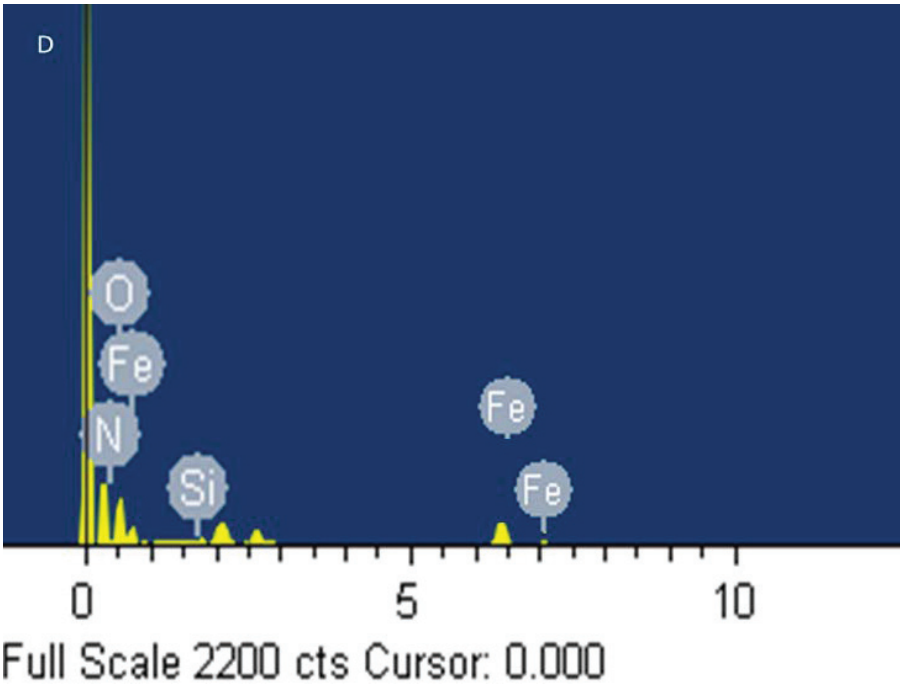

Figure 4: (A) FTIR spectrum of (a) bare Fe_3O_4 NPs, (b) APTES- Fe_3O_4 NPs and (c) GH-APTES-Fe_3O_4 NPs, (B) XRD pattern, (C) SEM image and (D) EDX spectrum of APTES-Fe_3O_4 nanoparticles.

3.3.4. Voltammetric study of the GH-APTES functionalized nanoparticles in the presence of divalent heavy metals

Prior to studying the voltammetric behavioral interaction of heavy metals with the modified electrode, each of the different elements were studied electrochemically to check for their respective signals. As shown in figure 5a, no observable peaks were detected with square wave voltammetry in the range between -1 and 1.5 V for the BDD electrode coated with APTES-Fe_3O_4 NPs. However, upon functionalization of the nanoparticles with GH, a peak appears at 1.1 V as indicated in figure 5b. This peak is characteristic of the oxidation of guanine at a BDD electrode [11, 24] and not the hydrazide function which is oxidized at a higher potential (1.8 V) [25]. The oxidation reaction of guanine in aqueous media is presented in Fig. 6 [11].

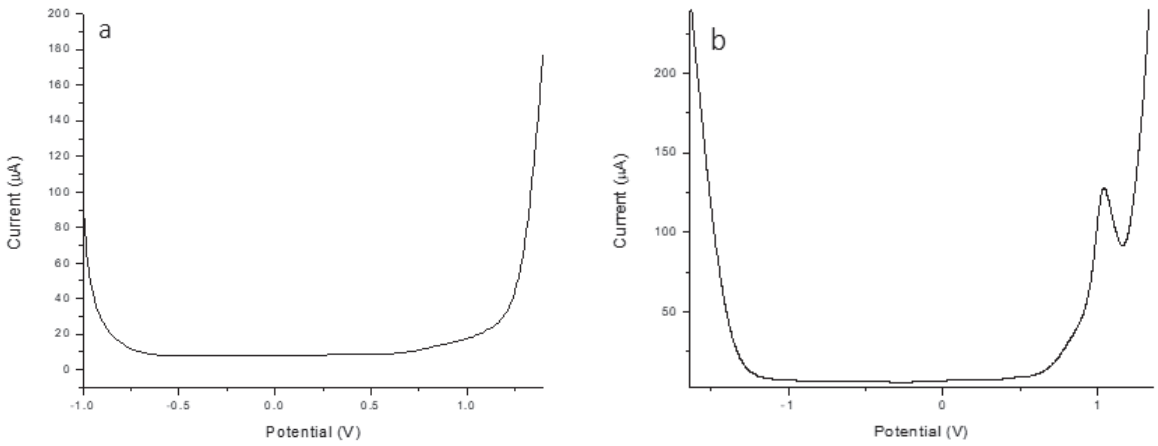

Figure 5: SWV of (a) APTES-Fe_3O_4 nanoparticles and (b) APTES-Fe_3O_4 nanoparticles functionalized with GH.

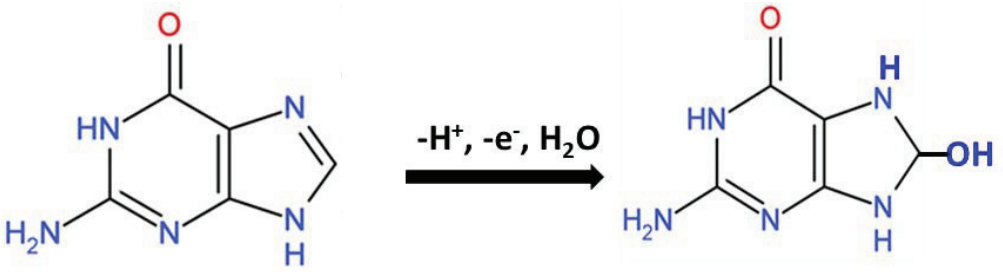

Figure 6: Oxidation reaction of guanine, in aqueous medium.

After confirming the identity of the signal obtained for the coated magnetic beads, the concentration of the magnetic nanoparticles used to modify the BDD electrode was optimized. APTES-Fe_3O_4 nanoparticles with varying concnetrations (50, 100 and 150 mg/L) were used to modify several electrodes. Copper ions were added and square wave voltammetry was run. Signals for the redox reaction of copper could be observed when the concentration of the magnetic nanoparticles was less than 100 mg/L (figure 7). Thus, for further electrode modifications, 100 mg/L of the magnetic nanoparticles was used.

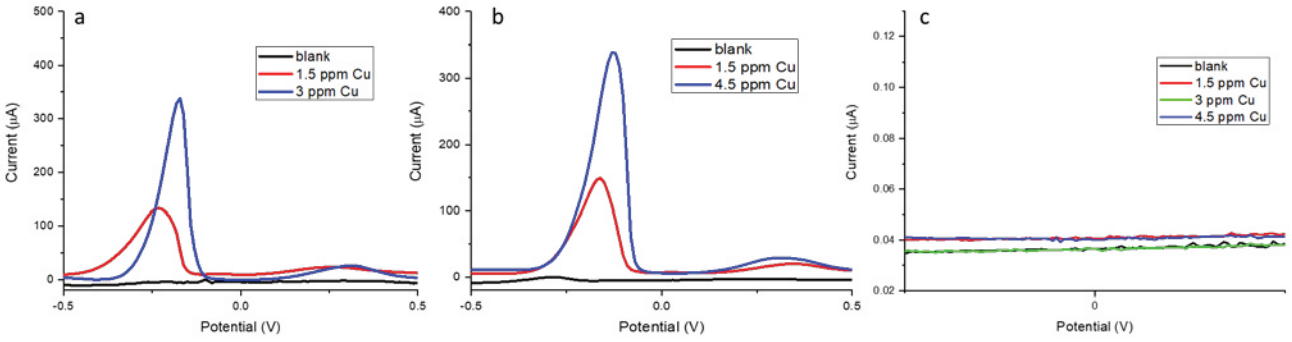

Figure 7: Effect of the addition of copper ions to BDD electrodes modified with (a) 50 mg/L APTES-Fe_3O_4 nanoparticles, (b) 100 mg/L APTES-Fe_3O_4 nanoparticles and (c) 150 mg/L APTES-Fe_3O_4 nanoparticles.

The effect of Cd (II) ions concentration on the oxidation signal of GH was then investigated after interaction in solution and using a bare BDD (data not shown). Square wave voltammetry was applied for a solution of GH in citrate buffer (pH 4) with 0.5 mol/L KCl at the following optimized conditions: frequency 50 Hz; amplitude 50 mV; step potential 10 mV. Before adding cadmium, the oxidation peak of GH appeared at 1.1 V. The peak current decreased upon the addition of increasing concentrations of Cd^{2+} implying that the complex formation of cadmium ions with GH hinder the redox reaction of the guanine moiety.

Using a BDD electrode modified with GH functionalized nanoparticles, the same behavior was observed. The intensity of the peak current was found to decrease when the Cd (II) concentration increased. The same behavior was observed with all the studied heavy metal ions. The square wave signals in the presence of the different divalent heavy metals are shown in figure 8. The different metal ions were added up until there were no observable changes in the recorded peak intensity.

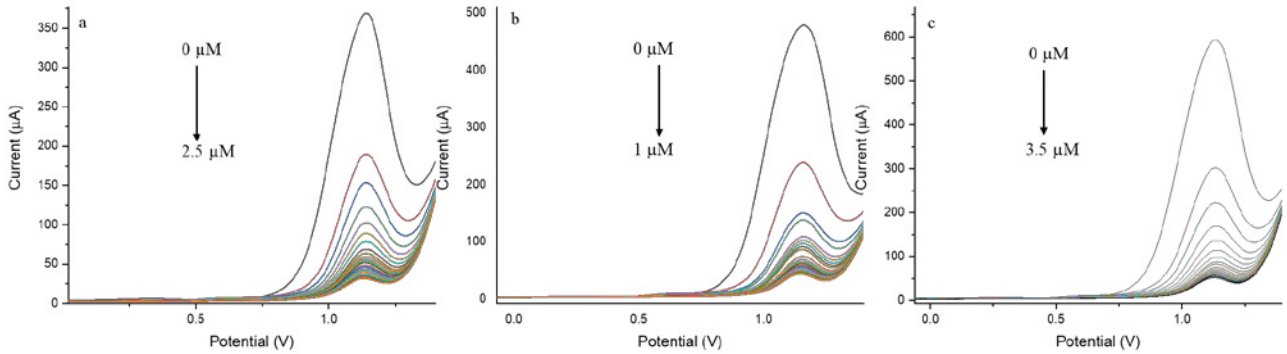

Figure 8: SWV of (a) Cd (II) at the GH-APTES-Fe_3O_4 NP electrode over a concentration range of 0 – 2.5 µM, (b) Pb (II) at the GH-APTES-Fe_3O_4 NP electrode over a concentration range of 0 – 1 µM and (c) Cu (II) at the GH-APTES-Fe_3O_4 NP electrode over a concentration range of 0 – 3.5 µM.

3.3.5. Adsorption isotherms of the divalent heavy metal ions on the GH-APTES functionalized nanoparticles

In order to characterize the interaction between heavy metals and the functionalized nanoparticles, adsorption isotherms were modeled. Adsorption isotherms are mathematical models describing the distribution of the adsorbate between the solution and the adsorbent. These models are

based on to the possibility of interaction between the adsorbate species, type of coverage and the homogeneity/heterogeneity of the adsorbent surface [26]. The variation of the peak maximum (ΔI) (mean value of triplicate) is proportional to the adsorbed concentration of the heavy metals at the modified electrode surface. It is calculated by subtracting the peak intensity after adding the heavy metals from the initial peak intensity before any addition. The adsorption isotherm of the heavy metals was then built from this value, the initial concentration of the heavy metals was not highly modified, due to the small surface area of the modified electrode in contact. Two models were tested: Langmuir and Freundlich.

i. Langmuir isotherm

The Langmuir model assumes that adsorption occurs on a structurally homogeneous adsorbent in a monolayer, or that the adsorption occurs at fixed sites that are identical and energetically equivalent. The linearized form of the Langmuir isotherm can be written as follows [27]:

$$c_e/\Delta I = 1/Q_0 b + c_e/Q_0$$

where Q_0 is the adsorption capacity (mg/g) and b is the energy of adsorption (L/mg). To calculate c_e, the concentration of each divalent metal adsorbed on the surface of the magnetic beads was calculated from the calibration curve. This value was then subtracted from the initial concentration of the divalent metals in the solution. Figure 9 shows the Langmuir plot $c_e/\Delta I$ versus c_e for the different heavy metals, each in their respective concentration range. The plots indicate that the experimental data are well fitted with the model with $r^2 > 0.999$. The values of the adsorption capacities were 400, 280.1 and 343.6 µg/g for Cu^{2+}, Cd^{2+} and Pb^{2+}, respectively. Moreover, the essential characteristics of the Langmuir model can be expressed as the dimensionless constant separation factor R_L as follows [27]:

$$R_L = 1/(1 + Q_0 b)$$

In the case of the three different metals, R_L falls in the range of 0 – 1 indicating that the nature of the adsorption isotherm is favorable. The adsorption capacity of the functionalized nanoparticles towards the studied heavy metal ions decreases in the following order: $Cu^{2+} > Pb^{2+} > Cd^{2+}$.

ii. Freundlich isotherm

Freundlich isotherm is another form of the Langmuir model describing a heterogeneous system with multiple adsorption sites. The linearized logarithmic form of the Freundlich model can be expressed as follows [28]:

$$\log \Delta I = \log K_F + (1/n) \log c_e$$

where K_F is the Freundlich constant (mg/g) and n is the Freundlich exponent. The different isotherms for each heavy metal are shown in figure 9 where log ΔI is plotted versus log c_e. It should be noted that the concentration range over which this model was linear was much smaller than that with the Langmuir model for all the studied metal ions. The values of n lie between 1 and 10, which implies that the adsorption is favorable and heavy metals are easily extracted from the solution. This result agrees with the values of R_L from Langmuir's isotherm. Langmuir and Freundlich model parameters and linear regression correlations calculated from curve fittings are shown in Table 1. Better regression correlations were calculated for Langmuir model suggesting that the Langmuir model is more convenient in describing the adsorption process. This signifies that the adsorption is of a typical monomolecular layer form [29]. It assumes that the adsorption is localized, all active sites have similar energies and no interaction between the adsorbed molecules exists [30]. The different affinities and adsorption capacities rely on both the adsorbent (mainly its guanine moities) and the adsorbate (ionic radius, electronegativity, charge…) [29,31]. Consequently, comparing the divalent metal ions, the orders of affinity and adsorption capacity decrease with increasing ionic radii and electronegativity.

Table 1: Constant parameters and correlation coefficients calculated for different adsorption models at different temperatures for Cu^{2+}, Cd^{2+} and Pb^{2+} adsorption.

Isotherm	**Langmuir**				**Freundlich**		
Constants	**Q_0 (µg/g)**	**b (L/µg)**	**R_L**	**r^2**	**N**	**k_F (µg/g)**	**r^2**
Cd^{2+}	280.1	0.087	0.0394	0.9999	6.4168	122.7	0.9677
Cu^{2+}	400	0.0707	0.0341	0.9998	5.125	142.5	0.9758
Pb^{2+}	343.6	0.1046	0.0271	0.9999	7.3986	168.7	0.9796

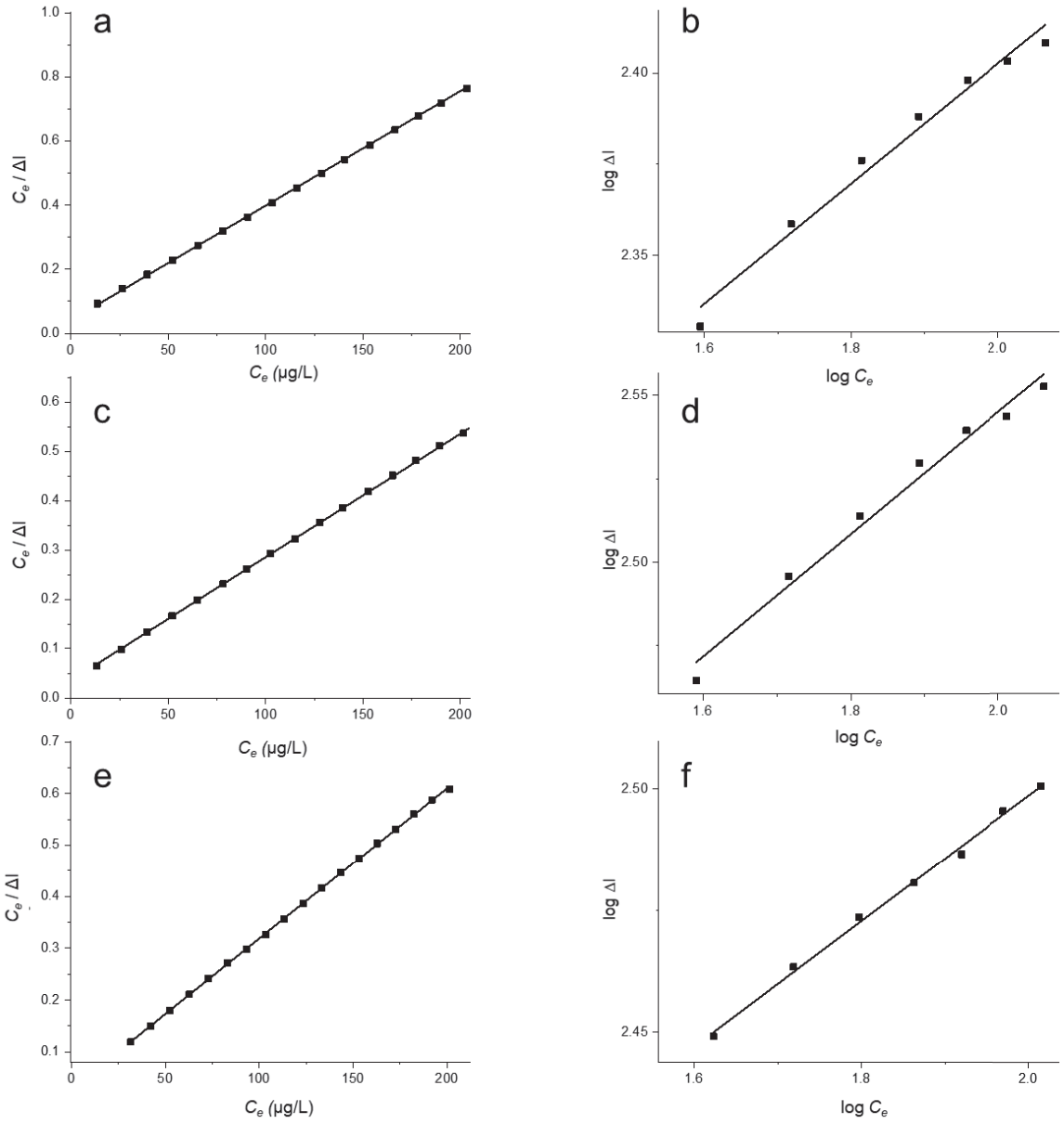

Figure 9: Langmuir adsorption isotherms for (a) Cd^{2+} in the range of 13 – 265 μg/L, (c) Cu^{2+} in the range of 13 – 229 μg/L and (e) Pb^{2+} in the range of 5 – 202 μg/L. Freundlich adsorption isotherms for (b) Cd^{2+} in the range 40 – 142 μg/L, (d) Cu^{2+} in the range 26 – 130 μg/L and (f) Pb^{2+} in the range 31 – 124 μg/L.

According to Roland and Sigel, guanine contains imidazole and pyridine-type nitrogens well suited for divalent metal ions binding [5], and in general the binding of metal cations is governed by the formation of energetically favorable coordination complexes [6]. The interaction of guanine or a guanine derivative G with a divalent metal ion M^{2+} yields $M(G)^{2+}$ complexes [32]. Most investigations about the complexation of the nucleobases with metal ions do not focus on the free nucleobases, but rather on DNA itself or DNA-resembling structures and related bio-molecules [4].

Nonetheless, it is reported that amongst divalent metal ions that can bind both the phosphate and the DNA base, copper (II) has the strongest affinity to the base [6], which confirms our findings. It was shown that copper can be coordinated to guanine through the N(7) and O(6) atoms, as well as a possible monocoordination to the N(7) position only, depending on the guanine tautomer [33]. Lead on the other hand is known to weakly interact with the N(7) and O(6) atoms of guanine [6] knowing that Pb^{2+} is an excellent oxidizer and strong Lewis acid [34]. Cadmium is classified as a soft metal that binds preferentially to DNA bases more than DNA phosphates. Notwithstanding the different studies dedicated to the interaction between Cd^{2+} and nucleobases, the exact nature of binding remains uncertain. It was suggested that cadmium most likely binds to guanine at its N(7) center in a 1:1 ratio [35].

Comparing the behavior of the three divalent heavy metals with guanine, it is evident that the highest adsorption capacity is observed for Cu (II) followed by Pb (II) and Cd (II). This trend comes in accordance with a study done by Hammud et al. on the interaction of some nucleobase derivatives with divalent metals. They found that it follows the ionic radii of the cations such that as the radius increases, the stability of the formed complexes increases [36]. This order is also in agreement with a report by Sharma et al. who potentiometrically studied the stability constant of a pyrimidine derivative with divalent metal ions. According to their observations, the trend depends on both the ionic radius and the second ionization energy [37]. Based on a recent study, different factors affect the stability of metal complexes including the nature of the central metal ion, nature of the ligand, chelating effect, macrocyclic effect, resonance effect and steric effect/hindrance [38]. Thus, this original and sensitive design can further help clarify the guanine-heavy metal interaction, with a possible application of these functionalized beads as advanced material for heavy metal ions complexation, removal and detection from aqueous solutions.

3.3.6. Voltammetric detection of divalent heavy metals with the GH-APTES-Fe_3O_4 modified BDD electrode

Following the adsorption isotherms, the plots of each heavy metal were assessed to study the analytical behavior of the guanine hydrazide functionalized nanoparticles. The peak intensities obtained in figure 8 were plotted as a function of the metals' concentrations, and the linear ranges were considered. Starting with cadmium in figure 10a, its plot can be divided into 2 linear parts: the first linear range was found between 0.232 and 0.809 µM (26 – 91 µg/L) with a correlation coefficient r^2 of 0.9274 and sensitivity of 101.4 µA/µM (0.9 $\mu A.\mu g^{-1}.L$) while the second linear range was observed between 0.925 and 1.815 µM (104 – 204 µg/L) with r^2= 0.9775 and sensitivity of 13.4 µA/µM (0.12 $\mu A.\mu g^{-1}.L$). Considering the first linear range, the obtained concentration range

and limit of detection are comparable to reported values using Fe_3O_4 nanoparticles for the detection of Cd (II) by square wave voltammetry (Table 2).

Table 2: Comparison of the linear detection range and sensitivity with previously reported values for the electrochemical detection of Cd (II).

Electrode modification	**Method**	**Concentration Range (µM)**	**LOD (µM)**	**Sensitivity (µA/µM)**	**Reference**
Polydopamine-Fe_3O_4	SWASV	0.02 – 0.59	9.2×10^{-5}	196	[39]
Reduced graphene oxide-Fe_3O_4	SWASV	0 – 0.8	0.056	14.82	[40]
Chitosan-Fe_3O_4	SWASV	1.2 – 1.7	0.0392	8.11	[1]
Fe_3O_4	SWASV	0.3 – 1.3	0.154	3.18	[41]
Terephthalic acid-Fe_3O_4	SWASV	0.4 – 1.1	0.2	12.15	[42]
GH-APTES-Fe_3O_4	SWV	0.232 – 0.809	0.077	101.4	Current work

The same behavior was noticed upon the subsequent addition of Pb (II) and Cu (II) respectively. The measurements were carried out in a citrate buffer solution pH 4. As shown in Fig. 10b, the calibration graph obtained for Pb (II) detection exhibited two linear response ranges of 0.0483 – 0.4521 µM or 10 – 94 µg/L (r^2 = 0.9113) and 0.550 – 1 µM or 114 – 207 µg/L (r^2= 0.98601) with the sensitivities of 156.38 µA/µM (0.75 $\mu A.\mu g^{-1}.L$) and 28.25 µA/µM (0.14 $\mu A.\mu g^{-1}.L$), respectively. By comparing the results obtained with previously reported electrochemical studies, a noticeable increase in sensitivity, similar to the case of Cd (II) was noticed (Table 3).

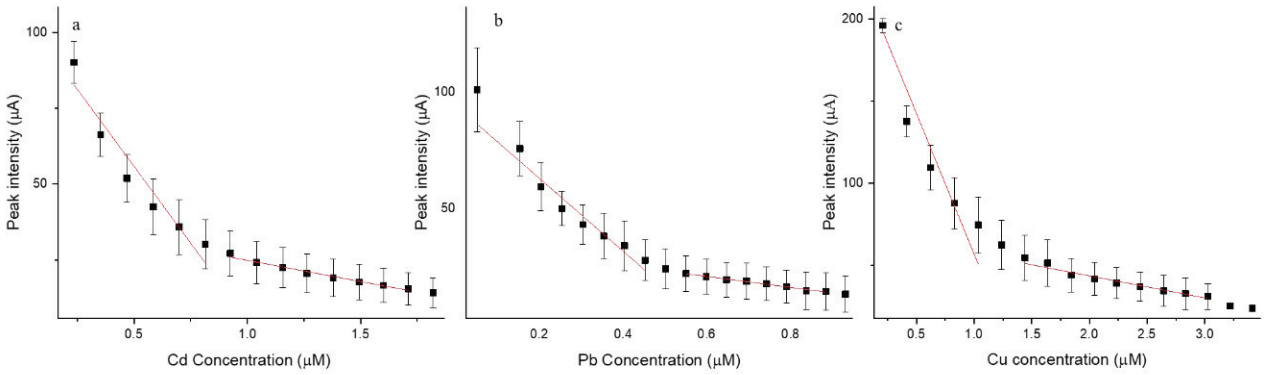

Figure 10: Linear ranges of (a) cadmium, (b) lead and (c) copper at the GH-APTES-Fe_3O_4 NP electrode.

Table 3: Comparison of the current concentration range and sensitivity with previously reported values for the electrochemical detection of Pb (II).

Electrode modification	**Method**	**Concentration Range (μM)**	**LOD (μM)**	**Sensitivity (μA/μM)**	**Reference**
Amine–Fe_3O_4	SWASV	0.5 – 8	0.15	10.07	[43]
Polydopamine-Fe_3O_4	SWASV	5×10^{-3} – 0.6	1.4×10^{-6}	235	[39]
Fe_3O_4	SWASV	0.3 – 1.3	0.119	14.9	[41]
Chitosan-Fe_3O_4	SWASV	0.1 – 1.3	0.0422	50.6	[1]
Terephthalic acid-Fe_3O_4	SWASV	0.4 – 1.1	0.04	8.56	[42]
GH-APTES-Fe_3O_4	SWV	0.0483 – 0.497	0.011	156	Current work

In the case of Cu (II), the calibration plots were divided between two linear ranges: the first range from 0.209 to 1.03 μM (13 – 65 μg/L) with r^2= 0.92098 and a sensitivity of 171.6 μA/μM (2.7 $\mu A.\mu g^{-1}.L$), and the second range from 1.44 to 3 μM (91 – 190.5 μg/L) with r^2= 0.94262 and a sensitivity of 13.5 μA/μM (0.2 $\mu A.\mu g^{-1}.L$) (figure 10c). It is worth mentioning that the sensitivity for

copper is much higher (more than tenfold) than in all other reported works using iron oxide nanoparticles [3, 11, 1, 41] with a comparable limit of detection of 0.069 µM.

Furthermore, the reproducibility among five independent GH functionalized Fe_3O_4 electrodes was evaluated by comparing the linear ranges with each of the studied heavy metals. The data in figure 9 show that the electrochemical sensor demonstrates a good reproducibility over five independent measurements such that the maximum relative standard deviation RSD is 4% in the case of Cu (II), 5% for Pb (II) and 10% for Cd (II).

3.4. Conclusion

In the present work, we report the development of a novel material, GH-APTES functionalized iron oxide nanoparticles. These nanoparticles were used to modify a BDD electrode in order to assess the interaction between guanine hydrazide and divalent heavy metal ions. The adsorption isotherms were investigated and it was proven that the data are better modelled with Langmuir isotherm, with adsorption capacities decreasing in the order: Cu^{2+}>Pb^{2+}>Cd^{2+}. This design allowed us to evaluate these ions such that the sensitivities and LODs were 171.61 µA/µM and 0.069 µM for Cu (II), 156 µA/µM and 0.0161 µM for Pb (II) and 101.4 µA/µM for 0.077 µM Cd (II), respectively. Moreover, the sensitivity obtained in the detection of copper was at least ten times greater than all reported sensitivities using iron oxide. We anticipate that the synthesized GH-APTES-Fe_3O_4 nanoparticles are promising materials that can be used rapidly and economically for heavy metal complexation and removal for water decontamination. Further tests utilizing the different hydrazide nucleobases derivatives for the detection of heavy metals could be of interest and could help better elucidate the sensitivity and the mechanism of interaction between nucleobases and heavy metal ions.

Acknowledgements The authors acknowledge the financial support of the EU H2020 research and innovation program entitled Kardia Tool grant #768686.

References

[1] S. F. Zhou , X. J. Han, Y. Q. Liu, SWASV performance toward heavy metal ions based on a high-activity and simple magnetic chitosan sensing nanomaterials, J Alloys Compd, 684 (2016) 1-7.

[2] S. K. Toor, P. Devi, B. K. S. Bansod, Electrochemical detection of trace amount of arsenic (III) at glassy carbon electrode modified with Au/Fe3O4 nanocomposites, Aquatic Procedia, 4 (2015) 1107-1113.

[3] L. Dedelaite, S. Kizilkaya, H. Incebay, H. Ciftci, M. Ersoz, Z. Yazicigil, Y. Oztekin, A. Ramanaviciene, A. Ramanavicius, Electrochemical determination of Cu (II) ions using glassy carbon electrode modified by some nanomaterials and 3-nitroaniline, Colloids Surf: A, 483 (2015) 279-284.

[4] S. Zhan, Y. Wu, L. Wang, X. Zhan, P. Zhou, A mini-review on functional nucleic acids-based heavy metal ion detection, Biosens Bioelectron, 86 (2016) 353-368.

[5] R. K. Sigel, H. Sigel, A stability concept for metal ion coordination to single-stranded nucleic acids and affinities of individual sites. Accounts of chemical research, 43(7) (2010) 974-984.

[6] V. G. Kanellis, C. G. Dos Remedios, A review of heavy metal cation binding to deoxyribonucleic acids for the creation of chemical sensors, Biophysical reviews, 10(5) (2018) 1401-1414.

[7] X. B. Zhang, R. M. Kong, Y. Lu, Metal ion sensors based on DNAzymes and related DNA molecules, Annual review of analytical chemistry, 4 (2011) 105-128.

[8] M. R. Saidur, A. A. Aziz, W. J. Basirun, Recent advances in DNA-based electrochemical biosensors for heavy metal ion detection: a review, Biosensors and Bioelectronics, 90 (2017) 125-139.

[9] H. Moriwaki, Complexes of cadmium ion with guanine bases detected by electrospray ionization mass spectrometry, Journal of mass spectrometry, 38(3) (2003) 321-327.

[10] J. V. Burda , J. Šponer, F. Šebesta, Metal Interactions with Nucleobases, Base Pairs, and Oligomer Sequences; Computational Approach, Handbook of Computational Chemistry, (2017) 1827-1874.

[11] P. Subramanian, G. Dryhurst, Electrochemical oxidation of guanosine formation of some novel guanine oligonucleosides, Journal of electroanalytical chemistry and interfacial electrochemistry, 224(1-2) (1987) 137-162.

[12] A. Afkhami, R. Moosavi, T. Madrakian, H. Keypour, A. Ramezani-Aktij, M. Mirzaei-Monsef, Construction and application of an electrochemical sensor for simultaneous determination of Cd (II), Cu (II) and Hg (II) in water and foodstuff samples, Electroanalysis, 26(4) (2014) 786-795.

[13] G. Wang, Y. Ma, Y. Tong, X. Dong, Synthesis, characterization and magnetorheological study of 3-aminopropyltriethoxysilane-modified Fe3O4 nanoparticles, Smart Materials and Structures, 25(3) (2016) 035028.

[14] D. Wu, Y. Li, Y. Zhang, P. Wang, Q. Wei, B. Du, Sensitive electrochemical sensor for simultaneous determination of dopamine, ascorbic acid, and uric acid enhanced by amino-group functionalized mesoporous Fe3O4@ graphene sheets, Electrochimica Acta, 116 (2014) 244-249.

[15] M. E. Khosroshahi, L. Ghazanfari, Synthesis and functionalization of SiO2 coated Fe3O4 nanoparticles with amine groups based on self-assembly, Materials Science and Engineering: C, 32(5) (2012) 1043-1049.

[16] J. P. Chen , P. C. Yang, Y. H. Ma, S. J. Tu, Y. J. Lu, Targeted delivery of tissue plasminogen activator by binding to silica-coated magnetic nanoparticle, International journal of nanomedicine, 7 (2012) 5137.

[17] M. Yamaura, R. L. Camilo, L. C. Sampaio, M. A. Macêdo, M. Nakamura, H. E. Toma, Preparation and characterization of (3-aminopropyl) triethoxysilane-coated magnetite nanoparticles, Journal of Magnetism and Magnetic Materials, 279(2-3) (2004) 210-217.

[18] Y. P. Yew, K. Shameli, M. Miyake, N.B.B.A. Khairudin, S.E.B. Mohamad, H. Hara , M.F.B.M Nordin, K.X. Lee, An Eco-Friendly Means of Biosynthesis of Superparamagnetic Magnetite Nanoparticles via Marine Polymer, IEEE Trans Nanotechnol, 16 (2017) 1047-1052.

[19] G. M. Swain, R. Ramesham, The electrochemical activity of boron-doped polycrystalline diamond thin film electrodes, Analytical chemistry 65(4) (1993) 345-351.

[20] A. Bee, R. Massart, S. Neveu, Synthesis of very fine maghemite particles, Journal of Magnetism and Magnetic Materials, 149(1-2) (1995): 6-9.

[21] D. Pulido, A. Sánchez, J. Robles, E. Pedroso, A. Grandas, Guanine-Containing DNA Minor-Groove Binders, European Journal of Organic Chemistry, 2009 (2009) 1398-1406.

[22] G. Karabanovich, J. Zemanova, T. Smutny, R. Szekely, M. Sarkan, I. Centarova, A. Vocat, I. Pavkova, P. Conka, J. Nemecek, J. Stolarikova, M. Vejsova, K. Vavrova, V. Klimesova, A. Hrabalek, P. Pavek, S.T. Cole, K. Mikusova, J. Roh, Development of 3,5-Dinitrobenzylsulfanyl-1,3,4-oxadiazoles and Thiadiazoles as Selective Antitubercular Agents Active Against Replicating and Nonreplicating Mycobacterium tuberculosis, J Med Chem, 59 (2016) 2362-2380.

[23] H. H. Hammud, M. H. El Dakdouki, N. M. Sonji, K. H. Bouhadir, Solvatochromic absorption and fluorescence studies of adenine, thymine and uracil thio-derived acyclonucleosides, European Journal of Chemistry, 6 (2015) 325 - 336.

[24] C. Prado, G.U. Flechsig, P. Grundler, J.S. Foord, F. Markenc, R.G. Compton, Electrochemical analysis of nucleic acids at boron-doped diamond electrodes, Analyst, 127 (2002) 329-332.

[25] H. Sun, L. Dong, H. Yu, M. Huo, Direct electrochemical oxidation and detection of hydrazine on a boron doped diamond (BDD) electrode, Russian Journal of Electrochemistry, 49 (2013) 883-887.

[26] P.S.V. Kumar, C.; Kirthika, K. and Kumar, K. Sathish, Kinetics and equilibrium studies of Pb2+ in removal from aqueous solutions by use of nano-silversol-coated activated carbon, Braz. J. Chem. Eng. [online], 27 (2010) 339-346.

[27] I. Langmuir, The Adsorption of Gases on Plane Surface of Gases on Plane Surface of Glass, Mica and Platinum, J. Am. Chem. Soc., 40 (1918) 1361-1403.

[28] J.L. Subramanyan Vasudevan, Ramasamy Vanathi, Electrochemical Coagulation for Chromium Removal: Process Optimization, Kinetics, Isotherms and Sludge Characterization, Clean 38 (2010) 9-16.

[29] K.Y. Kumar, T.N.V. Raj, S. Archana, S.B.B. Prasad, S. Olivera, H.B. Muralidhara, SnO2 nanoparticles as effective adsorbents for the removal of cadmium and lead from aqueous solution: Adsorption mechanism and kinetic studies, Journal of Water Process Engineering, 13 (2016) 44-52.

[30] V. Fierro, V. Torné-Fernández, D. Montané, A. Celzard, Adsorption of phenol onto activated carbons having different textural and surface properties, Microporous and Mesoporous Materials, 111 (2008) 276-284.

[31] W. Zhan, C. Xu, G. Qian, G. Huang, X. Tang, B. Lin, Adsorption of Cu(ii), Zn(ii), and Pb(ii) from aqueous single and binary metal solutions by regenerated cellulose and sodium alginate chemically modified with polyethyleneimine, RSC Advances, 8 (2018) 18723-18733.

[32] J.Z. Bin Song, Helmut Sigel, Rolf Griesser, Cordula Meiser, and Bernhard Lippert, Effects of (N7)-Coordinated Nickel(ii), Copper(ii), or Platinum(ii) on the Acid ± Base Properties of Guanine Derivatives and Other Related Purines, Chem Eur J, 5 (1999) 2374-2387.

[33] T. Marino, M. Toscano, N. Russo, A. Grand, Gas-phase interaction between DNA and RNA bases and copper (II) ion: A density functional study, International Journal of Quantum Chemistry, 98 (2004) 347-354.

[34] A. Dimkovikj, M.J. Banton, L.A. McDanel, K.N. Arndt, K.E. Unvert, E.K. Thorn, A.R. Marco, R.A. Hellmann-Whitaker, Characterization of tRNA(Leu) binding interactions with Cu(2+) and Pb(2+) and their biological implications, J Inorg Biochem, 171 (2017) 90-99.

[35] Z. Hossain, F. Huq, Studies on the interaction between Cd2+ ions and nucleobases and nucleotides, Journal of Inorganic Biochemistry, 90 (2002) 97-105.

[36] M.H.E.-D. Hassan H. Hammud, Nada Sonji, Ghassan Sonji & Kamal H. Bouhadir, Interactions of Some Divalent Metal Ions with Thymine and Uracil Thiosemicarbazide Derivatives, Nucleosides, Nucleotides and Nucleic Acids, 35 (2016) 259-276.

[37] B.S. Parvesh Sharma, S. Millal, R. K. Sharma, S. K. Sindhwani, Solution and molecular modeling studies on some bivalent metal complexes of higher analogues of biologically active 1,3-diaryl-4, 5, 6-pyrimidinetrione-2-thioxo-5-oxime, Indian Journal of Chemistry, 40A (2001) 1076-1081.

[38] S. Muthaiah, A. Bhatia, M. Kannan, Stability of Metal Complexes, Stability and Applications of Coordination Compounds. IntechOpen, 2020.

[39] Q. Song, M. Li, L. Huang, Q. Wu, Y. Zhou, Y. Wang, Bifunctional polydopamine@Fe3O4 core-shell nanoparticles for electrochemical determination of lead(II) and cadmium(II), Anal Chim Acta, 787 (2013) 64-70.

[40] Y.-F. Sun, W.-K. Chen, W.-J. Li, T.-J. Jiang, J.-H. Liu, Z.-G. Liu, Selective detection toward Cd2+ using Fe3O4/RGO nanoparticle modified glassy carbon electrode, Journal of Electroanalytical Chemistry, 714-715 (2014) 97-102.

[41] H.-L. Fan, S.-F. Zhou, J. Gao, Y.-Z. Liu, Continuous preparation of Fe3O4 nanoparticles through Impinging Stream-Rotating Packed Bed reactor and their electrochemistry detection toward heavy metal ions, Journal of Alloys and Compounds, 671 (2016) 354-359.

[42] S. Deshmukh, G. Kandasamy, R.K. Upadhyay, G. Bhattacharya, D. Banerjee, D. Maity, M.A. Deshusses, S.S. Roy, Terephthalic acid capped iron oxide nanoparticles for sensitive electrochemical detection of heavy metal ions in water, Journal of Electroanalytical Chemistry, 788 (2017) 91-98.

[43] S. Xiong, M. Wang, D. Cai, Y. Li, N. Gu, Z. Wu, Electrochemical Detection of Pb(II) by Glassy Carbon Electrode Modified with Amine-Functionalized Magnetite Nanoparticles, Analytical Letters, 46 (2013) 912-922.

Chapter IV: The use of voltammetry for sorption studies of arsenic (III) ions by magnetic beads functionalized with nucleobase hydrazide derivatives

Introduction

Arsenic is one of the most toxic heavy metal ions that can be released into the environment through natural and anthropogenic causes. It is known to cause several types of cancer due to long term exposure and irregularities in several systems due to slight contamination. It has four known oxidation states, of which trivalent As(III) and pentavalent As(V) are dominant in aqueous media. It has been classified as a carcinogen and the World Health Organization along with the Environmental Protection Agency have set a maximum permissible limit of 10 µg/L in drinking water.

Different nucleobase hydrazides were prepared by a base catalyzed Michael-type addition reaction between the various nucleobases and ethyl acrylate. After that, the obtained products were reacted with excess hydrazine hydrate to yield the different hydrazides. These hydrazides were used to functionalize iron oxide nanoparticles Fe_3O_4 NPs, prepared by a modified Massart's method, using glutaraldehyde as a crosslinking agent. The nanoparticles were characterized following each step of the synthesis using infrared spectroscopy to confirm the successful synthesis and functionalization with the nucleobase hydrazides.

The functionalized nanoparticles were used to modify a boron doped diamond electrode, and square wave voltammetry was applied in presence of different concentrations of arsenic. After optimizing the pH and upon increasing the concentration of arsenic, the signal intensity corresponding to the oxidation of the nucleobases decreased. Adsorption isotherms were investigated using Langmuir and Freundlich models, and Langmuir proved to be a better fit. Moreover, it was shown that magnetic nanoparticles functionalized with guanine hydrazide presented the highest adsorption capacity for arsenic ions followed by uracil hydrazide and adenine hydrazide. Kinetic studies showed that the adsorption process follows a pseudo-second order model signifying that chemisorption is involved in the process.

The experimental data presented in this report are a proof to earlier theoretical studies about the affinity of arsenic to different nucleobases. It was shown that the arsenic-guanine complex is much more stable compared to adenine and uracil complexes. It was also shown that arsenic prefers binding to purine rather than pyrimidine bases.

The electrochemical detection of arsenic was also investigated by applying the same conditions. Again, magnetic nanoparticles functionalized with guanine hydrazide showed the best results with the lowest limit of detection in the nanomolar range and the highest sensitivity compared to the other nucleobase hydrazides studied. Consequently, it was shown that guanine hydrazide-

magnetic nanoparticles are great adsorbents, in addition to their potential in being used for designing aptasensors.

The use of voltammetry for sorption studies of arsenic (III) ions by magnetic beads functionalized with nucleobase hydrazide derivatives

Material from: S. Sawan, K. Hamze, A. Youssef, K. Bouhadir, A. Errachid, R. Maalouf, N. Jaffrezic-Renault, The use of voltammetry for sorption studies of arsenic (III) ions by magnetic beads functionalized with nucleobase hydrazide derivatives, Electroanalysis, published 2021, Wiley.

ABSTRACT

The objective of this work is to study the interaction characteristics of nucleobases with As(III). Novel materials magnetic nanoparticles (MNPs) functionalized with adenine hydrazide (AH), guanine hydrazide (GH) and uracil hydrazide (UH) were elaborated. The adsorption isotherms were investigated electrochemically and it was shown that the adsorption capacity of the nanoparticles towards arsenic (III) increased in the following order: AH < UH < GH. The electrochemical detection of As(III) using the GH functionalized MNPs offered better results compared with the other functionalizations, with a sensitivity of 1.92 $\mu A.\mu g^{-1}.L$ (144 $\mu A/ \mu M$) and a limit of detection of 1.6 µg/L (21 nM).

Keywords: adsorption isotherm, arsenic, Fe_3O_4 nanoparticles, nucleobase-heavy metal interaction, nucleobase hydrazides

4.1. Introduction

The ubiquity of arsenic in the environment is of both anthropogenic and natural causes. Arsenic is the twentieth most abundant element in the earth's crust [1], whereas human activities such as smelting, mining, fossil fuel burning and pesticides and fertilizers usage are the major anthropogenic contributors of arsenic contamination [2]. Arsenic is an environmental contaminant that can be found in soil, water, air and food [3]. Long term exposure to arsenic is associated with several adverse effects including skin, liver, kidney and prostate cancer [4]. On the other hand, slight contamination can modify the functioning of the cardiovascular, gastrointestinal and nervous systems [1, 4] due to the fact that arsenic can accumulate in the body tissues and bind to the sulfhydryl sites

altering the functionality of proteins [2]. Arsenic can exist in four different oxidation states: As(-III), As(0), As(III) and As(V) [5] of which, inorganic oxyanions of arsenic as pentavalent arsenate As(V) and trivalent arsenite As(III) are predominant in aqueous environments [6]. Due to all its numerous undesirable effects, the International Agency for Research on Cancer has classified arsenic as group I human carcinogen. Moreover, several agencies including the World Health Organization and the United States Environmental Protection Agency have reduced the maximum permissible level of arsenic in drinking water to 10 μg/L [6]. Thus, sensitive and selective analysis, as well as removal of arsenic species from water in various environmental matrices is of high importance.

The removal of the inorganic trivalent forms of arsenite is of particular importance since As(III) is 60 times more toxic than As(V) [7]. The distribution of the charge and species depends on the pH and redox potential [4]. Numerous technologies have been employed for the removal of arsenic from water. These include ion exchange [8], photocatalysis [9], reverse osmosis [10], coagulation [11] and adsorption [12]. Among those, adsorption presents the most advantages including low cost, simple technology and sludge-free operation [13] without producing any byproducts compared to the other techniques. Various conventional adsorbents have been used for the removal of arsenic such as surfactants, synthetic activated carbon, industrial byproducts, mineral products and iron based materials [14]. Recently, Liu et al. reviewed and focused on novel materials such as carbon nanotubes, metal organic framework and nanoparticle-modified graphene oxide as sorbents and it was deduced that advanced materials are more effective treatment options compared to conventional sorbents [12].

Nanomaterials and nanotechnology have been rapidly developing in the past decades, opening new horizons in several domains including that of water purification [15]. Nanoparticles present the advantages of smaller size and hence larger surface area. Magnetic nanoparticles specifically were found to be very effective in the removal of arsenic because of their strong adsorption activities and ease of separation by applying an external magnetic field [15]. However, magnetite (Fe_3O_4) nanoparticles are known to aggregate as a result of magnetic dipole-dipole interactions among the particles. In order to overcome such drawback, Fe_3O_4 nanoparticles are usually coated or functionalized [16].

The efficiency of new adsorbents should always be evaluated through information such as adsorption mechanism, kinetics, capacity and affinity towards different adsorbates. Conventional adsorption studies involve batch experiments requiring the separation of the adsorbent prior to the analytical determination of heavy metals in the supernatant. Voltammetry has been long used for

heavy metal ion determination [17]. In adsorption studies, it offers the advantages of low cost, small volumes and no need to separate the adsorbent from the supernatant. Despite all that, only a few have reported the use of voltammetry in the adsorption of heavy metals [18]. Many researchers have described the design of sensitive and selective aptamer-based biosensors for arsenic detection [19-22]. Benefiting from the great affinity of heavy metals to nucleobases and aptamers, a high sensitivity and excellent selectivity are achieved.

Therefore, the objective of this work is to introduce a simple electrochemical system using magnetic nanoparticles functionalized with different nucleobase derivatives for the adsorption of As(III). Furthermore, the interaction of As(III) with nucleobases will be assessed through adsorption experiments. To the best of our knowledge, this is the first report using voltammetry as the method of choice for adsorption studies of arsenic ions. This work will help in selecting the most sensitive nucleobase fundamentally achieving a promising perspective for designing novel aptasensors for As(III) detection.

4.2. Materials and Methods

4.2.1. Chemical Reagents

All the reagents used in this study were of analytical grade and used as received without any further purification. Ammonium hydroxide (NH_4OH) (25% in H_2O), (3-aminopropyl)triethoxysilane (APTES) 99%, glutaraldehyde solution Grade II (25% in H_2O), potassium chloride (99 – 100.5%) and potassium citrate tribasic monohydrate (≥ 99%) were purchased from Sigma-Aldrich. Dimethyl sulfoxide (DMSO) (≥ 99.9%) was purchased from Riedel-de-Haën, sodium hydroxide (NaOH) (98.5 – 100%), arsenic standard from Fluka and ethanol (≥ 99.8%) from Honeywell. Ferric chloride hexahydrate $FeCl_3.6H_2O$ (98%) and ferrous chloride tetrahydrate $FeCl_2.4H_2O$ (99%) were purchased from Acros Organic. The reagents utilized in the synthesis and characterization of adenine hydrazide, guanine hydrazide and uracil hydrazide were purchased from Fluka Chemika, Merck or Sigma-Aldrich. All solutions were prepared using deionized water (with a resistivity of 18.2 MΩ.cm).

4.2.2. Apparatus

PalmSens 4 was used for performing all electrochemical measurements. A three-electrode system was utilized; the working electrode was a bare or modified boron doped diamond electrode,

the counter electrode was a Platinum plate and the reference electrode was Ag/AgCl. Square wave voltammetry was the technique of choice in all measurements with the following optimized conditions: frequency 50 Hz; amplitude 50 mV; step potential 10 mV; time of equilibration 2 min. A 300 mT cylindrical magnet was used to ensure the paramagnetic nanoparticles remain adhered to the BDD surface. Citrate buffered solutions (0.1 M, containing 0.5 M KCl, pH 4) were used as electrolytes for the various measurements.

4.2.3. Synthesis and characterization of the nucleobase hydrazides

The syntheses of the nucleobase derivatives were detailed in previous publications [20] and are briefly described below. The method employed a base catalyzed Michael-type addition reaction between the nucleobases and ethyl acrylate in refluxing ethanol followed by the reaction of the isolated products with excess hydrazine hydrate in refluxing ethanol to afford hydrazides in excellent yields. All the hydrazide derivatives were characterized using ^{1}H NMR, ^{13}C NMR, HRMS and FTIR.

4.2.3.1. Synthesis of adenine hydrazide

Adenine (16.7 g, 123 mmol) was dissolved in an ethanol:benzene mixture (8:1, 562 mL) and the flask was immersed in an ice-water bath. Sodium metal (175 mg) was carefully added followed by the dropwise addition of ethyl acrylate (5 mL) and the mixture was refluxed overnight, after which the solvent was evaporated under reduced pressure and the residue was triturated with cold ethanol, filtered and dried under reduced pressure to afford a colorless solid (26.7 g, 92%). Ethanol (300 mL) was added to 15 g of this solid and stirred at room temperature followed by the dropwise addition of hydrazine-hydrate (9.58 g, 191 mmol). The mixture was heated under reflux for 24 h and then the solution was cooled down to room temperature and the solvent was removed under reduced pressure. The residue was triturated with cold ethanol, filtered and dried under reduced pressure to obtain the adenine hydrazide as a colorless solid (13.9 g, 99%) [24].

4.2.3.2. Synthesis of guanine hydrazide

Synthesis started with the acetylation of the exocyclic amine of guanine to protect it. Guanine (10 g, 66.22 mmol) was solubilized in N,N-dimethylacetamide (30 mL), and acetic anhydride (16.5 mL, 168 mmol) was added. The reaction was kept stirring overnight under reflux. After cooling to room temperature, the solid was collected via suction filtration and placed under reflux at 80 °C for

2-3 hours in a water:ethanol 1:1 mixture (30 mL). The resultant precipitate was then recovered and dried under reduced pressure at 70°C to give a white solid. With the help of dimethylformamide (50 mL), the solid was transferred to a 500 mL round bottom flask along with an ethanolic solution of sodium ethoxide (2 mL, 25.9 mmol), and the mixture was stirred for 15 min. After that, the mixture was left under reflux at 165°C for 1h upon the addition of ethyl acrylate (3.8 mL, 34.96 mmol). After evaporating the solvent, the obtained residue was dissolved in methylene chloride and washed with distilled water. Methylene chloride and the residue were separated from water, dried, filtered and the solvent was evaporated under reduced pressure. The crude was then triturated with toluene (250 mL) with overnight stirring at room temperature. After collecting the precipitate, it underwent drying under reduced pressure and purification by column chromatography on silica gel (CH_2Cl_2/MeOH 98:2) to yield a white solid (2.85g). This solid (7 g, 23.9 mmol) was mixed with ethanol (70 mL) and $N_2H_4.H_2O$ (4.1 mL, 83.6 mmol), stirred and heated at 80°C for 24 h. The precipitate was finally collected and dried at 70°C under reduced pressure to yield a white solid (5.54 g, 98%) [25].

4.2.3.3. Synthesis of uracil hydrazide

Uracil (25 g, 223 mmol) was dissolved in sodium ethoxide (4.4 mL, 44 mmol) and ethanol (595 mL). The solution was stirred then ethyl acrylate (30.4 mL, 279 mmol) was added. The resulting mixture was heated under reflux for 7 h. The reaction mixture was concentrated under reduced pressure to afford a quantitative white precipitate. The obtained white solid was collected via suction filtration, washed thoroughly with cold ethanol and cold ethyl acetate, and dried under vacuum to yield the desired product as white crystalline material (26.63 g). The remaining filtrate was concentrated again under vacuum to give an orange-like oily substance. Cold ethyl acetate was added, the flask was cooled in the fridge and a white precipitate was recovered. The white precipitate was filtered under vacuum and dried to give the desired product. 25 g of the product were dissolved in ethanol (563 mL) and hydrazine hydrate (31.3 mL, 413 mmol) was then added, and the resulting mixture was stirred under reflux overnight. The reaction mixture was allowed to cool to room temperature. An off-white precipitate formed upon cooling, so it was filtered under vacuum, washed with cold ethanol and dried under vacuum to give the desired product as an off white solid (17.89 g, 77%) [23].

4.2.4. Fabrication and characterization of APTES-coated iron oxide nanoparticles

A modified Massart's method previously reported by our group [25] was used to synthesize the magnetic nanoparticles. The synthesis started by mixing $FeCl_3.6H_2O$ (2.7 g) and $FeCl_2.4H_2O$ (1.2 g) in a molar ratio of 2:1 and dissolving them in 90 mL of deionized water. Next, 100 mL of NaOH solution (1 M) were added dropwise under vigorous stirring and nitrogen gas at 0°C. The formation of iron oxide nanoparticles was evident by a change in color. The solution was left under stirring for 4 hours to guarantee nucleation and growth of magnetite nanoparticles. The NPs were recovered with an external magnet, washed repeatedly with water followed by ethanol, and finally dried under vacuum. Iron oxide nanoparticles were sonicated for 25 min followed by the addition of ammonium hydroxide and (3-aminopropyl)triethoxysilane under nitrogen atmosphere. The mixture was allowed to age for 24 hours to ensure APTES coating, after which the nanoparticles were also washed with water followed by ethanol, dried and stored for later use. To confirm the successful synthesis and coating of the magnetic nanoparticles, FTIR spectra were collected and assessed following each step using PerkinElmer Spectrum Two spectrometer. Scanning Electron Microscopy (SEM) images for the magnetic nanoparticles were also taken to check the morphology of the NPs using Tescan, Vega 3 LMU with Oxford EDX detector (Inca XmaW20).

4.2.5. Elaboration of the electrochemical sensor

Glutaraldehyde (GA) was used as a crosslinking agent to immobilize the nucleobase derivatives were on the APTES coated iron oxide nanoparticles. A 1 mg/mL solution of each nucleobase hydrazide dissolved in DMSO, and 100 mg/L of the APTES coated nanoparticles were mixed together. Then, on a clean Boron-doped diamond (BDD) electrode, 20 µL of the prepared mixture were dropped and left for 20 minutes in saturated glutaraldehyde vapor. After that, the solvent was left to evaporate at room temperature for subsequent use in electrochemical measurements. The preparation and procedure were previously detailed in chapter 3.

4.3. Results and Discussion

4.3.1. Synthesis of the nucleobase derivatives

The synthesis of 9-(2-hydrazidoethyl)adenine was initiated from the commercially available adenine (1) following a reported procedure [24]. In short, adenine was refluxed with ethyl acrylate in the presence of catalytic amounts of sodium ethoxide in ethanol for 18 hours to afford 3-(adenine-9-yl)propionic acid ethyl ester (2). The reaction was quenched when complete conversion of

nucleobases into esters was obtained (reaction monitored with TLC). Compound 2 was converted afterwards to nucleobase-hydrazide via overnight reflux with hydrazine (and ethanol) to yield compound 3. In comparison, the guanine hydrazide derivative was prepared following a reported procedure [25] from guanine (4) that was first acetylated and hydrolyzed to yield the N2-acetyl guanine adduct (5). Compound 5 underwent the Michael reaction with ethyl acrylate to afford the guanine ester (6). The desired guanine hydrazide (7) was prepared from the compound 6 in a similar procedure to the adenine adduct described above (figure 1).

The uracil hydrazide was prepared following a similar synthetic protocol starting with the commercially available uracil [26]. In short, uracil underwent the Michael addition to ethyl acrylate to afford the uracil ester intermediate that was transformed to uracil hydrazide by refluxing in an ethanolic solution of hydrazine monohydrate (figure 2). Uracil has two Ns in the ring, one is similar to an amide (N1) and the other is similar to an imide (N3). With NaOH, the more basic hydrogen on N3 is firstly abstracted, followed by the less basic H on N1. As a result, N1 will preferentially attack the double bond on the ethyl acrylate (no N3 attack at all). That is why there is no need for protection in this reaction as opposed to the guanine hydrazide preparation.

Adenine hydrazide, guanine hydrazide and uracil hydrazide were characterized using IR, ^{1}H and ^{13}C NMR. All characterization data were previously detailed and published [20]. The FTIR spectra are presented in the insets of figure 3.

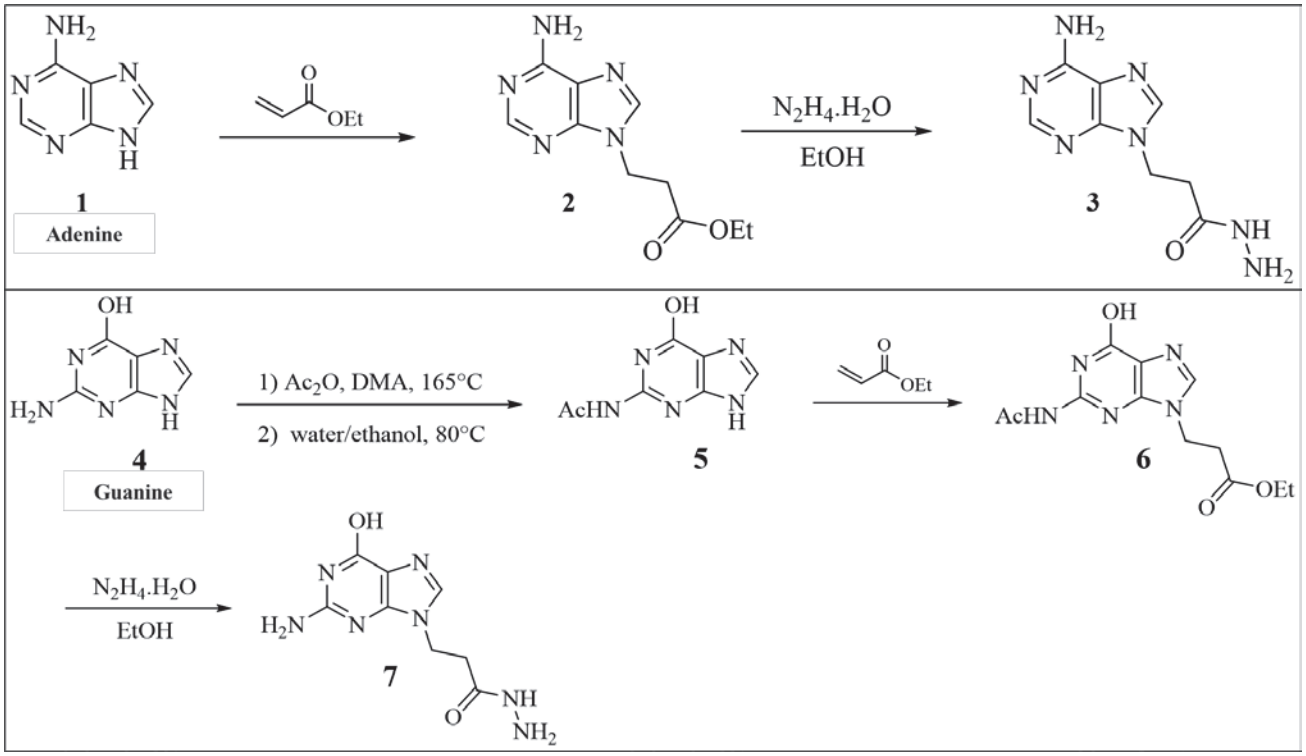

Figure 1: Synthesis of adenine hydrazide and guanine hydrazide.

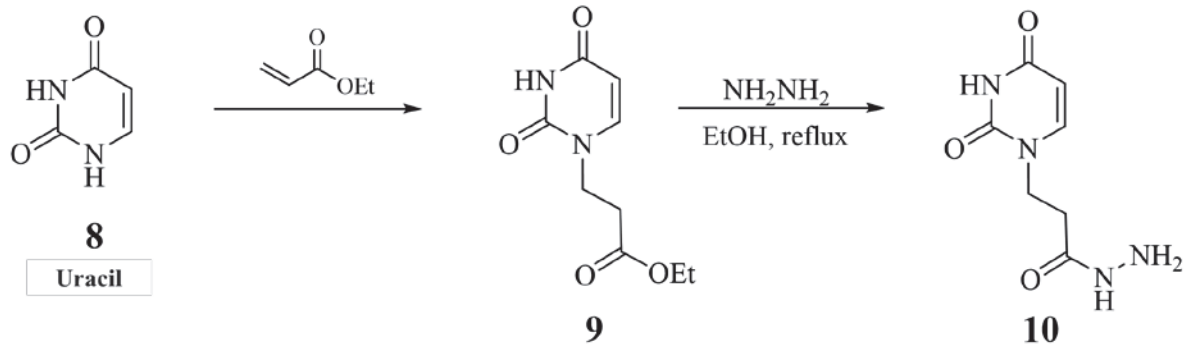

Figure 2: Synthesis of uracil hydrazide.

4.3.2. Functionalization of the magnetic beads

The successful synthesis and characterization of iron oxide (Fe_3O_4) nanoparticles coated with 3-aminopropyltriethoxysilane (APTES) have been earlier described by our team [25]. Figure 3D shows an SEM image of the magnetic nanoparticles capped with APTES. The obtained nanoparticles were spherical in shape, with a uniform size distribution of 45 nm. The APTES-coated magnetic beads were then functionalized with the different nucleobase derivatives in the presence of glutaraldehyde vapor.

The functionalization of the magnetic beads was proved using FT-IR with characteristic peaks proving the crosslinking between AH, GH or UH from one side and the APTES-coated Fe_3O_4

from the other side. Figure 3 shows FT-IR spectra of the bare and the coated nanoparticles. The spectrum of the bare nanoparticles showed only one peak at 550 cm^{-1} characteristic of the absorption of Fe-O. Coating of the Fe_3O_4 nanoparticles with (3- aminopropyl)triethoxysilane was confirmed by the appearance of new peaks. Bands at 3672 cm^{-1} and 1624 cm^{-1} attributed to the N-H stretching and NH_2 bending modes, respectively, of a free NH_2 group. Si-O-Si and SiO-H bands appeared at 1063 cm-^{1} and 1162 cm^{-1}. The stretching of -CH_2 was confirmed with bands at 2902 cm^{-1} and 2973 cm^{-1} [27]. The shift of the Fe-O band from 550 cm^{-1} to 562 cm^{-1} can be due to the overlap with the Fe-O-Si bond [28]. FT-IR measurements also showed the crosslinking of the nucleobase derivatives with the coated nanoparticles. Figure 3A shows the successful functionalization of the beads with adenine hydrazide. Bands at 1679 and 1422 cm^{-1} correspond to the C=O and C-N, respectively, of an amide function. N-H bands of an amine function appear at 3325 and 1647 cm^{-1} and the C=N of an aromatic-imine function appear at 1480 cm^{-1} [23]. In figure 3B, bands appear at 3366 cm^{-1} and 1604 cm^{-1} for N-H of an amine, 1698 cm^{-1} for the C=O of an amide, and 1567 cm^{-1} for C-N of an amide [25], thus confirming the presence of guanine hydrazide. The spectrum in figure 3C shows bands at 1675 and 1425 cm^{-1} for the C=O and C-N of an amide, 1613 and 3328 cm^{-1} for the N-H of an amine and 3080 cm^{-1} for the =C-H of a pyrimidine ring, confirming the functionalization of the magnetic beads with uracil hydrazide [23].

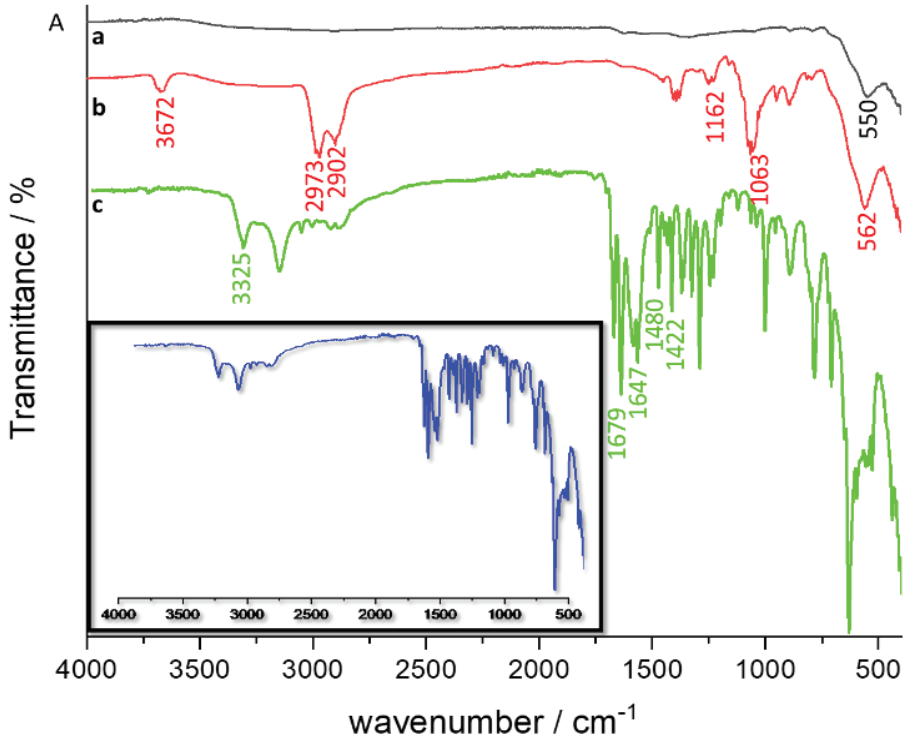

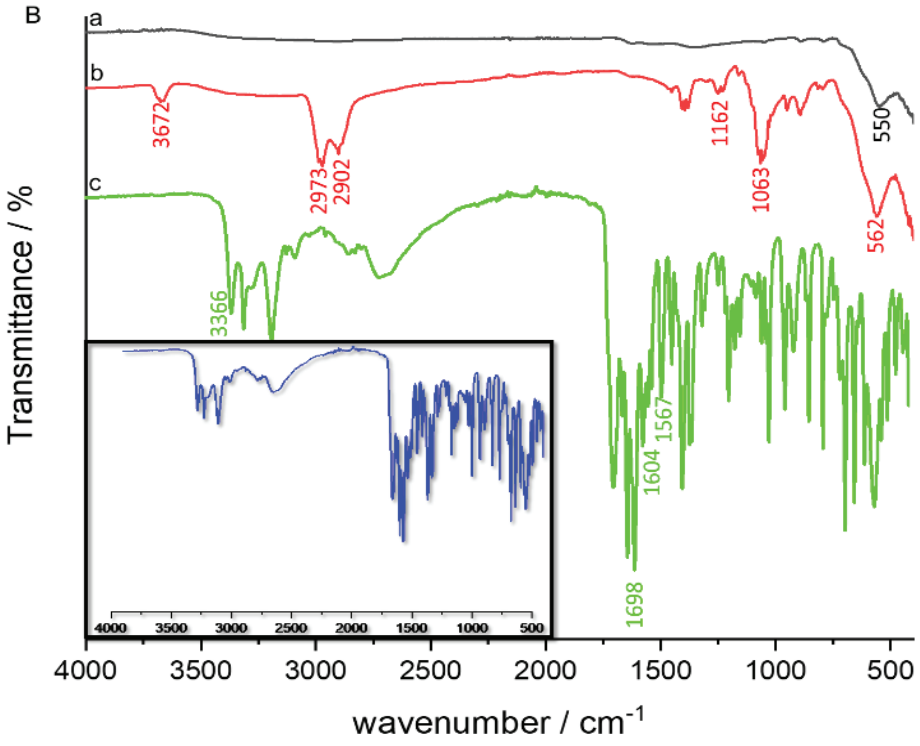
B
a
b
c
3672
2973
2902
1162
1063
550
562
3366
1698
1604
1567
Transmittance / %
4000 3500 3000 2500 2000 1500 1000 500
wavenumber / cm-1

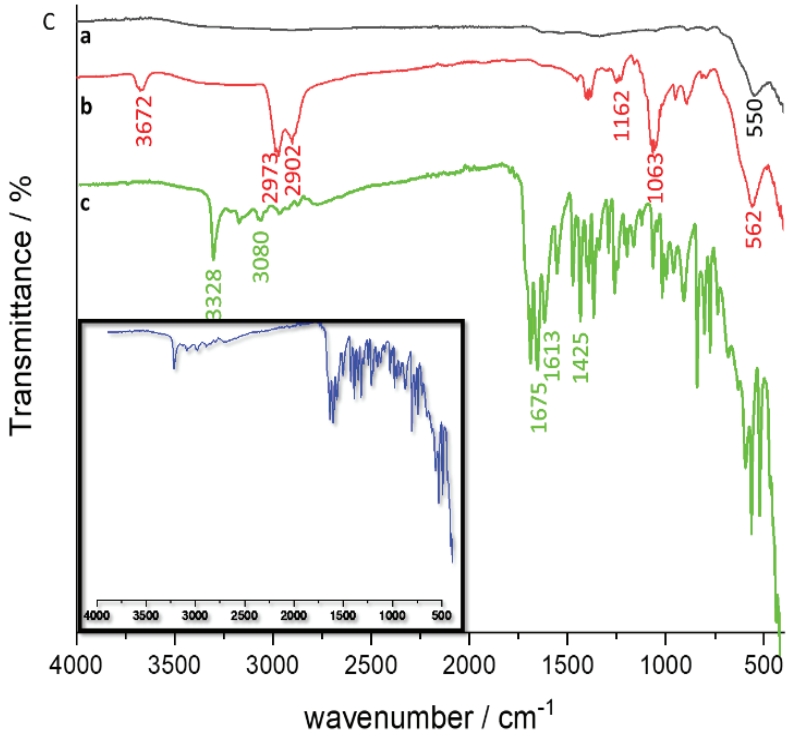
C
a
b
c
3672
2973
2902
1162
1063
550
562
3328
3080
1675
1613
1425
Transmittance / %
4000 3500 3000 2500 2000 1500 1000 500
wavenumber / cm-1

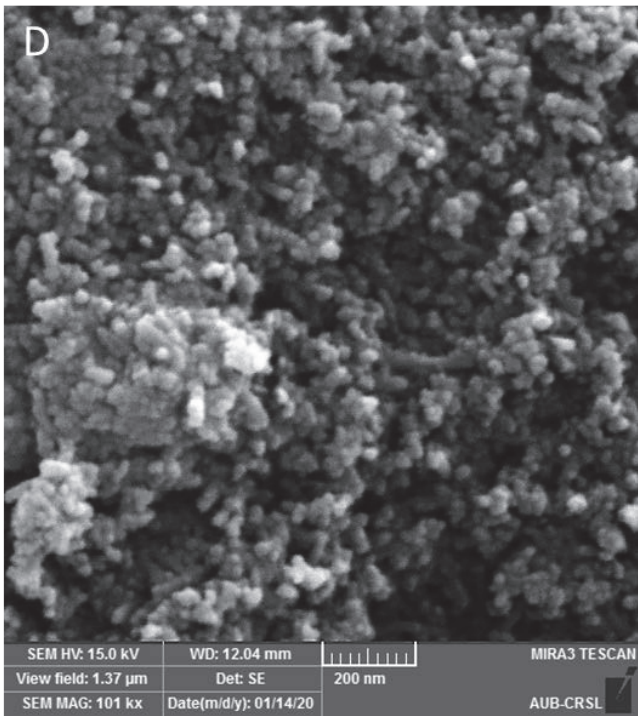

Figure 3: FTIR spectra of (A) (a) bare Fe_3O_4 NPs, (b) APTES-Fe_3O_4 NPs and (c) AH-APTES-Fe_3O_4 NPs, (B) (a) bare Fe_3O_4 NPs, (b) APTES- Fe_3O_4 NPs and (c) GH-APTES- Fe_3O_4 NPs and (C) (a) bare Fe_3O_4 NPs, (b) APTES- Fe_3O_4 NPs and (c) UH-APTES- Fe_3O_4 NPs; the insets correspond to FTIR spectra of the respective nucleobase hydrazides. (D) SEM image of APTES- Fe_3O_4 NPs.

4.3.3. Electrochemical signal of the different magnetic beads

Before starting with the sorption studies, it is important to determine the electroactive groups present to better elucidate the behavioral interaction between arsenic and the magnetic beads. Using square wave voltammetry, and as shown in figure 4, no observable peaks were detected in the range between -1 and 1.5 V for the BDD electrode coated with APTES-Fe_3O_4 NPs. Nevertheless, peaks appeared at 1.15, 1.1 and 1.22 V upon functionalization of the nanoparticles with AH, GH and UH, respectively. As it has been previously proven that the oxidation of the hydrazide function usually occurs at a potential of 1.8 V [29], it can be confirmed that these peaks are characteristic of the oxidation of the nucleobases at a BDD electrode [30].

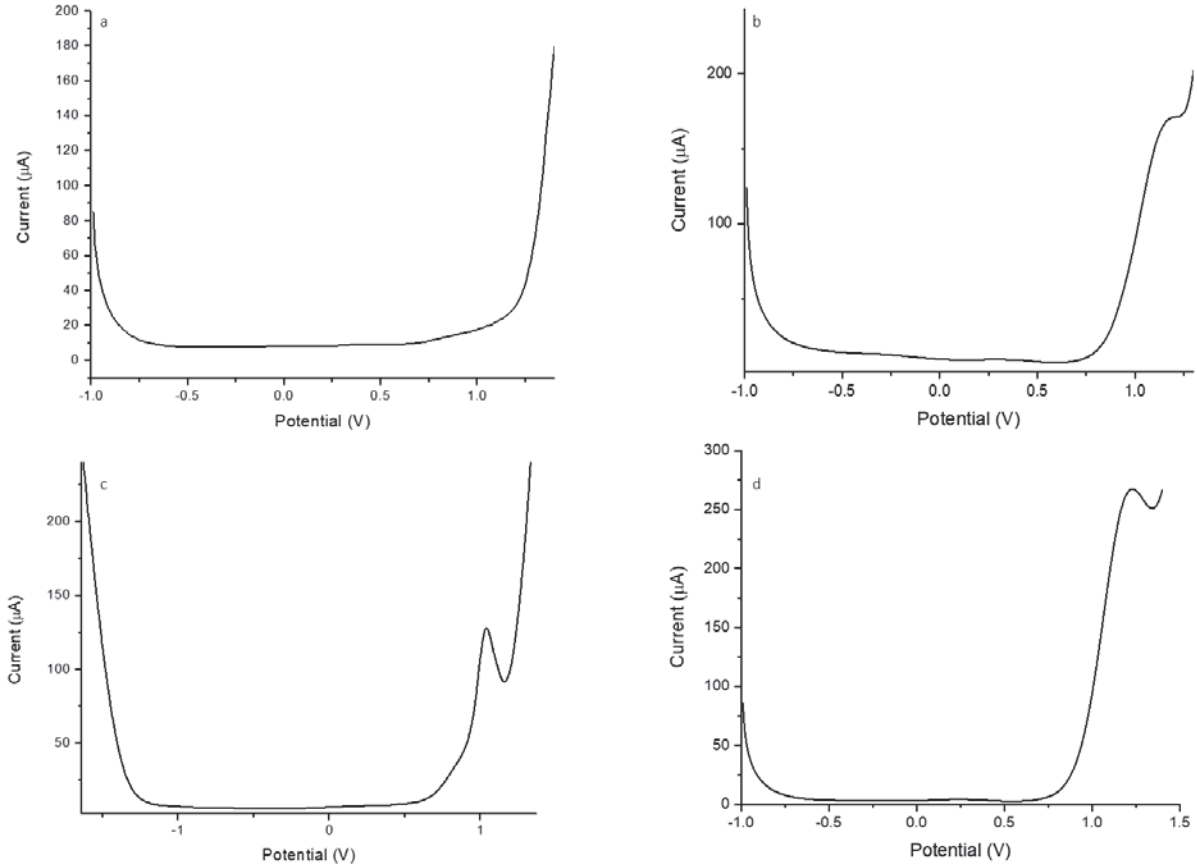

Figure 4: SWV of (a) APTES-Fe_3O_4 nanoparticles, (b) AH-APTES-Fe_3O_4 nanoparticles, (c) GH-APTES-Fe_3O_4 nanoparticles and (d) UH-APTES-Fe_3O_4 nanoparticles.

4.3.4. Effect of pH

The effect of the pH on the nucleobase hydrazide derivatives signal was first investigated. The pH of the solution is critical for both the adsorbent and the adsorbate. In the case of the adsorbent, the chemical state of the reactive groups (protonated or deprotonated) as well as its affinity towards the metal analyte are affected [31]. The pH was varied between 3 and 7 and the electrochemical signal was recorded at each pH. The highest peak intensities corresponding to the oxidation of the nucleobases were found when using the three nucleobases at pHs of 3 and 4. Considering the pK_{as} of each nucleobase, this was expected. Hence, pH 4.1 was chosen for further experiments. The purine nucleobases have 2 pk_{as}: guanine with pK_{a1} = 3.2 – 3.3 and pk_{a2} = 9.2 – 9.6 [32] and adenine with pk_{a1} = 4.2 and pK_{a2} = 9.8 [33]. Thus, at pH 4.1, guanine exists predominantly in the neutral keto tautomeric form, while adenine at a pH close to pKa1 related to the protonation of the pyrimidine nitrogen exists in both the positive and neutral forms. On the other hand, uracil has a pk_a of 9.45 [34] and is therefore neutral at the pH set for the experiments.

In the case of the adsorbate, the speciation of the metal in solution is generally affected by pH [31]. Arsenite has different species under different pH conditions along with their equilibrium constants as described below [35]:

$H_3AsO_3 \rightleftharpoons H_2AsO_3^- + H^+$; pka = 9.23 (1)

$H_2AsO_3^- \rightleftharpoons HAsO_3^{2-} + H^+$; pka = 12.1 (2)

$HAsO_3^{2-} \rightleftharpoons AsO_3^{3-} + H^+$; pka = 12.7 (3)

Thus, at pH 4.1, the dominant arsenite species is the neutral form of H_3AsO_3.

4.3.5. Effect of As(III) concentration

Using a bare BDD, the effect of different As(III) ion concentrations on the oxidation signal of GH was also examined in solution. SWV with the optimized conditions of frequency (50 Hz), amplitude (50 mV) and step potential (10 mV) were applied for a solution of GH in citrate buffer (pH 4.1) with 0.5 M KCl. Prior to the addition of arsenic, the oxidation peak of GH appeared at 1.1 V. Upon the addition of increasing concentrations of As^{3+}, the peak current decreased, indicating that redox reaction of the guanine moiety is hampered by the formation of a complex between arsenite and GH.

The same behavior was observed after immobilizing the magnetic beads on the BDD electrode. The intensity of the peak current was found to decrease with increasing As(III) concentration (figure 5b). The same pattern was also noticed with uracil hydrazide- and adenine hydrazide- functionalized magnetic beads (figure 5a, 5c).

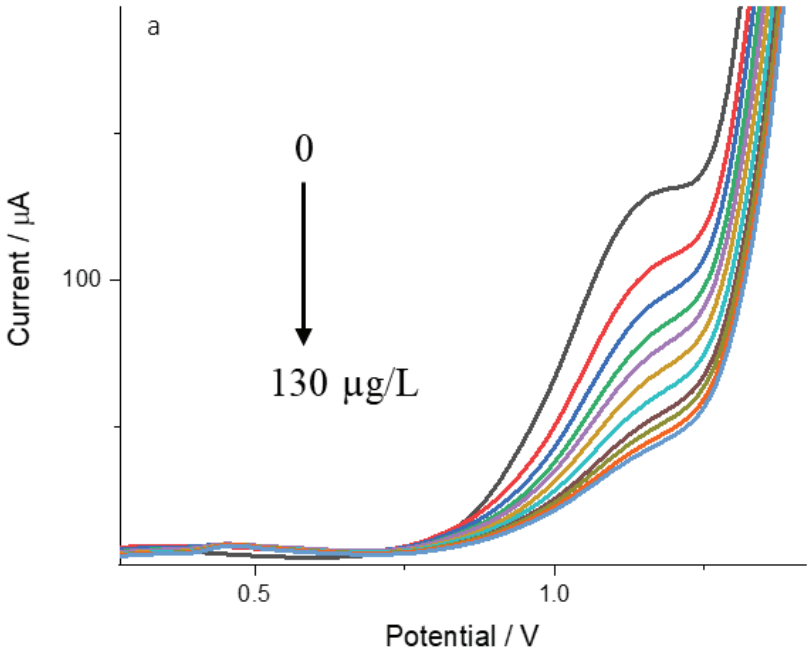
a
0
130 µg/L
Current / µA
100
0.5
1.0
Potential / V

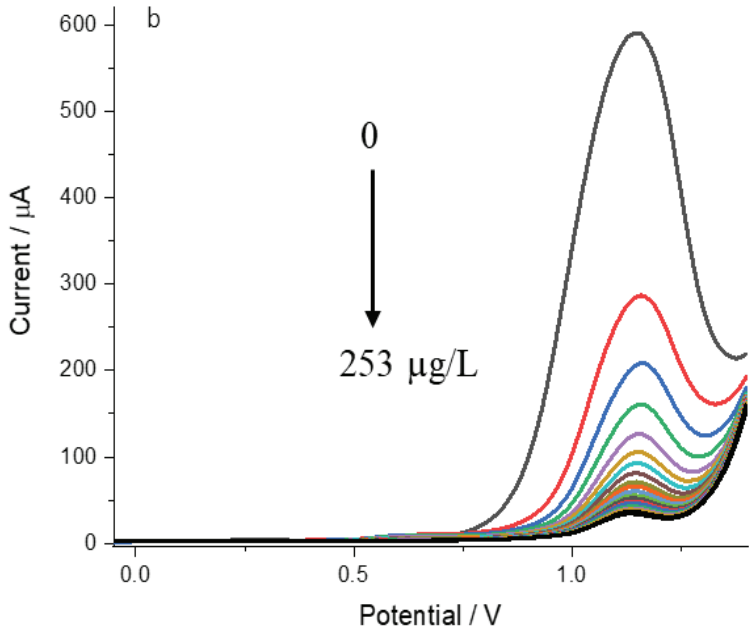
b
0
253 µg/L
Current / µA
600
500
400
300
200
100
0
0.0
0.5
1.0
Potential / V

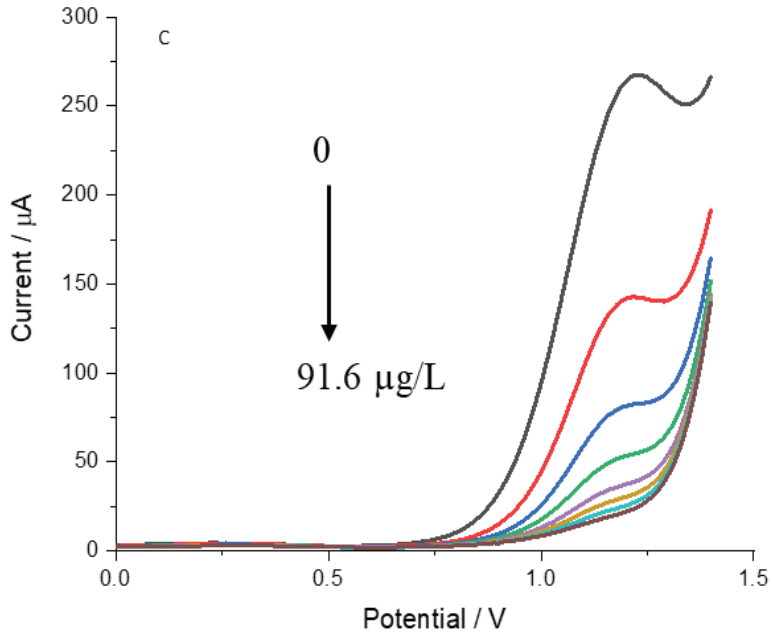

Figure 5: SWV of As(III) at the (a) AH-APTES- Fe_3O_4 NP electrode over a concentration range of 0 –130 µg/L, (b) GH-APTES- Fe_3O_4 NP electrode over a concentration range of 0 –253 µg/L and (c) UH-APTES- Fe_3O_4 NP electrode over a concentration range of 0 –91.6 µg/L.

4.3.6. Adsorption isotherms

Adsorption phenomenon on the surface of the hydrazide functionalized nanoparticles was studied using Langmuir and Freundlich isotherm models. The variation in peak current (ΔI) (average of triplicates) depends on the concentration of arsenite that was adsorbed at the surface of the modified electrode. The adsorption isotherms of arsenite were then built from this value. The two tested models were as follows:

4.3.6.1. Langmuir isotherm

The Langmuir model assumes that the adsorbent surface is homogeneous and that the adsorption takes place at similar and energetically comparable fixed sites. The mathematical linearized form of the Langmuir isotherm can be written as follows [36]:

$$c_e/\Delta I = 1/q_0 b + c_e/q_0$$

where c_e is the equilibrium concentration of the adsorbate, q_0 is the adsorption capacity ($\mu g.g^{-1}$) and b is the energy of adsorption ($L.\mu g^{-1}$). Figures 6a, 6b, and 6c show the Langmuir plot $c_e/\Delta I$ versus ce for the different functionalized nanoparticles, each in their separate concentration range. In

the case of functionalization with guanine hydrazide, the plots show that the experimental data are very well fitted with $r^2 > 0.9999$ and an adsorption capacity of 446.43 $\mu g.g^{-1}$. Fitting the experimental data of the functionalized magnetic nanoparticles with adenine hydrazide and uracil hydrazide resulted in smaller values of q_0 compared with that of GH, as well as r^2 values of 0.9682 and 0.9934, respectively.

Furthermore, the unitless constant separation factor R_L that predicts the efficiency of the adsorption process can be expressed as follows [36]:

$$R= = 1/(1 + q_0 b)$$

where adsorption is considered unfavorable if $R_L > 1$, linear if $R_L = 1$ and favorable if $0 < R_L < 1$ and irreversible if $R_L = 0$ [37]. In the case of the three functionalizations, R_L ranged from 0.0072 to 0.0475 demonstrating that the nature of the adsorption isotherm is favorable. The adsorption capacity of the functionalized nanoparticles towards arsenic (III) increases in the following order: AH < UH < GH.

4.3.6.2. Freundlich isotherm

Freundlich isotherm is considered a varying form of the Langmuir model that represents a heterogeneous system with multiple adsorption sites and a non-uniform distribution of the heat of sorption over the surface. The linearized logarithmic form of the Freundlich model can be expressed as follows [38]:

$$\log \Delta I = \log K_F + (1/n) \log c_e$$

where K_F is the Freundlich constant ($\mu g.g^{-1}$) and n is the Freundlich exponent. Only GH-APTES-Fe_3O_4 could be fitted using this model with an r^2 of 0.9656 (figure 6d) and a value of n lying between 1 and 10 implying that the adsorption is favorable and arsenic (III) can be easily removed from the solution therefore agreeing with the values of R_L calculated from Langmuir's isotherm.

Table 1 presents Langmuir and Freundlich model parameters and linear regression correlations calculated from curve fittings. In the case of GH-APTES-Fe_3O_4, and even though the data were fitted using both models, the Langmuir model could be considered more effectively in describing the adsorption process because of the better regression correlations calculated. On the other hand, data with AH-APTES- Fe_3O_4 and UH-APTES-Fe_3O_4 could only be fitted using the Langmuir model and in concentration ranges much smaller than that with GH-APTES- Fe_3O_4. This

suggests that the adsorption is of a characteristic monomolecular layer form [39]. All dynamic sites have comparable energies and no interaction occurs amongst the adsorbed molecules, assuming that adsorption is localized [40]. Properties of both the adsorbent and the adsorbate (ionic radius, electronegativity, charge…) are the basis of diverse affinities and adsorption capacities [31].

Table 1: Constant parameters and correlation coefficients calculated for different adsorption models for As(III) adsorption by the different functionalized nanoparticles.

Isotherm	**Langmuir**				**Freundlich**		
Constants	**q_0 (µg.g^{-1})**	**b (L.µg^{-1})**	**R_L**	**r^2**	**n**	**k_F (µg.g^{-1})**	**r^2**
AH	25.55	0.7854	0.0475	0.9682			
GH	446.43	0.0968	0.0226	0.9999	7.0522	211.12	0.9656
UH	43.27	3.1976	0.0072	0.9934			

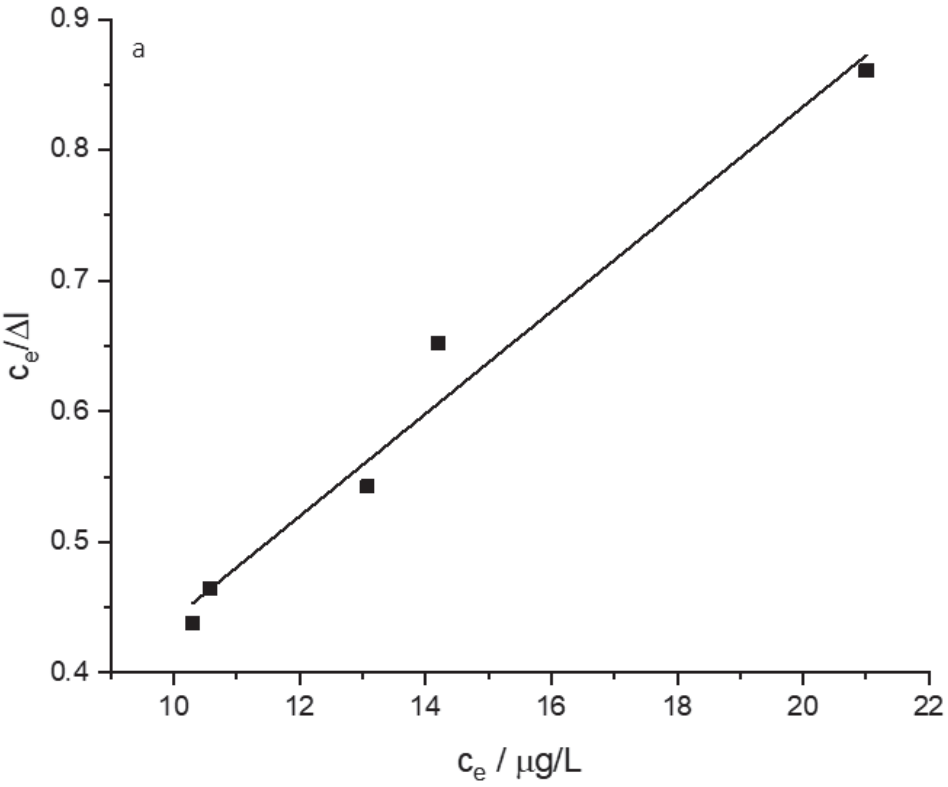
a
0.9
0.8
0.7
0.6
0.5
0.4
$c_e/\Delta I$
10
12
14
16
18
20
22
c_e / µg/L

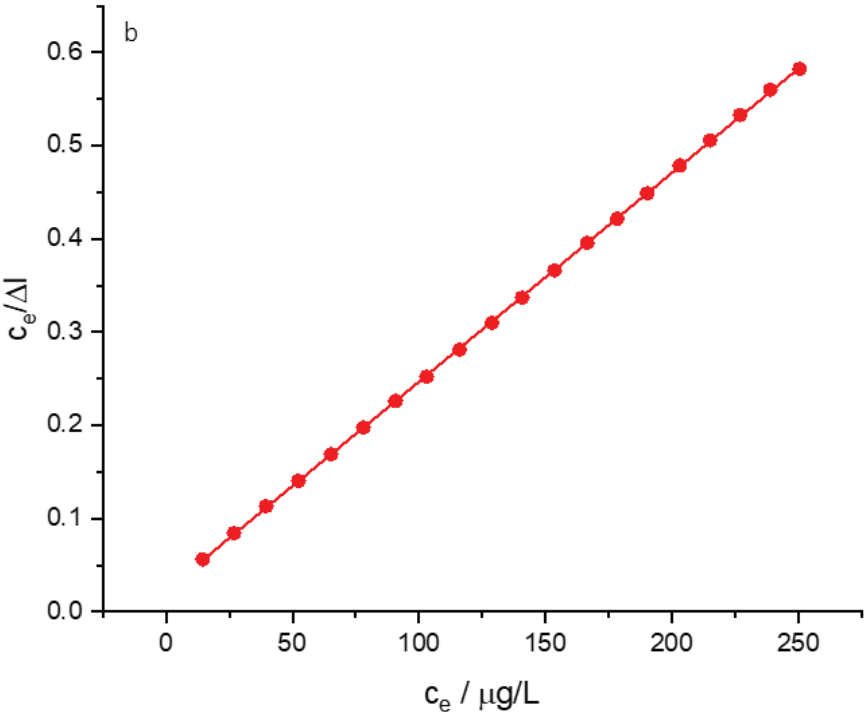
b
0.6
0.5
0.4
0.3
0.2
0.1
0.0
$c_e/\Delta I$
0
50
100
150
200
250
c_e / µg/L

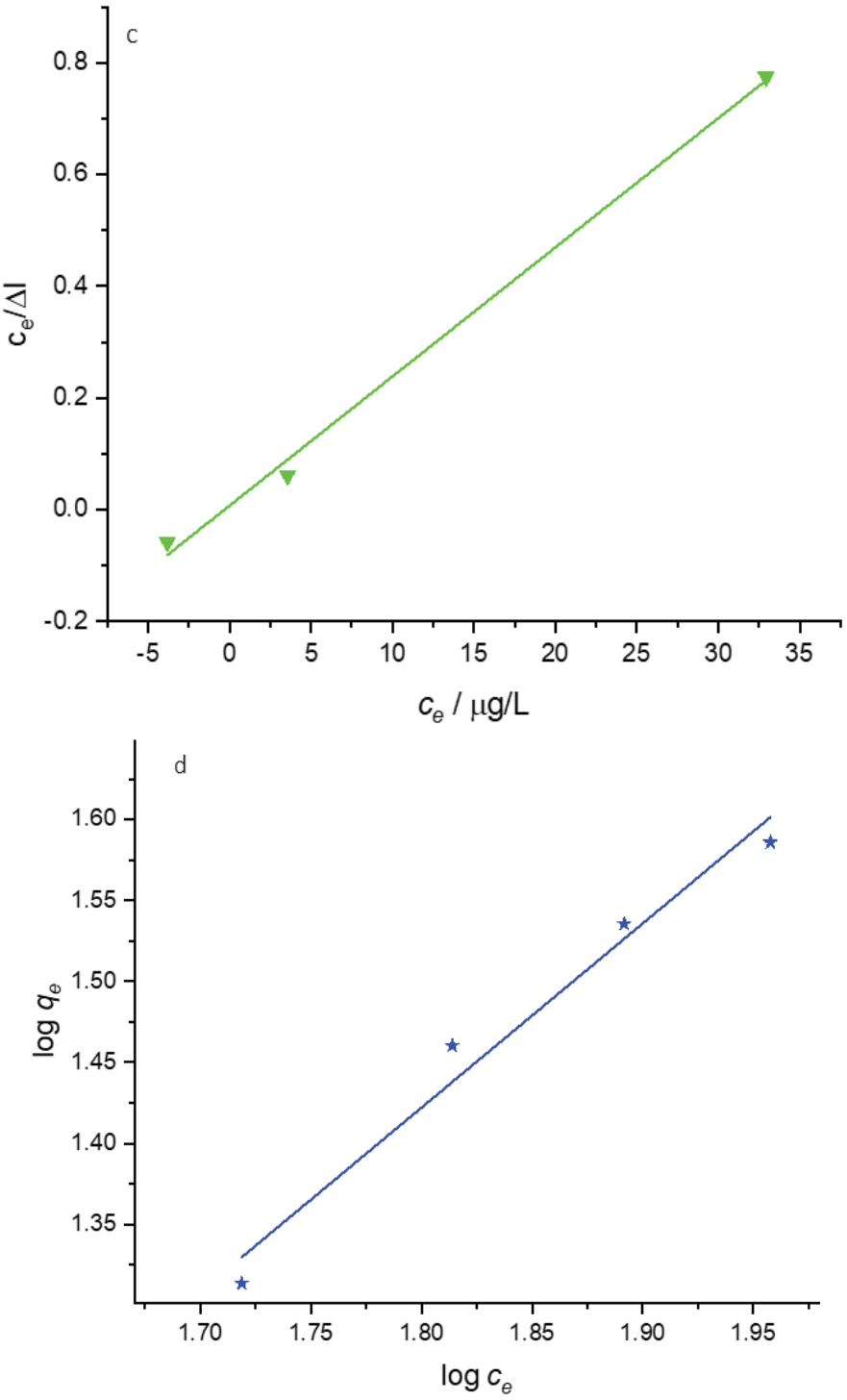

Figure 6: Langmuir adsorption isotherms for As (III) (a) on AH-APTES-Fe_3O_4 NP in the range of 10 –23 µg/L, (b) on GH-APTES- Fe_3O_4 NP in the range of 14 –250 µg/L and (c) on UH-APTES-Fe_3O_4 NP in the range of 0 –35 µg/L. Freundlich adsorption isotherms for As (III) (d) on GH-APTES- Fe_3O_4 NP in the range of 78 – 117 µg/L.

4.3.7. Adsorption kinetics

Studying the adsorption kinetics is crucial to understand the mechanisms, such as mass transfer and chemical reaction, controlling the adsorption [41]. For this reason, the linear pseudo-first order and pseudo-second order kinetic plots are usually used according to the following equations [42]:

$\log(q_e\text{-}q_t) = \log q_e - k_1 t/2.303$

$t/q_t = t/q_e + 1/k_2 q_e^2$

where q_e and q_t (mg/g) are the adsorption capacity of the adsorbent at equilibrium and at time t (min), respectively, and k_1 and k_2 are the pseudo first-order and pseudo-second order rate constants (min^{-1}). Normally by plotting $\log(q_e\text{-}q_t)$ as a function of time and t/q_t as a function of time, the kinetic data can be obtained. On the other hand, the non-linear pseudo-first order and pseudo-second order can be written as follows [42]:

$q_t = q_e(1\text{-}e^{-kt})$

$q_t = (k_2 q_e^2 t)/(1+k_2 q_e t)$

The experiments were performed starting with a concentration of 50 mg/L of arsenic ions in contact with the different magnetic beads. The electrochemical signal was measured every 2 minutes. Since the concentration of the adsorbed arsenic species on the surface of the functionalized magnetic beads is proportional to ΔI, the non-linear models can be plotted as ΔI as a function of time with correlation coefficients higher than 0.92 for the pseudo-first and 0.994 for the pseudo-second order (figure 7).

Using the linear models, the pseudo-first order and pseudo-second order were fitted with good correlation coefficients of higher than 0.98 and 0.992, respectively (figure 8). The correlation coefficients along with the rate constants obtained for the adsorption kinetics using the different nucleobase derivatives are summarized in table 2. A slightly better correlation coefficient suggests that the adsorption follows a pseudo-second order model. This model relies on the assumption that chemisorption may be the rate-limiting step. This implies that the arsenic ions form a chemical (usually covalent) bond with the adsorbent surface and tend to find sites that maximize their coordination number with the surface [41].

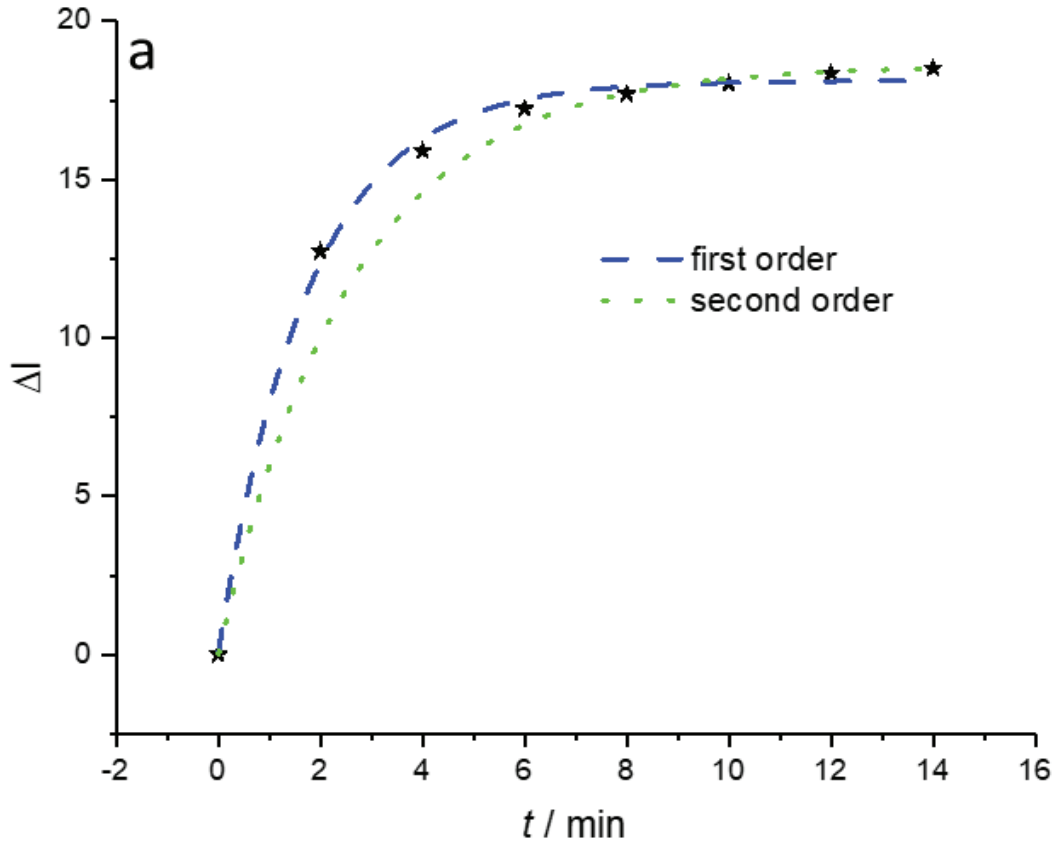
a
20
15
10
5
0
ΔI
-2
0
2
4
6
8
10
12
14
16
t / min
first order
second order

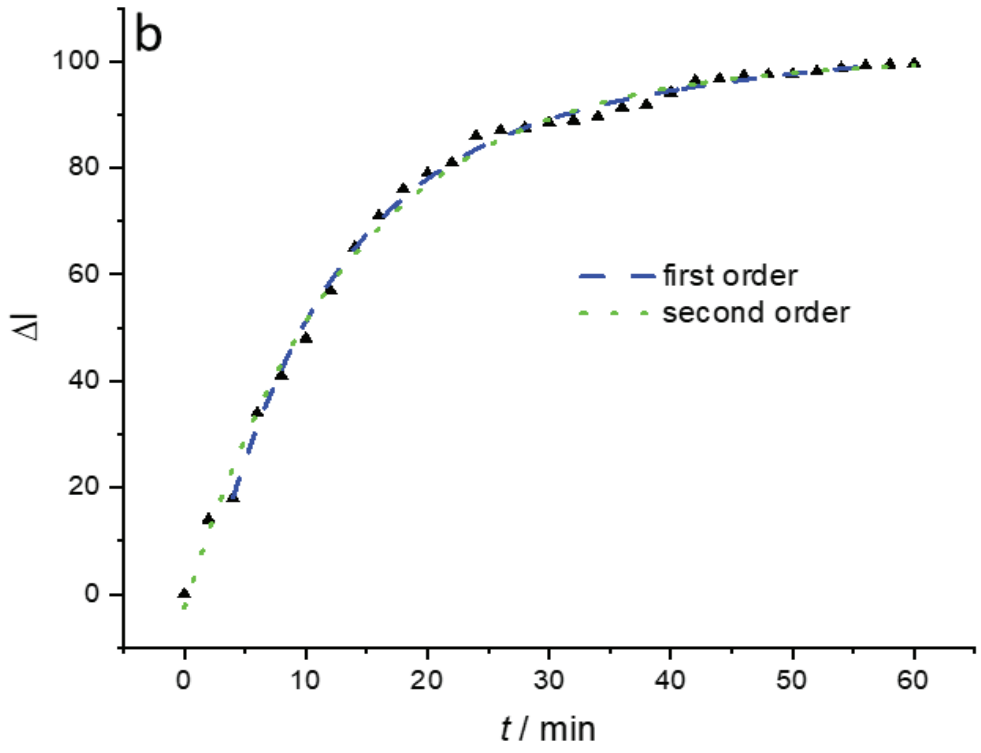
b
100
80
60
40
20
0
ΔI
0
10
20
30
40
50
60
t / min
first order
second order

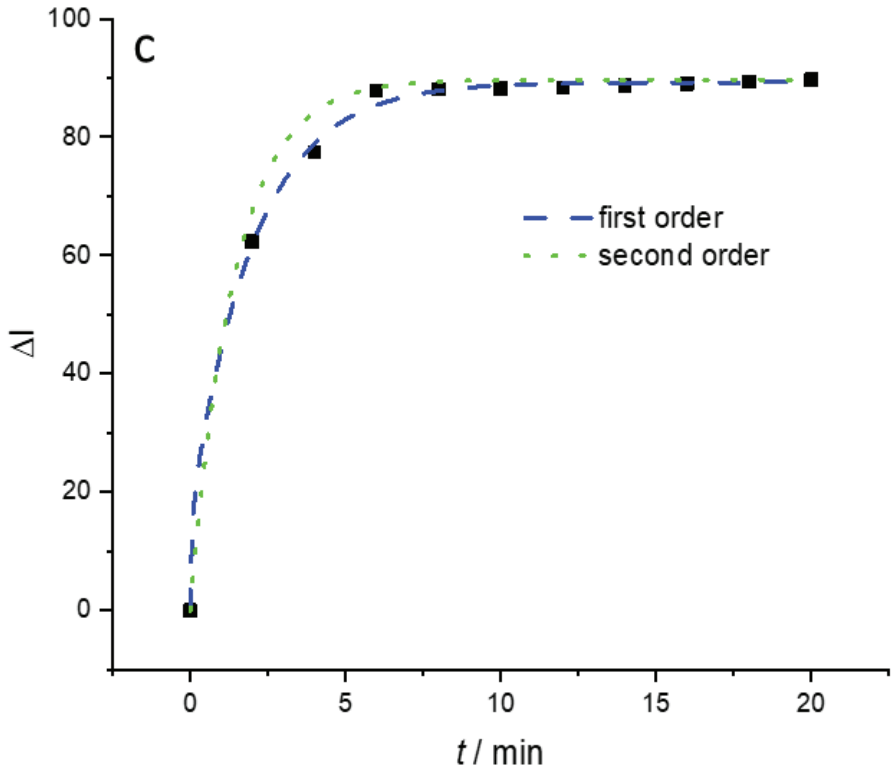

Figure 7: The non-linear plots of the pseudo-first and pseudo-second orders for (a) AH-APTES-Fe_3O_4, (b) GH-APTES- Fe_3O_4 and (c) UH-APTES- Fe_3O_4.

Table 2: Comparison between the pseudo-first order and pseudo-second order parameters for the adsorption of arsenite.

	Non-linear		***Linear***			
	r^2 (pseudo-first order)	**r^2 (pseudo-second order)**	**k_1 (min^{-1})**	**r^2**	**k_2**	**r^2**
AH	0.92062	0.99672	0.5967	0.99584	0.09	0.99585
GH	0.99491	0.99482	0.0846	0.98915	0.00057	0.99215
UH	0.98634	0.99767	0.5336	0.98309	0.0244	0.99854

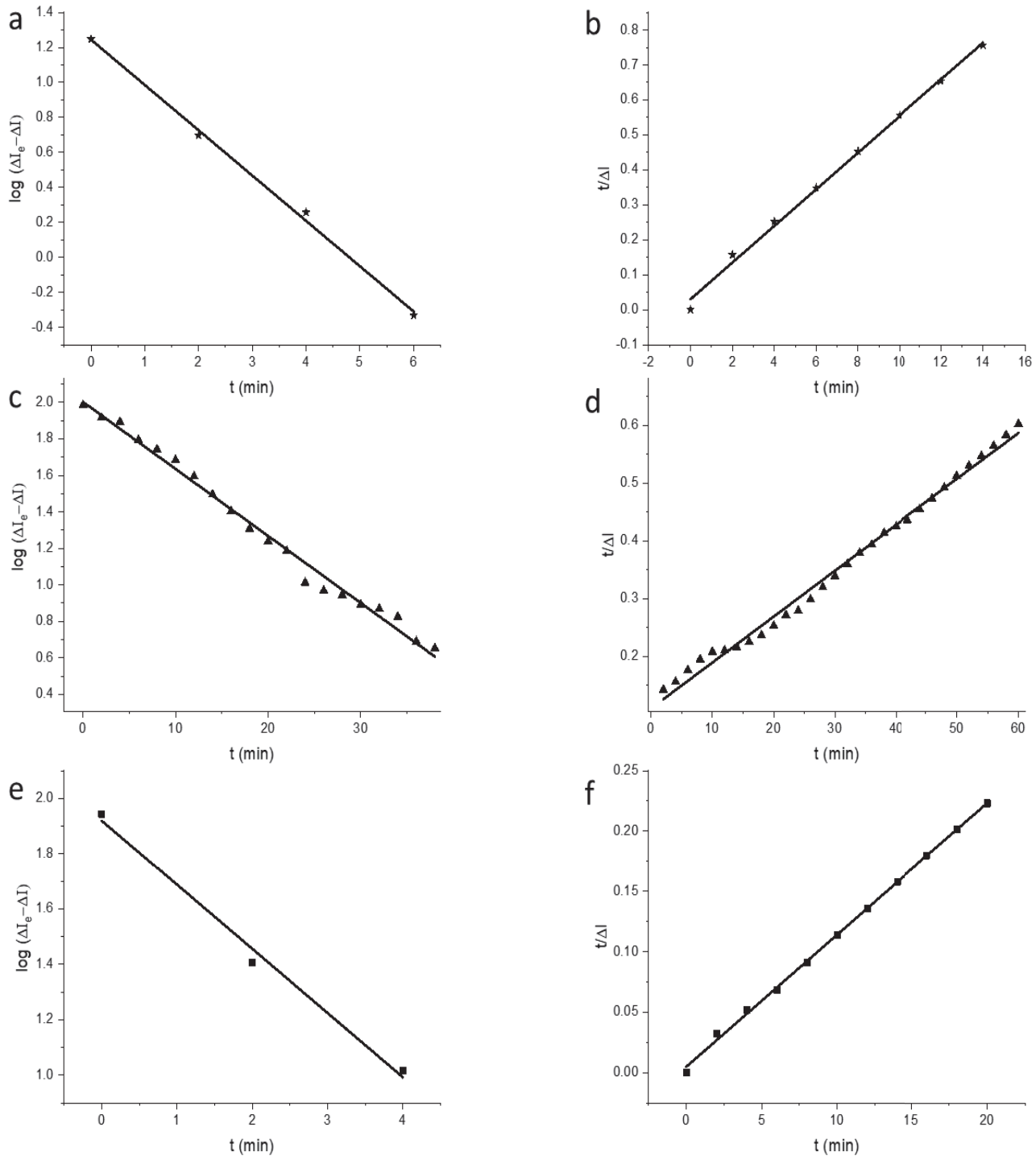

Figure 8: Linear pseudo-first order plots for As(III) adsorption on (a) AH-APTES-Fe_3O_4, (c) GH-APTES- Fe_3O_4 and (e) UH-APTES- Fe_3O_4 and the linear pseudo-second order plots for As (III) adsorption on (b) AH-APTES- Fe_3O_4, (d) GH-APTES- Fe_3O_4 and (f) UH-APTES- Fe_3O_4.

4.3.8. Voltammetric detection of arsenic (III) ions with the hydrazide nucleobase derivatives-APTES-Fe_3O_4 modified BDD electrode

Following the adsorption studies, the plots of arsenic (III) with the different functionalized nanoparticles were assessed. All plots can be divided into two linear ranges (figure 9). The most sensitive and the highest peak intensity was obtained when using GH-APTES- Fe_3O_4 modified BDD electrode. The first linear range was obtained between 13.3 and 65.8 µg/L (0.18 – 0.88 µM) with a correlation coefficient r^2 of 0.9636 and a sensitivity of 1.92 $\mu A.\mu g^{-1}.L$ (144 µA/µM) while the second linear range was between 117 – 241 µg/L (1.56– 3.21 µM) with r^2 of 0.9198 and sensitivity of 0.12 $\mu A.\mu g^{-1}.L$ (9 µA/µM). All the parameters for the three different functionalizations are summarized in table 3. The highest sensitivity of guanine to arsenic comes in accordance with literature proving that the highest stability of complexes formed between arsenic and nucleobases is for guanine [43]. Additionally, this sensitivity is higher than several previous reports [22, 44, 45]. The GH-APTES- Fe_3O_4 detection limit is in the nanomolar range and is lower than the limit of 10 µg/L set by the World Health Organization in drinking water. Moreover, and as shown in table 4, the LOD is lower than those obtained by non-electrochemical methods and can be compared with the LODs of electrochemical techniques.

Table 3: The concentration ranges, sensitivities and correlation coefficients obtained for the different electrode modifications.

	First linear range (µg/L)	**Sensitivity ($\mu A.\mu g^{-1}.L$)**	**r^2**	**Second linear range (µg/L)**	**Sensitivity ($\mu A.\mu g^{-1}.L$)**	**r^2**	**LOD**
AH	0 – 26.5	0.46	0.929	39.7 - 130	0.07235	0.919	6 µg/L 80 nM
GH	13.3 – 65.8	1.92	0.964	117 - 241	0.12497	0.920	1.6 µg/L 21 nM
UH	0 – 26.5	1.40	0.804	39.7 – 78.7	0.14851	0.787	20 µg/L 266 nM

Table 4: Comparison of the current LOD with those of some available aptamer-based sensors for the detection of arsenic.

Technique	**Nanomaterial**	**LOD (nM)**	**Reference**
Rayleigh Scattering	Gold	25.3	[46]
Colorimetry	Silver	79.8	[44]
Fluorescence	Fe_3O_4	50	[45]
Electrochemical	Gold	0.15	[19]
Electrochemical	-	0.27	[20]
Electrochemical	Carbon and gold	1.23	[21]
Electrochemical	-	800	[22]
Electrochemical	Fe_3O_4	21	This work

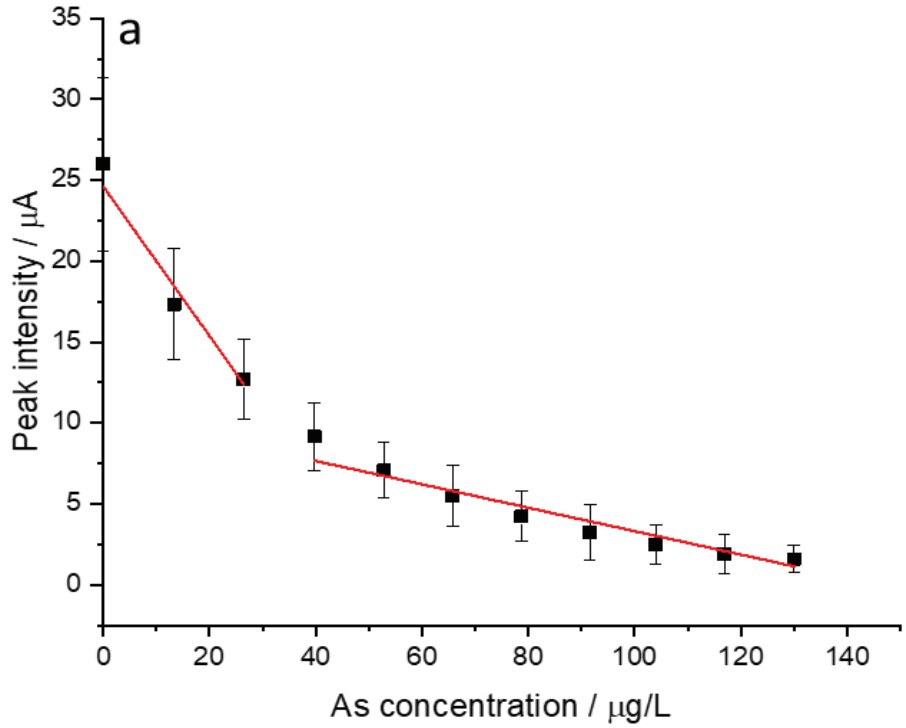
a
Peak intensity / μA
As concentration / μg/L
0
5
10
15
20
25
30
35
0
20
40
60
80
100
120
140

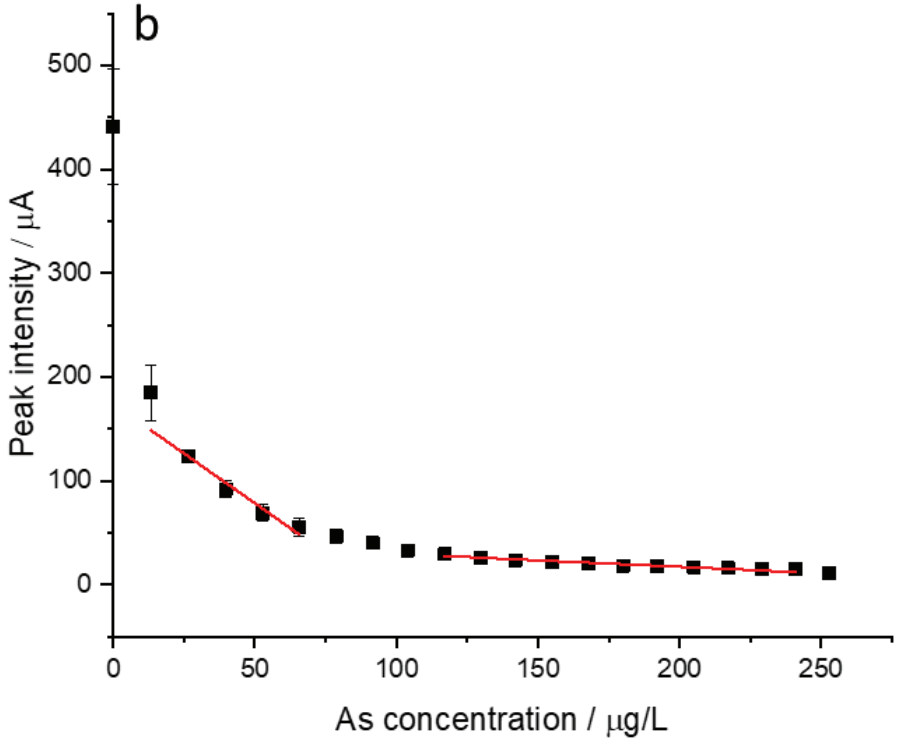
b
Peak intensity / μA
As concentration / μg/L
0
100
200
300
400
500
0
50
100
150
200
250

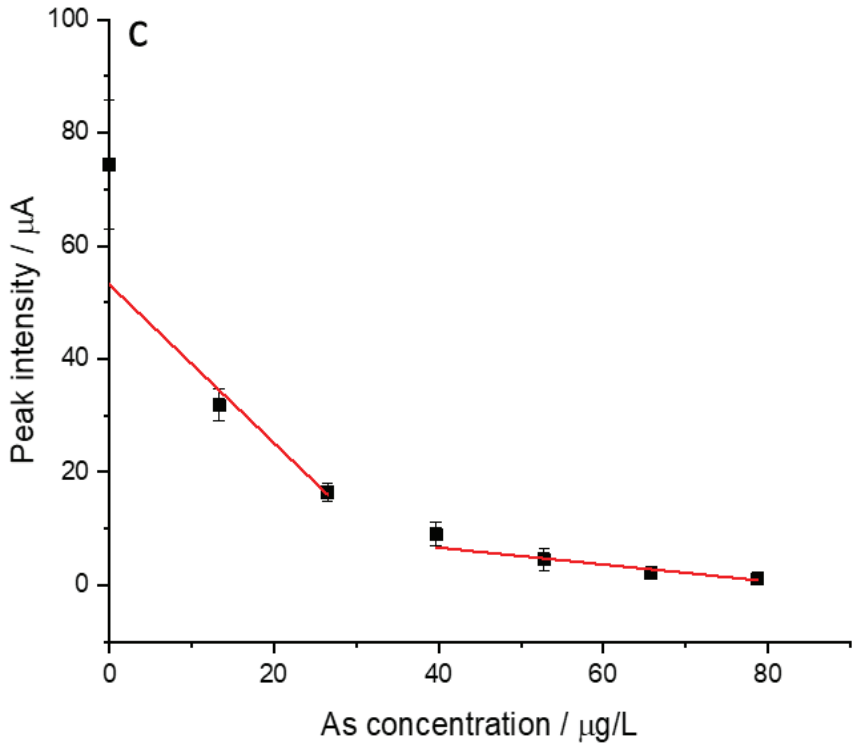

Figure 9: linear ranges of As (III) on (a) AH-APTES-Fe_3O_4 NP electrode, (b) GH-APTES-Fe_3O_4 NP electrode and (c) UH-APTES-Fe_3O_4 NP electrode.

Dong el al. investigated the structures, energies and electron affinities of As-nucleobase complexes using B3LYP density functional method [47]. The calculated formation energies were negative, showing that the formation of the complex is favored over the isolated ions and molecules: -26.3 kcal/mol for As-adenine, -27.0 kcal/mol for As–guanine and -25.2 kcal/mol for As–uracil, As-guanine being the most stable complex. The result shows that arsenic atom prefers to interact with purine rather than pyrimidine bases. To our knowledge, our work is the first experimental proof for this theoretical work.

4.4. Conclusion

In the present work, we have reported the use of some nucleobase derivatives for the electrochemical adsorption and detection of As(III) ions. The adsorption isotherms were evaluated and GH-functionalized MNPs presented the highest adsorption capacity towards arsenic. The adsorption process follows a pseudo-second order kinetic model, suggesting the involvement of chemisorption in the process. The possible binding sites for the adsorption of arsenic on the different

nucleobases were also discussed, it was experimentally demonstrated that the affinity for guanine was the highest, in agreement with previous theoretical measurements. Thus, we showed that voltammetry can be successfully used to study the adsorption of arsenic ions on functionalized MNPs offering its advantages over conventional adsorption techniques. Moreover, GH-functionalized MNPs showed the best limit of detection, in the nanomolar range, and the highest sensitivity towards arsenic compared to the different nucleobase derivatives studied. This point is of particular interest for the future design of aptasensors for arsenic.

References

[1] T.G. Asere, C.V. Stevens, G. Du Laing, Use of (modified) natural adsorbents for arsenic remediation: A review, Sci Total Environ, 676 (2019) 706-720.

[2] S.I. Siddiqui, M. Naushad, S.A. Chaudhry, Promising prospects of nanomaterials for arsenic water remediation: A comprehensive review, Process Safety and Environmental Protection, 126 (2019) 60-97.

[3] Q. Zhou, S. Xi, A review on arsenic carcinogenesis: Epidemiology, metabolism, genotoxicity and epigenetic changes, Regul Toxicol Pharmacol, 99 (2018) 78-88.

[4] S.I. Siddiqui, S.A. Chaudhry, A review on graphene oxide and its composites preparation and their use for the removal of As3+and As5+ from water under the effect of various parameters: Application of isotherm, kinetic and thermodynamics, Process Safety and Environmental Protection, 119 (2018) 138-163.

[5] R.S. Oremland, J.F. Stolz, The ecology of arsenic, Science, 300 (2003) 939-944.

[6] M.K.S. Jian Ma, Dongxing Yuan , Purnendu K. Dasgupta, Speciation and detection of arsenic in aqueous samples A review ofrecent progress in non-atomic spectrometric methods, Analytica Chimica Acta, 831 (2014) 1-23.

[7] V.K. Sharma, M. Sohn, Aquatic arsenic: Toxicity, speciation, transformations, and remediation, Environment International, 35 (2009) 743-759.

[8] A. Ortega, I. Oliva, K.E. Contreras, I. González, M.R. Cruz-Díaz, E.P. Rivero, Arsenic removal from water by hybrid electro-regenerated anion exchange resin/electrodialysis process, Separation and Purification Technology, 184 (2017) 319-326.

[9] P. Benjwal, M. Kumar, P. Chamoli, K.K. Kar, Enhanced photocatalytic degradation of methylene blue and adsorption of arsenic(iii) by reduced graphene oxide (rGO)–metal oxide (TiO2/Fe3O4) based nanocomposites, RSC Advances, 5 (2015) 73249-73260.

[10] R.Y. Ning, Arsenic removal by reverse osmosis, Desalination, 143 (2002) 237-241.
[11] F. Mohammadtabar, R.G. Pillai, B. Khorshidi, A. Hayatbakhsh, M. Sadrzadeh, Efficient treatment of oil sands produced water: Process integration using ion exchange regeneration wastewater as a chemical coagulant, Separation and Purification Technology, 221 (2019) 166-174.
[12] B. Liu, K.H. Kim, V. Kumar, S. Kim, A review of functional sorbents for adsorptive removal of arsenic ions in aqueous systems, J Hazard Mater, 388 (2020) 121815.
[13] X. Min, Y. Li, Y. Ke, M. Shi, L. Chai, K. Xue, Fe-FeS2 adsorbent prepared with iron powder and pyrite by facile ball milling and its application for arsenic removal, Water Sci Technol, 76 (2017) 192-200.
[14] S. Lata, S.R. Samadder, Removal of arsenic from water using nano adsorbents and challenges: A review, Journal of Environmental Management, 166 (2016) 387-406.
[15] S. Saif, A. Tahir, T. Asim, Y. Chen, S. Adil, Polymeric Nanocomposites of Iron–Oxide Nanoparticles (IONPs) Synthesized Using Terminalia chebula Leaf Extract for Enhanced Adsorption of Arsenic(V) from Water, Colloids and Interfaces, 3 (2019).
[16] M.E. Khosroshahi, Ghazanfari, Lida, Synthesis and functionalization of SiO2 coated Fe3O4 nanoparticles with amine groups based on self-assembly, Materials Science and Engineering: C, 32 (2012) 1043-1049.
[17] S. Sawan, R. Maalouf, A. Errachid, N. Jaffrezic-Renault, Metal and metal oxide nanoparticles in the voltammetric detection of heavy metals: A review, TrAC Trends in Analytical Chemistry, 131 (2020) 116014.
[18] J. Lalmalsawmi, D. Tiwari, D.J. Kim, Role of nanocomposite materials in the development of electrochemical sensors for arsenic: Past, present and future, Journal of Electroanalytical Chemistry, 877 (2020).
[19] L. Cui, J. Wu, H. Ju, Label-free signal-on aptasensor for sensitive electrochemical detection of arsenite, Biosensors and Bioelectronics, 79 (2016) 861-865.
[20] H. Gu, Y. Yang, F. Chen, T. Liu, J. Jin, Y. Pan, P. Miao, Electrochemical detection of arsenic contamination based on hybridization chain reaction and RecJf exonuclease-mediated amplification, Chemical Engineering Journal, 353 (2018) 305-310.
[21] T. Mushiana, N. Mabuba, A.O. Idris, G.M. Peleyeju, B.O. Orimolade, D. Nkosi, R.F. Ajayi, O.A.J.S. Arotiba, B.-S. Research, An aptasensor for arsenic on a carbon-gold bi-nanoparticle platform, 24 (2019) 100280.
[22] K. Vega-Figueroa, J. Santillán, V. Ortiz-Gómez, E.O. Ortiz-Quiles, B.A. Quiñones-Colón, D.A. Castilla-Casadiego, J. Almodóvar, M.J. Bayro, J.A. Rodríguez-Martínez, E. Nicolau, Aptamer-Based

Impedimetric Assay of Arsenite in Water: Interfacial Properties and Performance, ACS Omega, 3 (2018) 1437-1444.
[23] M.H.E.D. Hassan Hasan Hammud, Nada Mohamd Sonji and Kamal Hani Bouhadir, Solvatochromic absorption and fluorescence studies of adenine, thymine and uracil thio-derived acyclonucleosides, European Journal of Chemistry, 6 (2015) 325 - 336.
[24] D. Patra, N. Al Homsi, S. Jaafar, Z. Neouchy, J. Elaridi, A. Koubeissi, K.H. Bouhadir, Spectroscopic Evaluation of Novel Adenine/Thymine-Conjugated Naphthalenediimides: Preference of Adenine-Adenine over Thymine-Thymine Intermolecular Hydrogen Bonding in Adenine- and Thymine-Functionalized Naphthalenediimides, J Fluoresc, 29 (2019) 307-318.
[25] S. Sawan, K. Hamze, A. Youssef, R. Boukarroum, K. Bouhadir, A. Errachid, R. Maalouf, N. Jaffrezic-Renault, Voltammetric study of the affinity of divalent heavy metals for guanine functionalized iron oxide nanoparticles, Monatshefte für Chemie - Chemical Monthly, 152 (2021) 229-240.
[26] M. Diab El-Harakeh, R. Njeim, A. Youssef, N. Youssef, A.A. Eid, K.H. Bouhadir, Novel triazine-based pyrimidines suppress glomerular mesangial cells proliferation and matrix protein accumulation through a ROS-dependent mechanism in the diabetic milieu, Bioorganic & Medicinal Chemistry Letters, 29 (2019) 1580-1585.
[27] G. Wang, Ma, Yingying, Tong, Yu, Dong, Xufeng, Synthesis, characterization and magnetorheological study of 3-aminopropyltriethoxysilane-modified Fe3O4 nanoparticles, Smart Materials and Structures, 25 (2016).
[28] J.P. Chen, Yang, P. C., Ma, Y. H., Tu, S. J., Lu, Y. J., Targeted delivery of tissue plasminogen activator by binding to silica-coated magnetic nanoparticle, Int J Nanomedicine, 7 (2012) 5137-5149.
[29] H. Sun, L. Dong, H. Yu, M. Huo, Direct electrochemical oxidation and detection of hydrazine on a boron doped diamond (BDD) electrode, Russian Journal of Electrochemistry, 49 (2013) 883-887.
[30] C. Prado, G.U. Flechsig, P. Grundler, J.S. Foord, F. Markenc, R.G. Compton, Electrochemical analysis of nucleic acids at boron-doped diamond electrodes, Analyst, 127 (2002) 329-332.
[31] W. Zhan, C. Xu, G. Qian, G. Huang, X. Tang, B. Lin, Adsorption of Cu(ii), Zn(ii), and Pb(ii) from aqueous single and binary metal solutions by regenerated cellulose and sodium alginate chemically modified with polyethyleneimine, RSC Advances, 8 (2018) 18723-18733.
[32] W.A.G.I. Yun Hee Jang, Katherine T. Noyes, Lawrence C. Sowers, Sungu Hwang, and Doo Soo Chung, pKa Values of Guanine in Water: Density Functional Theory Calculations Combined with Poisson-Boltzmann Continuum-Solvation Mode, J. Phys. Chem. B 107 (2003) 344-357.

[33] J. Álvarez-Malmagro, F. Prieto, M. Rueda, A. Rodes, In situ Fourier transform infrared reflection absortion spectroscopy study of adenine adsorption on gold electrodes in basic media, Electrochimica Acta, 140 (2014) 476-481.
[34] M.G. Ilyina, E.M. Khamitov, A.G. Mustafin, S.L. Khursan, A theoretical quantitative estimation of acidity of uracil and its derivatives through the pKa values, Journal of the Chinese Chemical Society, 65 (2018) 1447-1452.
[35] S. Dutta, K. Manna, S.K. Srivastava, A.K. Gupta, M.K. Yadav, Hollow Polyaniline Microsphere/Fe3O4 Nanocomposite as an Effective Adsorbent for Removal of Arsenic from Water, Sci Rep, 10 (2020) 4982.
[36] I. Langmuir, The Adsorption of Gases on Plane Surface of Gases on Plane Surface of Glass, Mica and Platinum,, J. Am. Chem. Soc., 40 (1918) 1361-1403.
[37] C. Zou, J. Liang, W. Jiang, Y. Guan, Y. Zhang, Adsorption behavior of magnetic bentonite for removing Hg(ii) from aqueous solutions, RSC Advances, 8 (2018) 27587-27595.
[38] J.L. Subramanyan Vasudevan, Ramasamy Vanathi, Electrochemical Coagulation for Chromium Removal: Process Optimization, Kinetics, Isotherms and Sludge Characterization, Clean 38 (2010) 9-16.
[39] K.Y. Kumar, T.N.V. Raj, S. Archana, S.B.B. Prasad, S. Olivera, H.B. Muralidhara, SnO2 nanoparticles as effective adsorbents for the removal of cadmium and lead from aqueous solution: Adsorption mechanism and kinetic studies, Journal of Water Process Engineering, 13 (2016) 44-52.
[40] V. Fierro, V. Torné-Fernández, D. Montané, A. Celzard, Adsorption of phenol onto activated carbons having different textural and surface properties, Microporous and Mesoporous Materials, 111 (2008) 276-284.
[41] P.S.V. Kumar, C.; Kirthika, K. and Kumar, K. Sathish, Kinetics and equilibrium studies of Pb2+ in removal from aqueous solutions by use of nano-silversol-coated activated carbon, Braz. J. Chem. Eng. [online]. , 27 (2010) 339-346.
[42] N.K. S. Zafar, M. Daud and M.L. Mirza, Kinetic Studies of the Adsorption of Thorium Ions onto Rice Husk from Aqueous Media: Linear and Nonlinear Approach, The Nucleus, 52 (2015) 14-19.
[43] H. Yu, M. Yuan, H. Cao, T. Ye, J. Yu, F. Xu, A computational investigation of the interaction between As3+ and deoxynucleotides, Molecular Simulation, 45 (2019) 769-776.
[44] F. Divsar, K. Habibzadeh, S. Shariati, M.J.A.M. Shahriarinour, Aptamer conjugated silver nanoparticles for the colorimetric detection of arsenic ions using response surface methodology, 7 (2015) 4568-4576.

[45] B. Liu, J. Liu, DNA adsorption by magnetic iron oxide nanoparticles and its application for arsenate detection, J Chemical Communications, 50 (2014) 8568-8570.
[46] M. Tang, G. Wen, A. Liang, Z.J.L. Jiang, A simple and sensitive resonance Rayleigh scattering method for determination of As (III) using aptamer-modified nanogold as a probe, 29 (2014) 603-608.
[47] C. Dong, J. Yang, H. Ning, C. Li, Studies on structures, energetics, and electron affinities of As–nucleobases and their anions with density functional theory, Journal of Molecular Structure: THEOCHEM, 950 (2010) 64-71.

Conclusions and Perspectives

Several biosorbents for the potential removal and sensing of certain heavy metal ions such as arsenic, cadmium, copper and lead from water were successfully developed. The different adsorbents consisted of magnetic nanoparticles coated with (3-aminopropyl)triethoxysilane and functionalized with three nucleobase derivatives separately; adenine hydrazide, guanine hydrazide and uracil hydrazide. Experiments demonstrated that the best adsorption data and analytical performance with the different heavy metals were obtained when guanine hydrazide was used for the functionalization. Accordingly, it was shown that GH-APTES-Fe_3O_4 NPs can be used as a cheap, easy to prepare and manipulate adsorbent. It was also proven that the use of square wave voltammetry can be easily extended to study the adsorption properties of different species. Thus, combining the advantages of electrochemistry and adsorption, one can benefit from the easier and fast manipulation and smaller reagent volumes required compared to conventional adsorption studies. Consequently, the main objectives of this study have been achieved. However, a few points can be taken into consideration for further research and studies. Some recommendations for future studies are noted below:

- The regeneration of any adsorbent is very important; thus, the determination of a convenient regenerating solvent remains crucial. A quick test using GH-APTES-Fe_3O_4 NPs after adsorbing copper ions showed that a solution of guanine hydrazide of high concentration can be a suitable desorbent (appendix 1), but optimization of certain parameters was not achieved. Hence, for further studies, the concentration of the desorbing solvent and the contact time with the nanoparticles that have already adsorbed heavy metals should be studied.
- The studies were done with four heavy metals. There remain several other heavy metals and it would be exciting to study the interaction of these heavy metals with the proposed functionalized nanoparticles.
- In the laboratory, tests were done on solutions containing each heavy metal alone. Nevertheless, real water samples are a little more complex, possibly containing other heavy metal ions as well as other organic and inorganic contaminants. Consequently, further studies should take this point into consideration by checking how the combination of different heavy metals together can affect the adsorption properties of the magnetic beads to better elucidate the maximum adsorption capacity in natural water samples.

- The complexity of real water matrices extends to include anions in addition to the cations. Thus, it would be interesting to study whether the presence of some negatively charged ions can have an influence on the different nucleobases.
- Equilibrium studies were modelled using Langmuir and Freundlich isotherms only. Both models assume a homogeneous adsorbent surface. Consequently, other isotherm models such as Sips, Toth, Redlich-Peterson and Temkin isotherms could be investigated.

Appendix: Desorption Study

This appendix presents a brief description of the procedure and preliminary results for the desorption of the heavy metals after the adsorption process. This study is important for any adsorbent to validate its effectiveness to be regenerated and reused, thus enhancing its cost efficiency and applicability in real samples.

After a complete adsorption study, the magnetic beads that were functionalized with guanine hydrazide and used to adsorb copper ions were left on the boron doped diamond electrode. The solution that was in contact with the beads was removed and replaced with a guanine hydrazide solution of higher concentration (4 mg/mL). The guanine hydrazide solution was left for 1 hour. It was then removed and the magnetic beads were washed repeatedly with citrate buffer of pH 4 to ensure that all traces of the concentrated solution were removed. This was followed by filling the electrochemical cell with the citrate buffer, and running square wave voltammetry under the same conditions as before; frequency 50 Hz, amplitude 50 mV, step potential 10 mV and time of equilibration 2 min. This procedure was repeated three times using the same electrode functionalized with the magnetic beads. The signals were then analyzed. After each cycle in the desorbing solution, the reusability of the magnetic beads was also assessed by adding copper ions and performing square wave voltammetry.

Figure A1 represents the efficiency of desorption after each hour in the desorbing solution. The results show an excellent efficiency of more than 94% even after three adsorption-desorption cycles using the magnetic beads. This confirms that guanine hydrazide, with a concentration higher than that used to functionalize the magnetic beads, can be used as a desorbing solution to remove copper ions.

Not only was the adsorbent regenerated, but also used for three successive adsorption studies. Upon the addition of copper ions, the signal corresponding to the oxidation of guanine decreased. The results for three adsorption studies using the same magnetic beads are represented in figure A2. The analysis shows that the functionalized magnetic beads can be successfully reused up to three cycles with comparable sensitivities. This proves the excellent stability of our adsorbent and its cost effectiveness in practical applications.

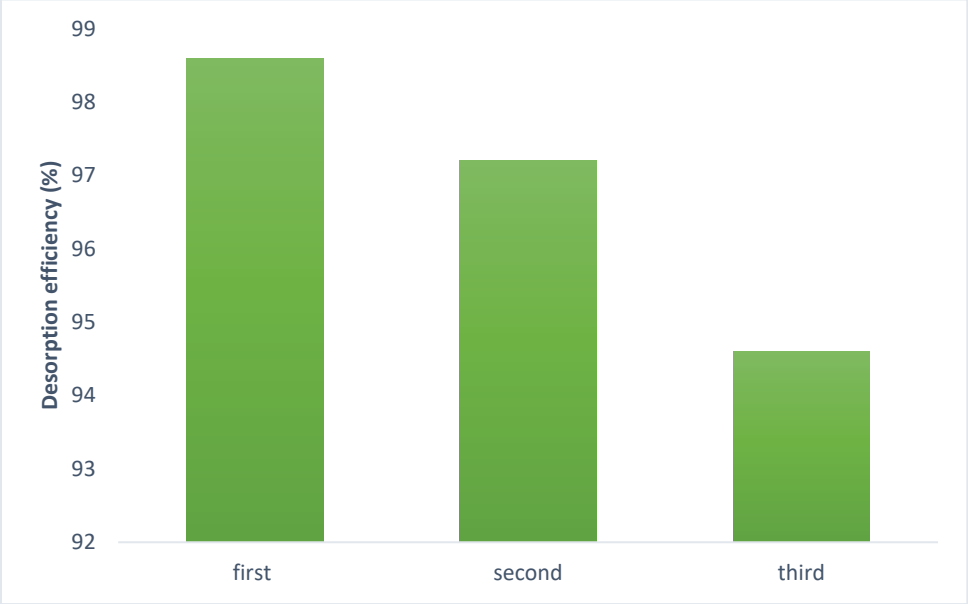

Figure A1: desorption efficiency of guanine hydrazide (4 mg/mL) after three desorption cycles.

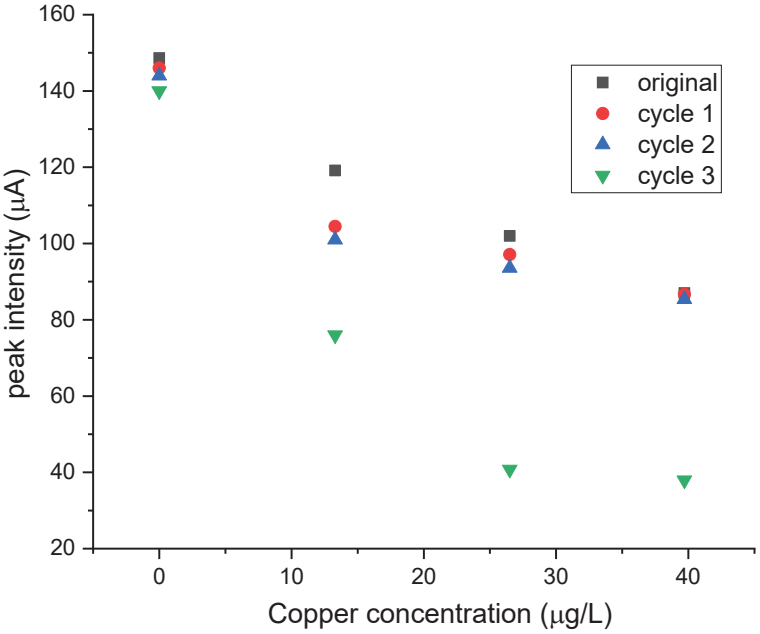

Figure A2: Response of GH-APTES-Fe_3O_4 NPs to the addition of copper (II) ions after 3 desorption-adsorption cycles.